

# **Wind induced upwelling and the response of surface chlorophyll in the Bay of Bengal**

*Thesis submitted in partial fulfillment of the requirements for the Degree of*

## **DOCTOR OF PHILOSOPHY in ATMOSPHERIC SCIENCE**

under the  
Faculty of Marine Sciences

by

**SMITHA A**



**Department of Atmospheric Sciences  
Cochin University of Science and Technology  
Cochin – 682016, India**

**September 2016**

## DECLARATION

I hereby declare that this thesis entitled *Wind induced upwelling and the response of surface chlorophyll in the Bay of Bengal* is an authentic record of the research work carried out by me and no part of this work has been submitted to any University or Institution for the award of any Degree or Diploma.

**Smitha A**

Cochin-682016  
September, 2016

Research Scholar  
Department of Atmospheric Sciences  
Cochin University of Science and Technology

## CERTIFICATE

This is to certify that the thesis entitled *Wind induced upwelling and the response of surface chlorophyll in the Bay of Bengal* is an authentic record of the research work carried out by Smt. Smitha A, under my supervision and guidance at the Department of Atmospheric Sciences, Cochin University of Science and Technology, in partial fulfillment of the requirements for the Ph. D. Degree of Cochin University of Science and Technology under the Faculty of Marine Sciences and that no part thereof has been submitted to any University or Institution for the award of any Degree or Diploma.

Prof. (Dr.) H. S. Ram Mohan

Supervising Guide

Professor (Retd.), Department of Atmospheric Sciences

& former Director, School of Marine Sciences

Cochin University of Science and Technology

Cochin-682016

September, 2016

## Acknowledgements

I would like to express my profound gratitude and regards to my guide Prof. (Dr). H. S. Ram Mohan for his guidance, valuable suggestions and encouragement, which enabled me to complete this thesis. This thesis would not have materialized without his support, constant encouragement, patience and enthusiasm in guiding my research. I wish to express my sincere gratitude to Sri. K. H. Rao and Dr. M. M. Ali, former scientists of Oceanography Division, NRSC, Hyderabad, who initiated me into my research career and introduced me to the field of satellite remote sensing of ocean which forms the basis of this thesis.

I take this opportunity to thank Dr. Ajith Joseph, Director of NERCI, Dr. Lasse Pettersson, Prof. Ola Johannessen and Dr. Nandini Menon for permitting me to carry out the thesis work alongside the project work and for providing the required facilities to carry out research during the last few years. I would like to thank Prof. Trevor Platt, Dr. Shubha Sathyendranath, Dr. N. R. Menon and Prof. P. V. Joseph for their support in the completion of the thesis.

I extend my sincere thanks to Dr. Santosh K. R., Member of my Doctoral Committee for taking keen interest in my work and providing valuable suggestions. I acknowledge all the support and help provided by Sri. B. Chakrapani, Head, Department of Atmospheric Sciences, for his valuable advice and encouragement and for providing the necessary facilities in the Department throughout the course of research. I extend my thanks to Dr. K. Mohanakumar, and Dr. C. A. Babu, Department of Atmospheric Sciences for their motivation and support.

I take this opportunity to thank my friends and colleagues from NERCI, CUSAT and NRSC for their help and support during the period of my thesis work. I am indebted to Krishnamohan, Johnson Zacharia, Jayaram and Lorna for their suggestions and for clearing my doubts on programming, statistical and mathematical techniques. I am grateful to Syam Sankar who helped me in programming, technical issues and during the last stage of submission. I would like to thank my friends Abish, Ajin,

Vijayakumar, Shaju, Shalin, Asha, Anila, Resmi, Swapna, Shinu and Sachin who in one way or other helped me in carrying out my research. I acknowledge the support provided by Dr. Bindu and Mr. Hariharan of NERCI during the course of my work. I would also like to acknowledge help rendered by Mr. Manuel of NERCI. I would like to mention my friends from NRSC, Debadatta, Jagadeesh, Sarika and Surendran who created a very pleasant and enjoyable atmosphere, gave many suggestions and supported me in my research and made my stay in Hyderabad memorable.

I would like to express my heartfelt thanks to the office staff of Department of Atmospheric Sciences for helping me carry out all administrative formalities and for providing a very cordial atmosphere. I would like to specially thank Dr. Sreedevi for the care and support she gave me during my research. I would like to express my heartfelt thanks to Mrs. Chandra Ram Mohan for her care and hospitality.

The Senior Research fellowship from CSIR is gratefully acknowledged. I acknowledge the use of Ferret and GrADS program for analysis and graphics in this thesis. Acknowledgements are due to NASA, NOAA, IFREMER and NCAR for providing data to carry out my work.

I express my gratefulness to my family who have been giving me unconditional love and support throughout my life and have enabled me to achieve this goal. I would like to mention my little kid Ishan who in his own way lightened the stress during last few months of my research work.

Finally, I would like to thank all those who supported me directly and indirectly throughout my research work.

**Smitha A**

*Dedicated to my parents...*

# Contents

<b>List of Figures</b>	x
<b>List of Tables</b>	xiv
<b>Glossary</b>	xv

## Chapters

<b>Chapter 1 – Introduction</b>	1-27
1.1. Wind forcing on the ocean surface	2
1.1.1. Wind	2
1.1.2. Wind stress	3
1.1.3. Wind stress curl	4
1.2. The Ekman layer	4
1.3. Ekman pumping	6
1.4. Importance of upwelling	8
1.4.1. Coastal upwelling	9
1.4.2. Equatorial upwelling	10
1.4.3. Open ocean upwelling	11
1.5. Chlorophyll in the upper ocean	12
1.6. Factors affecting surface chlorophyll concentration	13
1.7. Eddies in the ocean	15
1.8. Bay of Bengal - the study area and its characteristics	15
1.8.1. Winds	16
1.8.2. Circulation	17
1.8.3. Kelvin waves and Rossby waves	19
1.8.4. Salinity	20
1.8.5. Sea surface temperature and surface stratification	20
1.8.6. Chlorophyll and productivity	22

1.9. Ocean response to tropical cyclones	23
1.10. Objectives of the study	25
1.11. Significance of the study	26
<b>Chapter 2 - Data and Methodology</b>	<b>28-51</b>
2.1. Introduction	28
2.2. Remote sensing parameters and sensors	28
2.2.1. Sea surface winds	29
2.2.1.1. Scatterometer	29
2.2.1.2. QuikSCAT scatterometer	30
2.2.2. Sea surface temperature	33
2.2.2.1. TRMM Microwave Imager (TMI)	34
2.2.2.2. Terra Moderate Resolution Imaging Spectroradiometer (MODIS)	36
2.2.3. Sea level anomaly	37
2.2.3.1. Altimeter	38
2.2.4. Surface chlorophyll- <i>a</i> (chl- <i>a</i> ) concentration	39
2.2.4.1. Sea-viewing Wide Field of View sensor (SeaWiFS)	40
2.2.4.2. Terra MODIS	42
2.3. Model outputs	43
2.3.1. Water temperature	43
2.3.2. Primary production	44
2.3.3. Mixed layer depth	45
2.4. Methodology	45
2.4.1. Computation of monthly and seasonal climatology	45
2.4.2. Empirical Orthogonal Function analysis	47
2.4.3. Computation of geostrophic currents	48
2.4.4. Computation of Ekman vertical velocity	49
2.4.5. Analysis of depth of 20°C isotherm (D20) and surface chl- <i>a</i> concentration	50
2.4.6. Tropical cyclone studies	50

<b>Chapter 3 - Distribution of some physical and biological properties in the Bay of Bengal</b>	52-77
3.1. Introduction	52
3.2. Spatial distribution of wind stress curl	53
3.2.1. Seasonal mean distribution of wind stress curl	53
3.2.2. Monthly mean distribution of wind stress curl	55
3.3. Spatial distribution of sea surface temperature	59
3.3.1. Seasonal mean distribution of sea surface temperature	59
3.3.2. Monthly mean distribution of sea surface temperature	61
3.4. Spatial distribution of sea level anomaly	65
3.4.1. Seasonal mean distribution of sea level anomaly	65
3.4.2. Monthly mean distribution of sea level anomaly	66
3.5. Spatial distribution of surface chl- <i>a</i> concentration	69
3.5.1. Seasonal mean distribution of surface chl- <i>a</i> concentration	69
3.5.2. Monthly mean distribution of surface chl- <i>a</i> concentration	71
3.6. Summary	75
<b>Chapter 4 - Variability of wind stress curl and the Ekman pumping in the Bay of Bengal</b>	78-95
4.1. Introduction	78
4.2. Empirical Orthogonal Function analysis of wind stress curl	79
4.3. Wind stress during the southwest monsoon	82
4.4. Cold pool of the south-central Bay of Bengal and its inter-annual variation	84
4.5. Wind induced Ekman pumping and sea level variations	89
4.5.1. Southwestern Bay of Bengal	89
4.5.2. West-central Bay of Bengal	91
4.6. Summary	93
<b>Chapter 5 - Upwelling and its significance in relation to surface chlorophyll distribution</b>	96-127
5.1. Introduction	96
5.2. Variability of D20 in the Bay of Bengal	97

5.3. Annual mean distribution of D20	101
5.4. Relationship of D20 with physical and biological properties	102
5.4.1. Relation between D20 and Ekman vertical velocity	102
5.4.2. Relation between D20 and sea level anomaly	107
5.4.3. Relation between D20 and surface chl- <i>a</i> concentration	111
5.5. Seasonal and inter-annual variability of surface chl- <i>a</i> concentration	115
5.6. Influence of physical properties on surface chl- <i>a</i> distribution	119
5.6.1. Relation between surface chl- <i>a</i> concentration and Ekman pumping	119
5.6.2. Relation between surface chl- <i>a</i> concentration and sea level anomaly	120
5.7. Summary	124
<b>Chapter 6 - Upper ocean response to upwelling induced by tropical cyclones in the Bay of Bengal – Case studies</b>	128-148
6.1. Introduction	128
6.2. Tropical Cyclone 03B (TC 03B), 26 Nov – 6 Dec 2000	131
6.3. Response of physical and biological properties of ocean to TC 03B	132
6.4. Tropical cyclone 01B (TC 01B), 11-19 May 2003	138
6.5. Response of physical and biological properties of ocean to TC 01B	139
6.6. Summary	147
<b>Chapter 7 - Summary and conclusions</b>	149-157
<b>References</b>	158-175
<b>List of Publications</b>	176

## List of Figures

- |     |  |       |
|-----|--|-------|
| 1.1 | The balance between pressure gradient force, Coriolis force and friction (Figure is taken from <a href="http://ww2010.atmos.uiuc.edu/(Gh)/guides/mtr/fw/fric.rxml">http://ww2010.atmos.uiuc.edu/(Gh)/guides/mtr/fw/fric.rxml</a> )   | 5     |
| 1.2 | Ekman spiral in the northern hemisphere where the mass transport is directed to the right of the wind (Marshall and Plumb, 2013)   | 6     |
| 1.3 | Coastal Upwelling and downwelling when the wind blows parallel to the coast in the northern hemisphere with a) the coast to the left and the Ekman transport away from the coast causing upwelling, and b) the coast to the right and the Ekman transport towards the coast which cause downwelling (figure is taken from <a href="http://oceanmotion.org/html/background/upwelling-and-downwelling.htm">http://oceanmotion.org/html/background/upwelling-and-downwelling.htm</a> ).   | 10    |
| 1.4 | Bay of Bengal - study area   | 16    |
| 1.5 | Schematic representation of the circulation in the Indian Ocean during January and July. The abbreviations are as follows - SMC-Summer Monsoon Current; WMC-Winter Monsoon Current; EICC-East India Coastal Current; WICC-West India Coastal Current; SC-Somali Current; EC-Equatorial Current; SECC-South Equatorial Counter Current; EACC-East African Coastal Current; SEC-South Equatorial Current; LH-Lakshadweep high; LL-Lakshadweep low; and GW-Great Whirl. (The figure is taken from Shankar <i>et al.</i> , 2002) | 18    |
| 3.1 | Seasonal mean wind stress curl ( $\times 10^{-7} \text{ N m}^{-3}$ ) during a) Dec- Feb (DJF), b) Mar-May (MAM), c) Jun-Sep (JJAS), and d) Oct-Nov (ON) over the Bay of Bengal. Dashed lines indicate negative WSC   | 54    |
| 3.2 | Monthly climatology of wind stress curl ( $\times 10^{-7} \text{ N m}^{-3}$ ) over the Bay of Bengal. Dashed lines indicate negative wind stress curl  | 56-57 |
| 3.3 | Seasonal mean sea surface temperature ( $^{\circ}\text{C}$ ) during a) Dec-Feb (DJF), b) Mar-May (MAM), c) Jun-Sep (JJAS), and d) Oct-Nov (ON) of the Bay of Bengal  | 60    |
| 3.4 | Monthly climatology of sea surface temperature ( $^{\circ}\text{C}$ ) of the Bay of Bengal   | 62-63 |
| 3.5 | Seasonal mean sea level anomaly (cm) during a) Dec- Feb (DJF), b) Mar-May (MAM), c) Jun-Sep (JJAS), and d) Oct-Nov (ON) in the Bay of Bengal   | 66    |
| 3.6 | Monthly climatology of sea level anomaly (cm) in the Bay of Bengal   | 67-68 |
| 3.7 | Seasonal mean of surface chlorophyll- <i>a</i> concentration ( $\text{mg m}^{-3}$ ) during a) Dec-Feb (DJF), b) Mar-May (MAM), c) Jun-Sep (JJAS), and d) Oct-Nov (ON) in the Bay of Bengal   | 71    |
| 3.8 | Monthly climatology of surface chlorophyll- <i>a</i> concentration ( $\text{mg m}^{-3}$ ) in the Bay of Bengal   | 73-74 |

4.1	Annual mean of wind stress curl pattern ( $\times 10^{-7} \text{ N m}^{-3}$ ) over the Bay of Bengal from January 2000 to December 2007. Dashed lines indicate negative wind stress curl	79
4.2	(a) Variance in percentage associated with first 12 EOFs, and (b) cumulative variance in percentage of EOF modes	80
4.3	(a) Spatial pattern of wind stress curl ( $\times 10^{-7} \text{ N m}^{-3}$ ) for the first EOF and (b) the corresponding non-dimensional time series PC1	81
4.4	(a) Spatial pattern of wind stress curl ( $\times 10^{-7} \text{ N m}^{-3}$ ) for the second EOF and (b) the corresponding non-dimensional time series PC2	82
4.5	Spatial distribution of wind stress ( $\text{N m}^{-2}$ ) climatology for the years 2000 to 2007 superimposed with wind vectors from May to October covering the southwest monsoon season in the Bay of Bengal	83
4.6	Averaged sea surface temperature ( $^{\circ}\text{C}$ ) during Jun-Sep in the south-central Bay depicting the cold pool for the period of 2000 to 2007	84
4.7	(a) Average sea level anomaly (cm) superimposed with geostrophic currents in $\text{cm s}^{-1}$ (Jun-Sep) in the south-central Bay depicting the cold core eddy to the east of Sri Lanka and the intrusion of currents into the Bay of Bengal and (b) the mean wind pattern ( $\text{m s}^{-1}$ ) for the same period showing the region of maximum wind speed during summer monsoon period of 2000 to 2007	85
4.8	Sea surface temperature ( $^{\circ}\text{C}$ ) cooling in the south-central Bay of Bengal averaged over $3\text{-}10^{\circ}\text{N}$ depicting the cold pool that develops during the southwest monsoon season	87
4.9	Sea surface temperature ( $^{\circ}\text{C}$ ) cooling in the south-central Bay of Bengal averaged over $82\text{-}90^{\circ}\text{E}$ depicting the cold pool that develop during the southwest monsoon season	88
4.10	Monthly mean Ekman vertical velocity ( $\times 10^{-5} \text{ m s}^{-1}$ ) from May to October in the southwestern Bay of Bengal	89
4.11	Monthly mean sea level anomaly (cm) superimposed with geostrophic currents ( $\text{cm s}^{-1}$ ) in the southwestern Bay depicting evolution of the cold core eddy to the east of Sri Lanka and the intrusion of currents into the Bay of Bengal	90
4.12	Monthly mean Ekman vertical velocity ( $\times 10^{-5} \text{ m s}^{-1}$ ) from May to October in the west-central Bay of Bengal	91
4.13	Monthly mean sea level anomaly (cm) superimposed with geostrophic currents ( $\text{cm s}^{-1}$ ) in the west-central Bay depicting evolution of the cold core eddy and associated currents in the Bay of Bengal	92
5.1	Monthly mean of depth of $20^{\circ}\text{C}$ isotherm (m) in the Bay of Bengal	99-100
5.2	Annual mean of the $20^{\circ}\text{C}$ isotherm depth (m) in the Bay of Bengal ( <i>Boxed regions represent the four areas where further studies have been carried out</i> )	101

5.3	Monthly variations of depth of 20°C isotherm and Ekman vertical velocity indices for Box A (86-90°E, 18-21°N), Box B (84-88°E, 13-17°N), Box C (81-85°E, 7-11°N), and Box D (95-98°E, 7-11°N) in the Bay of Bengal	104
5.4	Monthly variations of depth of 20°C isotherm and sea level anomaly indices for Box A (86-90°E, 18-21°N), Box B (84-88°E, 13-17°N), Box C (81-85°E, 7-11°N), and Box D (95-98°E, 7-11°N) in the Bay of Bengal	108
5.5	Monthly variations of depth of 20°C isotherm and chl- <i>a</i> concentration indices for Box A (86-90°E, 18-21°N), Box B (84-88°E, 13-17°N), Box C (81-85°E, 7-11°N), and Box D (95-98°E, 7-11°N) in the Bay of Bengal	112
5.6	Monthly variations in surface chl- <i>a</i> concentration (mg m <sup>-3</sup> ) for Box A (86-90°E, 18-21°N), Box B (84-88°E, 13-17°N), Box C (81-85°E, 7-11°N), Box D (95-98°E, 7-11°N) and Bay of Bengal (75-100°E, 5-23°N)	117
5.7	Monthly variations of surface chl- <i>a</i> concentration and vertical velocity indices for Box A (86-90°E, 18-21°N), Box B (84-88°E, 13-17°N), Box C (81-85°E, 7-11°N) and Box D (95-98°E, 7-11°N) in the Bay of Bengal	119
5.8	Monthly variations of surface chl- <i>a</i> concentration and SLA indices for Box A (86-90°E, 18-21°N), Box B (84-88°E, 13-17°N), Box C (81-85°E, 7-11°N) and Box D (95-98°E, 7-11°N) in the Bay of Bengal	122
6.1	Track of tropical cyclone 03B during 26 Nov – 6 Dec 2000 (from Rao <i>et al.</i> , 2006)	131
6.2	Terra MODIS weekly sea surface temperature in °C: (a) 16-23 Nov before the cyclone; (b) 24 Nov-1 Dec during the cyclone; (c) 2-9 Dec; and (d) 10-17 Dec 2000 after the passage of cyclone	132
6.3	Ten day composite of sea surface height from altimeter data during: (a) 11-20 Nov and (b) 23 Nov-2 Dec 2000	133
6.4	Merged daily sea level anomaly during (a) 27 Nov 2000 before, and (b) 2 Dec 2000 after the passage of cyclone showing the decrease in sea level	134
6.5	Terra MODIS weekly chl- <i>a</i> concentration: (a) 16-23 Nov, prior to the cyclone formation; (b) 24 Nov-1 Dec during the cyclone; (c) 2-9 Dec; and (d) 10-17 Dec 2000, after the passage of cyclone showing the increase in chl- <i>a</i> concentration	135
6.6	MODIS weekly primary production: (a) before the cyclone (16-23 Nov); (b) during the cyclone (24 Nov-1 Dec); (c) 2-9 Dec; and (d) 10-17 Dec 2000 after the passage of cyclone showing the increase in production	136
6.7	Track of the tropical cyclone 01B during 11-19 May 2003 in the Bay of Bengal (Figure is taken from Smitha <i>et al.</i> , 2006)	138
6.8	Sea surface temperature in °C observed from Terra MODIS: (a) prior to the cyclone formation (1-8 May); (b) during the cyclone (9-16 May); (c) during 17-24 May; and (d) 25 May-1 Jun 2003 after the passage of cyclone	139
6.9	Weekly averaged TMI data showing sea surface temperature in °C: (a) before the cyclone (4-10 May); (b) during the cyclone when cooling	140

- occurs (11-17 May); (c) during 18-24 May; and (d) 25-31 May 2003, after the passage of cyclone
- 6.10 Modeled weekly mixed layer depth (m) in the Bay of Bengal during different stages of cyclone: (a) prior to the cyclone formation (1-8 May); (b) during the cyclone (9-16 May); (c) during 17-24 May; and (d) 25 May-1 Jun 2003 after the passage of cyclone 142
- 6.11 Weekly chl-*a* concentration in mg m<sup>-3</sup> observed from Terra MODIS during different stages of cyclone showing the increase in chl-*a* concentration in the cyclone affected area: (a) prior to the cyclone formation (1-8 May); (b) during the cyclone (9-16 May); (c) during 17-24 May; and (d) 25 May-1 Jun 2003 after the passage of cyclone 143
- 6.12 Difference images of (a) sea surface temperature in °C and (b) chl-*a* concentration in mg m<sup>-3</sup> from Terra MODIS depicting the changes occurred after the passage of cyclone in May 2003 144
- 6.13 Weekly mixed layer primary production during various stages of the cyclone: (a) prior to the formation of cyclone (1-8 May); (b) during the cyclone (9-16 May); (c) during 17-24 May; and (d) 25 May-1 Jun 2003, after the passage of cyclone showing the increase in production in the cyclone affected area 145

## List of Tables

5.1	Linear correlation coefficient of monthly mean D20 with surface chlorophyll- <i>a</i> concentration, sea level anomaly and vertical velocity	115
6.1	Tropical cyclones in the Bay of Bengal during 2000 to 2007. The categories of tropical cyclone with the maximum wind speed in brackets are given. CS - Cyclonic Storm (34-47 kts), SCS - Severe Cyclonic Storm (48-63) and VSCS - Very Severe Cyclonic Storm (64-119 kts)	129

## Glossary

ADEOS-II	Advanced Earth Observing Satellite-II
ASTER	Advanced Spaceborne Thermal Emission and Reflection Radiometer
AVHRR	Advanced Very High Resolution Radiometer
AVISO	Archiving, Validation and Interpretation of Satellite Oceanographic data
BoB	Bay of Bengal
$C_D$	Drag coefficient.
CDOM	Colored dissolved organic material
CERES	Clouds and Earth's Radiant Energy System
CERSAT	Centre de Recherche et d'Exploitation Satellitaire
Chl- <i>a</i>	Chlorophyll- <i>a</i>
COBE	Centennial <i>in-situ</i> Observation Based Estimates
CS	Cyclonic Storm
CZCS	Coastal Zone Colour Scanner
D20	Depth of the 20°C isotherm
DUACS	Data Unification and Altimeter Combination System
EACC	East African Coastal Current
EC	Equatorial Current
EICC	East India Coast Current
EOF	Empirical Orthogonal Function
ERS	European remote sensing satellite
FNMOCC	Fleet Numerical Meteorology and Oceanography Center
GAC	Global area coverage
GDAAC	NASA (GSFC) Distributive Active Archive Center
GSFC	Goddard Space Flight Center
GW	Great Whirl

IRS	Indian Remote Sensing Satellite
ITCZ	Inter Tropical Convergence Zone
JPL	Jet Propulsion Laboratory
LAC	Local area coverage
LH	Lakshadweep high
LIS	Lightning Imaging Sensor
LL	Lakshadweep low
M-AERI	Marine-Atmospheric Emitted Radiance Interferometer
$M_e$	Ekman mass transport
MISR	Multi-angle Imaging Spectroradiometer
MLD	Mixed layer depth
MOPITT	Measurements of Pollution in the Troposphere
NASA	National Aeronautical and Space Administration
NASDA	National Space Development Agency
NEM	Northeast Monsoon
NIO	North Indian Ocean
NOAA	National Oceanic and Atmospheric Administration
NSCAT	NASA scatterometer
OC4	Ocean Chlorophyll-4
OCM	Ocean Colour Monitor
OCTS	Ocean Color and Temperature Scanner
ONPP	Ocean Net Primary Production
OPP	Ocean primary productivity
OTIS/TOPS	Optimum Thermal Interpolation System / Thermodynamic Ocean Prediction System
PAR	Photosynthetically Available Radiation
PC	Principal component
PCA	Principal Component Analysis

PO.DAAC	Physical Oceanography Distributed Active Archive Center
PP	Primary production
PR	Precipitation Radar
RMS	Root Mean Square
RSS	Remote Sensing Systems
SC	Somali Current
SCS	Severe Cyclonic Storm
SeaWiFS	Sea-viewing Wide Field of view Sensor
SEC	South Equatorial Current
SECC	South Equatorial Counter Current
SLA	Sea level anomaly
SMC	Summer Monsoon Current
SSALTO	Ssalto multimission ground segment
SSH	Sea surface height
SST	Sea surface temperature
SVD	Singular value decomposition
SWM	Southwest Monsoon
TMI	TRMM Microwave Imager
TRMM	Tropical Rainfall Measuring Mission
$U_{10}$	Wind speed at 10 m
VGPM	Vertically Generalized Productivity Model
VIR	Visible and Infrared
VIRS	Visible and Infrared Scanner
VSCS	Very Severe Cyclonic Storm
VV	Ekman vertical velocity/pumping velocity
WICC	West India Coastal Current
WMC	Winter Monsoon Current
WOA	World Ocean Atlas

WOD	World Ocean Data
WSC	Wind stress curl
$f$	Coriolis force
$w_e$	Ekman pumping velocity
$\rho$	Density of air ( $1.225 \text{ kg m}^{-3}$ )
$\rho_o$	Density of sea water ( $1027 \text{ kg m}^{-3}$ )
$\sigma_o$	Normalized radar cross section
$\tau$	Wind stress
$\tau_x$ and $\tau_y$	x and y component of the wind stress
$\Omega$	Angular speed of the earth ( $7.292 \times 10^{-5} \text{ rad s}^{-1}$ )
$\phi$	Latitude

# Chapter 1

## Introduction

All the coastal nations of the world depend on oceans for fishing, oil and gas, minerals, rare earth metals, renewable energy and other living and non-living resources for their economic development. The Indian subcontinent has been blessed with enormous natural resources - both continental and marine - which have been determining our course of development over the last many centuries. Amongst these, a large portion of marine resources is believed to be unexplored or untapped in different regions. Sustainable development of natural resources of the ocean is imperative for high economic growth and development of the country. With a coastline of over 8000 km involving 9 maritime states and two island territories and an exclusive economic zone of about 2 million km<sup>2</sup>, the Indian marine fisheries sector alone contributes 1% to the country's GDP with a gross value of about 7 billion US\$. Detailed studies of the physical, chemical and biological properties of the Indian Ocean would be helpful to determine the future course of action towards development of the nation. In this regard, the present investigation is a small but definitive step in the study of some of the characteristics of the Bay of Bengal.

The North Indian Ocean is highly dynamic because of the seasonal reversal of the wind patterns associated with the Indian monsoons. The Indian subcontinent divides it into two basins, the Arabian Sea and the Bay of Bengal having distinct oceanographic features. The Bay of Bengal is a tropical basin, lying south of 22°N and its maximum zonal extent is about 1600 km with the eastern boundary intersecting the equator. It is a highly stratified basin that undergoes seasonal reversal of monsoon winds and ocean currents and is less productive compared to the Arabian Sea. It is one of the large marine ecosystems in the world ocean. The upper ocean physical processes have a large influence on its biological productivity. Oceanic eddies and fronts, surface currents, turbulence and vertical mixing and upwelling are

some of the factors that play major roles in influencing the upper ocean dynamics. Surface winds play a dominant role in the modification of ocean surface and drive the upper ocean circulation. Strong wind stress and wind stress curl cause coastal and open ocean upwelling under favourable conditions. It is established that most of the fishing grounds of the world oceans are located in the regions where upwelling occur. Coastal and open ocean upwelling can bring nutrients to the ocean surface thus increasing the productivity of the ocean which in turn influences the marine fisheries. Marine fishery resources are a significant component of the food security of countries and a major source of income for the people of coastal regions of the world. Changes in upwelling can result in large and significant changes in the chlorophyll biomass and productivity. Chlorophyll-*a* is the most important pigment involved in phytoplankton photosynthesis, and its concentration is used as a measure of phytoplankton biomass. For this reason, the variability in the surface chlorophyll-*a* concentration is a precursor to the changes in the primary production affecting the fisheries. Being a low productive basin with high surface stratification, understanding of the influence of wind forcing on upwelling and its effect on surface chlorophyll distribution in the Bay of Bengal is important.

## **1.1. Wind forcing on the ocean surface**

### **1.1.1. Wind**

Stull (1994) defined *the atmospheric boundary layer as the part of the troposphere that is directly influenced by the presence of the earth's surface, and responds to surface forcings with a time scale of about an hour or less*. The boundary layer thickness varies from hundreds of meters to few kilometers depending on space and time. The lowest part of the atmospheric boundary layer is the surface boundary layer which is influenced by the turbulent drag of the wind on the sea surface. Wind speed varies with height in the surface boundary layer, and hence the wind speed usually referred to is the winds at 10 m height. Surface winds influence the sea surface roughness, waves and the current systems. The wind driven circulation occurs mainly in the upper few hundreds meters and therefore is primarily a

horizontal circulation in contrast to the thermohaline circulation (Pickard and Emery, 1990). Wind is the largest source of momentum for the ocean surface. It is an important parameter in the determination of latent and sensible heat flux across ocean-atmosphere interface, momentum flux and wind stress in the ocean surface.

### 1.1.2. Wind stress

The horizontal force of the wind or the shear stress exerted by the wind on the sea surface is called the wind stress. Winds, through turbulent transfer of momentum across the atmospheric boundary layer, exert a stress on the ocean's surface which drives ocean currents (Marshall and Plumb, 2013). Stress is approximately constant with height near the surface.

Wind stress  $\tau$  (unit -  $\text{N m}^{-2}$ ) given by the bulk formulation method is,

$$\tau = \rho C_D U_{10}^2 \quad \text{-----(1.1)}$$

where  $\rho = 1.225 \text{ kg m}^{-3}$  is the density of air,  $U_{10}$  is wind speed at 10 m, and  $C_D$  is the drag coefficient.

For a neutrally stable boundary layer the drag coefficient is given by Large and Pond (1981) as,

$$C_D = 1.2 \times 10^{-3} \quad \text{for } 4 < U_{10} < 11 \text{ m s}^{-1} \quad \text{-----(1.2)}$$

$$C_D = 10^{-3} (0.49 + 0.065 U_{10}) \quad \text{for } 11 < U_{10} < 25 \text{ m s}^{-1} \quad \text{-----(1.3)}$$

Surface wind stress exerts a strong influence on the typical variation of wind through the lowest kilometer of the atmosphere (Sanders and Charnock, 2014). Turbulent, wind stirred motions confined to the near-surface layers of the ocean carry the wind stress downward. The layer affected by the surface wind stress is called the Ekman layer.

### 1.1.3. Wind stress curl

Wind stress curl (WSC) is a fundamental quantity that influences the wind driven ocean circulation. The curl of a field of vectors is a vector which measures the tendency of the vectors to induce rotation. WSC gives an idea about the strength of the rotation of the wind. WSC is calculated as the vertical component of the curl of wind stress  $\tau$ .

WSC is given by,

$$\text{curl}(\tau) = \frac{\partial \tau_y}{\partial x} - \frac{\partial \tau_x}{\partial y} \text{-----} (1.4)$$

where  $\tau_x$  and  $\tau_y$  are the x and y component of the wind stress. The unit of WSC is  $\text{N m}^{-3}$ .

WSC is an important factor in the vorticity budget of the upper ocean. It is the primary source of relative vorticity in the wind driven general circulation theories (Milliff and Morzel, 2001). WSC influences the upper ocean circulation of mesoscale and basin scale dimension. If the winds are cyclonic in the northern hemisphere then the WSC is positive. Positive WSC causes divergence in the Ekman layer and upward Ekman pumping leading to upwelling whereas negative WSC causes convergence in the Ekman layer and downward Ekman pumping leading to downwelling. The surface WSC is the forcing function in the equations of the vertically integrated water transport of the wind driven ocean currents (Hantel, 1970).

## 1.2. The Ekman layer

Steady winds blowing over the ocean surface create a thin boundary layer known as Ekman layer where the wind stress is communicated downward by turbulent, wind-stirred motions. In the absence of friction, pressure gradient force is balanced by the Coriolis force resulting in the geostrophic flow. On the ocean surface, frictional

coupling between the wind and water causes the water to move in the direction of wind. In the northern hemisphere, Coriolis force acts to the right of the direction of motion which makes the flow at the ocean surface to turn to the right of the wind. The balance of forces involves frictional force, which causes a departure from geostrophic flow and water moves across isobars from high pressure to low pressure areas (Fig. 1.1). Thus the flow in the Ekman layer is non-geostrophic.

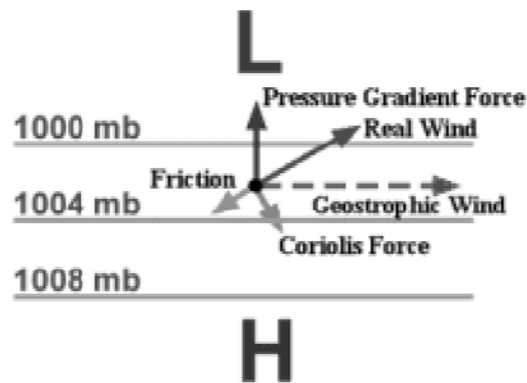


Fig. 1.1 The balance between pressure gradient force, Coriolis force and friction (Figure is taken from [http://ww2010.atmos.uiuc.edu/\(Gh\)/guides/mtr/fw/fric.rxml](http://ww2010.atmos.uiuc.edu/(Gh)/guides/mtr/fw/fric.rxml))

Stress exerted by the surface winds has the maximum effect at the ocean surface. The lower layers of the ocean move by the friction between the layers of water above. Consequently, the lower layer moves slower than the layer above and further turn to the right due to Coriolis force. The direct influence of wind forcing decreases gradually down the water column and stress reduces to zero at a depth called the Ekman layer depth which is about 100-150 m. Thus, an Ekman spiral is formed which rotates to the right and decays with depth in the Northern Hemisphere (Fig. 1.2). The Ekman spiral was first described mathematically by V Walfrid Ekman (Ekman, 1905) after whom it is named.

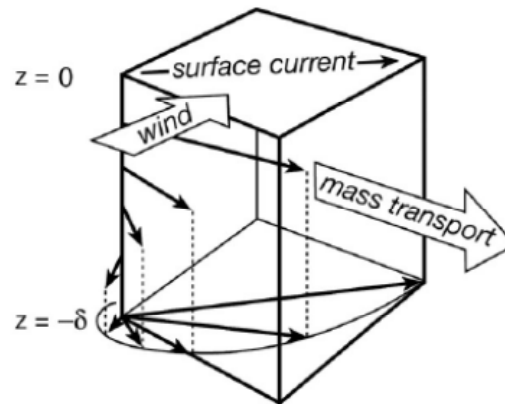


Fig. 1.2 Ekman spiral in the northern hemisphere where the mass transport is directed to the right of the wind (Marshall and Plumb, 2013)

Ekman layer depth is the depth at which the current velocity is opposite to the velocity at the surface and is about 4% of the surface current. The angle between the wind and the flow at the surface depends on latitude, and is near  $45^\circ$  at mid latitudes. Ekman mass transport is the net transport integrated over depth, and is at  $90^\circ$  to the right of the wind in the northern hemisphere and to the left in the southern hemisphere (Fig. 1.2).

The magnitude of Ekman mass transport  $M_e$  is given by,

$$|M_e| = |\tau/f| \quad \text{-----} \quad (1.5)$$

where  $\tau$  is the wind stress,  $f = 2 \Omega \sin(\phi)$  is the Coriolis force,  $\Omega$  is the angular speed of the earth ( $7.292 \times 10^{-5} \text{ rad s}^{-1}$ ),  $\phi$  is a latitude on the earth's surface, and the unit of  $M_e$  is  $\text{kg m}^{-1} \text{ s}^{-1}$  (Smith, 1968).

### 1.3. Ekman pumping

The horizontal variations in surface wind stress can result in horizontal variations in Ekman transport. This causes convergence or divergence in Ekman transport and vertical flow develops at the base of the Ekman layer to conserve the water mass. This process is known as Ekman pumping which results in a vertical upwelling or

downwelling velocity called Ekman vertical velocity or Ekman pumping velocity (hereafter VV).

The Ekman pumping velocity in  $\text{m s}^{-1}$  is given by Smith (1968) as,

$$w_e = \frac{1}{\rho_0} \left( \frac{\partial}{\partial x} \frac{\tau_y}{f} - \frac{\partial}{\partial y} \frac{\tau_x}{f} \right) \text{-----} (1.6)$$

$$i.e. \quad w_e = \hat{k} \cdot \nabla \times \frac{\tau}{\rho_0 f} \text{-----} (1.7)$$

where  $\hat{k}$  is a unit vector in the  $z$  direction,  $\tau_x$  and  $\tau_y$  are the wind stress components in  $\text{N m}^{-2}$ ,  $\rho_0 = 1027 \text{ kg m}^{-3}$  is the density of sea water,  $f = 2 \Omega \sin(\phi)$  is the Coriolis force,  $\Omega$  is the angular speed of the earth ( $7.292 \times 10^{-5} \text{ rad s}^{-1}$ ) and  $\phi$  is a latitude on the earth's surface.

VV is proportional to the horizontal gradient of the wind stress. According to Marshall and Plumb (2013), the flow within the Ekman layer is convergent in anticyclonic flow (negative WSC) and divergent in cyclonic flow (positive WSC). Convergence in the Ekman layer drives downward vertical motion and  $w_e$  is negative while divergence drives upward vertical motion and  $w_e$  is positive in the ocean surface. In the open ocean this convergence or divergence of water by Ekman transport leads to downwelling and upwelling respectively. Redistribution of water takes place to conserve the mass in the ocean and in the case of planetary scale flows, it leads to wind driven geostrophic currents. It is the convergence and divergence of Ekman transport induced by large scale wind patterns and the resulting flow that set up the large scale ocean gyres (Marshall and Plumb, 2013). Also steady winds blowing along the coastal regions on the sea surface produce an Ekman layer which causes a net transport of water at right angles to the wind direction which lead to coastal upwelling.

#### 1.4. Importance of upwelling

Upwelling is a process where the cooler subsurface waters from depths between 100 and 300 m move up towards the surface of the ocean, lower the sea surface temperature (SST) and affect the biological productivity of the ocean which in turn supports fisheries. Upwelling is important in ocean productivity as it brings the subsurface nutrient rich waters to the oligotrophic surface waters which enhance phytoplankton biomass and the surface chlorophyll concentration. Upwelling also affects the current pattern and the local weather of the region. The reverse process of surface waters sinking to subsurface depths is called downwelling. In the upwelling process, winds blowing across the ocean surface push the water away and subsurface water rise to replace the water that was pushed away. Surface wind cause divergence and convergence of surface water under favorable conditions leading to upwelling and downwelling respectively. Changes in upwelling can lead to considerable change in the productivity of the ocean. Upwelling regions which form only 0.1% of the oceanic water has high fish productivity compared to the extremely low fish productivity of the open ocean which constitute about 90% of the oceanic waters (Ryther, 1969). While open ocean produces 0.7% of the total fish production and coastal zone which makes up the 9.9% of the oceanic waters produces 54% of the fish, the upwelling regions produce 44% of the total fish production (Crisp, 1975). The enhanced primary production (PP) in the upwelling regions lead to an increase in secondary production of zooplankton and eventually fisheries thus contributing to the marine food web. Sachoemar *et al.* (2010) observed that high surface chlorophyll-*a* (chl-*a*) concentration occurred during the monsoon seasons in the Lampung Bay, Indonesia and during this time the abundance of pelagic fish was very high within this region.

The PP is high in upwelling regions as it depends on the availability of nutrients and sunlight. West coast of continents, equatorial Atlantic and Pacific during La Nina and western Indian Ocean are regions where nutrients are brought to the surface by wind mixing or upwelling (Martin, 2004). Generally, coastal upwelling occurs along

the western coasts of the continents. Some exceptions are along the northeastern African coast, Somali coast, east coast of Arabia and to some extent in the east coast of India (Madhu *et al.*, 2002). In the North Indian Ocean (NIO), upwelling off the coasts of Somalia and Arabia is strong. Lateral advection carries the nutrient-rich upwelled water from the coasts of Somalia and Arabia to the central Arabian Sea and increases the biological productivity in that region (Prasanna Kumar *et al.*, 2001). However, upwelling observed off the west and east coasts of India are relatively weak. In the NIO, the Bay of Bengal (hereafter BoB) is a less productive basin compared to the Arabian Sea (Prasanna Kumar *et al.*, 2002; Gomes *et al.*, 2000; Madhupratap *et al.*, 2003). Upwelling occurs in varying intensities along the west and east coast of India during the southwest monsoon (SWM). Upwelling has been reported at a few positions along the east coast of India during the SWM season (Lafond, 1957; Murty and Varadachary, 1968; Rao and Chamarthi, 1997).

Upwelling systems can be classified into two major categories based on the driving forces as wind driven and dynamic. Wind driven upwelling results from the divergence in the Ekman layer of the ocean by the wind stress acting on the ocean surface. Dynamic upwelling occurs when the flow of ocean currents causes surface water to diverge in the open ocean. Where adjacent ocean surface waters flow away from each other, deeper water rises to replace them (Conway and The Maryland Space Grant Consortium, 1997). Upwelling/downwelling process is divided into three categories based on the region of occurrence: (i) Coastal upwelling, (ii) Equatorial upwelling and (iii) Offshore or open ocean upwelling.

#### **1.4.1. Coastal upwelling**

Coastal upwelling is a near shore phenomenon in which subsurface water from depths is brought to the sea surface. When a spatially uniform along-shore wind stress acts on the sea surface with the coast to its left in the northern hemisphere, an Ekman mass transport develops which carries the water to the right of the wind direction. The surface water gets diverged, moves offshore and cooler subsurface

water rise to the surface near the coast (Fig. 1.3a). This process is called coastal upwelling.

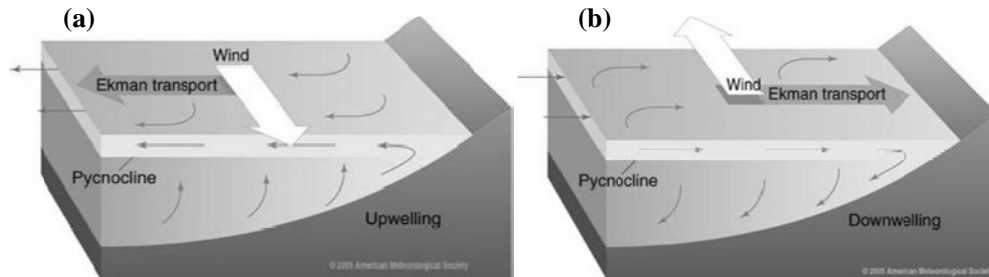


Fig. 1.3 Coastal Upwelling and downwelling when the wind blows parallel to the coast in the northern hemisphere with a) the coast to the left and the Ekman transport away from the coast causing upwelling, and b) the coast to the right and the Ekman transport towards the coast which cause downwelling (figure is taken from <http://oceanmotion.org/html/background/upwelling-and-downwelling.htm>).

But downwelling takes place if the wind blows in the opposite direction, i.e. when the coast is to the right of the wind in the northern hemisphere (Fig. 1.3b). In the Southern Hemisphere, coastal upwelling occurs when the wind blows with the coast on its right. For a steady and uniform wind blowing on the surface of a uniform and homogeneous ocean of infinite extent, Ekman (1905) showed that there exists a net transport of water in the surface layer due to the effect of the earth's rotation and frictional forces. According to Hidaka (1958), the most intense upwelling occurs when the wind makes an angle of  $21.5^\circ$  with the coastline in an offshore direction.

Coastal upwelling is common along the eastern boundaries of the oceans (Rao *et al.*, 2005; Rao *et al.*, 2008) and it exists also along the western boundaries of the oceans like BoB (Rao *et al.*, 1986). Coastal upwelling is closely related to human activities as it supports some of the most productive fisheries in the world.

#### 1.4.2. Equatorial upwelling

Large scale equatorial upwelling takes place along the equator due to the divergence in the Ekman layers. At the equator, the Coriolis parameter is zero but starts acting away from the equator. Hence, the westward flowing wind driven surface currents

near the equator turn northward on the north side of the equator and southward on the south side due to the Ekman transport (<http://oceanmotion.org/html/background/upwelling-and-downwelling.htm>). This results in the movement of surface water away from the equator and upwelling occurs along the equator to conserve the mass. This is called Equatorial upwelling. Easterly winds blowing along the Inter Tropical Convergence Zone (ITCZ) in both the Pacific and Atlantic Basins drive water to the right (northwards) of the wind in the Northern Hemisphere and to the left (southwards) in the Southern Hemisphere. This results in a divergence in the Ekman layer by which the cooler nutrient-rich water gets upwelled from below. Equatorial upwelling causes high chlorophyll concentration along the equator. In the tropical Indian Ocean, equatorial upwelling is not prominent compared to other two basins.

### 1.4.3. Open ocean upwelling

Away from the equator the Coriolis force becomes important, and the offshore water gets deflected to the right in the Northern Hemisphere and to the left in the Southern Hemisphere. The WSC can be regarded as a forcing function for oceanic motion. Positive WSC is favorable to upwelling in the Northern Hemisphere and downwelling in the Southern Hemisphere. Negative WSC is favorable to upwelling in the Southern Hemisphere and downwelling in the Northern Hemisphere (Rao and Shree Ram, 2005). WSC rotate surface water either in the cyclonic (anti-clock wise), or in the anti-cyclonic (clockwise) circulation (Hastenrath and Lamb, 1979). Upwelling and downwelling occur in the open ocean where surface winds cause ocean surface waters to diverge from a region leading to upwelling or converge toward some region causing downwelling (<http://oceanmotion.org/html/background/upwelling-and-downwelling.htm>). The open ocean upwelling does not have bottom influence. It has weak lateral advection and extends longitudinally. Areas of open ocean upwelling have high biodiversity and occupy large areas (Angel *et al.*, 1995).

### 1.5. Chlorophyll in the upper ocean

Phytoplankton are microscopic plants that are the principal photosynthetic organisms in the ocean and form the base of ocean food webs (Falkowski and Raven, 1997). Phytoplankton use photosynthesis to fix inorganic carbon into organic forms of carbon such as carbohydrates (Martin, 2004). Since phytoplankton can fix inorganic carbon and convert solar to chemical energy, phytoplankton contributes to the global carbon cycle. Their rate of growth and of carbon fixation is called PP (Martin, 2004). It can be also defined as the total chemical energy contained within an ecosystem as a direct result of photosynthesis (Bukata, 2005). Ocean primary productivity (OPP), defined as the sum of all photosynthetic rates within an ecosystem (Bukata, 2005) or the rate of carbon fixation as a direct result of photosynthesis in  $\text{mg C m}^{-2} \text{d}^{-1}$  plays an essential role in the global carbon cycle.

Photosynthetic pigments present in phytoplankton cell are chl-*a*, the accessory pigments chlorophyll-*b* and *c*, and the photosynthetic carotenoids (Martin, 2004). Chl-*a* concentration provides a measure of phytoplankton abundance and biomass as it is the only photosynthetic pigment present in all phytoplankton (Yoder and Kennelly, 2003). So Chl-*a* concentration has been used as a proxy for phytoplankton biomass (e.g. Ryther and Yentsch, 1957). The annual production of oceanic chlorophyll is about  $10^{12}$  kg (Jeffrey and Mantoura, 1997). According to Behrenfeld *et al.* (2001), phytoplankton in ocean are accountable for approximately half of the global biospheric net PP. Gregg *et al.* (2003a) point out that long term changes in ocean PP can affect the global carbon cycle. Many factors affect the growth of phytoplankton and hence they are a good indicator of change in their environment. Study of the variation in Chl-*a* concentration is important since the changes in ocean environment can affect growth and abundance of phytoplankton, which in turn influence the PP of the ocean and eventually fisheries.

## 1.6. Factors affecting surface chlorophyll concentration

Phytoplankton requires sunlight and nutrients for its growth and is present in the upper ocean layer known as euphotic zone (up to 50-100 m depth) where there is availability of sunlight to help in photosynthesis. In the tropical oceans where sunlight is abundant, availability of nutrients control the phytoplankton biomass of the upper layer. In warm stratified upper oceans, nutrients are used up by phytoplankton; hence the increase of phytoplankton depends on nutrient availability. Therefore, oceanic processes that bring nutrients into the euphotic zone influence the phytoplankton biomass and chlorophyll concentration in the upper ocean. According to Lin *et al.* (2003), nutrients can be brought to the surface by various processes that pump nutrient-rich deep water to the euphotic zone. Vinayachandran *et al.* (2004) listed coastal upwelling caused by alongshore winds, open ocean upwelling driven by Ekman pumping, entrainment due to wind stirring at the base of the mixed layer and horizontal advection due to ocean currents as the processes that bring nutrients to the surface of the ocean. Seasonal changes in the physical forcing influence these processes and in turn change the chlorophyll concentration at the surface depending on the latitude and regional characteristics.

Ocean phytoplankton biomass and thus chlorophyll concentration is highly variable in space and time (Yoder and Kennelly, 2003). Stratification, destratification and incident solar irradiance which vary with the season and latitude are some of the factors that influence the phytoplankton variability in the ocean (Longhurst, 1998; Gregg, 2001). Wind mixing in the tropics and subtropics can destratify the water column and bring nutrient-rich water to the sunlit ocean surface thus supporting the phytoplankton photosynthesis and growth (Yoder and Kennelly, 2003). During summer, strong stratification in these regions prevents the nutrients supply to upper layers which reduce photosynthetic rate and biomass (Yoder *et al.*, 1993). Warm ocean temperatures increase the mixed layer stratification, inhibiting the entrainment of nutrients from below to support ocean PP (Sarmiento *et al.*, 1998). According to Prasanna Kumar *et al.* (2002), apart from near-surface stratification caused by high SST and large freshwater influx, weak winds also inhibit the vertical mixing to a

shallow depth which prevent the upward transport of subsurface nutrients. The available nutrients in the surface layer is utilised in photosynthesis which makes the PP nutrient limited (Prasanna Kumar *et al.*, 2000). There exists an inverse relationship between temperature and nutrient concentration in the surface waters which vary seasonally depending upon the geographical locations except at higher latitudes (Kamykowski, 1987). Sathyendranath *et al.* (1991) has shown that the abundance of phytoplankton increase the absorption of radiation and influence seasonal evolution of SST. The nitrate transport into the open ocean by river inflow is significantly low as most of the nitrate is consumed biologically within the estuaries and coastal region (Prasanna Kumar *et al.*, 2002). Also the suspended sediments in the river inflow increases the turbidity of the water column and inhibits the light available for photosynthesis (Prasanna Kumar *et al.*, 2004).

Wind induced turbulence cause transport of nutrients into the euphotic zone and influence nutrient availability for the PP (Dwivedi *et al.*, 2004). Wind-stirring causes the vertically upward transport of nutrients from the upper thermocline into the euphotic zone by convective entrainment (Lee *et al.*, 2000). Vertical mixing by strong winds increases the mixed layer thickness and enrichment of nutrients in the upper layer, which in turn support high production (Prasanna Kumar *et al.*, 2000). Also seasonal cooling of surface waters and the cooling due to evaporation by strong winds generates convection which causes vertical mixing of water mass (Dwivedi *et al.*, 2004). Upwelling can bring nutrients to the ocean surface thus increasing the productivity of the ocean (Prasanna Kumar *et al.*, 2002). Nutrients could be brought to the surface by cyclones or high speed winds, in varying amounts that depends on location, intensity and residence time (Kumar *et al.*, 2004). Tropical cyclones can change the oligotrophic (nutrient depleted) condition of an ocean surface into a productive region by the associated intense wind stirring and surface divergence (Subrahmanyam *et al.*, 2002). Prasanna Kumar *et al.* (2004) proposed eddy pumping as a possible mechanism of vertical transfer of nutrients across the halocline to the oligotrophic euphotic zone during summer monsoon when the upper ocean is highly stratified. Upwelling in the cold core eddies bring nutrients to the surface layer,

which cause an increase in chlorophyll concentration and PP. When compared to the coastal upwelling driven by winds, upwelling associated with cold core eddies might start from greater depths (Ning *et al.*, 2004).

### **1.7. Eddies in the ocean**

Oceanic eddies are circulating water bodies and they are generally formed either by separation of a meander or due to the force exerted by the WSC (Madhusoodanan and James, 2003). It is a mesoscale feature of 10-100 km width and can last for weeks to months. In highly stratified waters, enhancement of biomass and PP occurs episodically when mesoscale physical phenomena increase the concentration of nutrients in the euphotic zone (Ning *et al.*, 2004). There are cold core eddies and warm core eddies in the ocean. Cold core eddies in the northern hemisphere rotate anti-clockwise causing the water to get diverged from the center which is replaced by cooler deep water. Thus a cyclonic eddy has raised thermocline, low SST and low sea level at the centre compared to the surrounding water. A cyclonic eddy occurs when the negative sea level anomaly (SLA) becomes less than 10 cm (Vinayachandran, 2009). Upwelling in the cold core eddy brings nutrients to the upper water column, which in turn increases the chl-*a* concentration and PP. Unlike the coastal upwelling due to winds, upwelling associated with cold eddies might start from greater depths (Ning *et al.*, 2004). When the nutricline and thermocline are coincident, enhanced phytoplankton production is expected in cyclonic eddies (Williams and Follows, 2003). Warm core eddies rotate clockwise and water converges at the center of the eddy in the northern hemisphere. These anti-cyclonic eddies have depressed thermocline, high SST and raised sea level at the center of the eddy compared to the surrounding water.

### **1.8. Bay of Bengal - the study area and its characteristics**

The BoB is a tropical basin of intense atmosphere-ocean interaction, experiences monsoon depressions and tropical cyclones, and receives large volume of fresh water from both river run-off and rainfall. The BoB is located at 5°- 22°N and 80°-100°E,

and bordered by Sri Lanka, India, Bangladesh and Myanmar (Fig. 1.4). On the west, the Bay is bounded by east coast of India and Sri Lanka, on the north by the deltaic region of the Ganges-Brahmaputra-Meghna river system, and on the east by the Myanmar peninsula extending up to the Andaman-Nicobar ridges. The Andaman and Nicobar Islands, separate it from the Andaman Sea to the southeast. The southern boundary of the Bay is approximately along the line drawn from Dondra Head in the south of Sri Lanka to the northern tip of Sumatra (Guo, 2006).

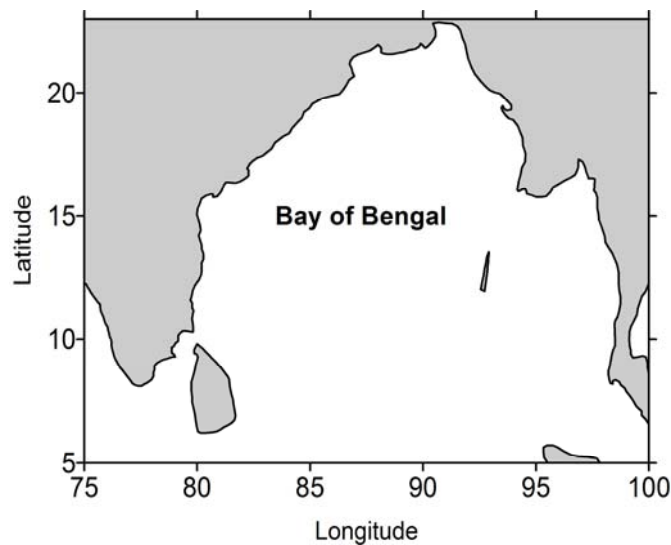


Fig. 1.4 Bay of Bengal - study area

### 1.8.1. Winds

The BoB comes under the influence of seasonally reversing winds associated with the Indian monsoon, i.e. SWM or summer monsoon (Jun-Sep) and Northeast monsoon (NEM) or winter monsoon (Nov-Feb). In the NIO, winds generally blow from the southwest during summer monsoon and are much stronger compared to the winds that blow from northeast during winter monsoon. Southwesterlies have an average wind speed of  $15 \text{ m s}^{-1}$  (Bauer *et al.*, 1991) and the northeasterlies are strongest in December, with an average speed of about  $5 \text{ m s}^{-1}$ . (Hastenrath and Lamb, 1979). Mar-Apr and October are months of transition between the monsoons and during this time winds are weakest (Shetye and Gouveia, 1998). These seasonally reversing

monsoon winds over the NIO force a seasonally reversing circulation in the upper ocean. The eastern boundary intersects the equator and because of the proximity to the equator the region can support rapidly propagating tropical planetary waves, and the seasonal winds are the mechanism for generating such low-frequency waves (Shetye *et al.*, 1996).

### 1.8.2. Circulation

Fig. 1.5 is a schematic representation of the large-scale circulation during January and July respectively in the NIO. The major seasonally reversing currents are the Somali Current (SC), which flows poleward (equatorward) along the coast of Somalia during the summer (winter) monsoon (Shetye and Gouveia, 1998; Schott and McCreary, 2001; Shankar *et al.*, 2002) and the current along the equator called Equatorial Current (EC), where eastward surface flow is observed during the transition periods between NEM and SWM during Apr–May and Oct–Nov (Shankar *et al.*, 2002; Schott and McCreary, 2001). The coastal circulations near Indian coast are East India Coastal Current (EICC) along the east coast of India (Shetye and Gouveia, 1998; Schott and McCreary, 2001; Vinayachandran *et al.*, 1996) and the West India Coastal Current (WICC) along the west coast of India. EICC is northeastward from February to September with the northward flow strong during Mar–Apr and southwestward from October to January with the strongest flow in November (McCreary *et al.*, 1996; Shankar *et al.*, 1996; Shetye *et al.*, 1996). The WICC flows southward from March to October with the peak strength in July and flows northward during the winter monsoon and is most developed during January (Schott and McCreary, 2001; Shenoi *et al.*, 2005).

The large scale seasonally reversing monsoon currents are also significant in the NIO and these currents transfer water masses between Arabian Sea and BoB. During winter, the Winter Monsoon Current (WMC) flows westward from the eastern BoB to the western Arabian Sea (Shankar *et al.*, 2002). During summer monsoon, the Summer Monsoon Current (SMC) flows eastward as a continuous current from the

western Arabian Sea to the BoB, replacing the westward WMC (Shankar *et al.*, 2002).

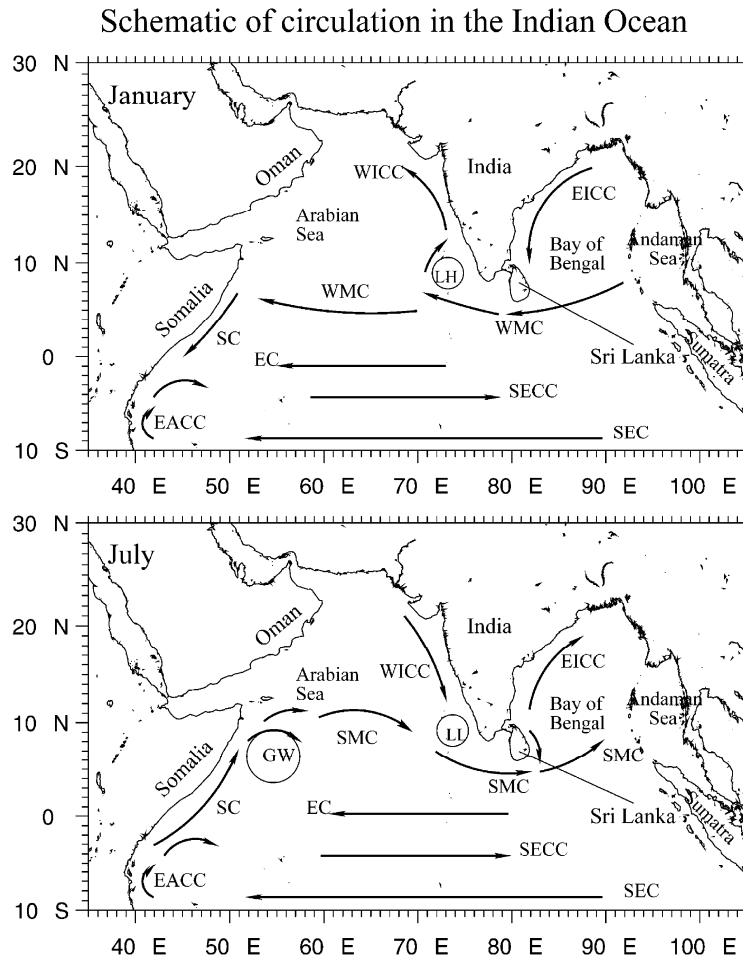


Fig. 1.5 Schematic representation of the circulation in the Indian Ocean during January and July. The abbreviations are as follows - SMC-Summer Monsoon Current; WMC-Winter Monsoon Current; EICC-East India Coastal Current; WICC-West India Coastal Current; SC-Somali Current; EC-Equatorial Current; SECC-South Equatorial Counter Current; EACC-East African Coastal Current; SEC-South Equatorial Current; LH-Lakshadweep high; LL-Lakshadweep low; and GW-Great Whirl. (The figure is taken from Shankar *et al.*, 2002)

During the pre-monsoon months (Mar-May) there is a well developed anticyclonic gyre in the Bay with a poleward EICC (Shetye *et al.*, 1993). The EICC flows equatorward all along the coast in Nov-Dec (Shetye *et al.*, 1996). During the summer

monsoon (Jun-Sep) the EICC flows poleward along the southern part of the Indian coast and equatorward farther north (Shetye *et al.*, 1991).

### 1.8.3. Kelvin waves and Rossby waves

Planetary waves such as Rossby waves and Kelvin waves can propagate over large distances and affect the ocean circulation in remote regions far from their origin. Coastal Kelvin Waves balance the Coriolis force against a topographic boundary such as shoreline. They always propagate with the shoreline on the right in the northern and on the left in the southern hemisphere. Equatorial Kelvin waves balance the Coriolis force in the northern hemisphere against its southern hemisphere counterpart. Thus, equatorial Kelvin waves are only possible for eastward motion. Oceanic Rossby waves move along the thermocline, and have low amplitude of the order of centimetres (at the surface) to meters (at the thermocline) when compared to its long wavelength. The zonal phase speed of Rossby waves is always westward and they may take months to cross an ocean basin.

Potemra *et al.* (1991) highlighted the role of these planetary waves in setting up of the seasonal circulation in the BoB. They showed that coastal Kelvin waves propagate along the entire perimeter of the BoB and these waves excite westward propagating Rossby waves into the interior of the Bay. The prominent feature of the annual cycle in the Bay are an anticyclonic gyre with a poleward EICC during Feb-May and an equatorward EICC during Oct-Dec. During the summer monsoon, the coastal current flow poleward in the south and equatorward in the north. Vinayachandran *et al.* (1996) used a general circulation model to suggest that this circulation can be linked to two coastal Kelvin wave pulses that originate along the eastern boundary of the Bay during the summer and winter monsoons. These two pulses contribute towards the circulation in the Bay by radiating Rossby waves. McCreary *et al.* (1993) further showed that the winds along the eastern rim of the BoB also trigger Kelvin waves, which not only influence the EICC, but also turn around the Sri Lanka to propagate poleward along the west coast of India, influencing the WICC.

#### 1.8.4. Salinity

Salinity and temperature are two properties that affect the density of the sea water and the stratification at the ocean surface. Salinity of the BoB is highly variable with very low salinity due to fresh waters at the surface in the northern Bay and saltier waters at the subsurface as well as to the south (Benshila *et al.*, 2014). Salinity near the surface in the northern BoB can be as low as 31 ppt because of the large freshwater influx due to rain and river runoff ([http://www.nio.org/index/option/com\\_nomenu/task/show/tid/2/id/140](http://www.nio.org/index/option/com_nomenu/task/show/tid/2/id/140)). Prasanna Kumar *et al.* (2010) has shown that during the pre-monsoon season, BoB experienced warm surface temperature ( $>29^{\circ}\text{C}$ ) and high salinity ( $>33$  psu) which decreases the stability of the water column. The authors also showed that during SWM and post-monsoon season, the salinity decreased by 4-6.5 psu especially in the northern Bay due to the fresh water influx from rivers and high precipitation. EICC which flows southward during Nov-Dec advects low salinity water along its path (Shetye *et al.*, 1996). The thin layer of fresh water that caps the northern half of the BoB influence the hydrography of the upper ocean by the formation of a barrier layer which affects the air-sea exchanges (Vinayachandran and Kurian, 2007). The shallow halocline and enhanced stability in the upper ocean help to maintain high heat content and SST throughout the year (Han and McCreary, 2001; Shenoi *et al.*, 2002). The stratification due to salinity prevents the cooling of ocean surface by cyclones and hence favours intense cyclones (Sengupta *et al.*, 2008). The salinity also influences the amplitude of intra-seasonal variability of SST in the BoB (Vinayachandran *et al.*, 2012).

#### 1.8.5. Sea surface temperature and surface stratification

Though located in the same latitudinal belt, Arabian Sea and the BoB exhibit distinct oceanographic features (Rao and Shree Ram, 2005). SST in the BoB is typically between  $22^{\circ}\text{C}$  and  $31^{\circ}\text{C}$  which is about  $1-2^{\circ}\text{C}$  less than the surface temperature in the Arabian Sea ([http://www.nio.org/index/option/com\\_nomenu/task/show/tid/2/id/140](http://www.nio.org/index/option/com_nomenu/task/show/tid/2/id/140)). The BoB is distinguished by a strong stratified surface layer. The BoB receives a

large volume of fresh water as river discharge and experiences more precipitation than evaporation resulting in an upper layer of less saline water for a large part of the year (Vinayachandran, 1992). On the other hand, Arabian Sea receives highly saline waters from the Persian Gulf and the Red Sea, and evaporation exceeds precipitation making an upper layer of high saline waters (Vinayachandran *et al.*, 1996). Since the surface salinity is very low in the BoB, the stratification in the upper layer is dominated by salinity gradients rather than temperature gradients (Shetye *et al.*, 1991). SST of the Bay remains above 28°C during most part of the year (Vinayachandran and Shetye, 1991) which is the threshold SST for active generation of large-scale convection/precipitation (Gadgil *et al.*, 1984). During the SWM season, the northern Bay is characterized by high SST, shallow surface layer of low salinity and weak wind compared to the Arabian Sea (Rao *et al.*, 2011). The weak winds cannot overturn the stratified low-salinity surface layer and hence the mixed layer becomes shallow. Once the strong stratification in the surface layer takes place, the SST is mainly driven by surface net heat flux (Rao *et al.*, 2011). As a consequence, though the Arabian Sea and BoB get almost same amount of net radiative heating, the SST over BoB is much warmer than that over Arabian Sea (Shenoi *et al.*, 2002). The intraseasonal SST changes can be associated with changes in the surface winds and atmospheric convection over BoB (Rao *et al.*, 2011). At the same time these atmospheric changes may be responsible for the observed SST variability over the Bay (Rao *et al.*, 2011).

Many major rivers of India flow into the BoB: in the north, the Ganges River (or Ganga), Meghna and Brahmaputra rivers, and in the east Mahanadi, Godavari, Krishna and Kaveri (or Cauvery) rivers. The Irrawaddy River of Myanmar also flows into the bay. The four major rivers Irrawaddy, Brahmaputra, Ganga, and Godavari, discharge annually approximately  $1.5 \times 10^{12} \text{ m}^3$  of fresh water into the Bay (Martin *et al.*, 1981). The Brahmaputra and Ganga rivers alone discharge approximately  $10^{12} \text{ m}^3 \text{ yr}^{-1}$  of fresh water into the Bay at its northern end (Martin *et al.*, 1981). The fresh water influx by Godavari in the middle of the east coast of India is about  $8.5 \times 10^{10} \text{ m}^3 \text{ yr}^{-1}$  (Martin *et al.*, 1981). About three fourths of all riverine influx occurs during the

SWM (Shetye *et al.*, 1996). During Aug-Sep, the combined discharge of Ganga and Brahmaputra has a peak of about  $70 \times 10^3 \text{ m}^3 \text{ s}^{-1}$  (Emery and Aubrey, 1989). The annual rainfall over the Bay varies between 1 m off the east coast of India to more than 3 m in the Andaman Sea and the coastal region north of it (Baumgartner and Reichel, 1975). The total runoff from the peninsular rivers, which peaks during summer monsoon, amounts up to about  $1.625 \times 10^{25} \text{ m}^3 \text{ yr}^{-1}$  (Subramanian, 1993). This large influx of fresh water through river runoff and precipitation results in a layer of low saline water at the ocean surface and leads to a strong stratified surface layer. The stability parameter in the BoB is 3-4 times greater than that in the Arabian Sea (Prasanna Kumar *et al.*, 2002) making it increasingly difficult to perturb the BoB except during the cyclonic storm period.

#### **1.8.6. Chlorophyll and productivity**

Biological productivity of the BoB is low compared to the Arabian Sea (Gomes *et al.*, 2000; Madhupratap *et al.*, 2003; Prasanna Kumar *et al.*, 2002). In contrast, very high biological production occurs in the western Arabian Sea in response to strong upwelling and favourable summer monsoon winds (e.g., Banse and English, 2000). During winter, convective mixing due to surface cooling leads to enhanced productivity in the northern Arabian Sea (Madhupratap *et al.*, 1996). Enhanced production in the central Arabian Sea is due to open ocean upwelling through Ekman pumping, wind driven vertical mixing and lateral advection, whereas high productivity along the southwest coast of India in summer is mainly due to coastal upwelling (Prasanna Kumar *et al.*, 2001; 2002). Coastal upwelling regions in the Bay tend to be rich in nutrients, whereas the extensive central regions are nutrient-deficient. Prasanna Kumar *et al.* (2002) attributed the relatively low production in the BoB to strong stratification, high SST and relatively weak winds. The winds are unable to erode the halocline, restricting turbulent vertical mixing and inhibiting the injection of subsurface nutrients into the mixed layer. The presence of eddies lead to high chlorophyll in the western BoB (Gomes *et al.*, 2000). They showed that physical processes such as ocean currents and eddies are able to erode the stratification and upwell nutrients leading to high chlorophyll in the western BoB.

Estimates by Prasanna Kumar *et al.* (2004) support the notion that eddies might be important in bringing subsurface nutrients into the well-lit surface layer of the Bay. Kumar *et al.* (1996) found that large regions in the Bay have pCO<sub>2</sub> levels far below the atmospheric value, which they attributed to high new production. Kumar *et al.* (2004) used measurements based on Nitrogen isotopes to show that new production in the Bay is high in both pre-monsoon and post-monsoon seasons. They estimated that only 20% of the nitrogen required to support the observed production comes from the rivers and atmosphere. The remaining 80% has to come from nitrate from deeper waters. It is possible that a significant part is due to entrainment of subsurface water by large disturbances such as cyclones.

### **1.9. Ocean response to tropical cyclones**

Tropical cyclones with strong wind and heavy rainfall represent the extreme cases of episodic disturbances that have profound influence on the abundance and production of marine phytoplankton (Chang *et al.*, 1996). Ramesh Kumar and Sankar (2010) have shown that the relationship between SST and maximum wind speed of tropical cyclones is complex over the BoB. One of the most striking effects of a tropical cyclone on the upper ocean is the marked cooling of SST. SST cooling is mainly due to the vertical mixing of cool subsurface water under the action of cyclonic winds. Mature cyclones exert strong stress on the ocean surface, creating large vertical shear of horizontal currents. The mixed layer deepens due to entrainment of cooler water from below. About 20% of the observed SST cooling is due to surface fluxes of latent and sensible heat to the atmosphere, and the remaining 80% due to vertical mixing at the base of the oceanic mixed layer (Jacob and Shay, 1999). Black (1983) reported upper ocean cooling of 1-6°C with mixed layer deepening by 20-50 m for fast, moderate and slow moving tropical storms in the Atlantic Ocean. Lin *et al.* (2003) reported SST cooling by as much as 6°C due to the slow moving tropical cyclone Kai-Tak in Jul 2000 in the South China Sea, associated with mixed layer deepening of 70m. Cooling of NIO SST by tropical cyclones has been studied by several authors (e.g. O'Brien and Reid 1967; Rao *et al.*, 2004). Premkumar *et al.* (2000) observed a 3°C fall in SST in association with a tropical cyclone in the

Arabian Sea. In the open ocean, tropical cyclones may deepen the mixed layer by 20-30 m (Malone *et al.*, 1993). Son *et al.* (2006) observed a decrease in SST by 2-4°C associated with an increase in the chlorophyll concentration by about 70% due to a typhoon in the Japan/East Sea.

Nutrients could be brought to the surface by the cyclones or high speed winds, in varying amounts that depend on location, intensity and residence time (Kumar *et al.*, 2004). Strong winds associated with tropical cyclones cause entrainment and upwelling in the tropical and subtropical oceans (Price, 1981; Emanuel, 1999). Tropical cyclones alter the generally prevailing oligotrophic conditions by brining deep layer nutrient-rich water in to the upper layer making it productive and lead to localized intense blooms. This fuels the photosynthetic activities in the light-replete euphotic zone and cause enhancement of PP (Lin *et al.*, 2003). According to Kumar *et al.* (2004), major part of the nitrogen required for the high new production during pre-monsoon and post-monsoon seasons is made available by cyclones through the entrainment of nutrient rich subsurface water.

The first study in the Indian Ocean about the influence of a tropical cyclone on phytoplankton (Subrahmanyam *et al.*, 2002) based on satellite chlorophyll observations showed phytoplankton blooms in response to an Arabian Sea cyclone in May 2001. Using Ocean Colour Monitor (OCM) on board Indian Remote Sensing Satellite (IRS-P4) data and an ocean model, the authors suggested that increase of mixed-layer depth (MLD) due to intense wind stirring leads to entrainment of nutrients into the surface layer. The injection of nutrients into the surface layer with near-zero nutrient concentration leads to strong phytoplankton blooms with 5-8 mg m<sup>-3</sup> of surface chl-*a* concentration. Vinayachandran and Mathew (2003) documented the occurrence of enhanced phytoplankton in the BoB during the NEM using chl-*a* from Ocean Color and Temperature Scanner (OCTS) and Sea-viewing Wide Field of view Sensor (SeaWiFS). During Nov-Dec, the chl-*a* in the open Bay is very low (<0.15 mg m<sup>-3</sup>), but patches of high chlorophyll concentrations were seen off the east coast of India during Nov-Dec 1996. The authors suggested that open ocean

upwelling driven by Ekman pumping caused the bloom and also cyclones which are common during this period helped to intensify the bloom in their region of influence.

### **1.10. Objectives of the study**

This work aims to achieve the following objectives

1. Analyse the temporal and spatial distributions of some of the physical properties that are important to upwelling and surface chl-*a* concentration in the Bay of Bengal.
2. Analyse the variations in the depth of 20°C isotherm (D20) in the BoB, and its relation to Ekman pumping, sea level variations and surface chl-*a* concentration.
3. Study the seasonal to inter-annual variations in surface chl-*a* concentration and its relation to Ekman pumping and sea level changes.
4. Examine the upper ocean response to the upwelling induced by tropical cyclones in the BoB.

The thesis is divided into seven Chapters with further subdivisions. Chapter 1 explains the importance of wind induced upwelling in the distribution of surface chlorophyll in the upper ocean. Physical and biological characteristics of the BoB and the importance of upwelling in the productivity of this Bay are described in detail in this Chapter. It also includes a detailed literature survey of the previous studies carried out on the physical and biological properties of the BoB. Chapter 2 describes different data sets used in the study and the methodology adopted for different analyses and computations. The satellite sensors and the retrieval methods of parameters by the sensors are described in detail.

In Chapter 3, the spatial and temporal distributions of the important physical and biological properties (WSC, SST, SLA and chl-*a*) in the BoB have been analysed based on seasonal and monthly climatology of eight years from 2000 to 2007. In Chapter 4, the variability of WSC in the BoB has been analysed using the Empirical Orthogonal Function (EOF) analysis. The analysis gives spatial patterns of WSC and associated time series. The spatial patterns of WSC associated with these modes

present the major elements of BoB climatology. The spatial distribution of wind stress in the BoB during the SWM has been analysed in Chapter 4. The inter-annual variations in the extent of the cold pool of southcentral Bay have been studied and the results are explained in this Chapter. VV has been computed from WSC and analysed in the regions of high wind stress in the BoB along with SLA.

Chapter 5 deals with the upwelling and its significance in relation to surface chlorophyll distribution in the BoB. In order to understand the sub-surface oceanographic structure, the monthly variations of D20 has been analyzed using NCAR reanalysis water temperature data. Based on prominent annual signatures of D20, four areas were considered for further study. Comparison of monthly variations of D20 indices have been carried out with VV, SLA, and chl-*a* indices and the results explained in this Chapter. The seasonal and inter-annual variations in the chl-*a* distribution have also been analysed and explained in this Chapter. The relationship of surface chl-*a* concentration with VV and SLA has been examined for the selected regions and the results explained.

In Chapter 6, the upper ocean response to the upwelling induced by tropical cyclones in the BoB has been analysed. The effect of strong winds during the cyclones on physical and biological processes has been examined by analyzing the changes in SST, surface chl-*a* concentration and PP in the cyclone affected area in the ocean. The analysis have been carried out for two intense tropical cyclones having wind speed more than 64 kts, one during May 2003 (pre-monsoon) which moved northward and another during Nov 2000 (post-monsoon) which moved westward. Chapter 7 contains the summary and conclusions of the thesis. References in the text and publications during research period are cited in the alphabetical order after Chapter 7.

### **1.11. Significance of the study**

The BoB is a highly stratified basin with low productivity compared to Arabian Sea in the NIO. Generally, the availability of nutrients is low in the central open ocean

of BoB leading to low PP whereas the coastal areas of BoB are nutrient rich with high PP. The low productivity of the BoB has been attributed to the presence of strong surface stratification and relatively weak winds which together prevent the nutrients from reaching the ocean surface. Hence the studies of physical processes that can break the stratification and bring nutrients to the ocean surface are of importance in the BoB.

Winds over the BoB play a major role in the dynamics of ocean surface which also cause divergence of surface waters and upwelling in the coastal and open ocean under favorable conditions. Seasonal to inter-annual changes in phytoplankton biomass and productivity are important components of the total variability associated with ocean biological and biogeochemical processes (Yoder and Kennely, 2003). Biomass turnover rates for plankton ecosystems are one hundred times faster than those for terrestrial ecosystems, thus making the relation between upper ocean ecology and physical forcing very important (Barnes *et al.*, 2003). Temporal variability of ocean chlorophyll provides information on PP and subsequent assessment of secondary and higher order production processes such as zooplanktons and marine fisheries (Dey and Singh, 2003). Phytoplankton patterns provide the basis for mesoscale and global marine ecosystem studies (Barnes *et al.*, 2003).

In this thesis, effect of wind on surface chlorophyll distribution in the BoB has been analysed. The study helps to understand the spatial distribution and seasonal to inter-annual variability of various physical properties of importance in upwelling in the BoB. The study also helps to understand the temporal and spatial variability of phytoplankton in the surface waters of BoB. Analysis of physical properties help to identify the upwelling zones in the BoB, the knowledge of which is highly beneficial in identifying the locations of biological importance and possible fishing grounds in the ocean.

## Chapter 2

# Data and Methodology

### 2.1. Introduction

The study of the influence of wind on surface chlorophyll distribution in the BoB has been carried out mostly using various remote sensing data from satellite observations. Some of the physical and biological parameters of importance that either influence or reflect the presence of upwelling in ocean are WSC, SST, SLA, water temperature, MLD and chl-*a* concentration. The spatial and temporal distributions of these parameters and their inter-relations in the BoB have been analyzed using satellite data. WSC is obtained from QuikSCAT scatterometer wind, SST from TRMM Microwave Imager (TMI) and Terra Moderate Resolution Imaging Spectroradiometer (MODIS), chl-*a* concentration from SeaWiFS and Terra MODIS, and SLA from merged altimeter observations. Modeled output of water temperature, PP and MLD has also been used for various analyses in the thesis.

### 2.2. Remote sensing parameters and sensors

Remote sensing from space provides a vantage point from which we can measure and map the ocean surface features on a global scale at different spatial resolution and can study reasonably fine details of ocean surface. Some of the important parameters related to upwelling such as sea surface winds, SST, surface chl-*a* concentration, sea surface height (SSH) can be measured using satellite sensors. Passive and active sensors like radiometer, scatterometer and altimeter and also optical scanner provide information of the above parameters. As with any other technique, remote sensing also has its limitations. It cannot provide the time series of measurements over a given geographic location with fine sampling as available with *in-situ* measurements. Also it can observe only the surface phenomenon; subsurface

phenomena, which provide recognizable surface signatures, cannot be measured using remote sensing data.

### **2.2.1. Sea surface winds**

Sea surface winds have an important role in the energy exchange at the air-sea interface since it influences the surface roughness and the wave climate. Sea surface winds drive the circulation of the upper ocean. The wind driven circulation is principally in the upper few hundred meters and therefore is primarily a horizontal circulation in contrast to the thermohaline circulation. Surface wind is an important parameter in the study of atmospheric forcing, ocean response and air-sea interaction mechanisms on various spatial and temporal scales. Wind velocity measurements by satellites are useful for studies on upwelling phenomena in the NIO, where large scale steady monsoon winds occur. Near-surface wind speed and direction are available from ship/buoys, atmospheric general circulation models, and satellite measurements of both scatterometer and radiometer. Among the three, satellite observations are more promising (Halpern *et al.*, 1998).

#### **2.2.1.1. Scatterometer**

Scatterometer is a side looking active microwave radar, but configured to measure the radar cross section of the target accurately rather than mapping it. From space-borne platforms, scatterometer is mainly used to measure the ocean surface wind speed and direction. The measured radar cross section of the ocean surface is highly correlated to the near-surface wind speed and direction. Because it measures the backscattered pulses produced by reflection or scattering effect, it is called a scatterometer.

Scatterometers transmit microwave pulses and receive backscattered energy from the ocean surface. Microwaves are Bragg scattered by short water waves and the backscattered energy is a function of wind speed and direction. Changes in wind velocity cause changes in ocean surface roughness that modifies the radar cross section of the ocean and the magnitude of backscattered power. Normalized radar

cross section ( $\sigma_0$ ) of the sea surface is estimated from this backscattered power reaching the scatterometer. Since the surface roughness is highly correlated with near-surface wind speed and direction, these parameters at a height of 10 m over the ocean surface are retrieved from scatterometer's backscattered power. Scatterometer data has many applications that include weather forecasting, storm detection, monitoring of El Niño and sea ice studies in the Polar regions. Combined with data from other scientific observations, scatterometer wind data is useful to understand mechanisms of global climatic change and weather.

### 2.2.1.2. QuikSCAT scatterometer

The SeaWinds scatterometer on QuikBird satellite is an active microwave radar designed specifically to measure near-surface wind speed and direction under all weather and cloud conditions over the earth's oceans. They are also useful for some land and sea ice applications. It was launched in June 1999 by National Aeronautical and Space Administration (NASA) into a sun-synchronous orbit at an altitude of 803 km and 98.6° inclination with a 0600 ascending equator crossing time. This instrument is referred to as QuikSCAT (or QSCAT) to distinguish it from the nearly identical SeaWinds scatterometer on Midori-II (Advanced Earth Observing Satellite-II, ADEOS-II), launched in December, 2002. This is a quick recovery mission to fill the gap created by the loss of data from the NASA scatterometer (NSCAT) when the ADEOS-I satellite lost power in June 1997 and came to an end in November 2009. The QuikSCAT sensor used a 1 m rotating dish antenna with two spot beams that swept in a circular pattern. The antenna radiated microwave pulses at a frequency of 13.4 GHz (Ku-band) across broad regions on Earth's surface. The instrument collected data in a continuous 1,800 km wide swath and cover 90% of earth's ocean in one day. QuikSCAT scatterometer provided wind speed measurements of 3 to 20  $\text{m s}^{-1}$ , with an accuracy of 2  $\text{m s}^{-1}$  and direction with an accuracy of 20° and had a spatial resolution of 25 km. Comparison with *in-situ* buoy data showed that QuikSCAT winds are accurate in calibrations and falls within the mission requirements of wind speed within 2 $\text{ms}^{-1}$  Root Mean Square (RMS), and wind direction within 20° RMS. But the mean difference between buoy and satellite wind

speeds is about  $-0.35\text{m s}^{-1}$ , indicating an overestimation of scatterometer wind speed estimates with respect to buoy measurements. The scatterometer winds underestimate at low winds and overestimate at high winds (*QuikSCAT Mean Wind Field User Manual*, 2002).

Other than surface wind speed and direction, rain information (*i.e.* the scatterometer derived rain flag) was available from QuikSCAT. Over the ocean, brightness temperature measurements are used to locate rain cells and flag the wind vector values, which can be contaminated by rain effects. In Polar regions, they are mainly useful to identify sea ice covered areas from open ocean since the surface emissivity of sea ice is almost twice that of seawater at the operating frequency of QuikSCAT. Scatterometer data is less accurate in rain; rain tends to result in erroneous cross track vectors and/or unrealistically high speeds. When rain is present, measurements of the ocean surface  $\sigma_0$  become contaminated for several reasons. Some of the transmitted energy is scattered back towards the scatterometer by rain and never reaches the ocean surface. Some of the transmitted energy is scattered and/or absorbed by rain and is never measured by the scatterometer. These respectively have the effect of increasing or attenuating the echo energy from ocean. Also the rain roughens the ocean surface and changes its radar cross section.

The monthly and weekly mean wind stress and WSC data used for the study were obtained from the Centre de Recherche et d'Exploitation Satellitaire (CERSAT), at IFREMER, Plouzané (France), (<http://www.ifremer.fr/cersat/en/>). They compute gridded mean wind fields from SeaWinds on QuikSCAT Level 2B data provided by Jet Propulsion Laboratory (JPL)/Physical Oceanography Distributed Active Archive Center (PO.DAAC). Wind vectors whose speed is not in the  $0.5 - 30\text{ m s}^{-1}$  range are skipped. Main parameters are wind speed, wind stress, WSC and divergence. QuikSCAT data cover global oceans from  $80^\circ\text{N}$  to  $80^\circ\text{S}$ , and  $180^\circ\text{W}$  to  $180^\circ\text{E}$ . Daily, weekly and monthly wind data is available on a rectangular  $0.5^\circ \times 0.5^\circ$  resolution geographical grid (*QuikSCat Mean Wind Field User Manual*, 2002).

IFREMER used bulk formulation method to estimate surface wind stress  $\tau$ .

$$\tau = (\tau_x, \tau_y) = \rho C_D W(u, v) \text{ ----- (2.1)}$$

where  $W$ ,  $u$  and  $v$  are wind speed, zonal component and meridional component respectively. The surface wind is assumed to be parallel to the stress vector.  $\rho = 1.225 \text{ kg m}^{-3}$  is the density of surface air.  $C_D$  is the drag coefficient.

The magnitude of the stress is:

$$|\tau| = \rho C_D W^2 \text{ ----- (2.2)}$$

The 10 m neutral coefficient formulation over the ocean is:

$$C_D = a + b W \text{ ----- (2.3)}$$

The values of  $a$  and  $b$  are determined for each wind speed range. This  $C_D$  estimate is given by Smith (1988).

Finite difference scheme is used by IFREMER for the computation of WSC,  $\text{curl}(\tau)$  from the resultant wind fields.

$$\begin{aligned} \text{curl}(\tau) &= \frac{(4/3)[\tau_y(i+1, j) - \tau_y(i-1, j)] - (1/3)[\tau_y(i+2, j) - \tau_y(i-2, j)]}{2dy} \\ &\quad - \frac{(4/3)[\tau_x(i, j+1) - \tau_x(i, j-1)] - (1/3)[\tau_x(i, j+2) - \tau_x(i, j-2)]}{2dx} \end{aligned} \text{ ----- (2.4)}$$

where,

- $u, v$  are the mean zonal and meridional components of the wind vector (as estimated by kriging),
- $\tau_x, \tau_y$  are the mean zonal and meridional components of the wind stress vector (as estimated by kriging),
- $i, j$  are the column and line index of the current grid cell,

- $dx, dy$  are the width and height of the current grid cell  
(excerpt from *QuikSCAT Mean Wind Field User Manual*, 2002).

### 2.2.2. Sea surface temperature

SST is a measure of the energy due to the motion of molecules at the top layer of the ocean. SST of the oceans has an important role in the exchange of energy, momentum, and moisture between the ocean and the atmosphere (Wentz *et al.*, 2000). It is a vital parameter in air-sea interaction including El Nino–La Nina cycle and climate variability. SST also influences the genesis and evolution of tropical storms and hurricanes. SST is an important parameter in detecting the upwelling regions in the world oceans which can be identified with the presence of low surface temperature. SST observations from satellite contribute to an understanding of regional variability and global climate change (Martin, 2004). It helps to delineate the ocean surface currents, eddies, fronts and upwelling zones by means of gradient patterns associated with these processes. Satellite observations of SST are useful for climate studies, global warming, fisheries, tropical cyclone studies and weather forecasting. Depending on the sensor, spaceborne measurements give us an unprecedented global measurement of SSTs every few days to a week.

SST can be measured from satellites using both infrared and microwave radiation. Radiometers are high sensitive receivers operating in different frequencies depending on the applications. Radiometers receive the natural electromagnetic radiation emitted by the target in the desired frequency and process it to provide the geophysical information. However, infrared SST retrievals have two significant limitations: 1) Retrievals cannot be done when clouds are present and 2) atmospheric aerosols from volcanoes and large fires can cause a spurious cooling in the SST retrieval (Reynolds, 1993). The aerosol problem is more when trying to construct multiyear time series to infer climate change (Reynolds *et al.*, 1989). The advantage for passive microwave radiometers over infrared radiometers is that the microwaves can penetrate clouds with little attenuation giving a clear view of the sea surface under all weather conditions except rain when the frequency is below about 12 GHz.

At these frequencies the surface radiance is proportional to SST and the microwave retrievals are not affected by aerosols (Wentz *et al.*, 2000). Ocean surface emissivity and atmospheric transmittivity depends on both frequency of microwave and variables like atmospheric water vapour and liquid water, SST, salinity, rain rate, wind speed and sea ice making microwave observations important in ocean remote sensing (Martin, 2004). Instead of the lenses and mirrors used in the Visible and Infrared (VIR), antennas are used with passive microwave radiometers to receive the earth emitted radiances, and with radars to transmit and receive energy pulses. Infrared radiometer operating at 11  $\mu\text{m}$  measures radiative temperature emitted from the top 30  $\mu\text{m}$  of the water column whereas microwave radiometer operating at 10 GHz measures the same emitted from the top 1-2 mm of the water column (Martin, 2004). Microwave retrievals are very sensitive to sea surface roughness while infrared retrievals are not. The radiation measured by passive microwave radiometers is expressed in terms of the brightness temperature. The sea surface roughness (which in turn depends on wind speed) and surface salinity are among the factors that influence the sea surface emissivity which influence SST retrieval from the measured radiance emitted by the sea surface (Bhat *et al.*, 2004). SST measurements by microwaves are useful in the study of marine boundary layer dynamics, tropical instability waves, and the prediction of hurricane intensity (Wentz *et al.*, 2000).

#### **2.2.2.1. TRMM Microwave Imager (TMI)**

The Tropical Rainfall Measuring Mission (TRMM) was launched in November 1997. It was a joint mission of the NASA and the National Space Development Agency (NASDA) of Japan designed to monitor and study tropical rainfall and the associated release of energy. TRMM was in a low inclination circular orbit at an altitude of 350 km and an inclination angle of 35° and covered the tropics between 40 N to 40 S. The orbit is not sun-synchronous so that over a month it samples the tropics at uniform intervals throughout the day (Martin, 2004). The TRMM satellite carried five instruments: a 3-sensor rainfall suite - Precipitation Radar (PR), TMI, Visible and Infrared Scanner (VIRS) and 2 related instruments (Lightning Imaging Sensor (LIS) and Cloud and Earth's Radiant Energy System (CERES)). TMI was a

multichannel, dual polarized, conical scanning passive microwave radiometer designed for SST retrievals in the tropical regions of heavy precipitation. It also measured rain rates, ocean surface wind speeds, columnar water vapor, and cloud liquid water. TMI measured electromagnetic radiation emitted by the ocean-atmosphere system at 10.7, 19.4, 21.3, 37, and 85 GHz (Halpern *et al.*, 2001). TMI had a resolution of about 50 km and a swath of 780 km and provided nighttime global SST maps. It is the first satellite sensor to measure SST accurately through clouds which are nearly transparent at 10.7 GHz. The TRMM satellite was shut down on April 2015.

Influence of atmospheric attenuation and sea surface roughness should be removed from the observations for the retrieval of SST from the microwave radiances. Wentz (1997) used a physically based retrieval algorithm to remove these effects. In the absence of rain, the attenuation is very small at 10.7 GHz and 97% of the sea surface radiation reaches the top of the atmosphere. The algorithm precisely estimates the 3% attenuation due to oxygen, water vapor, and clouds using the higher frequency channels (19.4 to 37 GHz). The horizontal to vertical polarization ratio of the measurements is used to estimate sea surface roughness (Wentz *et al.*, 2000). Raindrops with larger diameter than cloud droplets can significantly attenuate and scatter microwave radiation and hence SST retrievals are not reliable in the presence of rain. The 37 GHz channels are very sensitive to rain and are used to determine when rain is present in the radiometer's field of view (Wentz *et al.*, 2000).

Monthly and weekly mean (7-day average) TMI SST data provided by Remote Sensing Systems (RSS), Santa Rosa, CA (<http://www.remss.com/>) has been used in this study. The data are provided as daily maps (ascending and descending), 3-day, weekly (7day) and monthly mean maps and is available from December 1997 to March 2015. These data files contain SST, surface wind speeds, atmospheric water vapor, cloud liquid water, and rain rates. It covers a global region extending from 40°S to 40°N and has a pixel resolution of 25 km. A robust radiative transfer model was used by RSS to derive these ocean measurements from the instrument brightness temperatures. Two surface wind speeds are derived from 11 and 37 GHz channels of

TMI. Compared to infrared retrievals with high resolutions of 1 to 10 km, TMI SST has coarse resolution. The data range for SST is -3 to 35°C. Comparisons of TMI SST with the buoy measurements showed a root mean square difference of 0.5° to 0.7°C, which according to Wentz *et al.*, (2000) is partly due to the difference between ocean skin temperature and bulk temperature and the satellite-buoy spatial-temporal sampling mismatch. In BoB the mean difference between the SST from TMI and buoys is less than 0.1°C, and the RMS difference is about 0.6°C. Bhat *et al.* (2004) observed that TMI SST tends to be lower during periods with deep convection or winds stronger than 10 m s<sup>-1</sup>, or both.

#### 2.2.2.2. Terra Moderate Resolution Imaging Spectroradiometer (MODIS)

NASA launched the Terra satellite as the flagship mission of the Earth Observing System in December 1999 into a near-polar sun-synchronous orbit at an altitude of 705 km. Terra passes from north to south across the equator in the morning at 10.30 am, while Aqua, the sister ship of Terra launched in May 2002 passes from south to north over the equator in the afternoon at 13.30 pm. Terra carries five instruments: 1) Advanced Spaceborne Thermal Emission and Reflection Radiometer (ASTER), 2) CERES, 3) Multi-angle Imaging Spectroradiometer (MISR), 4) Measurements of Pollution in the Troposphere (MOPITT) and 5) MODIS. MODIS is a key instrument aboard Terra (EOS AM) and Aqua (EOS PM) satellites for the observation of oceanic and terrestrial phenomena. It is a hybrid cross-track scanning radiometer having a rotating double-sided scan mirror with 36 spectral bands in the range of visible to thermal infrared radiation at 0.4 - 14.4 µm. MODIS has a spatial resolution of 250 m to 1 km and a swath width of 2330 km and covers the Earth's surface every 1-2 days.

The MODIS use 3 bands (20, 22, and 23) between 3.6 – 4.1 µm and two bands (31 and 32) between 10.7 – 12.3 µm for SST retrievals. Because of the sensitivity to solar reflectance, 4 µm bands are used only for nighttime SST retrievals, whereas 11 µm bands are used all the time and their reflectances are an order larger than 4 µm bands (Martin, 2004). Also 4 µm bands are less sensitive to water vapour than 11 µm

bands and more sensitive to changes in surface temperature (Stewart, 1985). Apart from sea surface, atmosphere, cloud and land temperatures, ocean color, phytoplankton, aerosols, water vapor and cloud altitudes are obtained from MODIS. MODIS data are useful to understand the global dynamics and processes that occur on land, in oceans, and in the lower atmosphere. Application areas of MODIS include El Nino studies, climate change, air quality, volcanic eruptions, wildfire monitoring, weather forecast, agriculture, oil spills and floods.

The 8-day composite Terra MODIS SST data (11  $\mu\text{m}$  nighttime) at 4.0 km resolution used for the cyclone studies are obtained from NASA Goddard Space Flight Center (GSFC) Distributive Active Archive Center (GDAAC), <http://daac.gsfc.nasa.gov/>. The basis for the MODIS SST algorithm is the Miami Pathfinder SST (mpfsst) algorithm (Kilpatrick *et al.*, 2001). Comparison between MODIS SSTs and collocated skin SST measurements of the Marine-Atmospheric Emitted Radiance Interferometer (M-AERI; Minnett *et al.*, 2001) indicated that the SST values are within the required accuracy – bias error of 0.2K, rms 0.26K, using the empirical, Advanced Very High Resolution Radiometer (AVHRR) related coefficients.

### 2.2.3. Sea level anomaly

A sea level anomaly, as defined by National Oceanic and Atmospheric Administration's (NOAA) National Ocean Service, occurs when the 5-month running average of the interannual variation is at least 0.1 meters (4 inches) greater than or less than the long-term trend. SLA data is useful in tracking the movement of oceanic eddies and in the studies of upwelling caused by strong winds including the effect of tropical cyclones. SLA can be measured with satellite altimeters. Altimeter measurements of SLA provide information about mesoscale ocean properties and their variability (Martin, 2004). It can be used to study the seasonal variations in SSH, Rossby wave propagation and in the computation of geostrophic currents.

### 2.2.3.1. Altimeter

Radar altimeter is an active microwave sensor that transmits short pulses of energy vertically downward towards the ocean surface and then receives the reflected signal. It measures the travel time, the magnitude, and the shape of each return signal after reflection from the ocean surface: time difference between transmitted and received signal gives the distance between satellite and sea surface. The shape of the return signal gives the significant wave height and the magnitude gives the scalar wind speed (Martin, 2004). Satellite altimeters operate in Ku (13.8 GHz) and C (5.3 GHz) bands. Combined with precise satellite location data, altimetry measurements yield sea-surface heights. These measurements are used in the determination of changes in SSH due to tides, geographic currents and other oceanic phenomena to an accuracy of 2-3 cm. In altimeter measurements, SSH has to be measured relative to the geoid, which is defined as the shape of the ocean surface in the absence of all external forces and internal motion.

The merged SLA data generated by Ssalto multimission ground segment (SSALTO) / Data Unification and Altimeter Combination System (DUACS) has been used for the study. Observations from Saral/AltiKa, Jason-1, Jason-2, Cryosat-2, Envisat, European remote sensing satellite-1 (ERS-1), ERS-2, GFO, HY-2A are used for the generation of merged SLA. The all-satellite merged SLA takes into account all the satellites available (up to 4 satellites) making it the best possible sampling. These merged SLA is available on daily and monthly scales. The merged monthly gridded SLA data at  $0.25^\circ \times 0.25^\circ$  resolution is obtained from Archiving, Validation and Interpretation of Satellite Oceanographic data (AVISO, <http://www.aviso.altimetry.fr/>). It is the multi-mission gridded SSH computed with respect to a twenty-year mean profile (1993-2012), and includes the seasonal variability (no annual cycle is removed). This data is available from January 1993 onwards. Excerpts are taken from SSALTO/DUACS User Handbook, 2015. Daily and ten day averaged data has also been used to study the changes in SSH due the tropical cyclone.

#### 2.2.4. Surface chlorophyll-*a* (chl-*a*) concentration

Amongst the different photosynthetic pigments within phytoplankton cell, chl-*a* is the only pigment present in all phytoplankton and hence its concentration provides a measure of phytoplankton abundance and biomass. The annual production of oceanic chlorophyll is about  $10^{12}$  kg (Jeffrey and Mantoura, 1997). Chlorophyll is a measure of biomass while PP is a measure of phytoplankton growth (Martin, 2004). Oceanic processes that bring nutrients to the surface are open ocean upwelling driven by Ekman pumping, coastal upwelling driven by alongshore winds, entrainment due to wind stirring at the base of mixed layer and horizontal advection due to ocean currents (Vinayachandran *et al.*, 2004). Availability of nutrients and sunlight affect PP, hence growth occurs in regions of upwelling, or in regions with wind mixing that bring nutrients to the surface. Such regions occur along the west coast of continents, in the equatorial Atlantic and Pacific during La Nina and in the western Indian Ocean (Martin, 2004).

Chl-*a* concentration can be measured using satellite observations in the visible and near infrared region. Observations of ocean colour from satellite remote sensing can be used in the in models for the estimation of PP. Platt and Sathyendranath (1988) have shown that global productivity calculations are very sensitive to surface chlorophyll inputs. Ocean colour data is useful in understanding and quantifying the ocean carbon flux, studying the impact of El Nino, ocean biology and upper ocean processes, scientific analysis and management of the coastal zone which includes human-induced activities like fisheries and agriculture, occurrence of natural events like toxic blooms, erosion/sediment transport (IOCCG, 1999).

In infrared observations of ocean colour, the radiation is emitted from the top 10-100  $\mu\text{m}$  of the sea surface whereas ocean colour radiances in the blue-green upwell from depths of upto 50 m (Martin, 2004). Aerosol and molecular scattering dominate atmospheric attenuation in the visible range, and hence the water-leaving radiances comprise only about 10% of the total received radiance. Therefore, accurate determination of all other radiances is needed for the determination of water-leaving

radiances (Martin, 2004). Phytoplankton and its pigments, dissolved organic material which is also known as colored dissolved organic material (CDOM) and suspended particulate matter contribute to the colour change in the sea water. Oceanic waters are divided into *Case 1* and *Case 2* waters by Morel and Prieur (1977). *Case 1* waters are those waters in which phytoplankton (with their accompanying and covarying retinue of material of biological origin) are the principal agents responsible for variations in optical properties of the water. On the other hand, *Case 2* waters are influenced not just by phytoplankton and related particles, but also by other substances, that vary independently of phytoplankton, notably inorganic particles in suspension and yellow substances (IOCCG, 2000). One of the limitations of satellite remote sensing of ocean colour is that observations cannot be made under cloudy conditions. Also data is not available in the vertical. The first ocean colour sensor is Coastal Zone Colour Scanner (CZCS) instrument on the Nimbus-7 satellite was launched in 1978. In the thesis, chl-*a* observations from SeaWiFS and Terra MODIS have been used.

#### **2.2.4.1. Sea-viewing Wide Field of View Sensor (SeaWiFS)**

SeaWiFS onboard OrbView-2 spacecraft was launched in August 1997 into a sun-synchronous orbit at an altitude of 705 km and a 1200 descending equator crossing time. SeaWiFS is a cross-track scanner with a swath width of 2800 km and a revisit time of 1 day. The spatial resolution is 1.1 at the nadir. SeaWiFS contains 8 spectral bands in the visible and near infrared region. The central wavelengths are 412, 443, 490, 510, 555, 670, 765, and 865 nm. The 412 nm band is used for detection of CDOM, the 443, 490, 510 and 555 nm bands are used to determine chlorophyll concentrations, and the 670, 765 and 865 nm bands are used for atmospheric correction., 765 and 865 nm bands are also used for aerosol irradiance. SeaWiFS produced scientific data of two spatial resolutions: local area coverage (LAC) at 1.1 km resolution and global area coverage (GAC) at 4.5 km resolution.

There are two types of operational bio-optical algorithms for 400-550 nm bands called empirical and semi-analytic (O'Reilly *et al.*, 1998; Carder *et al.*, 1999).

Empirical algorithms are derived by statistical regression of radiance versus chlorophyll. These use satellite observations of water leaving radiance  $L_w(\lambda)$  or equivalently remote sensing reflectance ( $R_{rs}$ ) at several wavelengths as input: the output is chlorophyll concentration (Martin, 2004). Remote sensing reflectance  $R_{rs}$  is the ratio of  $L_w(\lambda)$  to the solar irradiance at the surface of the ocean and is a linear function of subsurface reflectance  $R(\lambda)$ . The use of empirical algorithms is restricted to *Case 1* waters since these give only chlorophyll. Semianalytic algorithms are useful to retrieve chlorophyll in the presence of CDOM or from both *Case 1* and *Case 2* waters (Martin, 2004). These algorithms use analytical, optical,  $R_{rs}$  models that can be inverted to derive chlorophyll, absorption coefficients of other optically active components in the water such as CDOM, or back scattering coefficient (O'Reilly *et al.*, 1998).

SeaWiFS maximum band ratio Ocean Chlorophyll-4 (OC4) empirical algorithm is written in terms of remote sensing reflectance  $R_{rs}(\lambda)$  ratios. OC4 makes use of a maximum band ratio that incorporates 443, 490, 510 and 555 nm bands. OC4 version 4 (OC4v4) relates band ratios to chl-*a* with a fourth order polynomial function given by the equation:

$$C_a = 10^{(0.366 - 3.067R_{4s} + 1.930 R_{4s}^2 + 0.649 R_{4s}^3 - 1.532R_{4s}^4)} \text{ ----- (2.5)}$$

$$\text{where } R_{4s} = \log_{10} (R_{555}^{443} > R_{555}^{490} > R_{555}^{510}) \text{ ----- (2.6)}$$

and  $C_a$  is the chlorophyll concentration (O'Reilly *et al.*, 2000).

When compared with *in-situ* chl-*a* concentration, the squared correlation coefficient  $R^2$  between *in-situ* and OC4v4 algorithm is 0.892 and the rms is 0.222 (O'Reilly *et al.*, 2000).

The monthly chl-*a* concentration at 9.0 km resolution used in the study is obtained from the NASA GSFC's Ocean Color Web, <http://oceancolor.gsfc.nasa.gov>. Global Level 3 chl-*a* data in various temporal resolutions ranging from daily, 8-day

composite, monthly, seasonal and annual composite at 4 km and 9 km spatial resolution are available from Ocean Color Web. The data is available from September 1997 till December 2010 when the SeaWiFS mission ended.

#### 2.2.4.2. Terra MODIS

The MODIS chl-*a* data that is used to study the changes in chl-*a* concentration due to the occurrence of tropical cyclones is based on the OC3M empirical algorithm described in the SeaWiFS Post-launch Technical Memorandum series (O' Reilly *et al.*, 2000). This empirical algorithm is based on the remote sensing reflectance ratio of 443 and 490 nm to 550 nm whichever is greater. The corresponding band numbers are 9, 10 and 12. In OC3M algorithm, the chl-*a* concentration  $C_a$  is given by the fourth order polynomial equation:

$$C_a = 10^{(0.283 - 2.753R_{3M} + 1.457R_{3M}^2 + 0.659R_{3M}^3 - 1.403R_{3M}^4)} \quad \text{----- (2.7)}$$

$$\text{where } R_{3M} = \log_{10} (R_{550}^{443} > R_{550}^{490}) \quad \text{----- (2.8)}$$

(O'Reilly *et al.*, 2000)

The 8-day composite Terra MODIS chl-*a* data at 4.0 km resolution used for the cyclone studies are obtained from NASA GDAAC (<http://daac.gsfc.nasa.gov/>). Blondeau *et al.* (2004) has shown that the SeaWiFS OC4v4 and the MODIS chl-*a* algorithms are less affected by CDOM. Comparison of MODIS chl-*a* concentration with *in-situ* data shows an  $R^2$  value of 0.754 and RMS error of 0.335 ([http://seabass.gsfc.nasa.gov/seabasscgi/search.cgi?search\\_type=val&id=1465764267642706](http://seabass.gsfc.nasa.gov/seabasscgi/search.cgi?search_type=val&id=1465764267642706)).

## 2.3. Model outputs

### 2.3.1. Water temperature

Ishii *et al.* (2006) carried out an objective analysis to estimate the monthly subsurface temperature and salinity with a horizontal resolution of  $1^\circ \times 1^\circ$  using observational data bases and an SST analysis. The analysis covered the topmost 700 m of the global ocean from 1945 to 2003. It followed the historical objective analysis of oceanic temperature carried out on a monthly basis for the period 1950 to 1998 by Ishii *et al.* (2003). The new analysis scheme improved the previous one by better representation of climate variations. The optimal interpolation based objective analysis scheme used by them was applied to an SST analyses (Ishii *et al.*, 2005) previously and it was successful in reducing the observational noise in the SST data.

They used data from World Ocean Data 2001 edition (WOD01; Boyer *et al.*, 2002) and COBE SST (COBE: Centennial in-situ Observation Based Estimates of variability of SST and marine meteorological variables; Ishii *et al.*, 2005). Seven steps were used in the quality control and data selection; location check, data thinning in the vertical, comparison against SST analysis, gross error check, comparison with nearby observations, erroneous profile check, and data merging in space and time. Application of these procedures helped to maintain the homogeneity of spatial and temporal data distribution and reduced the computational cost of objective analysis. The objective analysis scheme was based on a variational minimization with spatio-temporal covariance of background error. The major differences from the previous analysis by Ishii *et al.* (2003) were the use of a 3-D background error covariance, computation of isothermal layer depth and MLD prior to the analysis of temperature. The analysis errors were estimated in a framework of optimal interpolation. The analysis was able to present reasonable global mean variations of steric sea level for a period of 59 years. The trends of steric sea level estimated by the analysis were comparable to that of World Ocean Atlas 2005 (WOA05); Boyer *et al.* (2005) and Antonov *et al.* (2005).

### 2.3.2. Primary production

NASA GSFC used two models to calculate indices of ocean PP, denoted by P1 and P2. The P1 index was calculated using the Vertically Generalized Productivity Model (VGPM) by Behrenfeld and Falkowski (1997) and P2 index is given by a MLD production model called Howard, Yoder, Ryan model (Howard and Yoder, 1997). VGPM model estimates daily production over the euphotic zone whereas the P2 model estimates the production over the MLD. The main difference between these algorithms is their calculation of the photosynthetic yield efficiency and the depth of integration over the water column. Rao *et al.* (2002a) evaluated the applicability of Modeled PP (VGPM) along Paradip Coast during March 2002 and compared with measured values. These PP models were further evaluated along with other classes of similar models by Campbell *et al.* (2002).

The key model input data for the Ocean Net Primary Production (ONPP) models are 8-day composite averages of the MODIS chl-*a* concentration and daytime SST (11  $\mu\text{m}$ ) at 4.0 km resolution. Both models also use Photosynthetically Available Radiation (PAR) derived from surface incident short-wave surface flux estimates provided by NASA's Data Assimilation Office. For the P2 model, daily synoptic MLD at 1° resolution was provided by US Navy's Fleet Numerical Meteorology and Oceanography Center (FNMOC). This MLD was generated using Optimum Thermal Interpolation System/Thermodynamic Ocean Prediction System (OTIS/TOPS) Ocean MLD Model and averaged to the MODIS weekly period of 8 days. The accuracy of the PP models depends on the accuracy of the inputs data. MODIS chl-*a* input fields were validated using *in-situ* data at the daily level by Gregg *et al.* (2003b) who found an rms difference of 0.28. When compared with *in-situ* skin and bulk SST measurements MODIS SST values showed a bias of 0.16 and -0.14 K respectively with corresponding standard deviation of 0.42 and 0.51 K (Brown *et al.*, 2002). Also PAR fields were compared with SeaWiFS PAR and found an  $r^2$  of 0.92 and a slope of 1.09. The 8-day composite P2 model data at 4.0 km resolution used in the tropical cyclone study was obtained from NASA GDAAC, which they have discontinued presently.

### **2.3.3. Mixed layer depth**

The surface mixed layer is a feature of the open oceans where the temperature, salinity and density are almost vertically uniform. The mixed layer results from the turbulent mixing processes active near the ocean surface such as wind-stirring, waves and convective mixing. The MLD may be less than 20 m in the summer hemisphere whereas it may reach 500 m in the winter hemisphere sub-polar latitudes (Monterey and Levitus, 1997). The depth to which mixing takes place depends on the stability of the sea water and the energy input from wind. When the surface water is stable, the less mixing occurs and the mixed-layer will be shallow. MLD at 1° resolution by FNMOC averaged to the MODIS weekly period of 8 days has been used to study the changes in it due to tropical cyclone in the BoB. This weekly data at 4.0 km resolution was also obtained from NASA GDAAC.

## **2.4. Methodology**

### **2.4.1. Computation of monthly and seasonal climatology**

In Chapter 3, the spatial and temporal distribution of some of the physical and biological parameters in the BoB are analysed based on monthly and seasonal time scales. The physical properties are WSC, SST, and SLA and the biological parameter is the surface chl-*a* concentration. In this study, climatology is taken as the average of monthly mean data of eight years from 2000 to 2007. The four seasons for which the seasonal climatology is computed are 1) Dec-Feb (DJF), 2) Mar-May (MAM), 3) Jun-Sep (JJAS), and 4) Oct-Nov (ON). These periods represent the NEM, pre-monsoon, SWM and post-monsoon seasons respectively.

The monthly WSC at 0.5° x 0.5° spatial resolution from QuikSCAT scatterometer is used to compute the seasonal and monthly climatology of WSC of the BoB for the period 2000 to 2007. The spatial distribution and the temporal variations of WSC has been analysed using both seasonal and monthly climatology. Analysis of WSC is followed by the climatological analysis of seasonal and monthly SST of the BoB. SST used here is the monthly data at 0.25° x 0.25° spatial resolution from TMI

onboard TRMM satellite. The SLA analysed here is the merged altimeter data at  $0.25^\circ \times 0.25^\circ$  spatial resolution. Monthly and seasonal climatological analyses were carried out with the SLA data in the BoB.

The level 3 monthly *chl-a* concentration from SeaWiFS at a spatial resolution of 9.0 km has been used for the seasonal and monthly climatology study in Chapter 3. First the monthly data is regridded to  $0.25^\circ \times 0.25^\circ$  spatial resolution using a 2D regridding function in GrADS that employs box averaging transform method. This regridding function handles input grids which are cyclically continuous in longitude and excludes undefined input grid values from participation in the transform. If a valid transform cannot be made (i.e., insufficient defined data points), the output grid is set to undefined. Box averaging is simply the area-weighted integral of all input grid boxes which intersect an output grid box, divided by the area of the output grid box. This approach is most appropriate: 1) for transforming from fine to coarse grids; and 2) when approximate conservation of an integral quantity (e.g., global average) is desired.

Since *chl-a* observations cannot be made under cloud cover in the visible spectrum, gaps are likely to appear in the data especially during the monsoon season over the BoB. In order to reduce the data gap, a 3 point transformation which fills missing values with the average value of the surrounding grid points has been applied to the regridded data. The width of the averaging window is the number of points given as an argument to the transformation. All of the surrounding points are weighted equally, regardless of the sizes of the grid boxes, making this transformation best suited to axes with equally spaced points. If any of the surrounding points are invalid they are omitted from the calculation. If all of the surrounding points are invalid the gap is not filled. The monthly data thus obtained is used for the computation of seasonal and monthly climatology of *chl-a* concentration.

### 2.4.2. Empirical Orthogonal Function (EOF) analysis

In Chapter 4, the variability of the WSC in the BoB has been analysed using the Empirical Orthogonal Function (EOF) analysis. EOF analysis is an extensively used statistical method to analyse large meteorological and oceanographic data (Hannachi *et al.*, 2007; Preisendorfer, 1988; Ehret and O'Brien, 1989; Ludwig *et al.*, 2004). EOFs are used for pattern extraction and image compression. It helps to identify patterns in a dataset and to express the data in such a way as to highlight their similarities and differences (Smith, 2002). EOF analysis finds a new set of variables that capture most of the observed variance from the data through a linear combination of the original variables (Hannachi *et al.*, 2007). This analysis finds the first few orthogonal components to account for most of the variation in a data set so that the major characteristics of the data set can be more easily understood. A review of Principal Component Analysis (PCA) / EOFs can be found in Kutzbach (1967). EOF analysis (Lorenz, 1956, Hannachi, *et al.*, 2007) is an extensively used method in atmospheric science. This technique finds a set of orthogonal spatial patterns along with a set of associated uncorrelated time series or principal components (PC) for a space-time field (Hannachi *et al.*, 2007). EOF analysis avoids the problem of episodic events.

In the EOF analysis, eigen values and eigenvectors of the spatially weighted anomaly covariance matrix of the data field is computed to find out the EOFs. The area weight used here is  $\sqrt{\cos(\text{latitude} * 3.141 / 180)}$ . The eigen values give a measure of the percent variance explained by each of the EOF modes. Most of the variance is contained within the first few modes. The time series corresponding to each mode called PCs are determined by projecting the derived eigenvectors onto the spatially weighted anomalies. This will result in the determination of the amplitude of each mode over the period of record (<https://climatedataguide.ucar.edu/climate-data-tools-and-analysis/empirical-orthogonal-function-eof-analysis-and-rotated-eof-analysis>).

Singular Value Decomposition (SVD) technique (e.g. Linz and Wang 2003) is used to find the covariance matrix and the eigen values and eigen vectors. GrADS software is used to compute the EOF analysis (<http://cola.gmu.edu/grads>).

The annual mean of the WSC is first calculated from the monthly data for the years 2000 to 2007. It is then subtracted from the monthly data to obtain the WSC anomalies that have been used in the EOF analysis. EOF analysis of WSC data gives spatial patterns of WSC and associated time series. First 12 EOFs are retained in the analysis. EOF analysis identifies the significant patterns in large data sets and the variance explained by them. It is useful to understand the prominent modes of variability of WSC in terms of spatial and temporal patterns.

### 2.4.3. Computation of geostrophic currents

The spatial distribution of wind stress in the BoB during the SWM season has been analysed in Chapter 4. The monthly climatology of wind stress has been computed from May to October for the BoB to study about its spatial and temporal changes and to find the regions of strong wind stress. SST climatology for the southcentral Bay has been computed for the SWM season (JJAS) to illustrate the cold pool that develops during this season. This region of cold pool experiences strong wind stress during the SWM season. The geostrophic currents during JJAS have been computed from the SLA and used to understand the circulation pattern. The mean SLA superimposed with geostrophic currents shows the current flow into the southcentral Bay. Also the cyclonic eddy to the east of Sri Lanka and the anticyclonic eddy adjacent to it are observed in the SLA map.

In geostrophic current, the pressure gradient force is balanced by Coriolis force. The  $u$  and  $v$  components of the geostrophic equation are:

$$fu = -\frac{1}{\rho_0} \frac{\partial P}{\partial y} \quad \text{----- (2.10)}$$

$$fv = \frac{1}{\rho_0} \frac{\partial P}{\partial x} \quad \text{----- (2.11)}$$

where  $P$  is the pressure,  $u$  and  $v$  are the geostrophic velocities,  $\rho_0 = 1027 \text{ kg m}^{-3}$  is the density of water,  $f = 2\Omega \sin(\phi)$  is the Coriolis force,  $\Omega$  is the angular speed of earth ( $7.292 \times 10^{-5} \text{ rad s}^{-1}$ ) and  $\phi$  is a latitude on the earth's surface.

At the surface  $P = \rho_0 g \eta$  ----- (2.12)

where  $\eta$  is the sea surface height and  $g = 9.8 \text{ m s}^{-2}$  is the acceleration due to gravity

The  $u$  and  $v$  components of the surface geostrophic current are given by:

$$u = \frac{-g}{f} \frac{\partial \eta}{\partial y} \text{ ----- (2.13)}$$

$$v = \frac{g}{f} \frac{\partial \eta}{\partial x} \text{ ----- (2.14)}$$

where  $f = 2\Omega \sin(\phi)$  is the Coriolis force,  $\Omega$  is the angular speed of earth ( $7.292 \times 10^{-5} \text{ rad s}^{-1}$ ) and  $\phi$  is a latitude on the earth's surface.

The inter-annual variations in the extent of cold pool during SWM season have been studied with the help of monthly TMI SST and the results explained in Chapter 4. The mean wind stress is strong in the central and southcentral BoB during SWM season. The Ekman vertical velocity (VV) caused by the horizontal convergences and divergences of the Ekman transport has been computed from monthly WSC climatology for May to October and analysed in these two regions of strong stress in the BoB. Monthly mean geostrophic currents have been computed from SLA from May to October for these two regions which experience strong wind stress during SWM season. Geostrophic currents have been superimposed on SLA and analysed in the regions of strong wind stress.

#### 2.4.4. Computation of Ekman vertical velocity

In Chapter 4, VV has been computed from the monthly WSC climatology in the BoB. In Chapter 5, VV computations have been carried out using the monthly WSC data.

The Ekman pumping velocity  $w_e$  is calculated from Smith (1968) as,

$$w_e = \frac{1}{\rho_0 f} \nabla \times \tau \text{ ----- (2.15)}$$

(unit -  $\text{m s}^{-1}$ ), where  $\tau$  is the wind stress in  $\text{N m}^{-2}$ ,  $\rho_0 = 1027 \text{ kg m}^{-3}$  is the density of sea water, and  $f$  is the Coriolis force given by  $2 \Omega \sin(\phi)$  where  $\Omega$  is the angular speed of the earth ( $7.292 \times 10^{-5} \text{ rad s}^{-1}$ ) and  $\phi$  is a latitude on the earth's surface.

#### **2.4.5. Analysis of depth of 20°C isotherm (D20) and surface chl-*a* concentration**

Chapter 5 deals with the upwelling and its significance in relation to chl-*a* distribution in the BoB. Since the 20°C isotherm is located near the center of the main thermocline, it is used to represent the depth of thermocline in the ocean. In order to understand the sub-surface oceanographic thermal structure, the monthly variability of depth of 20°C isotherms (D20) is analyzed using water temperature data by Ishii *et al.* (2006). The upliftment of 20°C isotherms is considered to be the subsurface signature of upwelling. Based on prominent annual signatures of D20, four areas were considered for further study. Comparison of monthly variations of D20 indices is carried out with VV, SLA, and chl-*a* indices and the correlation coefficients have been computed. The seasonal and inter-annual variation in chl-*a* distribution has also been analysed and explained in Chapter 5. The relationship of chl-*a* concentration with VV and SLA has been examined for the selected regions and the correlation coefficients computed.

#### **2.4.6. Tropical cyclone studies**

In Chapter 6, the effect of tropical cyclones on physical and biological processes in the BoB has been studied. BoB has low biological productivity compared to the Arabian Sea. Passage of intense tropical cyclones cause marked cooling of SST together with an increase in chl-*a* concentrations in the upper ocean (Lin *et al.*, 2003). Intense wind stress on the ocean surface leads to the deepening of mixed layer (Black, 1983), and the entrainment of nutrient rich waters to the surface. The changes in SST, chl-*a* concentration and PP caused by tropical cyclones have been analysed for two cases of intense tropical cyclones in the BoB, one during November-December 2000 (pre-monsoon season) and the other during May 2003 (post-monsoon season). During November-December 2000 the very severe cyclonic storm

(VSCS) with a maximum wind speed of 102 kts developed in the southeastern BoB, moved westward and crossed the coast near Cuddalore. It emerged into the eastern Arabian Sea and weakened later. During May 2003 the VSCS with a maximum wind speed of 75 kts occurred in the central Bay. It moved northeastward and made the landfall in Burma coast.

For the VSCS in November-December 2000, the study has been carried out using 8 day composite SST and chl-*a* concentration from Terra MODIS and modeled PP (P2). Merged daily SLA from altimeter observations are also used to study about SSH variation. The altimeter values are point observations along the altimeter sub satellite tracks. For the 10 day composite SLA, the daily observations were interpolated to  $0.5^\circ \times 0.5^\circ$  spatial resolution using the Cressman scheme (Cressman, 1959). For the May 2003 VSCS, 8 day composite SST (from Terra MODIS and TMI), chl-*a* from Terra MODIS, modeled PP (P2) and MLD has been used. Difference in SST and chl-*a* concentration after the tropical cyclone is also calculated.

## Chapter 3

# Distribution of some physical and biological properties in the Bay of Bengal

### 3.1. Introduction

The spatial and temporal distributions of some physical and biological parameters in the BoB are analysed in this Chapter. The properties analysed are WSC, SST, SLA and surface chl-*a* concentration. The WSC has an important role in the generation of large scale oceanic currents or gyres and has large seasonal variability in the Indian Ocean (Rao, 2002). WSC causes divergence or convergence of the surface water that brings about vertical transport in the surface boundary layer of the ocean, known as Ekman pumping. Positive (negative) WSC cause divergence (convergence) in the Ekman layer and upward (downward) Ekman pumping leading to upwelling (downwelling). SST plays a major role in air-sea interaction processes over the tropical oceans. A dipole mode exists in the Indian Ocean characterized by warm SST anomalies in the western Indian Ocean and cold SST anomalies in the eastern Indian Ocean in its positive phase (Saji *et al.*, 1999). SST variability is associated with large-scale climate patterns such as La Nina and El Nino cycles in the equatorial Pacific. Satellite measurement of SST is useful in the identification of upwelling regions, delineation of ocean fronts, currents, and ocean eddies. SLA has applications in the study of mesoscale ocean properties and their variability. These include seasonal and long term variability of sea level, geostrophic flow, Rossby wave propagation and identification of eddies. Cyclonic (anticyclonic) eddies cause a decrease (increase) in sea level and elevations (depressions) in subsurface density surfaces. Eddy pumping associated with cyclonic eddies upwell nutrients and cause increased PP in the ocean surface (Falkowski *et al.*, 1991). Identification of ocean eddies in SLA data is feasible with these characteristics, where anticyclonic eddies are evident in the form of closed-contour positive SLA, while cyclonic eddies are

observed as closed-contour negative SLA (Faghmous *et al.*, 2015). Seasonal to inter-annual changes in phytoplankton biomass and productivity forms an important part of the total variability associated with ocean biological and biogeochemical processes (Yoder and Kennelly, 2003). Chl-*a* is the most important pigment involved in phytoplankton photosynthesis, and its concentration has been used as a proxy for phytoplankton biomass and photosynthetic potential for many decades (e.g. Ryther and Yentsch, 1957). Since chl-*a* is the only photosynthetic pigment that occurs in all phytoplankton, it provides a measure of phytoplankton abundance and biomass. The analysis of these four variables carried out in this Chapter is based on both the seasonal and monthly climatology of eight-year monthly mean data from 2000 to 2007. The four seasons taken into consideration are 1) Dec-Feb (DJF), 2) Mar-May (MAM), 3) Jun-Sep (JJAS) and 4) Oct-Nov (ON) during which the wind structure over the BoB undergoes considerable variations.

### **3.2. Spatial distribution of wind stress curl**

#### **3.2.1. Seasonal mean distribution of wind stress curl**

The seasonal variations in the spatial distribution of WSC over the BoB are analysed in this Section. Major seasonal features of WSC over the BoB, which undergoes seasonal reversal of the wind patterns, are presented in Fig. 3.1. During DJF, BoB comes under the influence of NEM and winds are northeasterly over the Bay (Vinayachandran *et al.*, 1996). At this time, weak negative (anticyclonic) WSC prevails over the BoB except for regions south of 10°N over the western side to nearly 7°N over the eastern side of the Bay. Over the northwestern Bay WSC is around  $-1 \times 10^{-7} \text{ N m}^{-3}$ . The maximum value of positive (cyclonic) WSC of  $\sim 2.5 \times 10^{-7} \text{ N m}^{-3}$  is observed near Sumatra Islands. It weakens during pre-monsoon season MAM and the positive maximum ( $1.5 \times 10^{-7} \text{ N m}^{-3}$ ) shifts to the eastern side of Sri Lanka. It is caused by the change in wind direction by the end of May when the winds start shifting to southwesterly as the SWM approaches. Also, negative (anticyclonic) WSC over the northern Bay increases to  $-1.5 \times 10^{-7} \text{ N m}^{-3}$  during this time.

BoB is influenced by the SWM winds during JJAS. The positive (cyclonic) WSC over the southwestern Bay increases to a maximum of  $4 \times 10^{-7} \text{ N m}^{-3}$  to the east of Sri Lanka near  $7.5^\circ\text{N}$  which is favourable for upwelling. Positive (cyclonic) WSC causes upward Ekman pumping and upwelling in the southwestern BoB (Vinayachandran and Mathew, 2003). Negative (anticyclonic) WSC over the northern Bay is replaced by comparatively high positive (cyclonic) WSC with a maximum of  $2 \times 10^{-7} \text{ N m}^{-3}$  over the northernmost region. Positive (cyclonic) WSC extends over the western Bay southward to  $11^\circ\text{N}$  during this season. South of  $16^\circ\text{N}$  on the eastern side, the BoB is under the influence of negative (anticyclonic) WSC and has a maximum ( $-3 \times 10^{-7} \text{ N m}^{-3}$ ) near the Malacca strait.

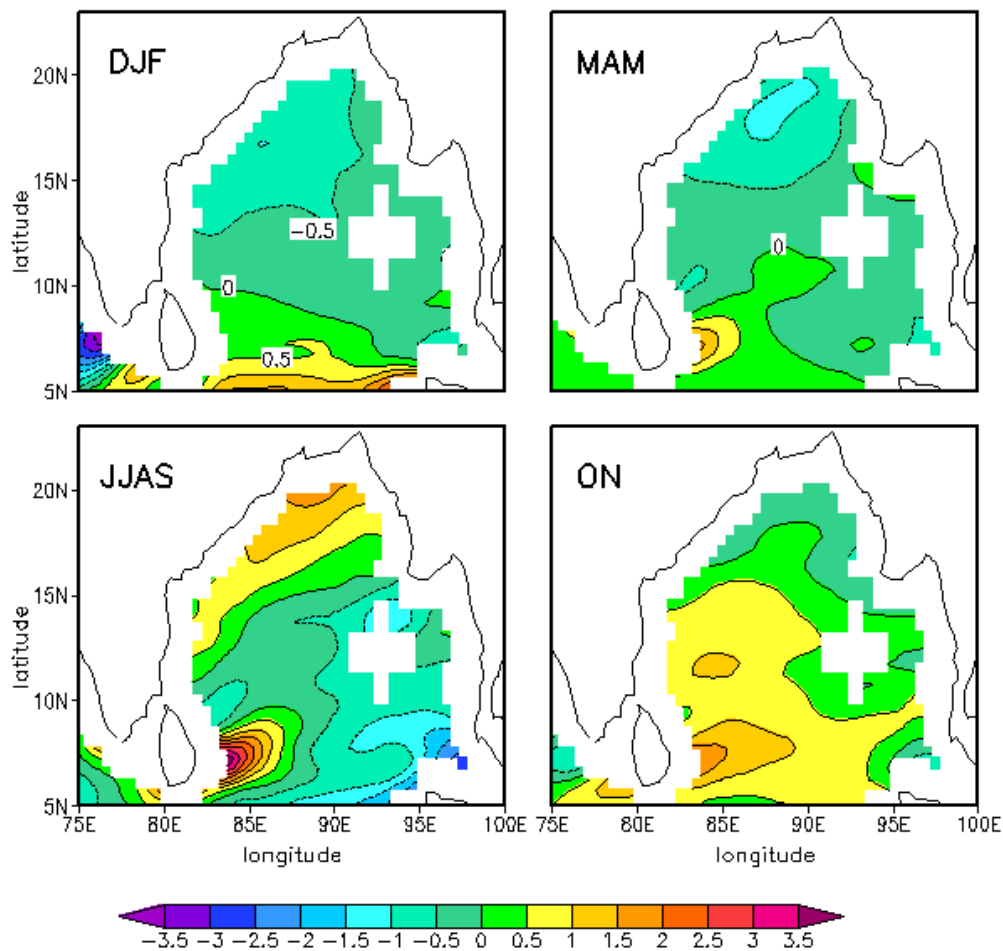


Fig. 3.1 Seasonal mean wind stress curl ( $\times 10^{-7} \text{ N m}^{-3}$ ) during a) Dec- Feb (DJF), b) Mar-May (MAM), c) Jun-Sep (JJAS), and d) Oct-Nov (ON) over the Bay of Bengal. Dashed lines indicate negative wind stress curl.

During ON, positive (cyclonic) WSC dominates the Bay and the negative values south of 15°N are replaced by positive (cyclonic) WSC. Over the eastern side of Sri Lanka, positive (cyclonic) WSC weakens to nearly  $2 \times 10^{-7} \text{ N m}^{-3}$  and over the northern Bay positive (cyclonic) WSC is replaced by weak negative (anticyclonic) WSC. WSC is mostly positive (cyclonic) off the southern tip of India during all the four seasons.

### **3.2.2. Monthly mean distribution of wind stress curl**

The spatial distribution of WSC over the BoB has been analysed using the monthly climatology of WSC illustrated in Fig. 3.2. In general from January to April and during December, the WSC is observed to be weak negative (anticyclonic) over the northern and central Bay and positive (cyclonic) over the southern Bay. The positive (cyclonic) WSC in the southern Bay is high during December and January with a maximum of  $2.5 \times 10^{-7} \text{ N m}^{-3}$  that decreases afterwards. In January and February, the negative (anticyclonic) WSC prevails over the BoB north of 8°N. An increase to  $\sim -1.5 \times 10^{-7} \text{ N m}^{-3}$  is observed over the head of the Bay in February, which extends over a larger area by March. Also by March, positive (cyclonic) WSC over the southern Bay extends northward up to 11°N on the eastern side. March and April are the transition period between the monsoons, and winds are weakest at these times (Shetye and Gouveia, 1998). During April, the negative (anticyclonic) WSC over the northern BoB increases to nearly  $-2.5 \times 10^{-7} \text{ N m}^{-3}$ , together with an increase in the positive values over the southwestern Bay. During May, positive (cyclonic) WSC over the eastern side of Sri Lanka strengthens to  $3.5 \times 10^{-7} \text{ N m}^{-3}$  and extends in a northeast direction caused by the shifting of wind to southwesterlies. Negative (anticyclonic) WSC over the northern Bay weakens when positive (cyclonic) WSC extends to the northern Bay from the south. At the same time negative (anticyclonic) WSC appears over the southern Bay, extending from south of Sri Lanka to 12°N over the eastern BoB with a maximum of  $-3 \times 10^{-7} \text{ N m}^{-3}$  over Malacca strait.

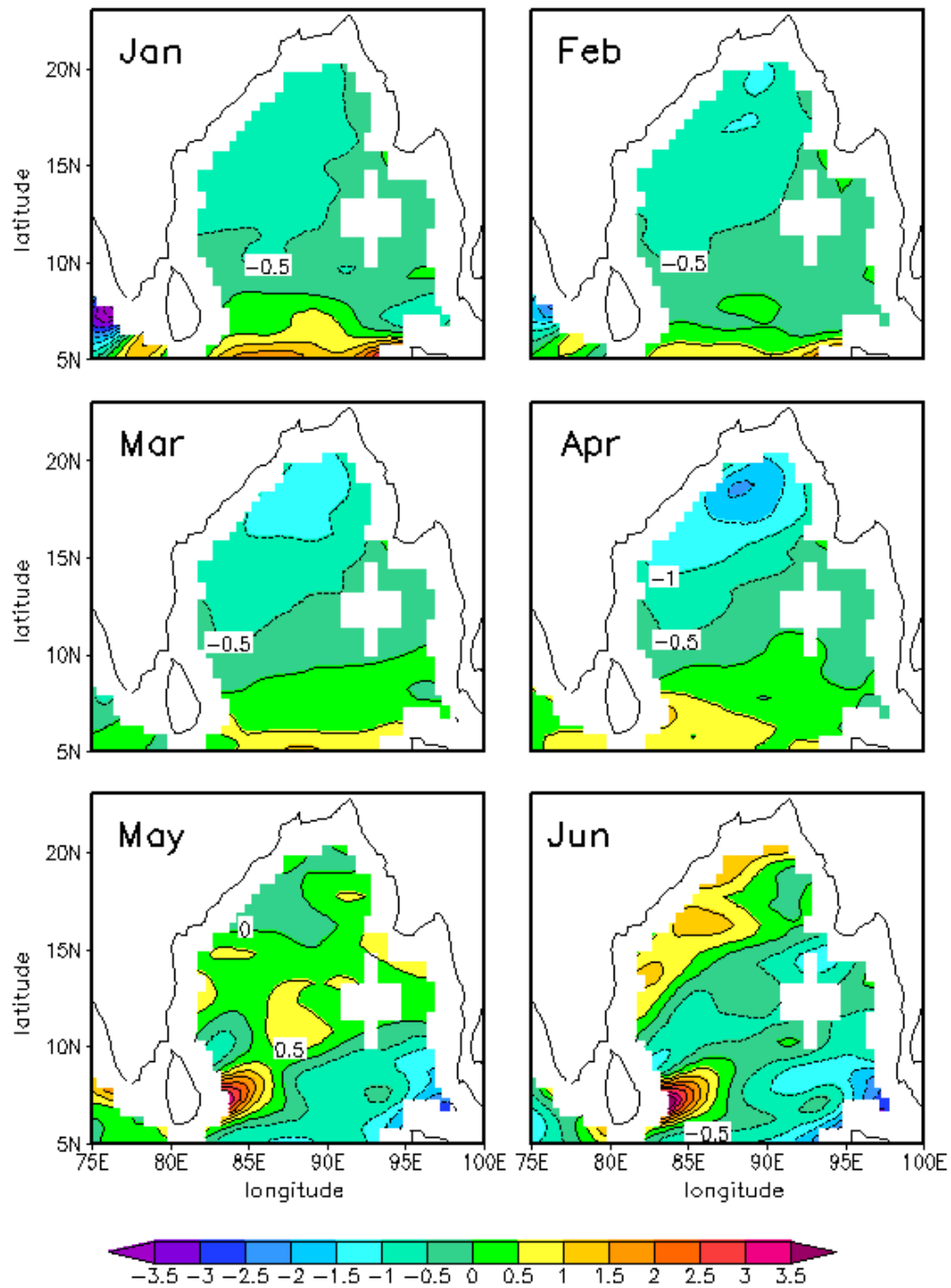


Fig. 3.2 Monthly climatology of wind stress curl ( $\times 10^{-7} \text{ N m}^{-3}$ ) over the Bay of Bengal. Dashed lines indicate negative wind stress curl

Continued...

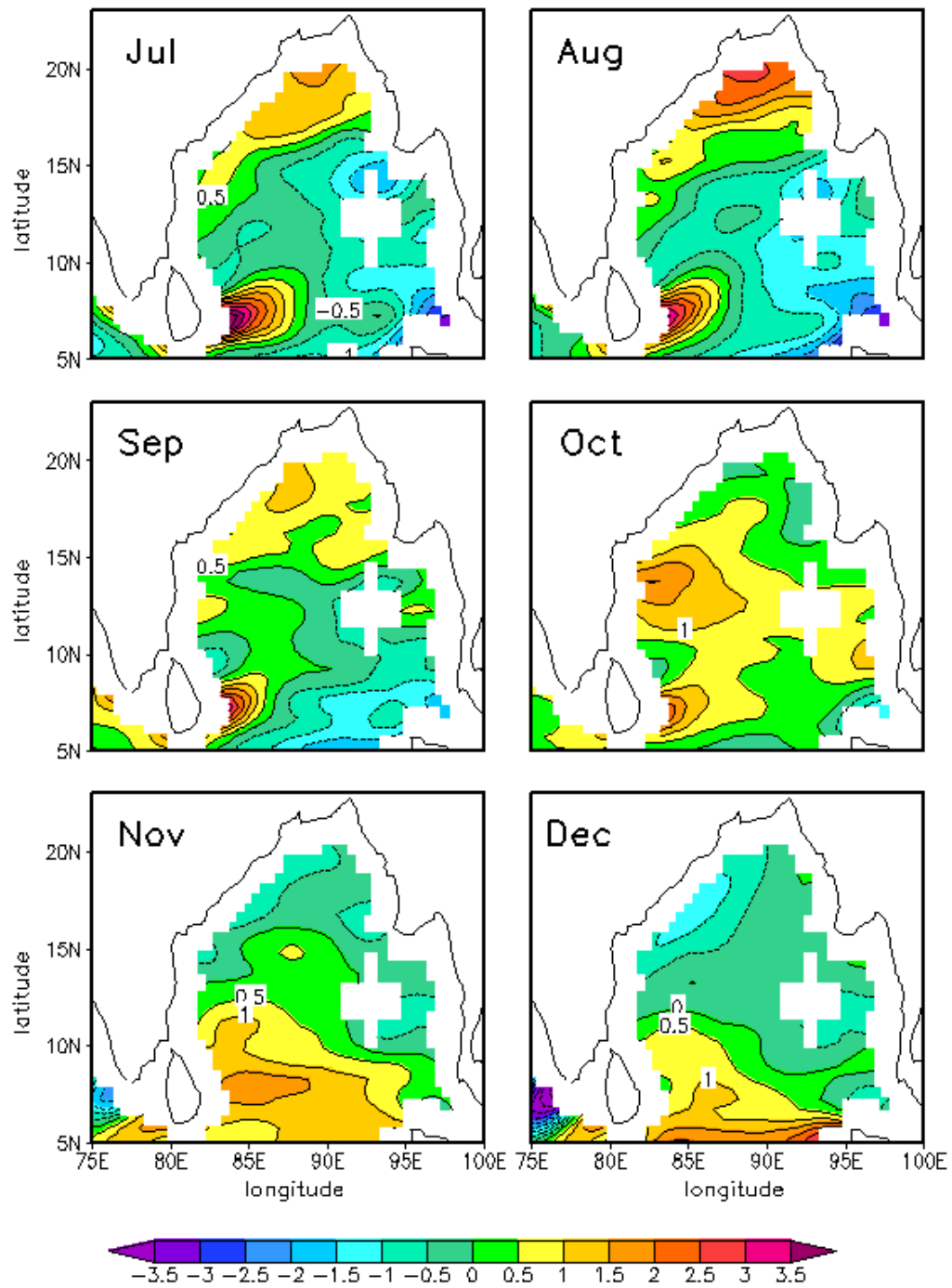


Fig. 3.2 Monthly climatology of wind stress curl ( $\times 10^{-7} \text{ N m}^{-3}$ ) over the Bay of Bengal. Dashed lines indicate negative wind stress curl.

In the BoB the southwesterlies strengthen during June, reach their peak during Jul-Aug, start decaying during September and vanish by October (Vinayachandran *et al.*, 1996). By the onset of SWM during June, the band of positive (cyclonic) WSC move northwestwards and lie over the northern and western BoB with a magnitude of approximately  $1.5 \times 10^{-7} \text{ N m}^{-3}$ . During the SWM season, positive (cyclonic) WSC prevails over the north and western Bay whereas negative (anticyclonic) WSC is observed over the central and southern Bay. In June, negative (anticyclonic) WSC over the south extends northward to  $16^{\circ}\text{N}$  over the central and eastern BoB. Positive (cyclonic) WSC over the northern Bay increases as the monsoon advances and reaches a high of  $\sim 3 \times 10^{-7} \text{ N m}^{-3}$  in August and thereafter decreases. Similarly negative values in the south increase to  $-3.5 \times 10^{-7} \text{ N m}^{-3}$  over the Malacca strait and to  $-2 \times 10^{-7} \text{ N m}^{-3}$  to the north of Andaman Islands in July, remains during August and thereafter decreases. The positive (cyclonic) WSC to the east of Sri Lanka increases as the monsoon advances and attains the maximum value of  $4.5 \times 10^{-7} \text{ N m}^{-3}$  during July and after that gradually decreases. This patch of positive (cyclonic) WSC extends up to  $10^{\circ}\text{N}$  in August, supporting upwelling in this region. Vinayachandran and Mathew (2003) have shown that positive (cyclonic) WSC cause upward Ekman pumping and upwelling in the BoB. By September, positive (cyclonic) WSC over the northern Bay decreases to  $1.5 \times 10^{-7} \text{ N m}^{-3}$  and over east of Sri Lanka to  $3 \times 10^{-7} \text{ N m}^{-3}$  with the withdrawal of SWM.

October is also a transition period between the monsoons, and winds are weak during this period (Shetye and Gouveia, 1998). During October, the BoB is dominated by positive (cyclonic) WSC and the negative (anticyclonic) WSC almost disappears from the BoB except for small patches near Sri Lanka, over Malacca strait and the southern Bay. Weak negative (anticyclonic) WSC appear over north and northwestern Bay replacing positive values of WSC and positive (cyclonic) WSC decreases to the east of Sri Lanka to below  $2.5 \times 10^{-7} \text{ N m}^{-3}$ . Positive (cyclonic) WSC of nearly  $2 \times 10^{-7} \text{ N m}^{-3}$  is observed over the west-central Bay which is replaced by weak negative (anticyclonic) WSC in November. Vinayachandran and Yamagata (1998) have documented the formation of a cyclonic gyre in this region by September which lasted till January. By the beginning of NEM in November, weak

negative (anticyclonic) WSC replaces positive values of WSC over the north, northwestern Bay and Andaman Sea. Over the central Bay positive (cyclonic) WSC decreases and is replaced by negative values of WSC in December. Also over the southern Bay an increase of positive (cyclonic) WSC is observed during November. The northwesterlies over the BoB reach their peak during December (Vinayachandran *et al.*, 1996), and the negative (anticyclonic) WSC over the northwestern Bay strengthens to  $-1.5 \times 10^{-7} \text{ N m}^{-3}$ . Positive (cyclonic) WSC reaches a maximum of  $3 \times 10^{-7} \text{ N m}^{-3}$  to the west of Sumatra. Off the southern tip of India WSC is positive (cyclonic) during all the months except in Jun-Aug.

### **3.3. Spatial distribution of sea surface temperature**

#### **3.3.1. Seasonal mean distribution of sea surface temperature**

The seasonal features of SST of the BoB are analysed in this section based on the seasonal mean of eight years from 2000 to 2007 (Fig. 3.3). During DJF, BoB experiences the maximum latitudinal variation in SST. The mean SST of the northern Bay ( $24^{\circ}\text{C}$ ) is the lowest amongst all the seasons. SST gradually increases towards southern and southeastern Bay. Maximum SST of about  $30^{\circ}\text{C}$  is observed in the Malacca strait. Off the southern tip of India, a cold pool is observed where the SST varies from  $27.5^{\circ}$  to  $28^{\circ}\text{C}$ . Luis and Kawamura (2000, 2001 & 2002) inferred that the wintertime SST cooling in the vicinity of the tip is a case of topography-monsoon-ocean interaction. During MAM, when the wind is weak and variable (Shetye and Gouveia, 1998), SST of the BoB increases abruptly and the latitudinal variation is minimum. SST is within the range  $29\text{-}30^{\circ}\text{C}$  in most parts of the Bay and the lowest SST (about  $28.5\text{-}29^{\circ}\text{C}$ ) is observed in the northern Bay, away from the coast. During this season, SST increases by  $4\text{-}5^{\circ}\text{C}$  in the northern Bay. The cooling off the southern tip of India ceases; and the Malacca strait and the eastern Andaman Sea experience the highest SST of more than  $30^{\circ}\text{C}$ .

.During JJAS, the spatial distribution of SST undergoes considerable change. An overall decrease in SST is observed with the occurrence of the mini cold pool off the southern tip of India where SST is  $26.5^{\circ}\text{C}$ . The cooler water from this region extends

to the south-central Bay up to 8°N, forming a cold pool where SST is in the range of 28-28.5°C. The mini cold pool has been well documented by Rao *et al.* (2006a), and has been attributed to the upwelling caused by the divergence in the near-surface circulation. Also the intrusion of this cooler upwelled water to the south-central Bay has been associated with the SMC that flows eastward south of Sri Lanka and then northeastward into the south-central BoB. The cold pool decays after September due to the arrival of a long Rossby wave, associated with the reflection of the spring Wyrki jet at the eastern boundary of the ocean (Vinayachandran and Yamagata, 1998). In the western and northern Bay, and to the east of Sri Lanka, SST is about 29-30°C. In the central Bay and Andaman Sea SST is 28.5-29°C. High SST (30°C) persists in Malacca strait during JJAS and ON.

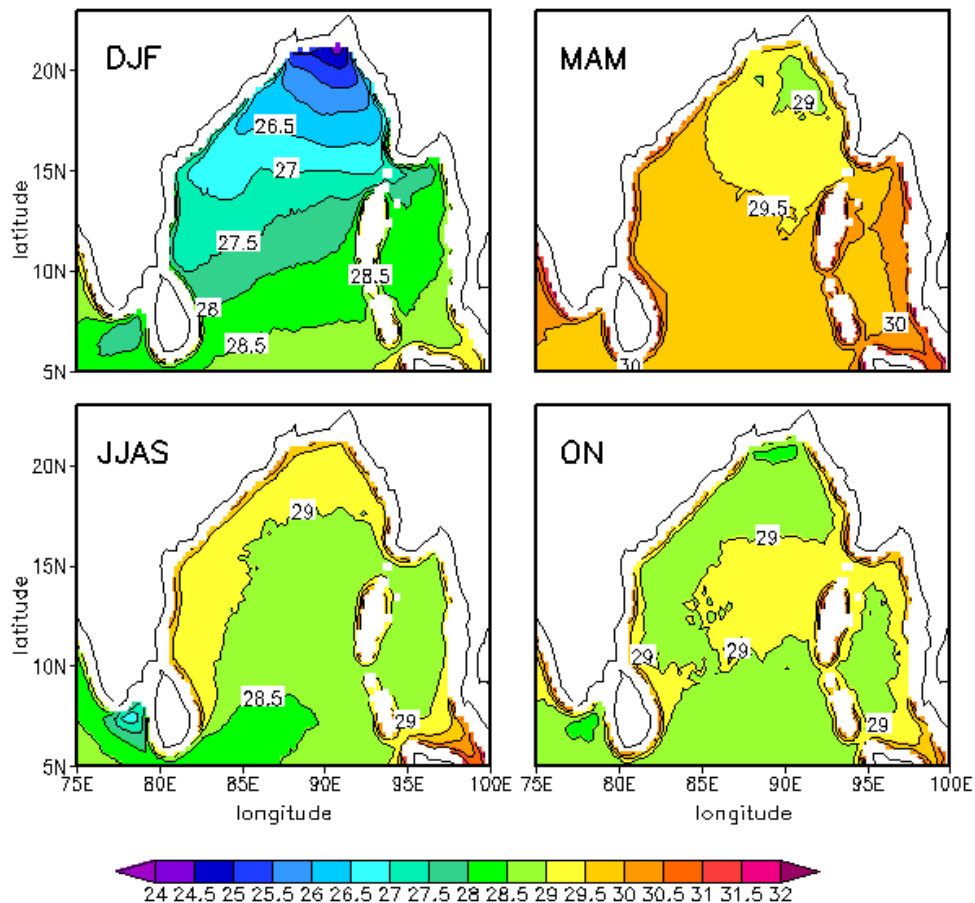


Fig. 3.3 Seasonal mean sea surface temperature (°C) during a) Dec-Feb (DJF), b) Mar-May (MAM), c) Jun-Sep (JJAS), and d) Oct-Nov (ON) of the Bay of Bengal.

The winds over the BoB weaken and the latitudinal variation in SST is less during ON. SST off the southern tip of India increases to about 28°C during ON, while a decrease is observed in the northern (28°C) and western Bay. In the central Bay extending to the western Andaman Sea, a pool of high SST (29-29.5°C) is observed during this time.

### **3.3.2. Monthly mean distribution of sea surface temperature**

Variations in the spatial distribution of SST in the BoB have been studied using the monthly climatology of SST, as illustrated in Fig. 3.4. During Dec-Feb, the spatial distribution of SST of the BoB shows little variability. The lowest temperature is observed in the head Bay, increasing gradually towards south and SST is highest in the Malacca Strait. During January, the BoB experiences the lowest SST (~23°C) of the year in the northern Bay: it gradually increases towards the south and southeast, reaching 29.5°C in Malacca strait. Slight cooling (27°C) is observed off the southern tip of India which diminishes by February. This cooling has been reported by Luis and Kawamura (2000 & 2001). SST distribution is similar during February with a slight increase in the entire Bay. By March when the winds over the Bay become weak (Shetye and Gouveia, 1998), there is an overall warming and the SST increases to 27°C in the north and northeastern Bay. In the southern Bay and Andaman Sea SST is 29-30°C, and in the Malacca strait an SST high of 30.5°C is observed. During April when the winds remain weak, SST of the BoB increases significantly to 29-31.5°C. The SST is 29-29.5°C in the northern Bay, and south of 15°N it is 30-30.5°C increasing further in the eastern Andaman Sea. In the Malacca strait, SST increases to nearly 31.5°C and remains high till July. SST remains high during May in the BoB with a latitudinal reversal in its spatial distribution. High SST (30.5-31°C) is observed along the western Bay and the lowest SST (29-29.5°C) is observed off the southern tip of India and in the south-central Bay, which develops into a cold pool during the SWM season. This cold pool has been studied in detail by Joseph *et al.* (2005). Vinayachandran and Yamagata (1998) suggested that the cold dome develops during the SWM in response to cyclonic curl in the local wind field. The

upward Ekman pumping induced by this cyclonic curl brings cooler water to the near-surface layers.

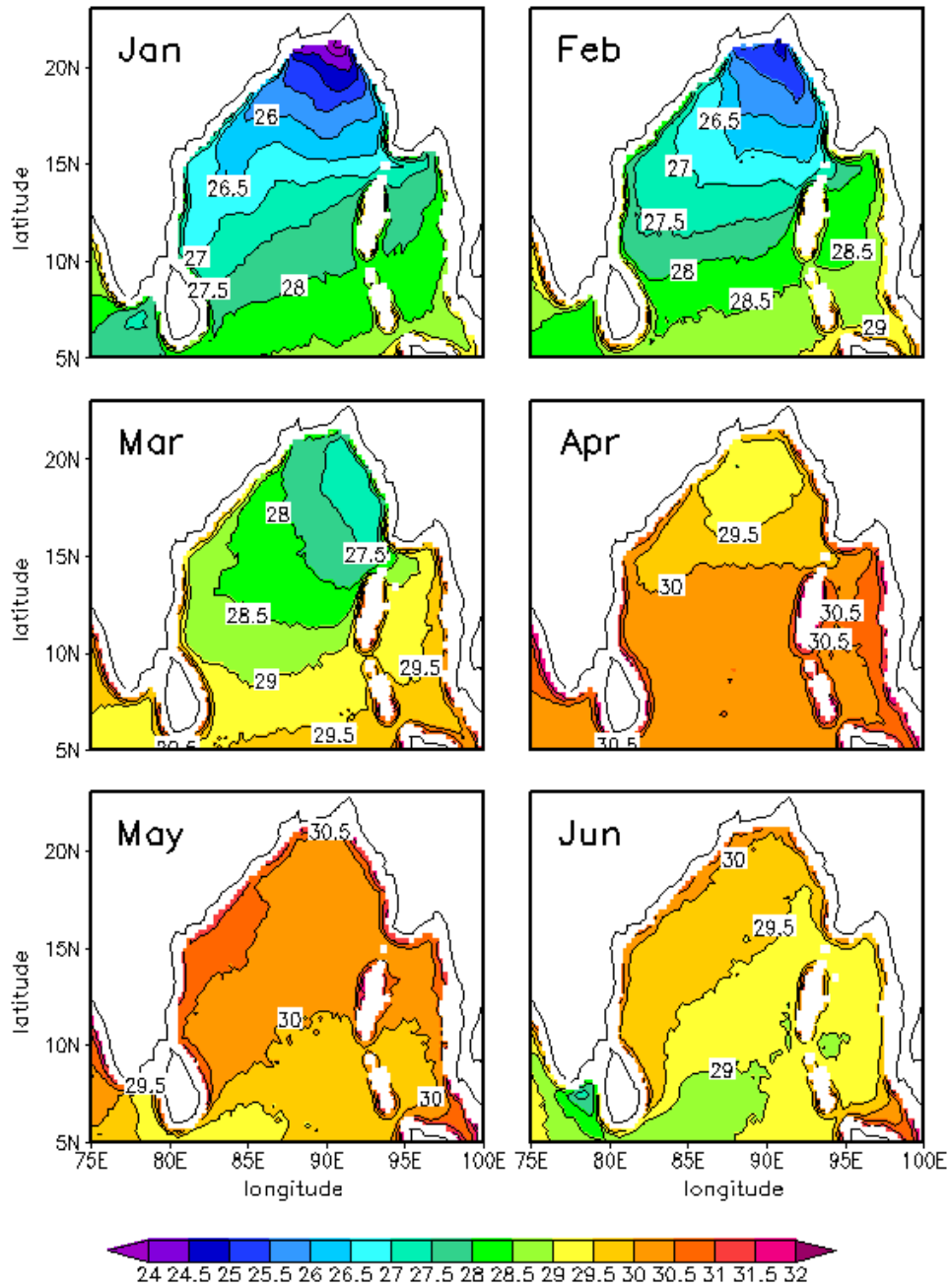


Fig. 3.4 Monthly climatology of sea surface temperature (°C) of the Bay of Bengal

Continued...

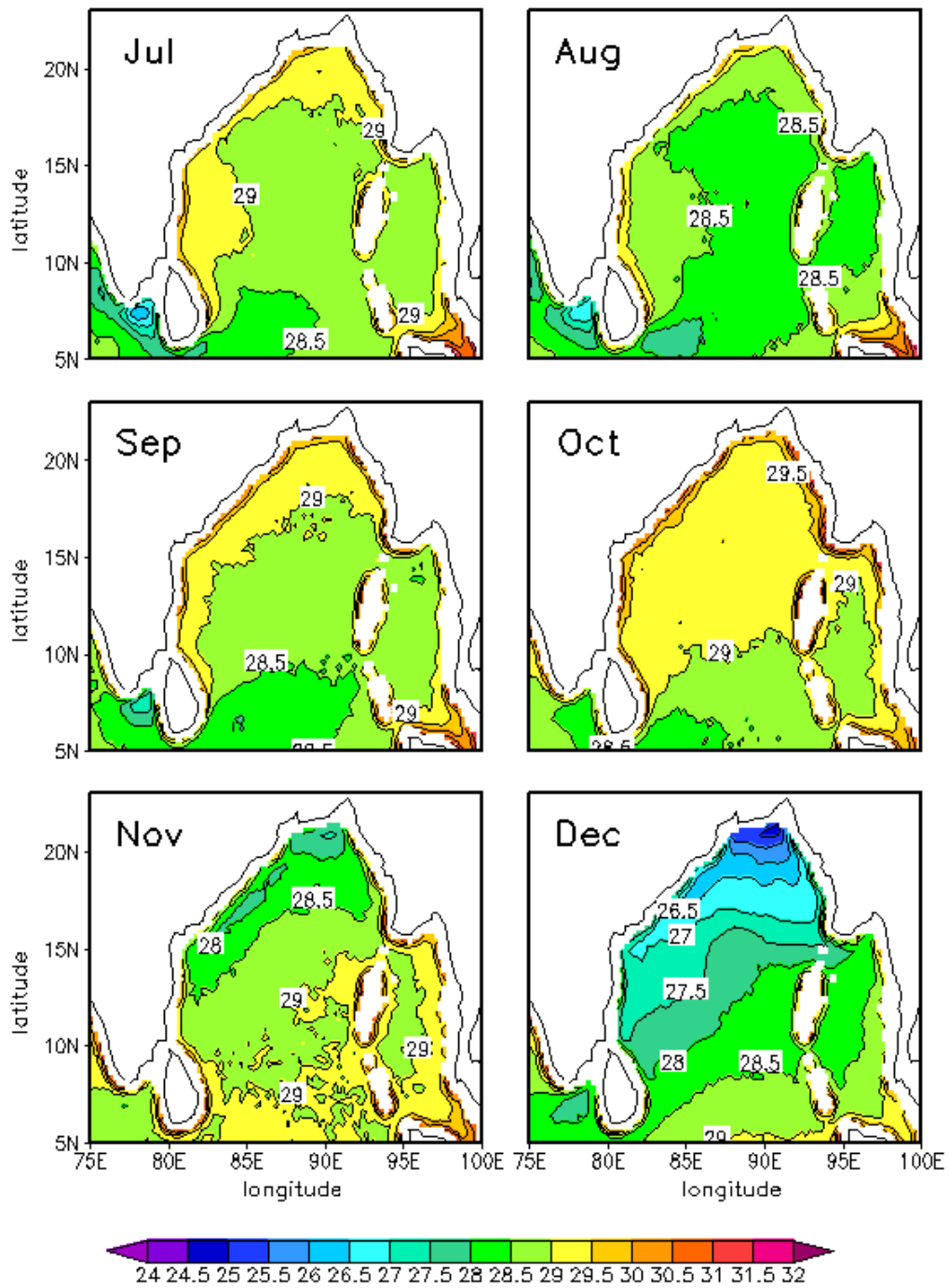


Fig. 3.4 Monthly climatology of sea surface temperature ( $^{\circ}$ C) of the Bay of Bengal

With the onset of SWM in June, SST of the BoB decreases. Off the southern tip of India a mini cold pool forms where SST is about 27°C. The cooler water advect eastward south of Sri Lanka and northward up to 9°N into the south-central Bay, forming a cold pool where SST varies between 28.5°C and 29°C. According to Rao *et al.* (2006a) the mini cold pool off the southern tip of India is driven by the upwelling caused by the divergence in the near-surface circulation. A cold pool is also observed in the Andaman Bay which seems to be an extension of the cold pool in the south-central Bay. As the monsoon progresses SST of the Bay decreases. During July, SST of the mini cold pool off the southern tip of India decreases to 26°C, which is the lowest temperature of the year in that region, while SST of the cold pool in the south-central Bay decreases by 0.5°C. As the monsoon progresses, intrusion of cooler water from the mini cold pool by the SMC causes a reduction in SST of the south-central Bay (Rao *et al.*, 2006a). SST is 29-30°C in the western and northern Bay. Slight cooling is observed in the Malacca strait during July which persists till December. During August, SST of the BoB further decreases by 0.5°C, and it is about 27.5-28°C in the south-central Bay, while an increase of 0.5°C is observed in the mini cold pool. SST of BoB increases during September as SWM weakens and its spatial distribution is similar to that during July. Also SST in the cold pool off the southern tip of India increases to 27°C. The decay of cold pool has been attributed to the arrival of a long Rossby wave (Vinayachandran and Yamagata, 1998).

The SST of the BoB further increases after the SWM withdraws. Along the coasts SST increase to 30.5°C and open ocean and Andaman sea experience an SST of 28.5-29.5°C during October. In November, SST shows a latitudinal variation in the BoB with low SST in the north and high SST in the south. In the north, SST drops by 2°C and cooler water of 27.5-28°C is observed along the north and northwestern Bay. SST increases to 29-29.5°C southwards and eastward in the BoB. The cold pool in the south-central Bay and off the southern tip of India disappears during November. During December, SST decreases significantly and its distribution is similar to that during January. SST drops by 3°C to nearly 24.5°C in the northern Bay, and also a slight decrease occurs in the Malacca strait. In the southern Bay SST is in the range

of 28.5-29°C, and off the southern tip of India a slight cooling (~27.5°C) is observed. According to Luis and Kawamura (2001) this SST cooling during the NEM is locally influenced by surface forcing in and offshore of the Gulf of Mannar.

### **3.4. Spatial distribution of sea level anomaly**

#### **3.4.1. Seasonal mean distribution of sea level anomaly**

The spatial distribution of SLA during different seasons in the BoB are analysed based on eight year merged data from 2000 to 2007 (Fig. 3.5). During DJF, a cyclonic eddy is observed in the western BoB indicating divergence and hence upwelling; also negative SLA is observed along the northern, eastern and southern BoB. Positive SLA is observed in the central and southwestern Bay. A strong anticyclonic eddy is observed in the northern Bay while a weak anticyclonic eddy is observed in the southwestern Bay during this season. During MAM, cyclonic eddy in the western Bay is replaced by a large anticyclonic eddy which had been documented by Shetye *et al.* (1993). In the regions near the Malacca strait, negative SLA is replaced by positive SLA. Also the negative SLA near the north and northeastern coasts weakens during this season.

During JJAS, negative SLA prevails to the west of 88°E while it is positive to the east and north. The anticyclonic eddy in the western Bay during MAM becomes weak during this period. Two cyclonic eddies are observed during the SWM season: one in the northwestern Bay and the other in the southwestern Bay. Also SLA becomes negative off the southern tip of India. The cyclonic eddy to the east of Sri Lanka develops due to the open ocean Ekman pumping (Vinayachandran and Yamagata, 1998). Sea level is high along the northern BoB and in Martaban Bay during JJAS. During ON, the cyclonic eddy in the northwestern Bay intensifies together with the formation of another cyclonic eddy in the western Bay. The existence of the cyclonic eddy in the northwestern Bay forced by Ekman pumping has been reported by Vinayachandran and Yamagata (1998). All along the coast, positive SLA is observed during this time. Off the southern tip of India, SLA

becomes positive again. In the Palk Strait high positive SLA is observed during ON and DJF.

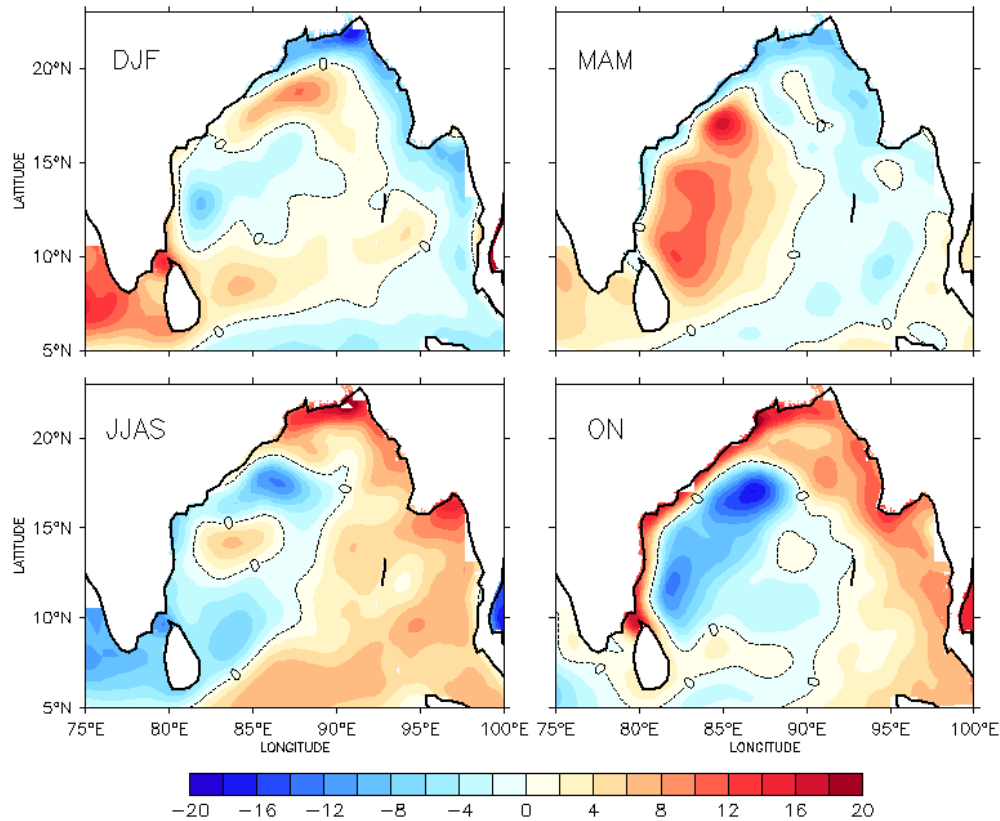


Fig. 3.5 Seasonal mean sea level anomaly (cm) during a) Dec- Feb (DJF), b) Mar-May (MAM), c) Jun-Sep (JJAS), and d) Oct-Nov (ON) in the Bay of Bengal.

### 3.4.2. Monthly mean distribution of sea level anomaly

SLA variations in the BoB have been analysed using monthly climatology data (Fig. 3.6). In January, the central BoB is dominated by positive SLA. Also SLA is positive to the south of India. A large anticyclonic eddy is observed in the northern Bay during January. SLA is negative in the north and also in the eastern and southern Bay. A cyclonic eddy is observed in the western Bay near 12°N. During February, the eastern Bay is dominated by negative SLA and western Bay by positive SLA. The existing anticyclonic eddies in the northwestern and southwestern Bay develops

further during this time. The negative SLA is high along the coast in the north and northeastern BoB during February and March. The distribution pattern of SLA remains the same during Feb-Mar. In April, there is an overall decrease in the negative SLA in the BoB. The anticyclonic eddy in the southwestern Bay strengthens during this time. The entire Bay is dominated by positive SLA during May except for a cyclonic eddy in the northwestern Bay around 18°N. The anticyclonic eddy in the western BoB which lies to the south of cyclonic eddy develops further during this time.

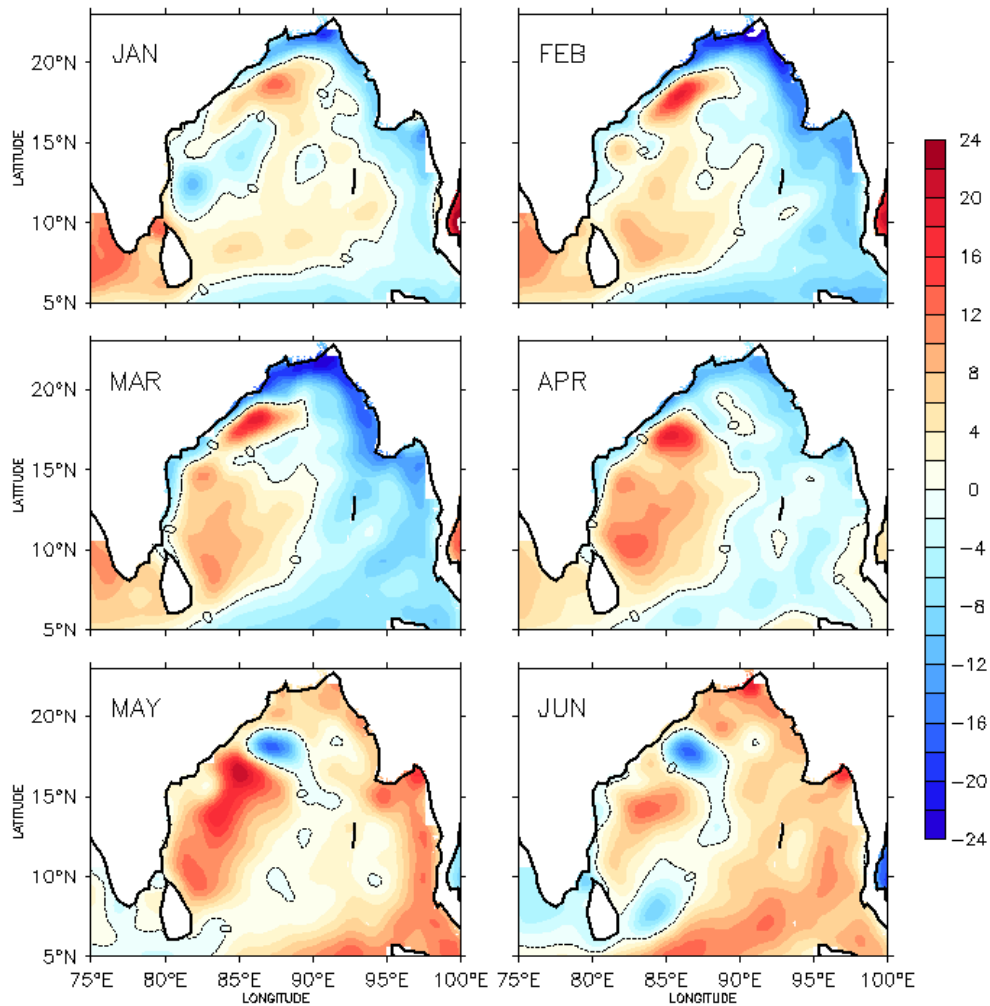


Fig. 3.6 Monthly climatology of sea level anomaly (cm) in the Bay of Bengal

Continued...

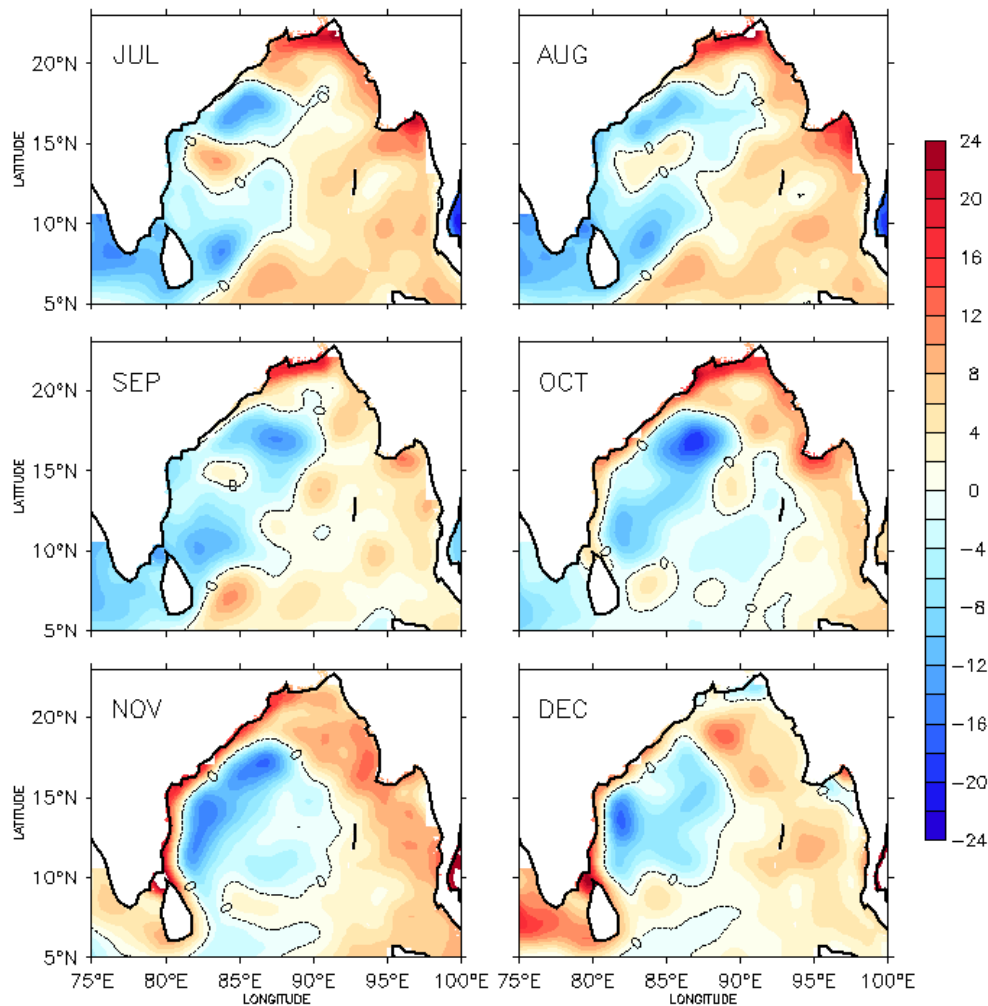


Fig. 3.6 Monthly climatology of sea level anomaly (cm) in the Bay of Bengal

In June, with the onset of SWM season the anticyclonic eddy in the western Bay weakens while in the southern Bay, weak anticyclonic eddies develop. A cyclonic eddy forms to the east of Sri Lanka during June which develops further during July within which upwelling takes place. Negative SLA extends more in the western BoB during July. The positive SLA along the northern Bay and Martaban Bay becomes high during this time and persists in August while the anticyclonic eddies weaken in the southern Bay and in the western Bay. At this time the western Bay is dominated by negative SLA. The SLA distribution does not undergo much variation during August and September. A decrease in positive SLA especially in the Martaban Bay is observed during September.

In October with the retreat of SWM, the cyclonic eddy in the northern BoB intensifies and the negative SLA extends to central Bay. In November during the NEM season, negative SLA decreases, but the cyclonic eddies in the western Bay remains intense which support upwelling in this region. SLA becomes positive to the south of India during November. In December the extent of negative SLA in the western Bay decreases and the BoB is dominated by positive SLA. The cyclonic eddies that are observed during the SWM and during Oct-Nov are documented by Vinayachandran and Yamagata (1998). Eddies also form during the months Apr-May and Oct-Nov in the vicinity of EICC during the tropical cyclone season in the BoB. The importance of eddy pumping of nutrients and resultant enhanced biological productivity in the BoB during fall and spring inter monsoons were reported by Prasanna Kumar *et al.* (2007).

Han and Webster (2002) used a reduced gravity ocean model to show that SLA in the BoB results largely from wind variability. The SLA in the northern and eastern boundaries was predominantly caused by equatorial winds which generate coastal Kelvin waves that propagate into the Bay along the eastern boundary. The SLA in the western boundary is influenced by Bay winds and equatorial winds. In the central Bay, SLAs are produced primarily from westward propagating Rossby waves generated by equatorial wind variability. They also found minimal effect of freshwater flux, heat fluxes and river discharges on SLA.

### **3.5. Spatial distribution of surface chl-*a* concentration**

#### **3.5.1. Seasonal mean distribution of surface chl-*a* concentration**

The seasonal changes in the distribution of surface chl-*a* of the BoB are analysed based on the seasonal mean of chl-*a* concentrations ( $\text{mg m}^{-3}$ ) as illustrated in Fig. 3.7. During DJF, chl-*a* concentration is very low ( $0.1\text{-}0.4 \text{ mg m}^{-3}$ ) in the central BoB. The chl-*a* concentration increases in the coastal region. Chl-*a* concentration is about  $4 \text{ mg m}^{-3}$  in the northern Bay and in the Martaban Bay during this time. In the eastern BoB near the coast, chl-*a* concentration is lesser (about  $3 \text{ mg m}^{-3}$ ) and in the Malacca strait and Gulf of Mannar it is about  $2 \text{ mg m}^{-3}$ . Chl-*a* concentration is comparatively

low along the western and northwestern Bay during this time. During MAM, the chl-*a* concentration of the entire open ocean decreases becomes less than  $0.2 \text{ mg m}^{-3}$ . In the Malacca Strait, chl-*a* decreases from  $2 \text{ mg m}^{-3}$  to  $1 \text{ mg m}^{-3}$  during this time. Near the southern tip of India, chl-*a* increases to  $3 \text{ mg m}^{-3}$ , while to the south of Sri Lanka and along the western and northwestern Bay, chl-*a* increases to about  $1 \text{ mg m}^{-3}$ .

During JJAS, the chl-*a* concentration is highest in the BoB. The extent of high chl-*a* increases in the northern Bay, near the southern tip of India, and south of Sri Lanka. To the south of Sri Lanka chl-*a* concentration increases to  $3 \text{ mg m}^{-3}$  while in the northern Bay and near the southern tip of India, chl-*a* increases to about  $7 \text{ mg m}^{-3}$ . In the northwestern Bay near the coast above  $15^{\circ}\text{N}$  near the Godavari river mouth, chl-*a* increases to about  $3 \text{ mg m}^{-3}$  during this time. High chl-*a* is observed in the southwestern Bay to the east of Sri Lanka where it increases to about  $1.5 \text{ mg m}^{-3}$ . Coastal upwelling driven by monsoon winds causes the increase in chl-*a* concentration in the southern coast of Sri Lanka. The SMC advect the upwelled water into the southwestern BoB increasing the chl-*a* concentration in that region (Vinayachandran *et al.*, 2004). Open ocean upwelling by Ekman pumping also contribute to the high chl-*a* concentration in the southwestern BoB. During ON, there is an overall decrease in chl-*a* concentration in the BoB. Chl-*a* concentration in the southwestern Bay decreases to about  $0.4 \text{ mg m}^{-3}$  and near the southern tip of India chl-*a* decreases to  $3 \text{ mg m}^{-3}$ . Also chl-*a* concentration along the northwestern and northern BoB decreases during this season. At the same time an increase in chl-*a* concentration up to  $1.0 \text{ mg m}^{-3}$  is observed in the Malacca strait.

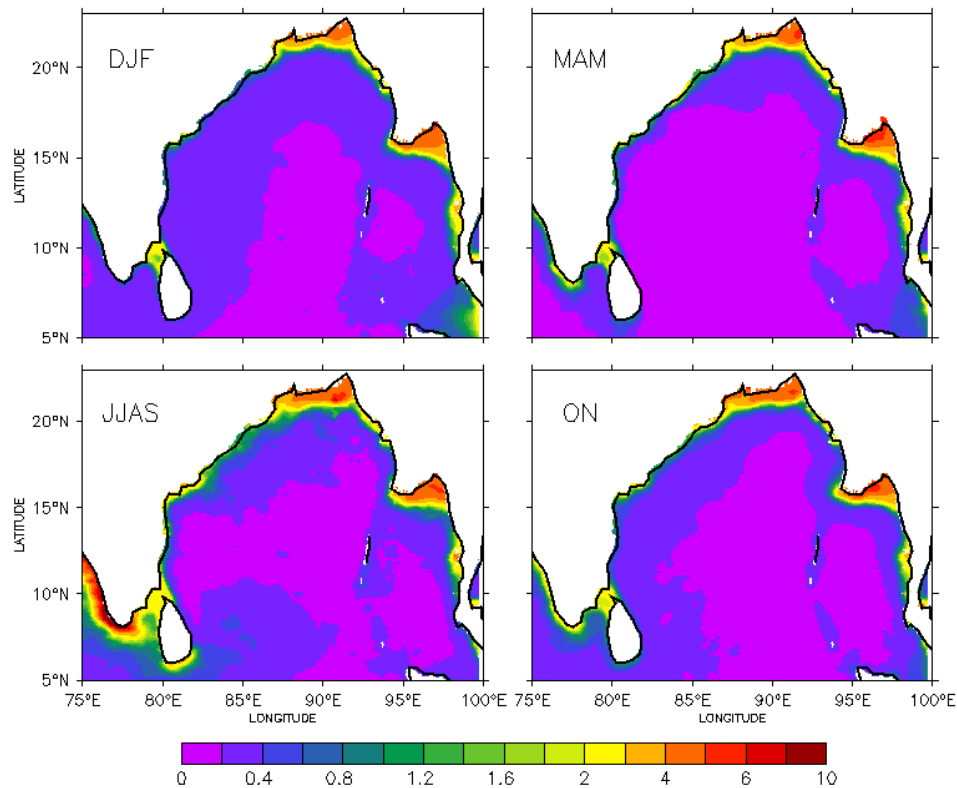


Fig. 3.7 Seasonal mean of surface chlorophyll-*a* concentration ( $\text{mg m}^{-3}$ ) during a) Dec-Feb (DJF), b) Mar-May (MAM), c) Jun-Sep (JJAS), and d) Oct-Nov (ON) in the Bay of Bengal.

### 3.5.2. Monthly mean distribution of surface chl-*a* concentration

Spatial distribution of surface chl-*a* has been studied using the monthly climatology of chl-*a* concentration (Fig. 3.8). During January, chl-*a* concentration in the central BoB and Andaman Sea varies from 0.1 to 0.3  $\text{mg m}^{-3}$  and it gradually increase towards the coastal regions. Highest chl-*a* concentration of about 3-4  $\text{mg m}^{-3}$  is observed in the northern Bay and Martaban Bay. In the Malacca strait, eastern Bay and in the Gulf of Mannar, chl-*a* concentration has a maximum of 3  $\text{mg m}^{-3}$ . In the Godavari basin near 16°N, chl-*a* concentration is about 2  $\text{mg m}^{-3}$ . In February, chl-*a* concentration reduces to less than 0.2  $\text{mg m}^{-3}$  in the open ocean while along the coastal region it does not undergo considerable change. In March, chl-*a* concentration increases to about 5  $\text{mg m}^{-3}$  in the Martaban Bay. The chl-*a* distribution does not vary much during April except for a decrease in the Malacca

strait. Chl-*a* blooms appear to the south of Sri Lanka ( $\sim 2 \text{ mg m}^{-3}$ ), and to the southern tip of India ( $\sim 5 \text{ mg m}^{-3}$ ) during May. There is an increase in chl-*a* concentration in the northern Bay and in the Martaban Bay during this time. Also scattered patches of high chl-*a* occur along the east coast below  $15^{\circ}\text{N}$ .

In June, high chl-*a* concentration is observed over a large area to the south of India and Sri Lanka, with a maximum of nearly  $7 \text{ mg m}^{-3}$  occurring close to the southern tip of India. High chl-*a* from the bloom extends from the south of India and Sri Lanka to the southwestern Bay by the advection of SMC in the ocean. According to Rao *et al.* (2006a), upwelling off the southern tip of India results in both shoaling of the thermocline and enhanced blooming of chl-*a*. During June, chl-*a* concentration in the northern BoB is about  $4\text{-}5 \text{ mg m}^{-3}$  and along the northeastern coast increase of chl-*a* concentration upto  $3 \text{ mg m}^{-3}$  is observed. There is an overall increase of chl-*a* concentration in the BoB during July. Chl-*a* concentration increases in the northwestern BoB near the Krishna-Godavari river mouth with small blooms ( $\sim 2\text{-}3 \text{ mg m}^{-3}$ ) in July. This is due to the increased river runoff during the SWM season which brings more nutrients into the ocean. In July, the bloom in the southwestern Bay extends northward upto  $10^{\circ}\text{N}$  within which chl-*a* concentration increase to about  $1\text{-}1.5 \text{ mg m}^{-3}$ , whereas it is about  $0.2 \text{ mg m}^{-3}$  in the surrounding waters. The bloom to the south of India and Sri Lankan coast extends over a larger area and persists till September. The bloom to the south of Sri Lanka is attributed to the coastal upwelling driven by monsoon winds that cause enrichment of nutrients in the surface layer (Vinayachandran *et al.*, 2004). The SMC flowing eastward south of Sri Lanka, and then into the BoB advect the upwelled waters eastward along its path. The chlorophyll rich waters from the Indian coast also advect along with the monsoon current towards Sri Lanka. East of Sri Lanka the open ocean upwelling associated with the Sri Lanka Dome is also found to be an important process that upwell nutrients (Vinayachandran *et al.*, 2004). The chl-*a* concentration off the southern tip of India reaches upto  $9 \text{ mg m}^{-3}$  in August. Also during August, there is a further increase in chl-*a* concentration in the northwestern Bay near Krishna-Godavari river mouth. Chl-*a* concentration in the northern Bay increases to  $5\text{-}6 \text{ mg m}^{-3}$  during this time which sustain in September. After August, an overall decrease of chl-*a*

concentration in the open ocean is observed in the BoB. The bloom in the southwestern Bay and in the northern Bay diminishes in September.

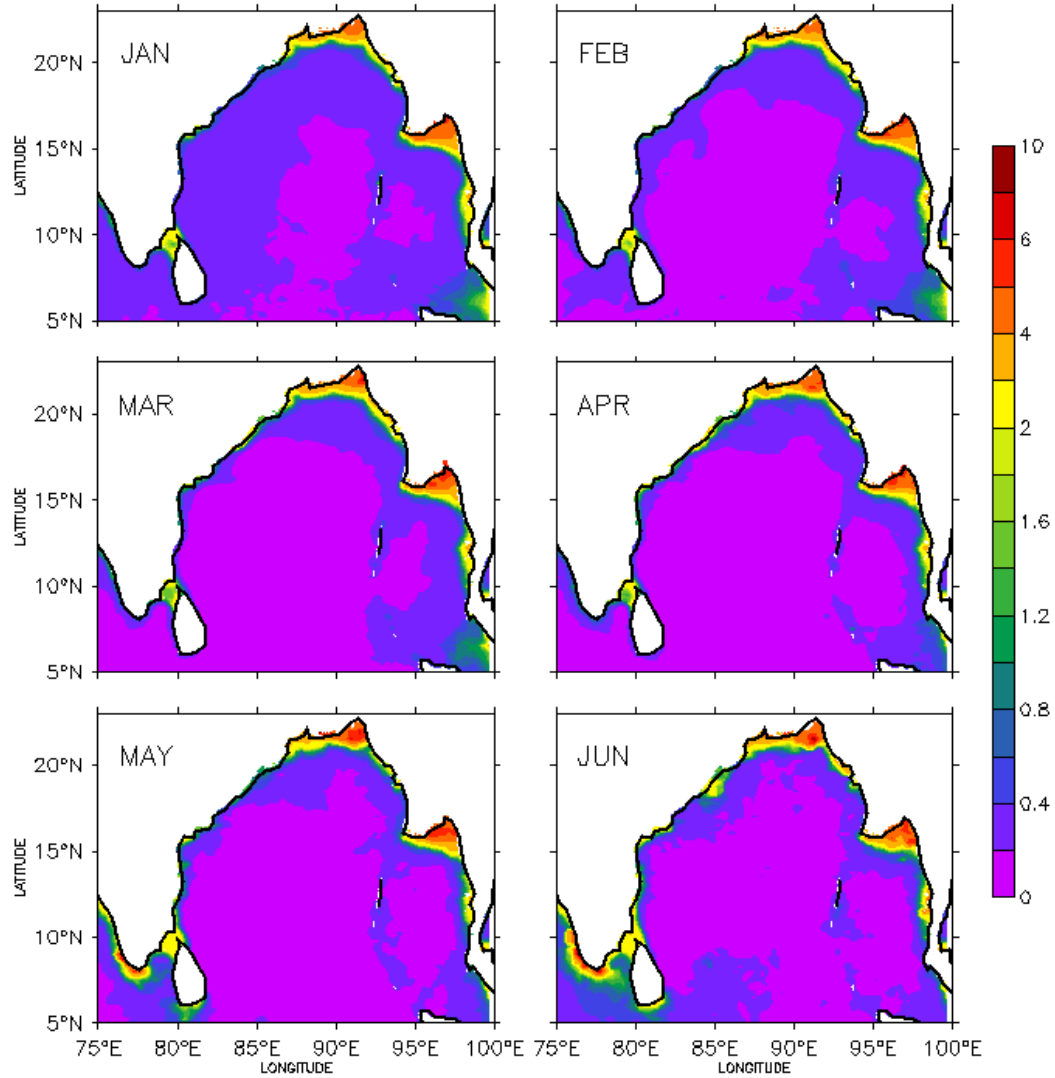


Fig. 3.8 Monthly climatology of surface chlorophyll-*a* concentration (mg m<sup>-3</sup>) in the Bay of Bengal

Continued...

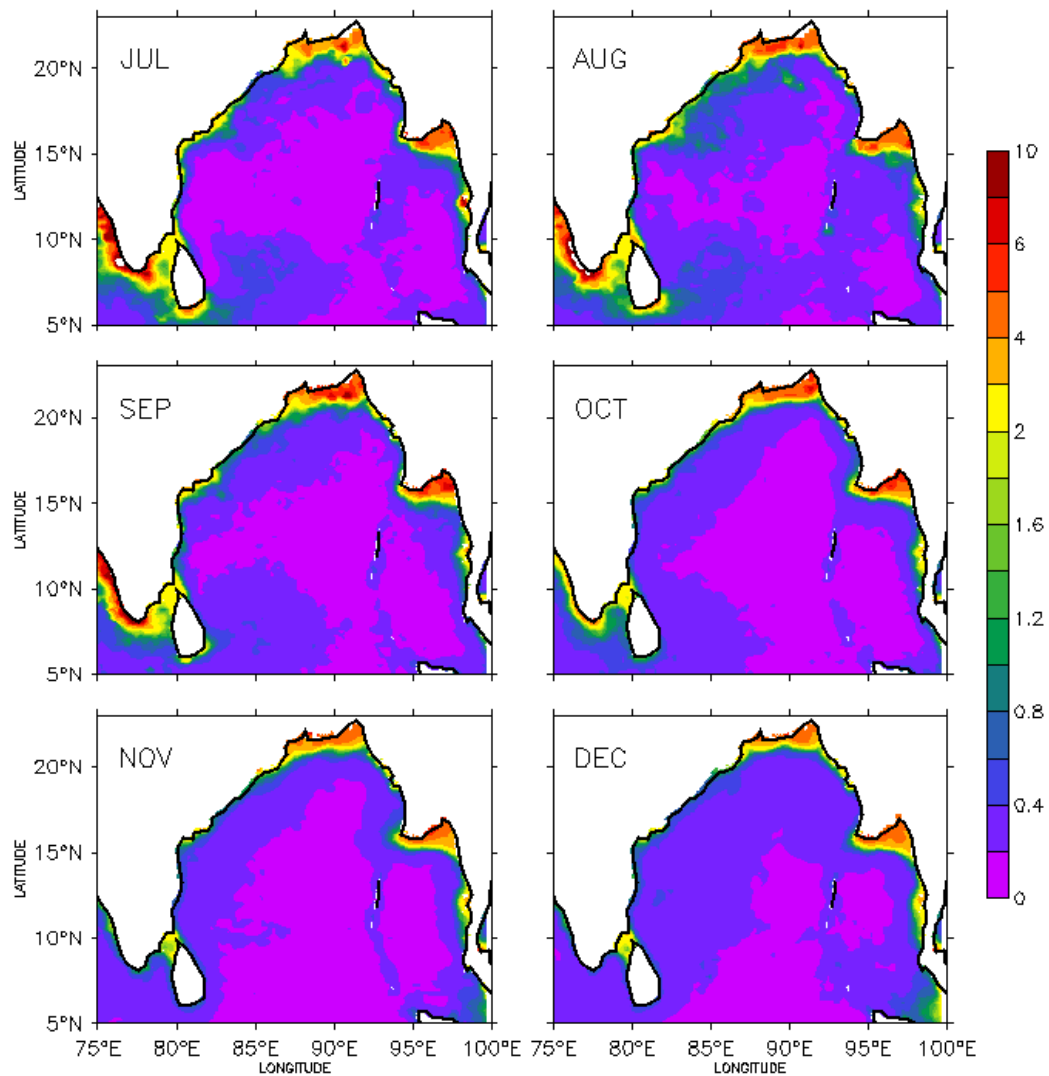


Fig. 3.8 Monthly climatology of surface chlorophyll-*a* concentration ( $\text{mg m}^{-3}$ ) in the Bay of Bengal

By October, when the SWM withdraws, the chlorophyll bloom in the southwestern Bay disappears and the bloom off the Krishna-Godavari river mouth diminishes. Chl-*a* concentration in the northern Bay and Martaban Bay decreases to  $4\text{--}5 \text{ mg m}^{-3}$ . Chl-*a* concentration off the southern tip of India and to the south of Sri Lanka decreases to about  $2 \text{ mg m}^{-3}$  during this time. During November, a decrease in chl-*a* concentration is observed in the northern BoB and to the south of India and Sri Lanka. In the Malacca strait, chl-*a* concentration increases to about  $2 \text{ mg m}^{-3}$ , that

extends westward during December. There is little difference in the spatial distribution of chl-*a* concentration in December when compared to November.

### **3.6. Summary**

The climatological variations of WSC, SST, SLA and surface chl-*a* concentration in the BoB during the period 2000-2007 have been analysed in this Chapter. The spatial distribution of WSC over the BoB changes in correspondence with the prevailing surface winds which undergo seasonal reversals associated with changing seasons over the BoB. Positive (cyclonic) WSC is observed over the southern Bay during the NEM season (Dec-Feb) with the maximum ( $3 \times 10^{-7} \text{ N m}^{-3}$ ) over the west of Sumatra Islands in December. During this season, weak negative (anticyclonic) WSC exist over the north and central Bay. During pre-monsoon months (Mar-Apr), WSC over the Bay is comparatively weak as the winds are weak and variable. During SWM season from June to September, positive (cyclonic) WSC is observed over the north and northwestern parts of the BoB, extending and increasing in intensity, to a maximum of  $3 \times 10^{-7} \text{ N m}^{-3}$  during August and thereafter diminishing. Strong positive (cyclonic) WSC is observed over the southwestern Bay from May to September which increases as the monsoon advances. It attains maximum strength ( $\sim 4.5 \times 10^{-7} \text{ N m}^{-3}$ ) to the east of Sri Lanka in July and then gradually decreases. High positive (cyclonic) WSC induce divergence of the ocean surface and upwelling in the southwestern Bay, north and northwestern Bay during SWM season. During this season high negative (anticyclonic) WSC with a maximum of  $-2.5 \times 10^{-7} \text{ N m}^{-3}$  which induce convergence of the surface waters and downwelling is observed over the southeastern Bay. Positive (cyclonic) WSC dominates the Bay during the post-monsoon months of October and November. Over the southwestern Bay positive WSC is about  $2 \times 10^{-7} \text{ N m}^{-3}$  during this season. High positive (cyclonic) WSC in the west-central Bay during October supports upwelling in this region.

SST of the BoB undergoes large variations in its spatial distribution in a year. During the NEM, SST reaches the lowest ( $\sim 23^\circ\text{C}$ ) in January in the northern Bay and increases southward. During the pre-monsoon months when the winds are weak, SST

of the Bay increases abruptly and is greater than 29°C in April and May. With the onset of the SWM in the BoB, SST decreases and its distribution pattern changes. The Bay experiences low SST in the southern part which gradually increases towards the north and northwestern Bay. A cold pool forms in the south-central Bay during May and intensifies as the SWM progresses. The cold pool reach the maximum extent with a temperature of 27.5°C during the peak of monsoon in Jul-Aug and disappear by October. The upward Ekman pumping induced by high positive (cyclonic) WSC brings the cooler subsurface water to the ocean surface thus reducing the SST of the cold pool (Vinayachandran and Yamagata, 1998). Also the decay of the cold pool is attributed to the arrival of a long Rossby wave. A mini cold pool forms off the southern tip of India in June reaches the minimum SST of 26°C in July and diminishes by October as the SWM withdraws. The mini cold pool develops due to the upwelling caused by the divergence in the near-surface circulation (Rao *et al.*, 2006a). In October the SST of the Bay increases, and in November the latitudinal distribution changes again with low SST to the north and high SST to the southern Bay. SST distribution of December resembles that during January with slightly less cooling in the northern Bay.

In general, the mean SLA of the BoB undergoes considerable change during the year. The variations in SLA are mainly caused by Rossby and Kelvin waves in the BoB which are generated by equatorial winds (Han and Webster, 2002). From February to April, negative SLA dominates the eastern Bay while anticyclonic eddies are observed in the western Bay. These anticyclonic eddies are replaced by cyclonic eddies during the SWM season. Also the negative SLA in the eastern Bay is replaced by positive SLA during SWM season. Strong cyclonic eddies that cause upwelling are observed during the SWM and post-monsoon season in the western and southwestern Bay. The cyclonic eddy in the southwestern Bay develops as a result of the open ocean Ekman pumping by the positive WSC (Vinayachandran and Yamagata, 1998). During NEM, positive SLA dominates the Bay and a strong anticyclonic eddy is observed in the northwestern Bay, which cause downwelling in this region.

Seasonal and monthly variability is minimum in the Bay except at certain locations such as southwestern Bay, east coast of India, northern BoB and Malacca strait. The spatial variation of surface chl-*a* is low in the BoB especially in the open ocean where it is in the range of 0.1 to 0.4 mg m<sup>-3</sup> during all the seasons. Generally chl-*a* concentration increases towards the coasts up to 3-5 mg m<sup>-3</sup> and especially during SWM it reaches as high as 8-9 mg m<sup>-3</sup>. During NEM season, chl-*a* concentration increases to about 4 mg m<sup>-3</sup> in the northern Bay and in the Martaban Bay. Chl-*a* concentration is lowest (<0.2 mg m<sup>-3</sup>) in the entire central Bay during the pre-monsoon season. High chl-*a* concentration is observed during the SWM season in the BoB. During the SWM season, a chlorophyll bloom develops off the southern tip of India and in the southwestern Bay. As the SWM intensifies, spatial extent of the bloom increases and by October the bloom disappears completely. The chl-*a* concentration within the bloom is about 1-1.5 mg m<sup>-3</sup> which is high compared to the surrounding waters. During the entire SWM season, chl-*a* concentration south of Indian and Sri Lankan coast remain very high, reaching up to 7-9 mg m<sup>-3</sup>. This increase is caused by the coastal upwelling driven by monsoon winds along the coasts of Sri Lanka. The occurrence of bloom during SWM in southwestern Bay is caused by the open ocean upwelling driven by Ekman pumping together with the advection of upwelled waters from the southern coasts of Sri Lanka by the SMC (Vinayachandran *et al.*, 2004). East coast of India experiences changing current patterns and river inputs from Krishna and Godavari, which cause increased chl-*a* concentration in that region especially during SWM season. Northern and northwestern Bay also experience high chl-*a* concentrations during the summer monsoon months.

## Chapter 4

# Variability of wind stress curl and the Ekman pumping in the Bay of Bengal

### 4.1. Introduction

The WSC is a measure of the sense and strength of rotation in the wind. WSC is positive if the winds are cyclonic in the northern hemisphere. In Ekman pumping, WSC generates ocean-surface divergence or convergence, which forces water upward or downward. In the open ocean, this results in large-scale upwelling at the centre of low-pressure areas, and downwelling in high-pressure areas (Pickett and Paduan, 2003). Horizontal convergences and divergences of the Ekman transport are compensated for by a vertical upwelling or downwelling velocity at the base of the Ekman layer, known as Ekman vertical velocity (VV). Based on WSC studies, Chelton (1982) suggested that Ekman pumping is important in bringing nutrients to the surface waters. Upwelling has importance well beyond its physical significance, because it brings the subsurface nutrient rich waters to the surface where phytoplankton blooms. Changes in upwelling can result in large and significant changes in the productivity of the ocean.

In the first section of this Chapter, monthly data on WSC for a period of eight years (2000-2007) has been used to study the spatial and temporal variability of WSC over the BoB. EOF analysis has been performed on WSC field, resulting in spatial patterns of WSC and associated time series. EOF analyses identify the significant patterns in large data sets and the variance explained by them. These help us to understand the prominent modes of variability of WSC in terms of spatial and temporal patterns.

The spatial distribution of wind stress in the BoB during the SWM season has been analysed in second section of the Chapter. The cold pool of the BoB lies in a region of intense wind stress: the interannual variations in the extent of the cold pool have been studied with the help of TMI SST and the results have been explained. VV has been computed from WSC and analysed in the regions of strong wind stress during SWM season in the BoB. Positive VV denote upward Ekman pumping while negative VV denote downward Ekman pumping in the Ekman layer. SLA has also been analysed in the regions of intense wind stress. High positive VV and intense negative SLA (cyclonic eddies) indicate the occurrence of upwelling in the ocean.

#### 4.2. Empirical Orthogonal Function analysis of wind stress curl

EOF analysis has been applied to WSC over the BoB to quantify the major seasonal and inter-annual patterns in the WSC during the period 2000 to 2007. The analysis gives a set of orthogonal spatial patterns and associated uncorrelated time series called principal components (PCs). Fig. 4.1 represents the annual mean distribution of WSC during the study period.

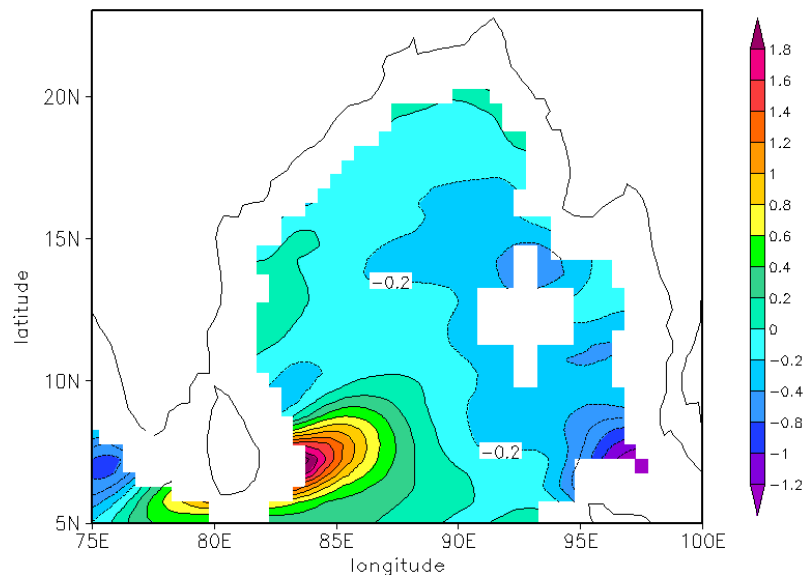


Fig. 4.1 Annual mean of wind stress curl pattern ( $\times 10^{-7} \text{ N m}^{-3}$ ) over the Bay of Bengal from January 2000 to December 2007. Dashed lines indicate negative wind stress curl.

Annual mean of WSC depict the most pronounced features in the spatial distribution of WSC over the BoB during the years 2000 to 2007. It is observed that in the BoB annual WSC varies between  $-1.4 \times 10^{-7} \text{ N m}^{-3}$  and  $2 \times 10^{-7} \text{ N m}^{-3}$ . Weak negative (anticyclonic) WSC is observed over most part of the BoB except over the southwestern Bay. Comparatively high negative (anticyclonic) WSC of about  $-1.4 \times 10^{-7} \text{ N m}^{-3}$  is observed near the Malacca strait. Positive (cyclonic) WSC of high magnitude is observed over the southwestern Bay with a maximum of  $2 \times 10^{-7} \text{ N m}^{-3}$  centered at  $7.5^\circ\text{N}$  which is favourable to upwelling events. This high WSC is caused by the prevailing southwesterlies in the BoB during the SWM season. Also weak positive (cyclonic) WSC is observed over the western side of the Bay between  $11^\circ\text{N}$  and  $15^\circ\text{N}$  and over the head Bay in the north.

First twelve EOFs have been retained in the EOF analysis of WSC. Fig. 4.2a shows the variance associated with the first 12 EOF modes. First EOF mode contributes to 36% and the second mode 15.1% of the total variance. WSC fields vary mainly according to the first modes of variance and hence the associated patterns are most typical. The rest of the EOF modes are of minor significance corresponding to very small eigen values, and contribute very little to the total variance. The cumulative variance in percentage (Fig. 4.2b) shows that the 12 EOF modes represent 83% of the total variance and the first four EOFs alone represent 64% of the total variance of the WSC field. The spatial patterns of the WSC associated with these modes depict the major components of WSC climatology.

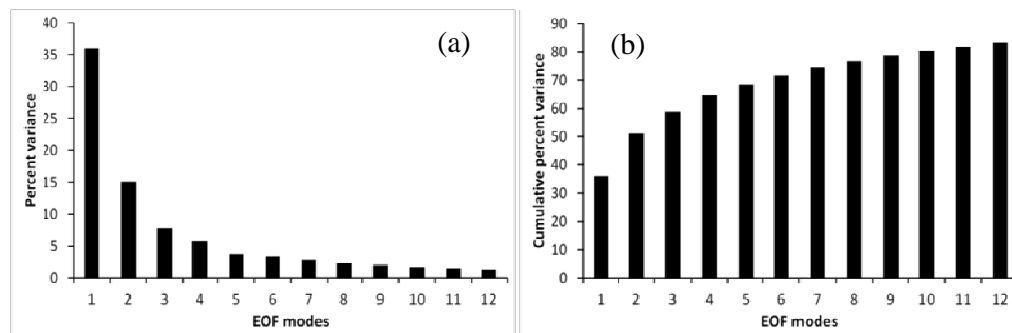


Fig. 4.2 (a) Variance in percentage associated with first 12 EOFs, and (b) cumulative variance in percentage of EOF modes

Spatial patterns of the WSC and a non-dimensional time series are associated with each EOF mode. The first EOF accounts for 36% of the total variance of the WSC field. EOF1 (Fig. 4.3a) shows high positive values in the northwestern Bay and in the southwestern Bay to the east of Sri Lanka. Negative high values are observed in the southeastern Bay. This pattern is similar to the JJAS climatology of WSC (Fig.3.1c).

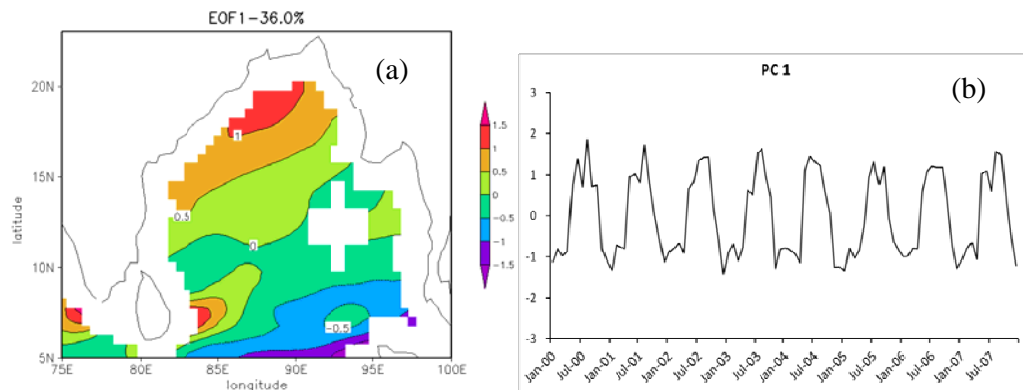


Fig. 4.3 (a) Spatial pattern of wind stress curl ( $\times 10^{-7} \text{ N m}^{-3}$ ) for the first EOF, and (b) the corresponding non-dimensional time series PC1

The first EOF is dominated by annual periodicity associated with summer monsoon which is clearly revealed in the time series coefficient PC1 (Fig. 4.3b). The positive peaks in the time series graph are more pronounced than the negative peaks. From 2000 to 2003 and during 2007 the positive peak occurred during August while during 2005 and 2006 the peak occurred in July. The interannual variations in WSC are brought out in the graph. Negative peaks occur during December and January which also shows interannual variations. From the analysis of EOF1 and corresponding PC1 it has been observed that a positive high occurs in the northwestern and southwestern Bay during Jul-Aug which becomes negative during Dec-Jan months. Also another annual variation observed is the negative high in the southeastern Bay during Jul-Aug which turns to a positive high during Dec-Jan.

The second EOF accounts for 15.1% of the total variance which is associated primarily with northeast monsoon having annual periodicity. In EOF2 (Fig. 4.4a), negative high values are observed in the central Bay and positive high in the northern and southern Bay. Annual periodicity is observed in the associated time series plot of

PC2 (Fig. 4.4b) which also shows the inter-annual variability. The negative peaks are prominent compared to positive peaks in the time series plot. Seasonal variability is less during 2003, 2004 and 2006. Primary negative peaks occur generally during October and November while positive high occur mostly during summer monsoon months. Comparison between EOF2 and PC2 reveals that the negative high in the central Bay is associated with the variance during northeast monsoon.

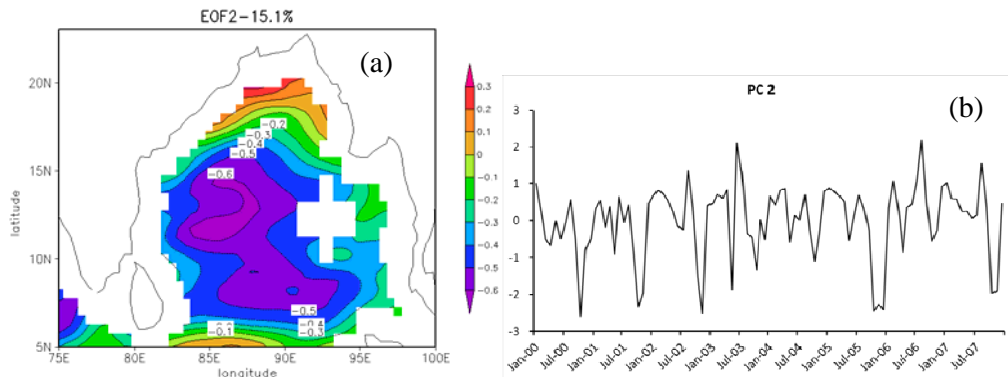


Fig. 4.4 (a) Spatial pattern of wind stress curl ( $\times 10^{-7} \text{ N m}^{-3}$ ) for the second EOF and (b) the corresponding non-dimensional time series PC2

EOF analysis of curl field shows that most of the variance of WSC in the BoB is contained in annual frequencies associated with the monsoon. The possible processes contributing to the remaining 36% of the total variance could be attributed to factors such as intraseasonal variability of summer monsoon (active and break phases), monsoon depressions and intra-seasonal variability of the equatorial (zonal) wind stress.

### 4.3. Wind stress during the southwest monsoon

The spatial distribution of wind stress in the BoB during the SWM has been analysed for the study period 2000 – 2007 (Fig. 4.5). The wind stress is high in the southeastern side of Sri Lanka and also in the west-central Bay away from coast between 12 to 20°N during the SWM season. A tongue of high wind stress ( $0.2 \text{ N m}^{-2}$ ) is observed to the southeastern side of Sri Lanka in May which increased to  $0.22 \text{ N m}^{-2}$  during Jun-Jul and later weakened. In the west-central Bay, strong wind stress of  $\sim 0.2 \text{ N m}^{-2}$  is observed during June over a large area. In August, the wind stress

increases to  $0.21 \text{ N m}^{-2}$  along  $88^\circ\text{E}$ ,  $15\text{-}16^\circ\text{N}$  and by September wind stress in the west-central Bay becomes weak (less than  $0.15 \text{ N m}^{-2}$ ). The strong wind stress observed in the BoB is due to the strong wind flow during the SWM season in these regions. Wind stress is very weak in the southeastern Bay ( $0.04\text{-}0.05 \text{ N m}^{-2}$ ) during the SWM followed by the east coast of India south of  $16^\circ\text{N}$  and in the southwestern Bay at around  $8^\circ\text{N}$  to the east of Sri Lanka ( $0.06\text{-}0.07 \text{ N m}^{-2}$ ). The wind stress minimum in the southwestern Bay is situated above the region of maximum wind stress. The cold pool of the BoB (Vinayachandran and Yamagata, 1998) develops in the south-central Bay where the stress of the wind is high during the SWM season. The inter-annual variations of the cold pool have been analysed using SST data. The VV has been computed and analysed along with SLA in the southwestern and west-central Bay where high wind stress is experienced during the SWM season in the BoB to understand the upwelling in these regions.

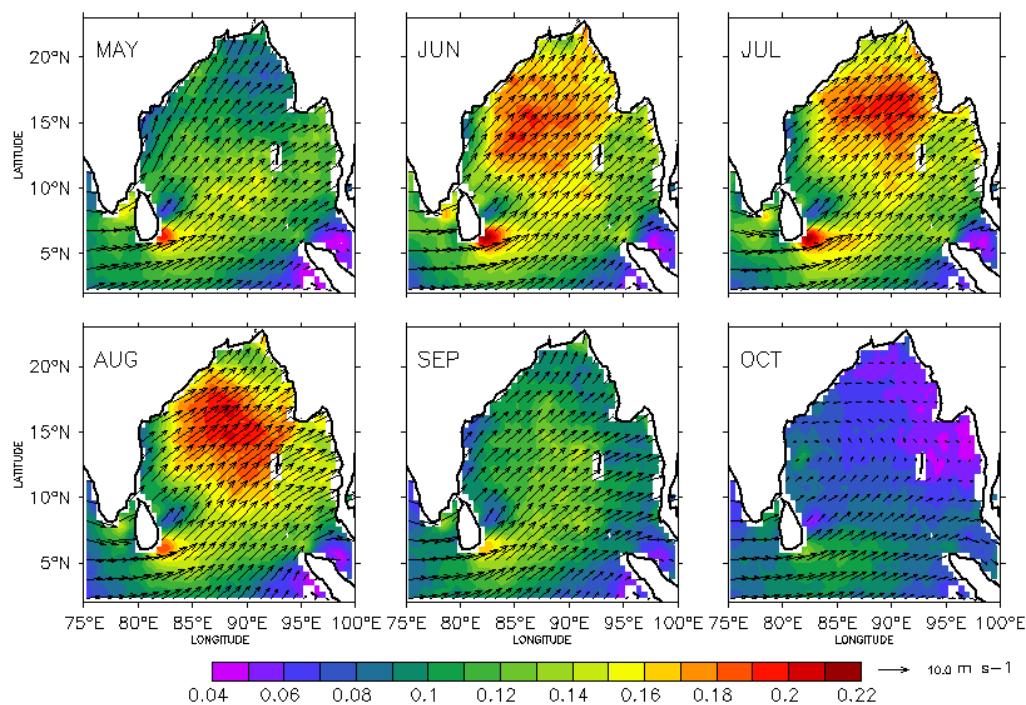


Fig. 4.5 Spatial distribution of wind stress ( $\text{N m}^{-2}$ ) climatology for the years 2000 to 2007 superimposed with wind vectors from May to October covering the southwest monsoon season in the Bay of Bengal

#### 4.4. Cold pool of the south-central Bay of Bengal and its inter-annual variation

The SST climatology for JJAS (Fig. 4.6) in the south-central BoB depicts the cold pool that is observed during the SWM season. This cold pool has been well documented by Vinayachandran and Yamagata (1998) and Joseph *et al.* (2005). The cold pool lies between 3-10°N and extends to about 90°E in the south-central BoB. Within the cold pool, the lowest temperature observed is about 28°C to the southeastern side of Sri Lanka, which is the area that experiences high wind stress (Fig. 4.5) during this season. The strong positive (cyclonic) WSC in the southwestern BoB (Fig. 3.1c and Fig. 3.2) causes open ocean upwelling by Ekman pumping, which contributes to the reduction in SST. Vinayachandran and Yamagata (1998) related the development of this cold pool to the cyclonic curl in the local wind field and the decay to the arrival of a long Rossby wave, associated with the reflection of the spring Wyrтки jet at the eastern boundary of the ocean.

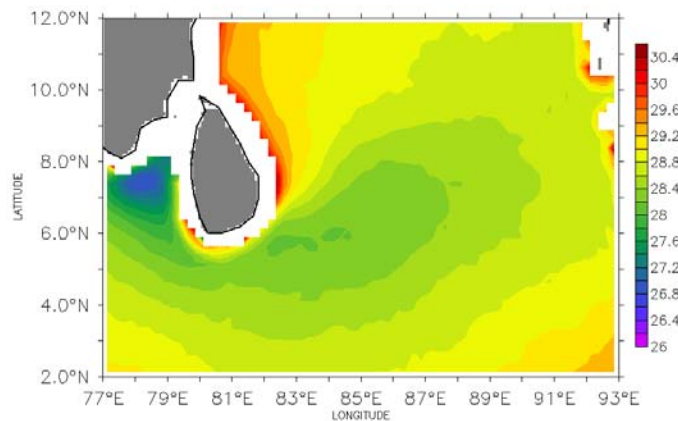


Fig. 4.6 Averaged sea surface temperature (°C) during Jun-Sep in the south-central Bay depicting the cold pool for the period of 2000 to 2007

The summer monsoon winds cause coastal upwelling in the southern coast of Sri Lanka (Vinayachandran *et al.*, 2004) and the upwelled cooler waters get advected into the BoB by the SMC which flow eastward south of Sri Lanka. This contributes to the cooling in the south-central Bay apart from the open ocean upwelling in that region. Cooler water from the mini cold pool off the southern tip of India also gets advected into the south-central BoB by the SMC (Rao *et al.*, 2006a).

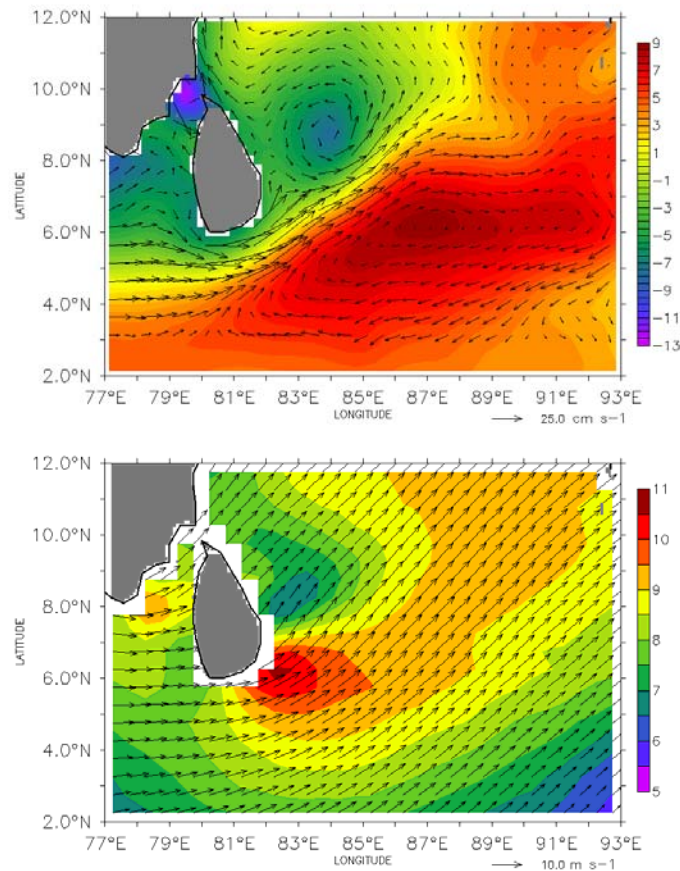


Fig. 4.7 (a) Average sea level anomaly (cm) superimposed with geostrophic currents in  $\text{cm s}^{-1}$  (Jun-Sep) in the south-central Bay depicting the cold core eddy to the east of Sri Lanka and the intrusion of currents into the Bay of Bengal and (b) the mean wind pattern ( $\text{m s}^{-1}$ ) for the same period showing the region of maximum wind speed during summer monsoon period of 2000 to 2007

The mean SLA and the estimated geostrophic currents (Fig. 4.7a) during JJAS illustrate the cyclonic eddy to the east of Sri Lanka and the anticyclonic eddy adjacent to it. The geostrophic currents clearly show the intrusion of SMC northeastward into the south-central BoB, the northern edge of which forms part of the cyclonic eddy to the east of Sri Lanka. The cyclonic eddy is centered at 9°N, 84°E and the SLA is about -8 cm in the core of the eddy. The anticyclonic eddy is centered at 6°N, 87°E. Though the lowest temperature in the cold pool is observed to the southeast of Sri Lanka (Fig. 4.6), the cyclonic eddy lies further north around 9°N. The evolution of the cyclonic eddy during SWM can be observed in Fig. 3.6. Though

the eddy is located to the east of Sri Lanka during June, by September it moves northward and lay centered at  $10^{\circ}\text{N}$ . The decay of the cold pool begins in September when a strong northward flow east of Sri Lanka, which is separated from the coast by a southward current, replaces the cyclonic eddy (Vinayachandran and Yamagata, 1998). As a result, warm water advected from the east occupies the south-central Bay whereas the cold water patch moves northeast forming an eastward tongue. The EICC flows northeastward north of  $10^{\circ}\text{N}$  from February until September, with a strong peak in Mar-Apr and weaker flow from June to September (McCreary *et al.*, 1996). South of  $10^{\circ}\text{N}$ , along Sri Lanka the EICC flows northward only during March and April. The absence of flow during the rest of the year is due to the interior Ekman pumping which drives a strong southward current. During NEM, the EICC flows equatorward all along the coast driven by winds along the east coast of India and Ekman pumping in the interior Bay (Shetye *et al.*, 1996). The mean surface wind speed during JJAS illustrated in Fig. 4.7b is high to the southeastern side of Sri Lanka ( $\sim 10 \text{ m s}^{-1}$ ) which is observed to be the region of low SST (Fig. 4.6) during this season.

The interannual variations in the strength and extend of the cold pool in the south-central BoB during the SWM season have been explained using Hovmoller plots (Fig. 4.8 and Fig. 4.9). In Fig. 4.8, the SST averaged over  $3\text{-}10^{\circ}\text{N}$  between  $82\text{-}90^{\circ}\text{E}$  for the months from May to October have been plotted. The longitudinal extent of the cold pool and its intraseasonal and interannual variations are observed in these plots. In general, the temperature within the cold pool is lowest during August, with 2005, 2006 being exceptions during which the lowest SST occurred in September. During 2007, apart from August and September, the cooling extends to October. The cold pool is most developed during 2000 and has the lowest SST ( $\sim 27.6^{\circ}\text{C}$ ) in August followed by 2001, 2004 and 2006. The cold pool is weakest during 2007 followed by 2003. Depending on how prominent and well defined is the cold pool, the longitudinal extent varies with each year. When the cold pool is most developed, the cooling extends eastward upto  $88\text{-}89^{\circ}\text{E}$ : during 2000, the lowest SST is observed between  $83\text{-}87^{\circ}\text{E}$ .

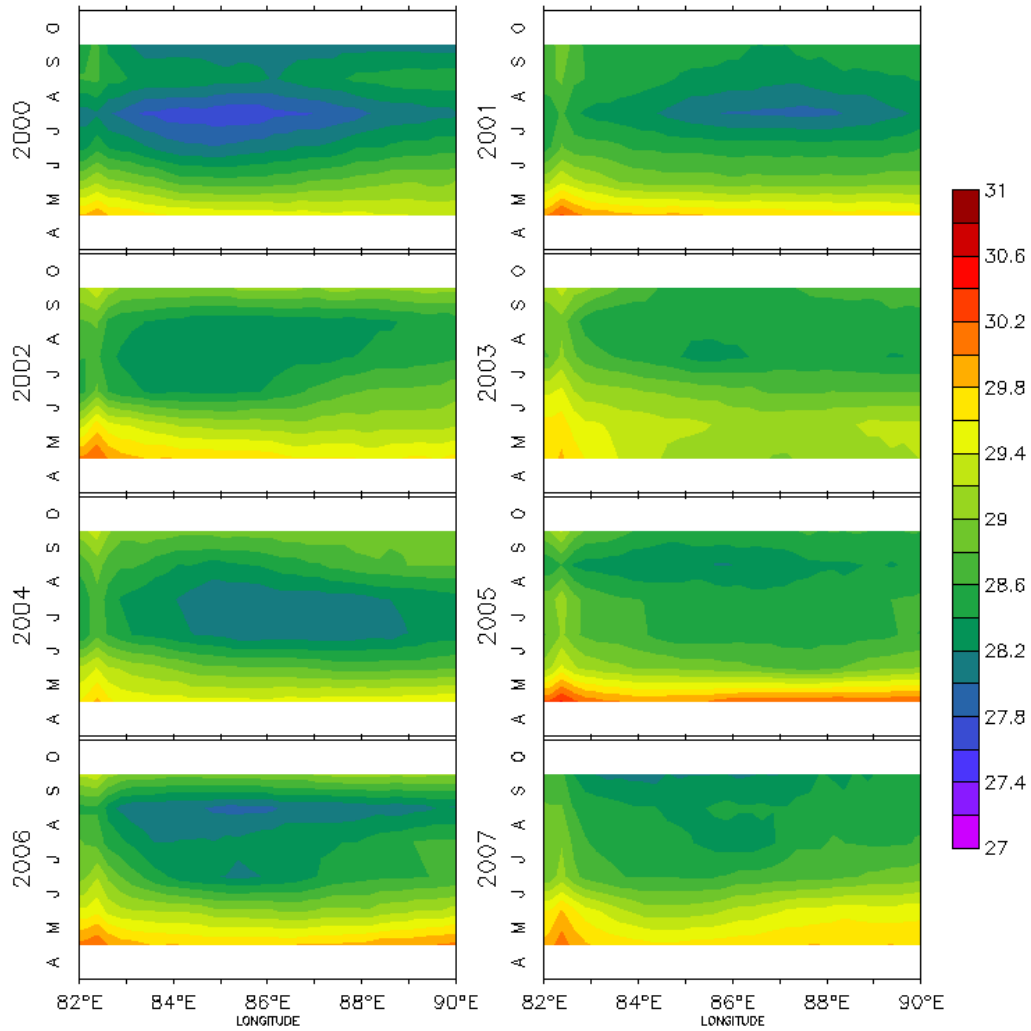


Fig. 4.8 Sea surface temperature ( $^{\circ}\text{C}$ ) cooling in the south-central Bay of Bengal averaged over  $3\text{-}10^{\circ}\text{N}$  depicting the cold pool that develops during the southwest monsoon season

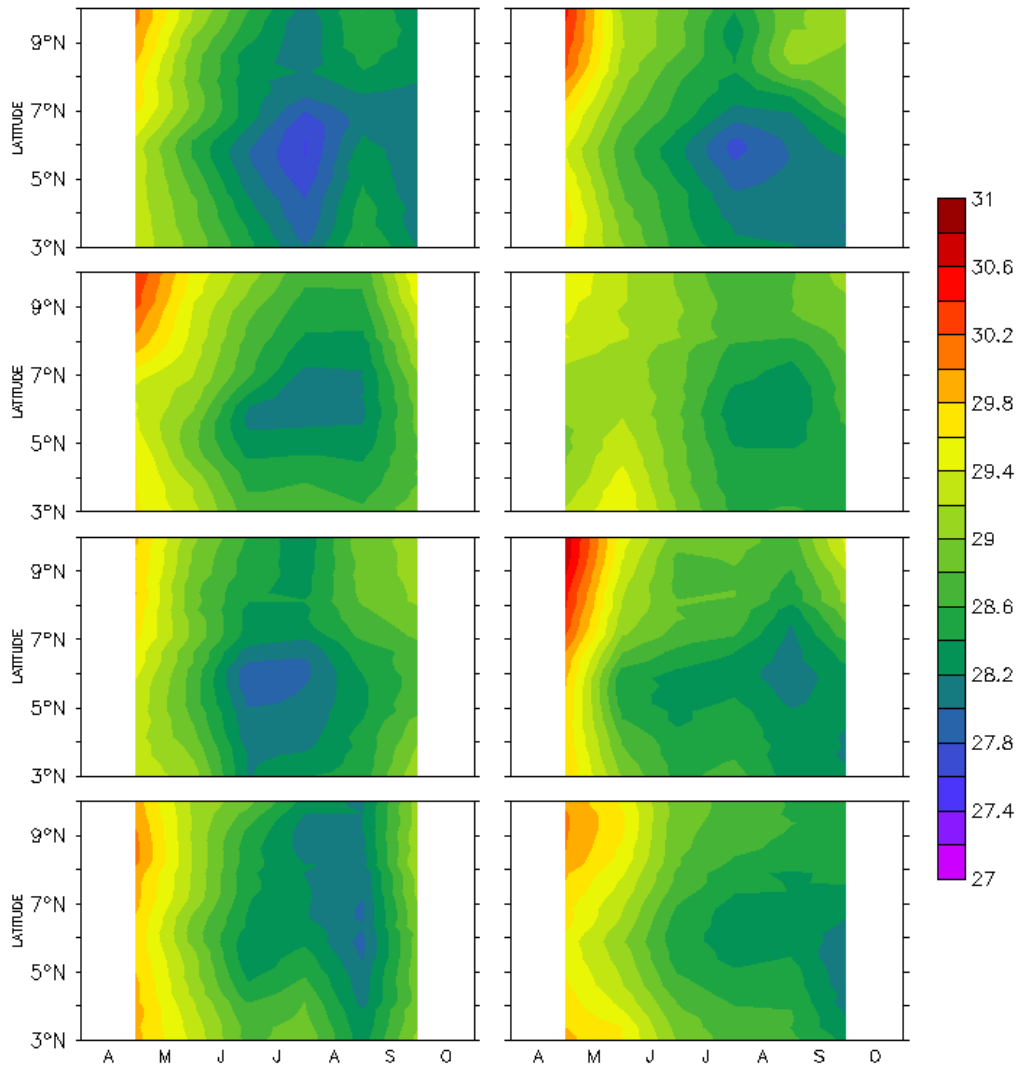


Fig. 4.9 Sea surface temperature ( $^{\circ}\text{C}$ ) cooling in the south-central Bay of Bengal averaged over  $82\text{-}90^{\circ}\text{E}$  depicting the cold pool that develop during the southwest monsoon season

The intraseasonal and interannual variations in the cold pool of the south-central BoB are also observed in the Hovmoller plots of SST (Fig. 4.9) averaged over  $82\text{-}90^{\circ}\text{E}$  between  $3\text{-}10^{\circ}\text{N}$  for May to October. From these plots, it is observed that the cold pool is most developed during 2000, followed by 2001, 2004 and 2006, while during 2007 and 2003 it is least developed. The lowest SST of the cold pool occurs during August in most of the years, except for 2005 and 2006 when it occurred in

September. In general, the lowest SSTs are observed between 4-7°N. The latitudinal extent varies each year depending on the strength of the cold pool.

#### 4.5. Wind induced Ekman pumping and sea level variations

The monthly mean VV for the period May to October of the years 2000-2007 has been computed for two regions: a) southwestern Bay, and 2) north-central Bay, where the wind stress during the SWM (Fig. 4.5) is highest in BoB. The corresponding SLA together with the computed geostrophic currents has also been used to analyse the response of sea level to high wind stress in these regions.

##### 4.5.1. Southwestern Bay of Bengal

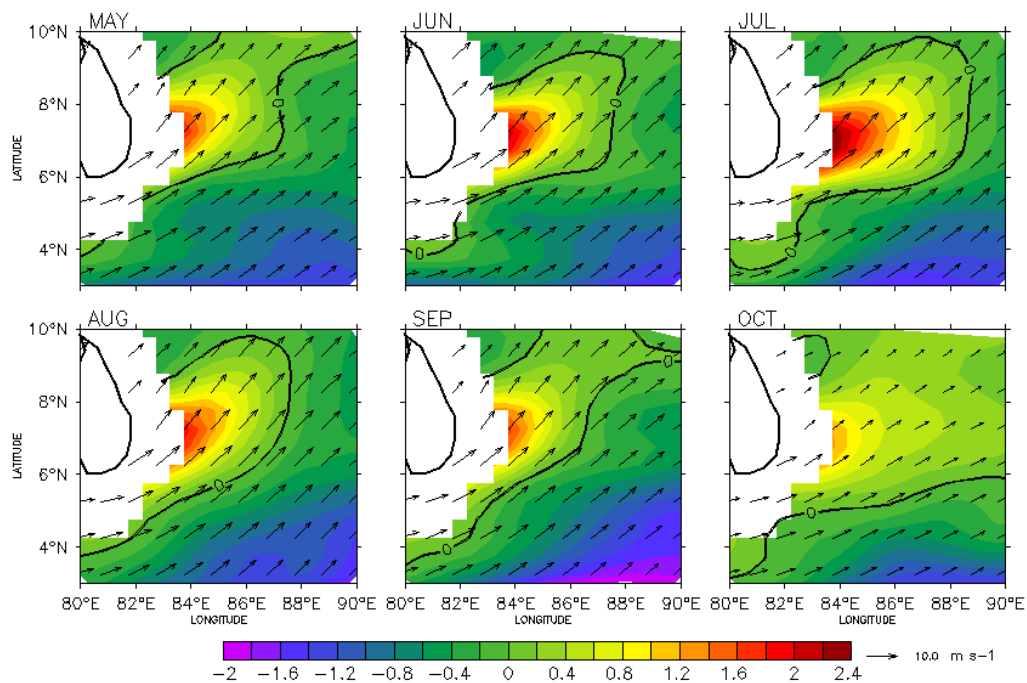


Fig. 4.10 Monthly mean Ekman vertical velocity ( $\times 10^{-5} \text{ m s}^{-1}$ ) from May to October in the southwestern Bay of Bengal

The monthly mean of VV for the southwestern Bay are plotted in Fig. 4.10 depicting the intra-seasonal variations during the summer monsoon season. The VV is about  $1.6 \times 10^{-5} \text{ m s}^{-1}$  to the east of Sri Lanka during May which increases and extends

eastwards into the Bay as the SWM advances. The VV is strongest during July and it is about  $2.4 \times 10^{-5} \text{ m s}^{-1}$  around  $84^\circ\text{E}$ ,  $7^\circ\text{N}$  to the east of Sri Lanka and the tongue of strong VV extends eastward upto  $86^\circ\text{E}$ . Positive VV is an indication of the upwelling in that region. The strong cyclonic curl in the southwestern Bay (Fig. 3.2) during SWM season causes divergence in the surface layer and upward Ekman pumping causing upwelling. By August, the strength of the VV slightly decreases and the direction of the tongue of strong VV shifts northeastward into the Bay. During September, the VV reduces to  $1.6 \times 10^{-5} \text{ ms}^{-1}$  to the east of Sri Lanka and thereafter decreases.

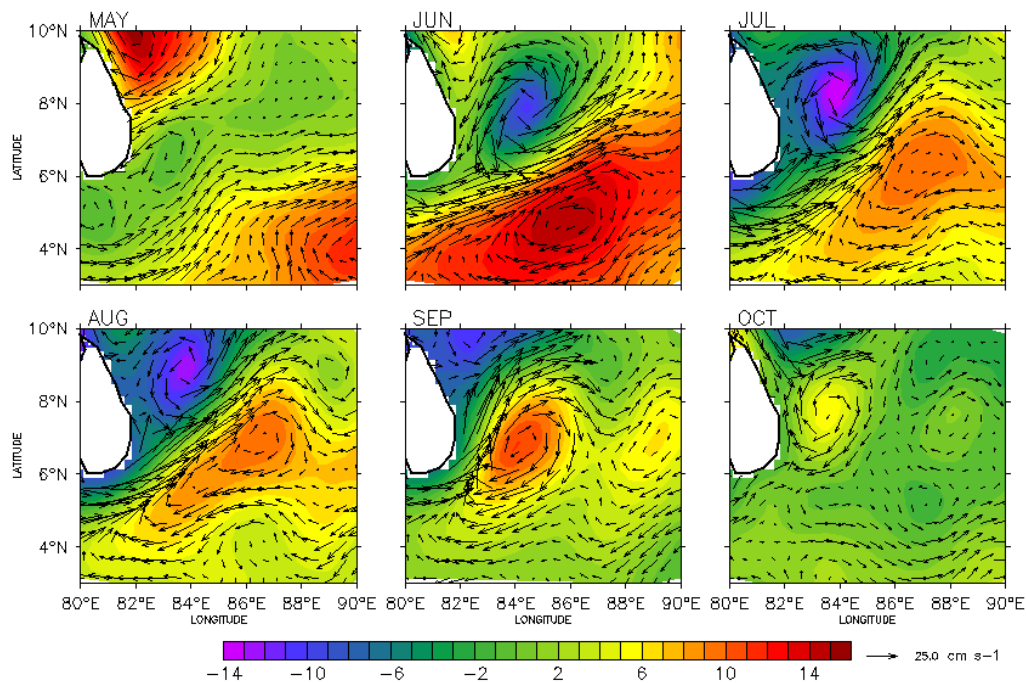


Fig. 4.11 Monthly mean sea level anomaly (cm) superimposed with geostrophic currents ( $\text{cm s}^{-1}$ ) in the southwestern Bay depicting evolution of the cold core eddy to the east of Sri Lanka and the intrusion of currents into the Bay of Bengal

The monthly mean SLA in the southwestern BoB illustrated in Fig. 4.11 shows the cyclonic eddy that develops during the SWM season. During June, with the onset of SWM, a cyclonic eddy develops to the east of Sri Lanka centered at  $84^\circ\text{E}$  between  $7^\circ\text{N}$  and  $9^\circ\text{N}$  and is flanked by an anticyclonic eddy centered at  $86^\circ\text{E}$  just to the south of it.

The western flank of the cyclonic eddy is a southward coastal current that flows against local winds. The geostrophic currents during this time show the intrusion of SMC into the southwestern BoB which forms the southern flank of the cyclonic eddy. Currents are very strong (about  $25\text{-}40\text{ cm s}^{-1}$ ) in this region. The eastern flank of the cyclonic eddy is a northward flow, that moves westward with the progress of SWM (Vinayachandran and Yamagata, 1998). The cyclonic eddy is most developed during July and within the eddy the SLA is about  $-14\text{ cm}$ . The cyclonic eddy is pushed northward by the anticyclonic eddy as the monsoon progresses and in August cyclonic eddy is centered at  $9^\circ\text{N}$ ,  $83^\circ\text{E}$  to the east of Sri Lanka. During September, the cyclonic eddy is located to the northeast of Sri Lanka, while the anticyclonic eddy shifts to the east of Sri Lanka replacing the cyclonic eddy. By October, the anticyclonic eddy to the east of Sri Lanka also becomes weak.

#### 4.5.2. West-central Bay of Bengal

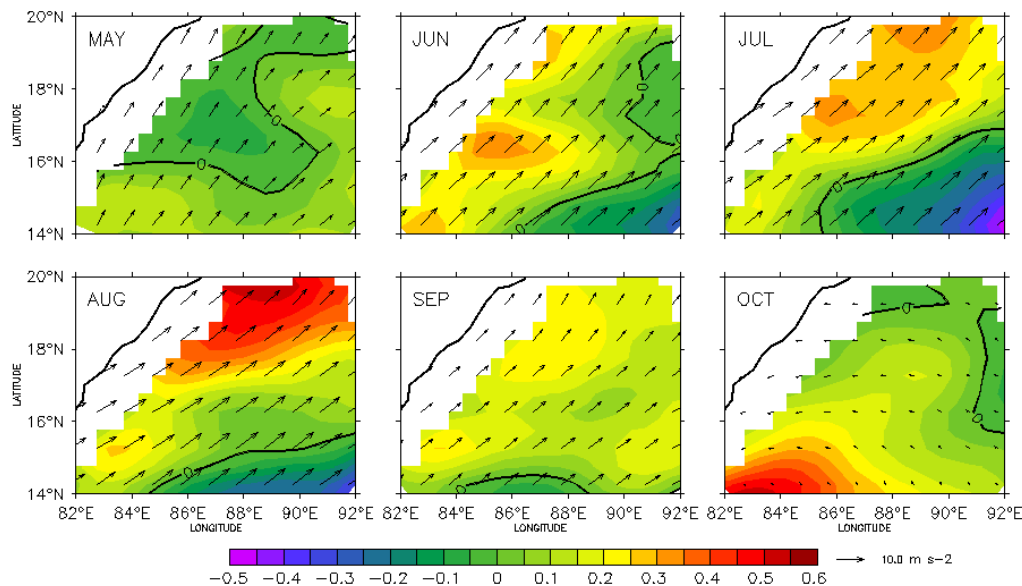


Fig. 4.12 Monthly mean Ekman vertical velocity ( $\times 10^{-5}\text{ m s}^{-1}$ ) from May to October in the west-central Bay of Bengal

The monthly mean VV of the west-central Bay are plotted in Fig. 4.12 depicting the intraseasonal variations during the SWM season. West-central Bay is an area of intense wind stress during this season. During May, the VV is negative on the western side and by the onset of SWM in June, the VV becomes positive and is about

$0.35 \times 10^{-5} \text{ m s}^{-1}$  at  $17^\circ\text{N}$ . By July the area of strong positive VV moves northward and during August, positive VV becomes very prominent ( $0.55 \times 10^{-5} \text{ m s}^{-1}$ ). Strong positive VV lies north of  $18^\circ\text{N}$  which indicate the upwelling in this region. In September, there is an overall decrease and the VV becomes less than  $0.25 \times 10^{-5} \text{ m s}^{-1}$ . During October, VV in the northern side further decreases while to the south between  $82\text{--}88^\circ\text{E}$ , an increase ( $\sim 0.55 \times 10^{-5} \text{ m s}^{-1}$ ) is observed which favours upwelling.

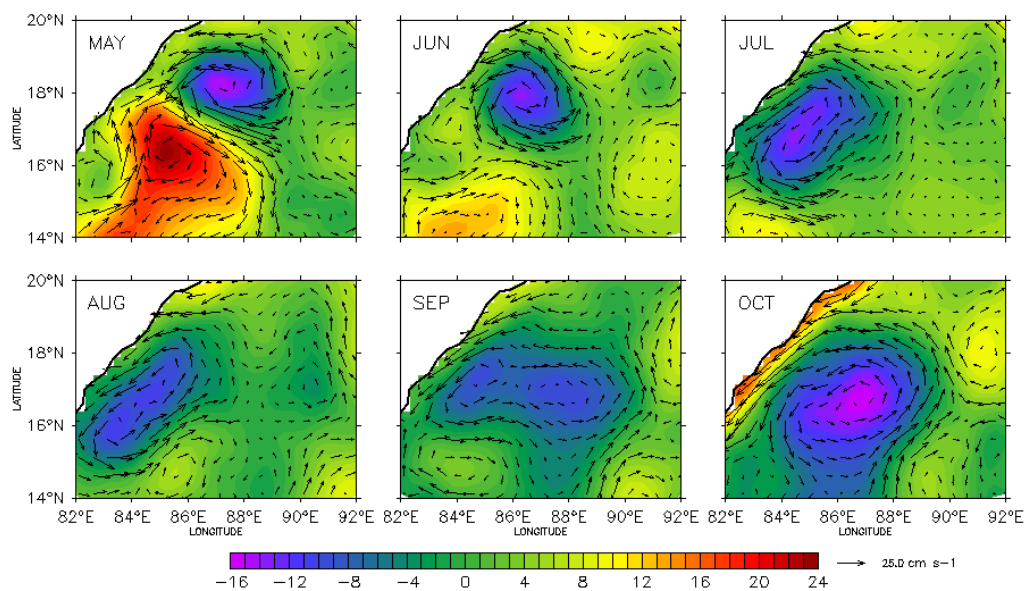


Fig. 4.13 Monthly mean sea level anomaly (cm) superimposed with geostrophic currents ( $\text{cm s}^{-1}$ ) in the west-central Bay depicting evolution of the cold core eddy and associated currents in the Bay of Bengal

A strong anticyclonic eddy flanked by a cyclonic eddy is observed during May in the west-central Bay (Fig. 4.13). During June, the anticyclonic eddy weakens and moves southwards. The cyclonic eddy extends along the western side in July, within which the SLA is about  $-14 \text{ cm}$ . By September, the cyclonic eddy becomes large and extends into the central Bay. The eddy appear to have two cold cores lying between  $16\text{--}18^\circ\text{N}$  in the central Bay. During October, the cyclonic eddy becomes well defined with an SLA of  $-16 \text{ cm}$  at  $87^\circ\text{E}$ ,  $18^\circ\text{N}$  within the eddy. During the entire SWM

season the western side of the cold core eddy is flanked by EICC which flows southwards along the coast in the northern Bay.

#### **4.6. Summary**

The variability of WSC over the BoB has been investigated using EOF analysis of monthly data of eight years (2000-2007) in this Chapter. EOF analysis technique is utilized to extract the patterns in the WSC data. The analysis gives spatial patterns of WSC and associated time series. The first four EOF modes represent more than 64% of the total curl variance with the first mode contributing to 36% of the total variance of the WSC field. The second EOF represents 15.1% of the total variance in curl data. The spatial patterns of WSC associated with these modes describe the major elements of BoB climatology. EOF 1 and EOF 2 represent the dominant features associated with monsoon seasons. From the associated time series, it has been observed that most of the variance is contained in annual frequencies and the first mode EOF1 and the second mode EOF2 have annual periodicity associated with southwest and northeast monsoon respectively.

The spatial distribution of wind stress in the BoB during the SWM has been analysed in this Chapter. The wind stress is found to be maximum to the southeastern side of Sri Lanka in the southwestern BoB ( $0.22 \text{ N m}^{-2}$ ) in July and in the west-central Bay during August ( $0.21 \text{ N m}^{-2}$ ). During this time, the lowest wind stress is observed in the southeastern Bay ( $0.04\text{-}0.05 \text{ N m}^{-2}$ ) followed by the east coast of India south of  $16^{\circ}\text{N}$  and in the southwestern Bay at around  $8^{\circ}\text{N}$  to the east of Sri Lanka ( $0.06\text{-}0.07 \text{ N m}^{-2}$ ).

The cold pool of the BoB lies between  $3\text{-}10^{\circ}\text{N}$  in the south-central BoB and extends to about  $90^{\circ}\text{E}$  to the east of Sri Lanka. The SST average for JJAS shows that lowest temperature is about  $28^{\circ}\text{C}$  to the southeastern side of Sri Lanka, which is the area that experiences high wind stress. The high wind stress along the southern coast of Sri Lanka leads to coastal upwelling and contributes to the SST reduction in this region. The cooler water is advected into the south-central Bay by the SMC which flow eastward south of Sri Lanka. The development of the cold pool is also due to

the cyclonic curl in the local wind field which causes open ocean upwelling (Vinayachandran and Yamagata, 1998). The mean geostrophic currents during JJAS show a cyclonic eddy with high negative SLA centered at 9°N, 84°E to the east of Sri Lanka in the southwestern Bay and an anticyclonic eddy with high positive SLA (centered at 6°N, 87°E) to the southeast of it. The geostrophic currents show the intrusion of SMC into the south-central BoB; the cyclonic eddy to the north being flanked by this current. Cold pool starts decaying in September, when a strong northward flow east of Sri Lanka replaces the cyclonic eddy (Vinayachandran and Yamagata, 1998). In the southwestern Bay, a wind speed maximum of about 10 m s<sup>-1</sup> during JJAS is observed over the southeastern side of Sri Lanka.

From the analysis of the interannual variations of cold pool in the south-central Bay (3-10°N, 82-90°E), it is observed that the lowest SST within the cold pool occurs generally during August: however, the years 2005 and 2006 were exceptions with the SST reaching the lowest values in September. The cold pool was most developed in 2000 and the SST reached the lowest of ~27.6°C within the cold pool during August, while in 2007 it was least developed followed by 2003. During 2007, the low SST of the cold pool was about 28.4°C which was observed during Aug-Oct. Also it has been observed that, in general, the lowest SST occurs between 4-7°N and extend eastward depending on the strength of the cold pool.

VV has been computed from WSC and analysed in the southwestern and west-central Bay where the intensity of wind stress is high. SLA has also been analysed in these regions of intense wind stress. Strong positive VV and high negative SLA indicate the occurrence of upwelling in a region. The VV to the eastern side of Sri Lanka increases in strength and extends eastward into the Bay as the SWM advances. A cyclonic eddy also develops during this time to the east of Sri Lanka which is flanked by an anticyclonic eddy to the south of it. VV attains the maximum intensity of about  $2.4 \times 10^{-5}$  m s<sup>-1</sup> in July at around 84°E, 7°N and extends upto 86°E, and thereafter weakens. The cyclonic eddy is most developed during July and the geostrophic currents are very strong about 25-40 cm s<sup>-1</sup> in this region. Geostrophic currents show the intrusion of SMC northeastward into the Bay which flanks the

eastern side of the cyclonic eddy. Ocean surface divergence and upward Ekman pumping by high positive WSC cause upwelling in the southwestern BoB. With the progress of SWM, anticyclonic eddy moves the cyclonic eddy northward and by September cyclonic eddy is located to the northeast of Sri Lanka.

In the west-central Bay, in May before the onset of SWM, the VV is mainly negative. During this time, a strong anticyclonic eddy flanked in the north by a cyclonic eddy is observed in the west-central Bay and this anticyclonic eddy weakens during June. During the SWM season, VV becomes positive with its intensity increasing as the monsoon advances. The area of high positive VV shifted gradually northward and reaches a high ( $0.55 \times 10^{-5} \text{ m s}^{-1}$ ) during August near  $20^{\circ}\text{N}$ . Strong positive VV north of  $18^{\circ}\text{N}$  indicate the presence of upwelling in this region. The cyclonic eddy further develops as the SWM advances and has two cold cores - one to the west and the other to the east during September. The strength of positive VV decreases considerably in September, and during October towards the southern side of this region between  $82\text{-}88^{\circ}\text{E}$ , positive VV increases to about  $0.55 \times 10^{-5} \text{ m s}^{-1}$ . During this time, the cold eddy develops more and is centered about  $87^{\circ}\text{E}$ ,  $18^{\circ}\text{N}$  with a depressed sea level anomaly of  $-16 \text{ cm}$ . The southward flowing EICC along the coast during SWM season forms the western side of the cold-core eddy.

## Chapter 5

# Upwelling and its significance in relation to surface chlorophyll distribution

### 5.1. Introduction

Thermocline is a distinct layer in the ocean where temperature decreases more sharply with depth than it does in the layers above and below it. It is the transition layer that separates the surface mixed layer from the calm cooler water below. The depth and strength of the thermocline shows considerable seasonal and annual variations. The change in depth of the 20°C isotherm (D20) is often taken as a proxy for thermocline anomalies (McPhaden, 1993; Harrison and Vecchi, 2001). Apart from being an appropriate index for the thermocline variability, D20 is also a good proxy for the pycnocline variability (Yu, 2003) and has been generally used as the thermocline in many studies (Kessler, 1990; Meinen and McPhaden, 2000) since D20 is located near the centre of the main thermocline. Schott *et al.* (2009) used D20 to represent the thermocline depth in the NIO and showed that it is shallow in regions of upwelling. Variations in D20 are important as they indicate upwelling in the ocean by means of the shoaling of thermocline.

Several studies have looked into the variability of thermocline on seasonal, inter-annual, and longer time scales (Rao *et al.*, 1993; Rao *et al.*, 2002b; Vinayachandran and Saji, 2008; Yu, 2003). Yu (2003) used XBT observations along 6°N to investigate the variability of the 20°C isotherm on seasonal and inter-annual timescales. They found that local Ekman pumping and remote Kelvin/Rossby wave propagation are the two leading forcing mechanisms responsible for thermocline variability. On seasonal timescales, the phase of the semi-annual variations are determined by a remote forcing signal, whereas on inter-annual timescales, the 20°C isotherm is sensitive to the remote equatorial wind variability, with local forcing

variability being the secondary contributor. Girishkumar *et al.* (2013) investigated the characteristics and possible causes of the intraseasonal thermocline variability in the BoB. They showed that in the thermocline region a persistent intra-seasonal variability on 30–120 day time scale having three distinct periods (30–70 day, near 90 day, and near 120 day) existed. They argued that the 90 day and 120 day thermocline variability is driven primarily by the variability of equatorial zonal wind stress; whereas the 30-70 day variability is influenced by the interior Ekman pumping in the Bay and also by the zonal wind stress in the equatorial Indian Ocean and alongshore wind stress in the eastern BoB.

In order to understand the subsurface thermal structure of the BoB, monthly variability of D20 has been analysed based on the subsurface temperature data by Ishii *et al.* (2005, 2006). The annual mean of D20 has been computed for the period 2000-2007 to bring out its salient features. Based on the prominent signatures of D20 observed in the annual mean, four areas have been selected for further study. Comparison of monthly variations of D20 indices were carried out with Ekman vertical velocity (VV), SLA and surface chl-*a* concentration indices in these boxes. The seasonal to inter-annual variations and the relation of D20 with these three variables have been studied in this Chapter.

Further, the seasonal to inter-annual variations of surface chl-*a* concentration in the four selected regions in BoB have been analysed and explained. The relationship of surface chl-*a* concentration with VV and SLA has been examined for these regions and the results explained.

## **5.2. Variability of D20 in the Bay of Bengal**

Monthly mean of D20 in the BoB has been plotted in Fig. 5.1 to understand the spatial and temporal variability of thermocline. It is observed that D20 is deep (~135 m) in the central Bay extending from the western Bay to the south of Andaman Islands in a southeastward direction. Shallow D20 of 95-100 m is observed in the eastern Bay and north of Sri Lanka in the western BoB. In February, D20 increases

in the western Bay and is deepest (~145 m) at around 86°E, 17°N. D20 becomes shallow in the rest of the BoB and decreases to about 80 m in the eastern Bay. During March, D20 increases further along the western Bay with the deepest D20 observed between 12-17°N (~ 145-150 m). During April, a similar pattern is observed in the spatial distribution of D20 except for the deepening of isotherms in the eastern Bay. Also the area of deeper isotherms in the western Bay reduces considerably. By May, there is an overall increase in D20 in the BoB. D20 is deepest (~150 m) in the western Bay between 12-18°N. During the same time, D20 increases to 140 m in the eastern and southeastern BoB. In the central Bay and extending from southwest to north, a comparatively shallow D20 (110-120 m) exists.

In June, with the onset of SWM, D20 in the western Bay decreases slightly whereas in the northern and eastern Bay it increases. Shoaling of D20 up to 90 m off the southern tip of India and southwestern Bay to the east of Sri Lanka occurs during this time. The spatial distribution of D20 undergoes considerable change in July, and lasts till October. A large decrease in D20 is observed in the entire BoB at this time. Shoaling of D20 is maximum (75 m) east and north of Sri Lanka in the southwestern Bay during July which indicates occurrence of upwelling. D20 decreases by about 60 m in the northern Bay and the depth is ~90 m around 18-20°N, indicating strong upwelling in this region. A slight increase of D20 (140 m) is observed in a small area near 87°E in the southern Bay during this time while on the eastern Bay it decreases to 130 m. D20 distribution remains almost the same during August except for the shoaling of D20 in the eastern and southern Bay. The D20 gets deeper east and northeast of Sri Lanka towards the central Bay forming a tongue like feature. During September, the extent of shallow D20 in the western Bay decreases as the SWM withdraws. Also a slight decrease in D20 is observed in the eastern Bay.

During October, shoaling of D20 intensifies in the western Bay while D20 increases in the eastern Bay. Around 9°N in the southwestern Bay, D20 decreases to 80 m signifying the shoaling of thermocline and occurrence of upwelling. Upwelling also

occurs in the northwestern Bay where D20 is shallow. In November a strong positive gradient of D20 from west to east is clearly discernible along the entire length of the Bay. There is deepening of D20 to 145 m in the northeastern BoB whereas D20 in the western Bay is about 100 m during this time. Deepening of D20 also occurs off the southern tip of India. In December, D20 decreases along the eastern and western periphery of the Bay, where as it continues to increase in the northern and southern Bay. D20 decreases to ~80 m in the eastern Bay while it increases to ~140 m in the northern Bay. A slight decrease of D20 (to ~90 m) is observed in the western Bay which is carried over from November indicative of the winter upwelling in this region.

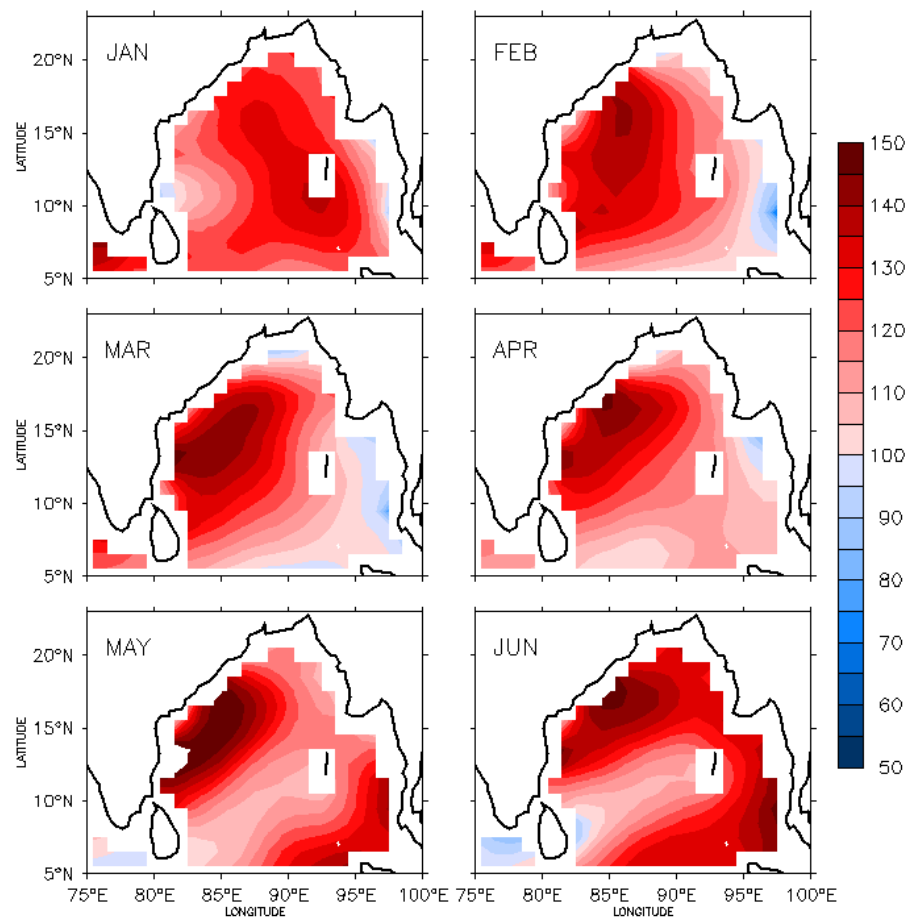


Fig. 5.1 Monthly mean of depth of 20°C isotherm (m) in the Bay of Bengal

Continued...

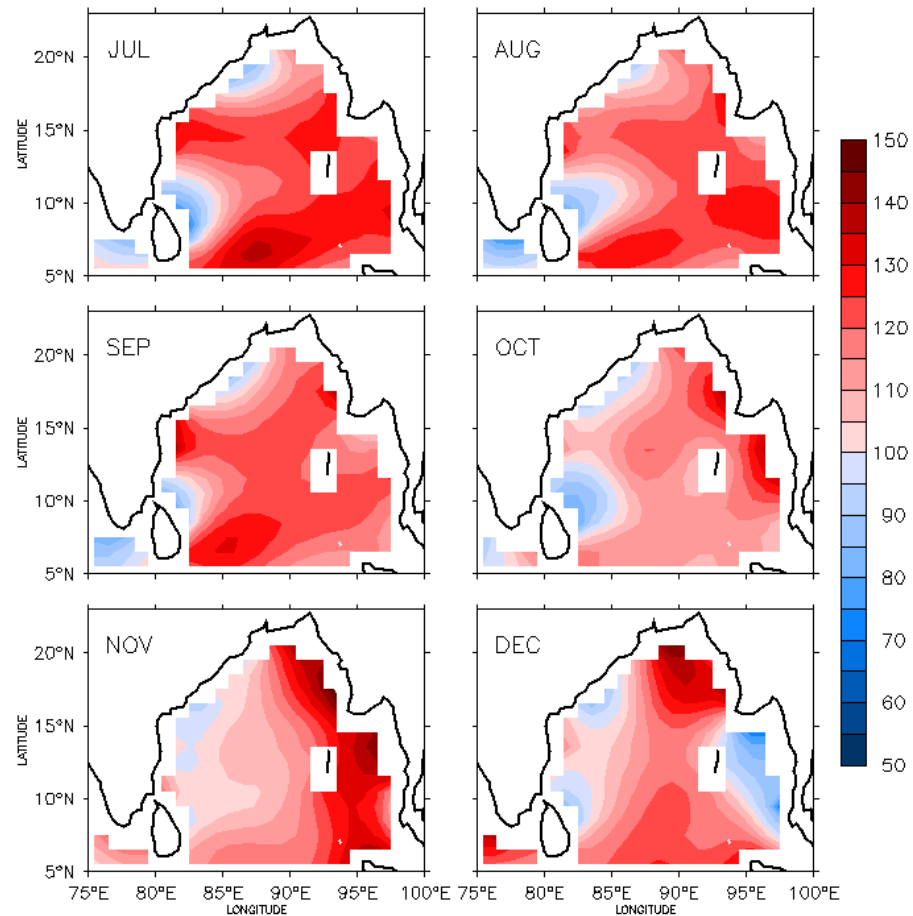


Fig. 5.1 Monthly mean of depth of 20°C isotherm (m) in the Bay of Bengal

It has been observed that D20 is deep during Jan-Apr in the BoB especially in the western Bay. In May, D20 becomes shallow across the Bay from southwest to northeast. It remains shallow in the southwestern and northern BoB during SWM season. D20 is shallow to the north and east of Sri Lanka in the southwestern Bay in July, indicative of the shoaling of thermocline and upwelling during this season. During post-monsoon season, there is a westward decrease in D20 and it is deep in the eastern Bay and shallow in the western Bay. Shallow thermocline exists in the western Bay during this reason which is associated with upwelling.

### 5.3. Annual mean distribution of D20

Fig. 5.2 depicts the annual mean pattern of D20 in the BoB: the prominent spatial signatures of D20 are evident from the figure. D20 is generally deep in the Bay especially in the central Bay where it is ~130 m in and around 87°E, 15°N. D20 is very shallow in the northern Bay (~103 m) and to the east and northeast of Sri Lanka (~107 m) in the southwestern Bay. D20 is also shallow in the eastern Bay. In the western Bay near 13°N, D20 reaches a maximum depth of ~130 m. Based on these significant features, four different areas have been selected for the study of monthly variations of D20 and its relation to VV, SLA and surface chl-*a* concentration.

The selected areas are:

1. Box A : 86-90°E, 18-21°N - Northern Bay
2. Box B : 84-88°E, 13-17°N - West-central Bay
3. Box C : 81-85°E, 7-11°N - Southwestern Bay
4. Box D : 95-98°E, 7-11°N - Andaman Sea

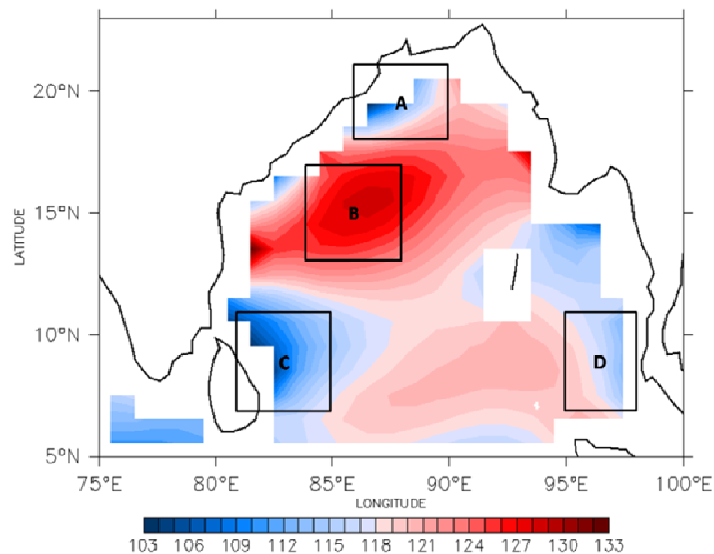


Fig. 5.2 Annual mean of the 20°C isotherm depth (m) in the Bay of Bengal (Boxed regions represent the four areas where further studies have been carried out)

Box A in the northern Bay is influenced by precipitation and large fresh water influx from Ganga and Brahmaputra rivers which result in low salinity and highly stratified surface layer. These two rivers discharge  $\sim 7.2 \times 10^{11} \text{ m}^3$  during Jun-Oct into the northern Bay which contributes to  $\sim 70\%$  of the total river discharge into the BoB (Martin *et al.*, 1981; Shetye *et al.*, 1993). Box B in the west-central Bay comes under the influence of seasonally reversing EICC (Shetye and Gouveia, 1998; Schott and McCreary, 2001). EICC is northeastward from February to September which is strong during Mar-Apr and southwestward from October to January with the strongest flow in November (Shankar *et al.*, 1996). Box C in the southwestern Bay is influenced by the seasonally reversing monsoon currents (Shankar *et al.*, 2002) and EICC. Vinayachandran *et al.* (2004) have shown that the SMC which flows eastward south of Sri Lanka and into the BoB advects the upwelled water from the southern coast of Sri Lanka along its path. East of Sri Lanka, the open ocean upwelling by cyclonic winds is associated with the cold pool formation during SWM and the intensification of chl-*a* concentration. During NEM, open ocean upwelling caused by Ekman pumping leads to high chl-*a* concentration in the southwestern Bay (Vinayachandran and Mathew, 2003). Box D lies in the Andaman Sea and is influenced by the eastern boundary currents. This region is influenced by Kelvin waves which efficiently transmit the wind input energy to the eastern boundary of the BoB (Yu *et al.*, 1991). McCreary *et al.* (1996) have shown that there exists a southward flow from October to January driven by interior Ekman pumping and local alongshore winds along the eastern and western coasts of BoB.

#### **5.4. Relationship of D20 with physical and biological properties**

##### **5.4.1. Relation between D20 and Ekman vertical velocity**

The monthly variability of D20 and VV indices (standardised anomaly) for the four selected areas are shown in Fig. 5.3(a-d). Positive anomalies of VV and negative D20 anomalies are indicative of upwelling. The inverse relation between VV and D20 has been brought out in these figures. The seasonal to inter-annual variations in

the VV and D20 are clearly seen in each box. Fig. 3.1 and Fig. 3.2 which show the WSC variations in BoB support the changes in VV observed in Fig. 5.3(a-d).

In box A in the northern BoB, VV anomaly is positive during the SWM season (Jun-Sep) which denotes upwelling (Fig. 5.3a). Positive VV anomalies sometimes extend to May and October. Annual maximum of positive VV anomaly occurs during Jul-Aug. During other months, VV anomalies are negative and its maximum is observed mostly during April. During Aug 2006 and 2007, very high VV anomaly is observed in this region. D20 is negative in March and from July to October with the maximum in July indicating the upwelling which is in agreement with VV anomalies. During other months, D20 anomalies are positive, the highest positive anomalies indicating downwelling in this region. In 2006, D20 anomaly is negative during Feb-May when VV anomaly is negative. D20 anomaly is negative in Nov 2007, reflecting the effect of a VSCS SIDR (11-16 Nov 2007) with the wind speed more than 64 kts in the shoaling of thermocline. VV does not reflect the effect of strong winds, which is due to the averaging of coarse temporal resolution data to produce the monthly mean data. The linear correlation coefficient between VV and D20 is -0.291 in the northern Bay.

In box B (Fig. 5.3b) in the west-central Bay, VV anomaly is positive from May to October, sometimes extending to November. In most of the years highest positive VV anomaly occurs during October indicating upwelling. During other months, VV anomalies are generally negative with its maximum observed mostly in April that denotes downwelling. A gradual decrease in the positive VV anomaly is observed from 2000 to 2006 which increases in 2007. High positive VV anomaly during Oct 2000 could be partially attributed to the strong winds associated with the cyclonic storm during 15-19 Oct 2000. The corresponding high negative D20 anomaly indicating the shoaling of thermocline supports the same. D20 anomaly is generally negative from July to December with its maximum in November or December indicating the shoaling of thermocline. During the rest of the period, D20 anomaly remains positive. The high positive VV anomaly in Nov 2002 could be due to the severe cyclonic storm during 10-12 Nov 2002 and the cyclonic storm during 23-28

Nov 2002 which affected this region. High positive anomaly of VV in May 2003 is attributed to the passage of a VSCS (10-19 May 2003) with a wind speed of more than 64 kts. D20 anomaly however remains positive during this time. During the occurrence of a cyclonic storm Baaz, (28 Nov-2 Dec 2005) with a wind speed of 45 kts, the D20 anomaly decreased and VV anomaly was positive. From 2002 to 2004 the variations in positive VV anomaly during Jun-Oct are erratic. The correlation between VV and D20 is -0.303 in the west-central region.

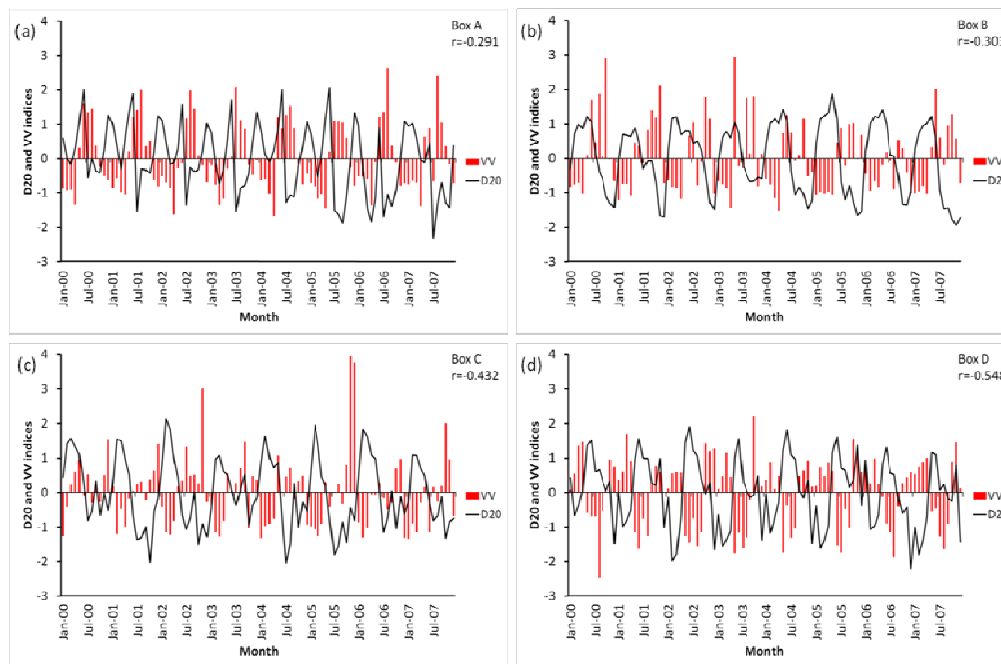


Fig. 5.3 Monthly variations of depth of 20°C isotherm and Ekman vertical velocity indices for Box A (86-90°E, 18-21°N), Box B (84-88°E, 13-17°N), Box C (81-85°E, 7-11°N), and Box D (95-98°E, 7-11°N) in the Bay of Bengal

In Box C in the southwestern Bay, VV anomaly is positive from May-Jun to Nov-Dec in general while for the rest of the year it is negative (Fig. 5.3c). The years 2000, 2006 and 2007 are exceptions when VV anomalies are variable during Jun-Nov. Also in 2000, VV anomalies are positive during Mar-Apr as opposed to other years. The positive maximum of VV anomaly occurs during November or December in general, with 2003, 2004 and 2007 being exceptions. D20 anomalies are positive during Jan-May and negative during the rest of the year. During high positive VV anomaly, the

corresponding D20 anomaly is negative. The negative maximum of VV anomaly occurs during Jan-Mar and is usually associated with high positive anomaly of D20. The effect of a VSCS with a maximum wind speed of 77 kts during 23-28 Dec 2000 in the southwestern Bay has been observed in the figure as high positive VV anomaly. Also the effects of cyclonic storms Baaz (28 Nov-2 Dec 2005) and Fanoos (6-10 Dec 2005) have been observed as very high positive VV anomaly during Nov-Dec 2005. D20 anomaly is negative during the same period. The correlation between VV and D20 is -0.432 in the southwestern Bay.

In box D region in the Andaman Sea in Fig. 5.3d, VV anomaly pattern is well defined with negative anomaly occurring mostly during May-Sep. In 2005, the negative VV anomaly occurs from June to September. During other months, VV anomaly is positive. D20 anomalies are positive during May-Nov in most years, while they last only till August in 2003, 2006 and 2007. Negative D20 anomalies are observed generally during Dec-Apr which is in an inverse relation with the positive anomalies of VV. Positive maximum of VV anomaly occur mostly during March when the D20 anomalies are negative and high indicating shoaling of thermocline. Maximum of negative VV anomaly occurs mostly in Jul-Aug during which D20 anomaly is positive. The correlation between VV and D20 in the Andaman Sea is found to be -0.548.

It has been observed from the analysis that D20 and VV undergo considerable seasonal variations in all the four selected regions in the BoB. Except for the Andaman Sea, D20 anomaly is generally negative and VV anomaly positive during the SWM and post-monsoon seasons. Negative D20 anomaly extends till December in west-central and southwestern Bay. Negative anomaly signifies shallow D20 and thermocline which could signify upwelling while high positive VV cause divergence of surface water and upwelling in the BoB. The maximum of negative D20 anomaly occurs generally during July in northern Bay, Nov/Dec in west-central Bay, whereas in the southwestern Bay it is variable. The maximum of positive VV anomaly occurs normally during Jul/Aug in northern Bay, October in west-central Bay and Nov/Dec

in southwestern Bay. In these three regions, D20 anomaly is positive and VV anomaly negative during NEM and pre-monsoon season. The maximum of positive D20 anomaly occurs generally during June in northern Bay, May in west-central Bay, and February in southwestern Bay. Negative maximum of VV occurs during April in northern and west-central Bay, while in southwestern Bay it is either January or February. In the Andaman Sea, D20 anomaly is negative during NEM and pre-monsoon season (Dec-Apr) whereas VV anomaly is positive during Oct-Apr with the maximum occurring in February or March. During other months D20 anomaly is positive (maximum in June) and VV anomaly negative with maximum in Jul/Aug. High positive VV induced by the strong cyclonic winds of severe tropical cyclones that cause upwelling, and the associated shoaling of thermocline depicted by the increase in negative D20 anomaly is also observed.

The low correlation between D20 and VV in northern Bay could be attributed to the low salinity caused by large river run-off and precipitation especially during SWM and the subsequent stratified layer which prevents the divergence of surface water and shoaling of thermocline. Ganga and Brahmaputra together discharge about  $7.2 \times 10^{11} \text{ m}^3$  of fresh water in to the northern Bay during Jun-Oct (Martin *et al.*, 1981; Shetye, 1993). Strong winds even during the SWM are unable to erode the intense stratification (Shenoi *et al.*, 2002) in the BoB. The equatorward EICC during NEM force coastal downwelling and advect the river discharge as a coastally trapped low-salinity plume (Shetye *et al.*, 1996) that can influence D20 variation in the west-central BoB. The correlation is better for the southern BoB. By November, the equatorward EICC that transports low saline fresh water is present all along the east coast causing a sharp decrease in salinity along the coast (Shetye *et al.*, 1996). When the EICC flows poleward in February it forces coastal upwelling and raise the salinity along the east coast (Shetye *et al.*, 1993). Though strong positive VV is observed in the southwestern Bay, the response of D20 is influenced by the EICC. Also the SMC that flows eastward advects the upwelled water from the Arabian Sea into the BoB. Open ocean upwelling by positive WSC which shoals the D20 occurs during NEM in the southwestern Bay. To the east of Sri Lanka, open ocean

upwelling associated with the Sri Lanka dome results in the shoaling of D20. During summer and winter monsoons, two coastal Kelvin waves originate along the eastern boundary of the BoB (Vinayachandran *et al.*, 1996). McCreary *et al.* (1993) suggested that remote alongshore winds excite coastal Kelvin waves that propagate anticlockwise round the perimeter of the Bay as well as Rossby waves that radiate westward from the eastern boundary.

#### **5.4.2. Relation between D20 and sea level anomaly**

The monthly variability of D20 and SLA indices (standardised anomaly) for the selected regions are shown in Fig. 5.4(a-d). Negative anomalies of SLA and D20 indicate shoaling of thermocline. The direct relation between SLA and D20 has been clearly brought out in these figures. Also the seasonal and inter-annual variations in the SLA and D20 are seen in each region.

In box A in the northern BoB (Fig. 5.4a), SLA is generally positive from May/June till the end of the year. During other months, SLA is negative with years 2002 and 2006 dominated by negative SLA. D20 anomaly is generally negative in March and July-Oct indicating the shoaling of thermocline. Except for Mar 2007 when D20 is positive, for all other years SLA and D20 show a positive correlation in March. But during SWM season, SLA is generally positive showing a negative correlation with D20. The negative SLA in Nov 2002 could be related to the severe cyclonic storm that developed during 10-12 Nov 2002, but D20 anomaly was positive and failed to show the shoaling of thermocline. The negative D20 anomaly of Nov 2007 reflects the effect of the VSCS SIDR during 11-16 Nov 2007 in the shoaling of thermocline. The SLA however does not show the reduction in sea level. It has been observed that there is no significant correlation between D20 and SLA in the northern Bay.

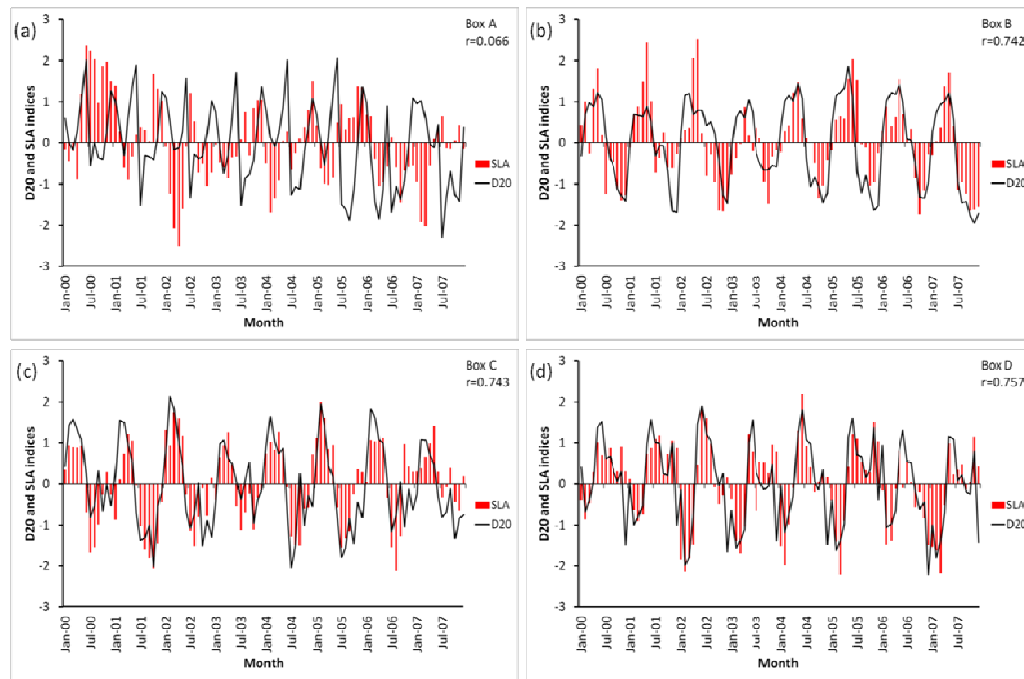


Fig. 5.4 Monthly variations of depth of 20°C isotherm and sea level anomaly indices for Box A (86-90°E, 18-21°N), Box B (84-88°E, 13-17°N), Box C (81-85°E, 7-11°N), and Box D (95-98°E, 7-11°N) in the Bay of Bengal

The seasonal and inter-annual variations in SLA of box B in the west-central BoB is clearly seen in Fig. 5.4b. SLA is generally positive during Jan-Jun and negative for the rest of the year. Negative SLA indicates divergence of water and upwelling during SWM season till the end of the year. D20 anomaly is also negative from July to December mostly, depicting the shoaling of thermocline and is positive during other months which indicate the deepening of thermocline. SLA is highly variable during Jan-Aug 2003. The lowest values of SLA are observed during Oct/Nov during which D20 anomaly also remains negative and high. The lowest SLA could be related to the occurrence of a severe cyclonic storm (10-12 Nov 2002) and two cyclonic storms (15-19 Oct 2000 and 23-28 Nov 2002) in this region. Positive high of SLA occurs during Apr-May and except for 2002, D20 high is observed during April, showing a positive correlation with SLA. Thus D20 and SLA are highly correlated and have a positive correlation of 0.742 in west-central Bay.

The seasonal to inter-annual variations in SLA and D20 in box C in the southwestern Bay are clearly seen in Fig. 5.4c. D20 anomalies are generally positive from January to May/June and negative from June/July to December. The corresponding SLA follows a similar pattern except in 2005 (negative SLA during June-October) and 2006 (negative SLA during June-September). Also during July-December 2007, SLA is variable in southwestern Bay. It has been observed from the figure that D20 and SLA are positively correlated in the southwestern BoB with a high correlation of 0.743. The maximum positive D20 anomaly is observed during February/March during which SLA is also maximum. During the occurrence of a VSCS in the southwestern Bay (23-28 Dec 2000) with a maximum wind speed of 77 kts, D20 and SLA decreased. D20 also decreased due to the passage of cyclonic storms Baaz (28 Nov-2 Dec 2005), and Fanoos (6-10 Dec 2005), but SLA remained positive during this time.

In box D region in the Andaman Sea (Fig. 5.4d), there is a positive correlation between D20 and SLA. In general, D20 anomalies are positive during May-November and negative during December-April. In 2003, 2006 and 2007 positive D20 anomalies are observed only from during May-August and remain negative for the rest of the year indicating a shallow thermocline. SLA is generally negative during January-April that shows a positive correlation with D20 anomaly. In 2002 and 2006, negative SLA is observed also during September-December and the corresponding D20 anomaly is negative. Negative maximum of SLA occurs during February/March during which D20 anomaly is lowest indicating a shallow thermocline. Also the occurrence of positive maximum of D20 (deep thermocline) in June is associated with positive SLA. Thus Andaman Sea has a high correlation of 0.757 between D20 and SLA.

Low sea level could be associated with divergence of surface water and shoaling of thermocline by upwelling. SLA in the northern Bay is in general positive during SWM till December and negative during other months. During NEM and pre-monsoon season, SLA is positive in boxes B and C, and negative in box D. SLA is negative during the SWM and post-monsoon season in west-central and southwestern Bay indicating shoaling of thermocline, whereas it is positive in the

Andaman Sea. Positive maximum of SLA occurs during Apr/May in west-central Bay, Feb/Mar in southwestern Bay and Jun/Jul in Andaman Sea. Negative maximum of SLA occurs during Oct/Nov in west-central Bay, whereas it is variable in southwestern Bay. In Andaman Sea, negative maximum occurs during Feb/Mar. Strong winds during tropical cyclones cause divergence at the ocean surface and upwelling which decreases sea level, and is associated with the shoaling of D20.

Yu (2003) suggested that SLA and D20 relation in the BoB is not linear because large variation in salinity also contributes to the sea level variability. The low correlation between D20 and SLA in the northern Bay when compared to the other three regions can be attributed to the large influx of fresh water from river discharge which affects the SLA (Girishkumar *et al.*, 2013). The freshening of the northern BoB where box A is located follows the precipitation maximum in June and the river discharge in August (Akhil *et al.*, 2014). Girishkumar *et al.* (2011) used buoy data to show that there is significant high correlation between SLA and 23°C isotherm in the southern BoB and suggested that SLA can be used as a good proxy to study the intraseasonal thermocline variability. The zonal winds along the eastern equatorial Indian Ocean play a dominant role in modulating the thermocline depth, SLA and MLD variability in the southern BoB (Girishkumar *et al.*, 2011, Sengupta *et al.*, 2007). Southern BoB and west-central Bay show high correlation between SLA and D20. The first and second baroclinic mode Kelvin waves and Rossby waves generated remotely by winds from the equatorial Indian Ocean and alongshore wind stress in the eastern BoB contribute significantly to the thermocline variability in BoB (Girishkumar *et al.*, 2013). The SLA anomalies also exhibit semi-annual variability similar to that of D20 due to the dominant baroclinic response of the BoB to the surface wind forcing. Coastal Kelvin waves that propagate into the Bay along the eastern boundary generated by equatorial wind variability are the main cause for the SLA near the eastern and northern boundaries (Han and Webster, 2002). The SLA in the west-central Bay, is influenced by the EICC which flows polewards during summer and equatorward during winter. In this region the sea level is mainly

determined by remote forcing through Rossby waves propagating from the interior of the bay (Eigenheer and Quadfasel, 2000).

### **5.4.3. Relation between D20 and surface chl-*a* concentration**

The relation between D20 and surface chl-*a* concentration has been analysed for the four selected regions in the BoB. Fig. 5.5(a-d) shows the relation between D20 and chl-*a* concentration by means of standardised anomaly. Increase in chl-*a* concentration caused by upwelling should be accompanied by the shoaling of thermocline which appears as increase in the negative anomaly of D20. The negative correlation between chl-*a* concentration and D20 is evident from these figures.

The seasonal and inter-annual variations in chl-*a* anomaly and its relation with D20 anomaly in box A in the northern BoB have been depicted in Fig. 5.5a. It has been observed that chl-*a* anomaly is generally positive from Jul-Aug to Oct-Nov showing an increase in concentration during the SWM and post-monsoon seasons. Its maximum occurs mostly in August and is accompanied by a decrease in D20 anomaly. During other months, chl-*a* anomaly is negative showing a decrease from the mean. An increase in chl-*a* anomaly in Oct 2000 could be due to the occurrence of the cyclonic storm during 25-28 Oct, 2000. In Sep 2005, high positive chl-*a* anomaly is observed caused by the passage of the cyclonic storm PYARR during 17-21 Sep 2005 which is accompanied by high negative D20 anomaly depicting the shoaling of thermocline. Also in Nov 2007 similar changes of lower magnitudes were observed due to the cyclonic storm SIDR (11-16 Nov 2007). High chl-*a* anomaly is observed during Jul 2001 and Aug 2006 during which D20 anomaly is negative. D20 and chl-*a* concentration have an inverse correlation of -0.527 in the northern BoB.

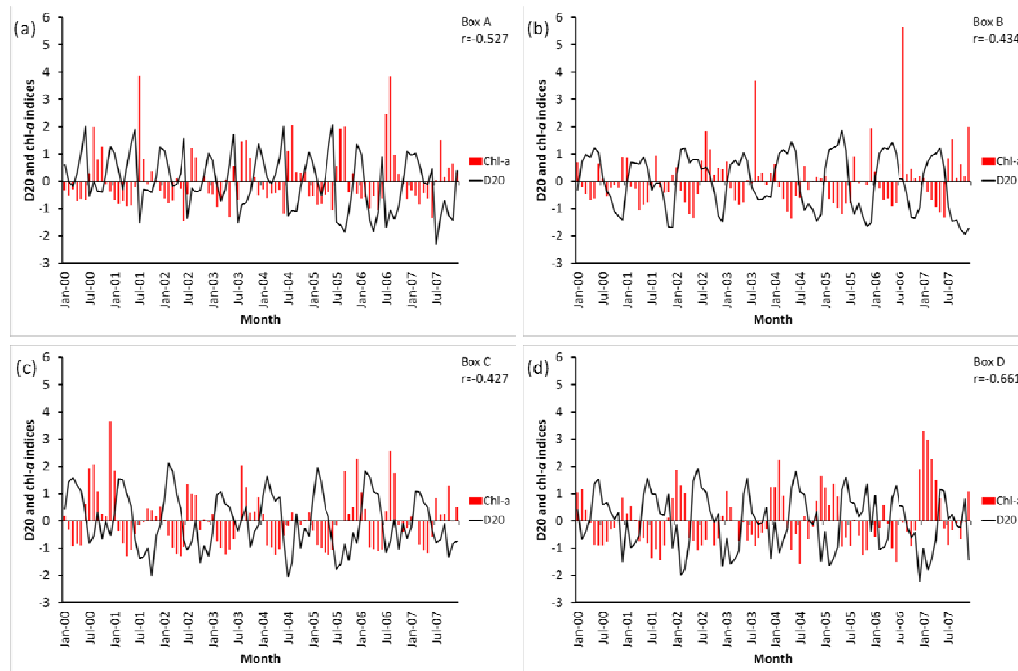


Fig. 5.5 Monthly variations of depth of 20°C isotherm and chl-*a* concentration indices for Box A (86-90°E, 18-21°N), Box B (84-88°E, 13-17°N), Box C (81-85°E, 7-11°N), and Box D (95-98°E, 7-11°N) in the Bay of Bengal

In box B in the west-central BoB (Fig. 5.5b), the inverse relation between surface chl-*a* concentration and D20 is evident especially when chl-*a* anomaly is negative and D20 anomaly is positive during Feb-Jun. The inverse relation during Jul-Dec is not well defined when the D20 anomaly is negative and chl-*a* anomaly is variable. The maximum of negative chl-*a* anomaly occurs during Apr/May during which positive D20 anomaly is high. During 2002-2003 and 2006-2007, the chl-*a* anomaly is mostly positive from July till December and the associated D20 anomaly is negative. The anomalous high chl-*a* anomaly during Aug 2003 is attributed to the presence of a bloom in this region. Another high chl-*a* anomaly in Dec 2005 is caused by the presence of a bloom which developed due to the cyclonic storm Baaz during 28 Nov-2 Dec 2005. The correlation between D20 and chl-*a* anomalies in the western BoB is -0.434.

The seasonal and inter-annual variations in surface chl-*a* concentration and D20 anomaly and its interrelation in box C in the southwestern BoB have been projected in Fig. 5.5c. Chl-*a* anomaly is negative during Feb-Jun in general during which D20 anomaly is positive with maximum during Feb/Mar. Positive anomalies of chl-*a* concentration are observed in the second half of the year during SWM and post-monsoon season and the associated D20 anomaly is negative. In Dec 2000, an anomalous high in chl-*a* anomaly is observed, caused by the bloom which developed due to the VSCS that occurred in the southwestern Bay during 23-28 Dec 2000 with a maximum wind intensity of 77 kts. The effect of another VSCS during 11-16 Dec 2003 could be the reason for a slight increase in the chl-*a* anomaly in Dec 2003. Two cyclonic storms Baaz (28 Nov-2 Dec 2005) and Fanoos (6-10 Dec 2005) caused an increase in chl-*a* anomaly in Dec 2005 in box C. D20 anomaly is negative during the occurrence of cyclones. The correlation between D20 and chl-*a* anomaly for this region is -0.427.

The inverse relation between D20 and chl-*a* anomalies in the box D in the Andaman Sea is clearly observed in Fig. 5.5d. Chl-*a* anomaly is generally negative during Apr-Oct sometimes extending to November. The corresponding D20 anomalies are positive in general during this time. In 2005, chl-*a* anomaly is negative during May-Dec and extending to February 2006, while in 2007 it is from June to November. Chl-*a* anomaly is positive during NEM and pre-monsoon season in this region with the maximum observed during Jan/Feb. 2006 is an exception with negative anomaly during this time. High positive chl-*a* anomalies are observed during Jan-Apr 2007 during which D20 anomaly is negative. The inverse relation between D20 and chl-*a* anomaly is high with a correlation of -0.661 in the Andaman Sea.

It has been observed that chl-*a* anomaly is generally positive during SWM and post-monsoon seasons in the northern, west-central and southwestern Bay, and negative during NEM and pre-monsoon season. Chl-*a* anomaly in the Andaman Sea is positive during NEM and pre-monsoon and negative from April to October sometimes extending to November. The positive maxima occurs during August in

northern Bay, while in the southern Bay it is variable. In Andaman Sea, the maximum chl-*a* anomaly occurs during Jan/Feb. The negative maximum of chl-*a* anomaly in the northern Bay occurs during Feb/Mar while in the west-central and southwestern Bay it occurs during Apr/May. In Andaman Sea, the negative maximum occurs during Jun-Jul. The occurrences of tropical cyclones tend to increase the chl-*a* concentration in the BoB, which is normally a low productive ocean (Smitha *et al.*, 2006, Rao *et al.*, 2006b).

The correlation between D20 and chl-*a* concentration is high in all the regions. Precipitation and large quantity of fresh water influx from the rivers especially during SWM season carry nutrients into the northern BoB increasing the chl-*a* concentration and D20 in this region. At the same time, they reduce the surface salinity and temperature thus making the BoB highly stratified (Shetye *et al.*, 1996). Northern Bay is also affected by strong positive VV during SWM. During SWM the EICC flows equatorward in the north and poleward in the south (Vinayachandran *et al.*, 1996). This current carries chl-*a* rich water from the northern Bay to the south along the northwestern coast thus influencing the chl-*a* concentration in the west-central Bay. The equatorward EICC during NEM forces coastal downwelling and also advects the nutrient rich water from the north thus increasing the chl-*a* concentration along the western BoB. The bifurcation of EICC which flows equatorward during NEM from the eastern coast results in high chl-*a* in the open ocean east of Sri Lanka (Vinayachandran *et al.*, 2005) thus influencing the chl-*a* concentration in southwestern Bay. Poleward moving EICC in February forces coastal upwelling and raises the salinity along the east coast (Shetye *et al.*, 1993). Advection of upwelled water from the south of Sri Lanka into the BoB by SMC increases the chl-*a* concentration (Vinayachandran *et al.*, 2004) in the southwestern Bay. Open ocean upwelling by strong WSC associated with Sri Lanka Dome causes upwelling during SWM thus increasing the chl-*a* concentration in the south-western Bay which also decreases D20. Also during NEM season, Ekman pumping causes open ocean upwelling in the southwestern BoB, which contributes to the increase in chl-*a* concentration (Vinayachandran and Mathew, 2003). The correlation is

maximum in the Andaman Sea, which is affected by Kelvin waves. In the eastern coast of the Bay, the winds are favourable for upwelling during NEM and pre-monsoon which increases the chl-*a* concentration and decreases D20 in the Andaman Sea. McCreary *et al.* (1996) showed the existence of a southward flow along the eastern and western coasts of the BoB during Oct-Jan which is driven by interior Ekman pumping and local alongshore winds. Table 5.1 lists the linear correlation coefficients of monthly D20 with chl-*a*, SLA and VV for the four regions illustrated in Fig. 5.2 with 99% confidence interval except for SLA in box A in the northern BoB.

Table 5.1 Linear correlation coefficients of monthly mean D20 with surface chlorophyll-*a* concentration, sea level anomaly and Ekman vertical velocity

<b>Linear Correlation Coeff.</b>	<b>Chl-<i>a</i></b>	<b>SLA</b>	<b>VV</b>
Box A (Northern Bay)	-0.527*	0.066	-0.291*
Box B (West-central Bay)	-0.434*	0.742*	-0.303*
Box C (Southwestern Bay)	-0.427*	0.743*	-0.432*
Box D (Andaman Sea)	-0.661*	0.757*	-0.548*

\* indicates a confidence interval of 99% for the effective degrees of freedom.

### 5.5. Seasonal and inter-annual variability of surface chl-*a* concentration

The seasonal to inter-annual variations in chl-*a* concentration in the four selected regions illustrated in the Fig. 5.2 have been analysed in this section. Fig. 5.6 shows the monthly mean variations in chl-*a* concentration for Box A (86-90°E, 18-21°N), Box B (84-88°E, 13-17°N), Box C (81-85°E, 7-11°N), and Box D (95-98°E, 7-11°N) in the BoB.

It has been observed that surface chl-*a* concentration is highest (upto about 1.8 mg m<sup>-3</sup>) in box A in the northern Bay compared to other boxes. Chl-*a* concentration is high during SWM season with the maximum concentration occurring mostly in August. Chl-*a* concentration in this region is in the range of 0.25 to 1.8 mg m<sup>-3</sup> with a mean of 0.68 mg m<sup>-3</sup> and during the SWM the average surface chl-*a* concentration increases to about 0.93 mg m<sup>-3</sup>. Strong cyclonic WSC that is observed during the SWM season (Fig. 3.1 and Fig. 3.2) and large river discharge that bring nutrients into the northern Bay occur during this season, together contribute to the increase in surface chl-*a* concentration. Ganga and Brahmaputra rivers have a peak discharge of about 0.07 x 10<sup>6</sup> m<sup>3</sup> s<sup>-1</sup> during Aug-Sep (Emery and Aubrey, 1989). During other seasons, chl-*a* concentration is less in northern Bay, but still remains high (>0.4 mg m<sup>-3</sup>) most of the time compared to other regions. Chl-*a* concentration is the lowest in northern Bay mostly during pre-monsoon season (Mar-May). During this time, winds are weak over the BoB and the river inflow less. Anomalously high surface chl-*a* concentration is observed during Jul 2001 and Aug 2006.

In general, chl-*a* concentration in the west-central and southwestern Bay and Andaman Sea are less than 0.4 mg m<sup>-3</sup> except in some months. A semi-annual variation is observed in chl-*a* concentration in the west-central Bay with the maxima occurring mostly in August followed by Dec-Jan. High positive WSC is observed during SWM season in the western Bay (Fig. 3.2) which causes upwelling and increase of chl-*a* concentration in the west-central Bay. Chl-*a* concentration is in the range of 0.1 to 0.66 mg m<sup>-3</sup> with a mean of 0.2 mg m<sup>-3</sup> in this region and during the SWM season the average chl-*a* concentration is 0.23 mg m<sup>-3</sup>. The EICC which flows equatorward in the north during SWM season transports chl-*a* rich water from the northern Bay leading to an increase in surface chl-*a* concentration in the west-central Bay. During the NEM season, the equatorward EICC carries the river runoff as a coastally trapped low salinity plume from the north (Shetye *et al.*, 1996). Vinayachandran (2009) suggested that the advection of these nutrient rich waters southward along the western side during NEM cause an increase in surface chl-*a* concentration in the west-central Bay. High chl-*a* concentration of ~ 0.67 mg m<sup>-3</sup>

compared to other months is observed during Aug 2006. The lowest chl-*a* concentration occurs in west-central Bay during the pre-monsoon season (Apr-May).

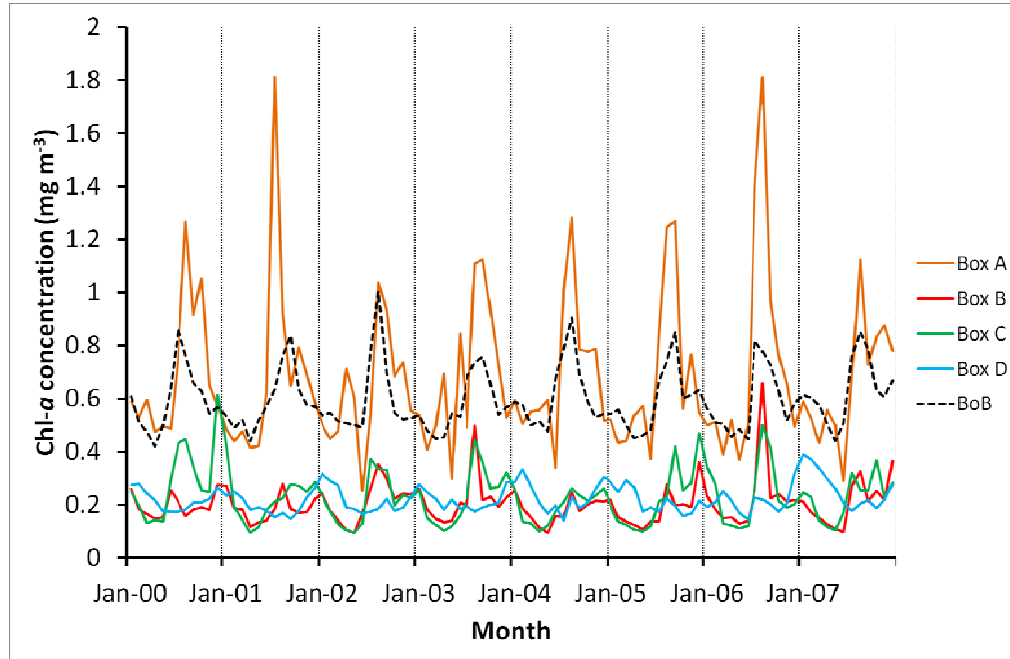


Fig. 5.6 Monthly variations in surface chl-*a* concentration ( $\text{mg m}^{-3}$ ) for Box A ( $86\text{--}90^\circ\text{E}$ ,  $18\text{--}21^\circ\text{N}$ ), Box B ( $84\text{--}88^\circ\text{E}$ ,  $13\text{--}17^\circ\text{N}$ ), Box C ( $81\text{--}85^\circ\text{E}$ ,  $7\text{--}11^\circ\text{N}$ ), Box D ( $95\text{--}98^\circ\text{E}$ ,  $7\text{--}11^\circ\text{N}$ ) and Bay of Bengal ( $75\text{--}100^\circ\text{E}$ ,  $5\text{--}23^\circ\text{N}$ )

Surface chl-*a* concentration in box C in the southwestern Bay is slightly high compared to west-central Bay with SWM being the major influencing factor. Surface chl-*a* concentration is in the range of  $0.1\text{--}0.62\text{ mg m}^{-3}$  in this region with a mean of  $0.23\text{ mg m}^{-3}$  and during the SWM the average concentration increases to  $0.28\text{ mg m}^{-3}$ . High chl-*a* concentration is observed during Jul-Dec and is lowest during Mar-Apr. Chl-*a* maximum occurs mostly during Aug/Sep in the southwestern Bay. In Dec 2000, high chl-*a* concentration of about  $0.614\text{ mg m}^{-3}$  was observed due the VSCS in the southwestern Bay during 23-28 Dec 2000. VSCS during 11-16 Dec 2003 increased the chl-*a* concentration in Dec 2003. High chl-*a* concentration ( $0.5\text{ mg m}^{-3}$ ) in Dec 2005 was caused due to the presence of cyclonic storms Baaz (28 Nov-2 Dec 2005) and Fanoos (6-10 Dec 2005). Vinayachandran and Mathew (2003) showed that open ocean upwelling driven by Ekman pumping cause chl-*a* bloom in the

southwestern Bay during NEM. Advection of upwelled water from the south of Sri Lanka into the southwest Bay by the SMC (Vinayachandran *et al.*, 2004) and the open ocean upwelling to the east of Sri Lanka associated with the Sri Lanka Dome during SWM caused the increase in surface chl-*a* concentration in the southwestern Bay.

Surface chl-*a* concentration in box D in the Andaman Sea is within the same range as that in the west-central Bay. The chl-*a* pattern is quite different in Andaman Sea compared to other regions. Surface chl-*a* concentration is high during NEM and pre-monsoon season in general with the maximum occurring in Jan/Feb. The chl-*a* concentration is within the range of 0.14-0.38 mg m<sup>-3</sup> with a mean of 0.22 mg m<sup>-3</sup> which decreases to about 0.19 mg m<sup>-3</sup> during the SWM. In this region chl-*a* concentration is high during the NEM and pre-monsoon season compared to SWM and is in the range 0.2-0.38 mg m<sup>-3</sup>. McCreary *et al.* (1996) observed the existence of a southward flow driven by interior Ekman pumping and local alongshore winds during Oct-Jan along both the eastern and western coasts of the BoB. Vinayachandran, (2009) attributed the high surface chl-*a* concentration during Jan-Feb in the Andaman Sea to the local coastal upwelling. Chl-*a* minimum is observed mostly during Jun/Jul in this region. The chl-*a* concentration of the BoB is within the range of 0.14-0.39 mg m<sup>-3</sup>. Chl-*a* concentration is high during SWM season with the maximum occurring mostly during August in the BoB. It is low during pre-monsoon season when the winds over the Bay are weak and variable and the minimum chl-*a* concentration occurs mostly during April. It has been observed that SWM is the major season influencing the increase in surface chl-*a* concentration, followed by NEM. Severe cyclonic winds during the occurrence of tropical cyclones are able to erode the highly stratified surface layer of the BoB causing the upwelling of nutrient rich water to the surface and the increase of surface chl-*a* concentration in that region.

## 5.6. Influence of physical properties on surface chl-*a* distribution

### 5.6.1. Relation between surface chl-*a* concentration and Ekman pumping

The effect of Ekman VV on surface chl-*a* concentration has been analysed in the four regions illustrated in Fig. 5.2 and the correlations between the two are computed. Fig. 5.7 (a-d) of the standardised anomaly of chl-*a* concentration and VV for each region shows the relation between both and its seasonal to inter-annual variations.

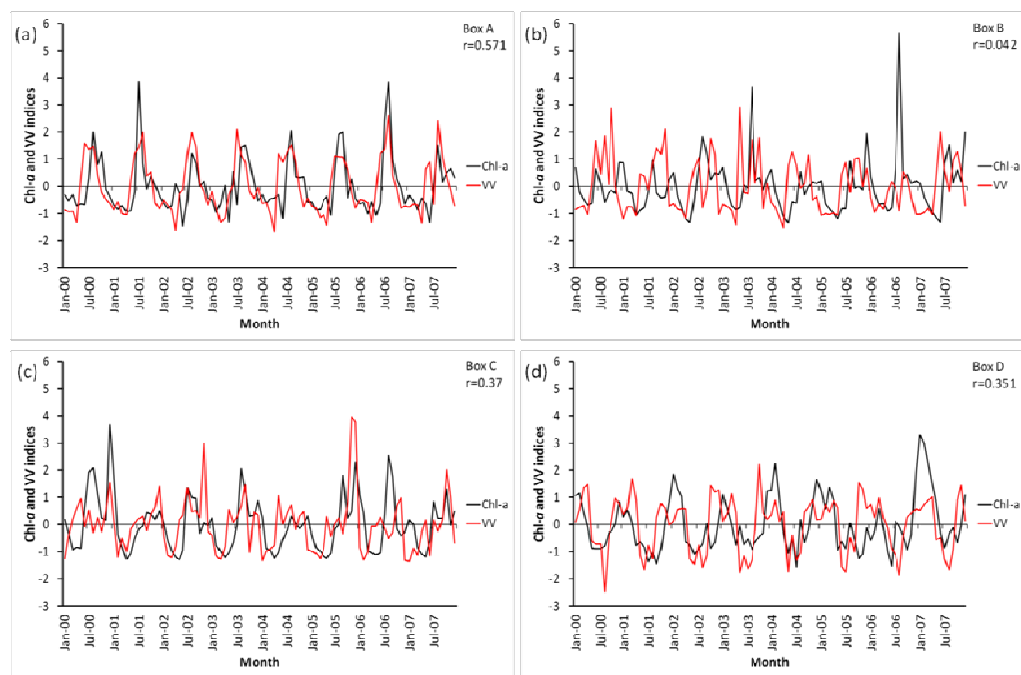


Fig. 5.7 Monthly variations of surface chl-*a* concentration and vertical velocity indices for Box A (86-90°E, 18-21°N), Box B (84-88°E, 13-17°N), Box C (81-85°E, 7-11°N) and Box D (95-98°E, 7-11°N) in the Bay of Bengal

The correlation between VV and surface chl-*a* concentration in box A in the northern Bay is maximum compared to other boxes. The correlation is 0.571 with a clear lag of about one month with the increase in VV preceding an increase in chl-*a* concentration (Fig. 5.7a). The high positive chl-*a* anomaly during the SWM is associated with high positive VV. Apart from VV that causes upwelling, the large river run-off that brings nutrients into the northern BoB especially during SWM

season increases the surface chl-*a* concentration in this region. Both Ganga and Brahmaputra which discharge  $\sim 7.2 \times 10^{11} \text{ m}^3$  of water into the northern Bay during Jun-Oct constitute about 70% of the total inflow into the BoB (Martin *et al.*, 1981; Shetye *et al.*, 1993). Since a highly stratified region due to the low salinity at the surface caused by fresh water inflow, VV is not fully efficient in breaking the stratification to cause upwelling and increase in chl-*a* concentration. In box B in the west-central Bay, chl-*a* concentration does not respond much to the increase in positive VV and the correlation is very low ( $r = 0.042$ ). Though VV is high during NEM, equatorward EICC forces coastal downwelling along the western Bay (Shetye *et al.*, 1996) thus preventing the increase in surface chl-*a* concentration in the west-central Bay.

In box C and box D in the southern BoB, the correlation between VV and chl-*a* concentration is 0.37 and 0.351 respectively. In box C in the southwestern Bay, strong Ekman VV associated with thihg positive WSC causes open ocean upwelling and an increase in surface chl-*a* concentration. The SMC that flows eastward south of Sri Lanka to the BoB during the SWM season advects high chl-*a* from the south and east coast of Sri Lanka into the BoB contributing to the formation of bloom during this season (Vinayachandran *et al.*, 2004). A lag of one month is observed in the southwestern Bay with high chl-*a* succeeding high positive VV. In box D in the Andaman Sea, the high surface chl-*a* concentration during NEM and pre-monsoon is associated with positive VV but not fully dependent on it. Vinayachandran, 2009 attributed the high chl-*a* concentration during Jan-Feb in the Andaman Sea to the local coastal upwelling. This region is affected by coastal Kelvin waves. Interior Ekman pumping and local alongshore winds drive a southward flow along the eastern and western BoB during Oct-Jan (McCreary *et al.*, 1996).

### **5.6.2. Relation between surface chl-*a* concentration and sea level anomaly**

The relation between surface chl-*a* concentration and SLA has been analysed in the four selected regions illustrated in Fig. 5.2. Fig. 5.8 (a-d) shows the standardised

anomaly of surface chl-*a* concentration and SLA and the inverse correlation between the same.

Correlation between surface chl-*a* concentration and SLA is the lowest in box A in the northern Bay. Chl-*a* concentration remains higher in the northern Bay compared to other regions and the maximum is observed during the SWM season. Northern Bay, a highly complex region, receives large quantity of fresh water from precipitation and river inflow which reduce the salinity thereby increasing the stratification especially during SWM season which is reflected in Fig. 6.11a. Riverine inflow brings nutrients into the ocean which increases surface chl-*a* concentration in the northern Bay. Normally strong positive WSC cause upwelling, decrease sea level and increase the surface chl-*a* concentration. But in the northern Bay it is difficult to erode the strong stratification which reduces the effect of strong winds in increasing chl-*a* concentration. In box B in the west-central Bay, the inverse correlation between surface chl-*a* concentration and SLA increases considerably (-0.444). This region is affected by the EICC which flows poleward along the southern part of east coast of India and equatorward in the north during SWM season (Shetye *et al.*, 1991, Vinayachandran *et al.*, 1996). This carries chl-*a* rich water from the northern Bay equatorward along the western side leading to an increase in chl-*a* concentration in west-central Bay. During NEM, the EICC flows equatorward all along the western side of the Bay, and carries the nutrient rich river inflow from the northern Bay, causing an increase in chl-*a* concentration in the west-central Bay. The SLA is low during SWM and post-monsoon seasons in west-central Bay. During SWM season, coastal upwelling also contributes to the high surface chl-*a* concentration in the west-central Bay, when SLA is low.

In box C and box D in the southwestern Bay and Andaman Sea, the inverse correlation between chl-*a* concentration and SLA is -0.661 and -0.606. The meandering of EICC off the coast leads to an increase in chl-*a* in the open ocean (Vinayachandran *et al.*, 2005). SMC transports nutrient rich upwelled water from the south of Sri Lanka into the BoB, thus increasing the chl-*a* concentration in the

southwestern Bay (Vinayachandran *et al.*, 2004) during SWM season. Open ocean upwelling caused by positive WSC associated with the Sri Lanka Dome also cause increase in chl-*a* concentration in this region during which period SLA decreases. Also, open ocean upwelling driven by the Ekman pumping increases the surface chl-*a* concentration in the southwestern Bay during NEM season (Vinayachandran and Mathew, 2003) together with a decrease in SLA. A southward flow exists along the eastern and western coasts of the BoB during Oct-Jan which is driven by interior Ekman pumping and local alongshore winds (McCreary *et al.*, 1996). Occurrence of high chl-*a* concentration during January coincides with this southward flow along with low SLA. Vinayachandran (2009) has attributed the high surface chl-*a* concentration during Jan-Feb to the local coastal upwelling.

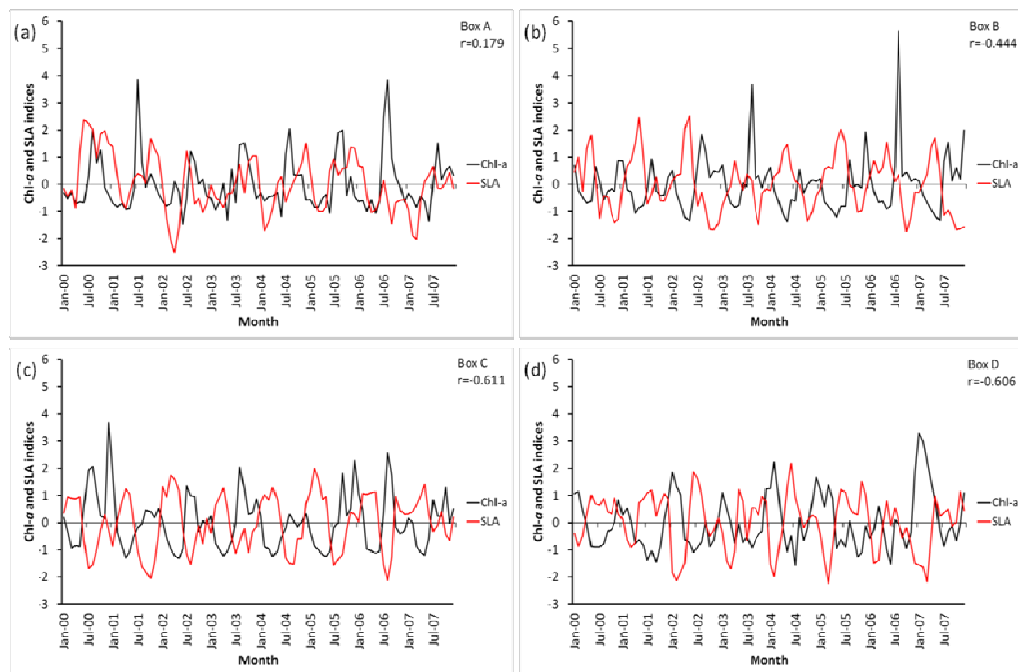


Fig. 5.8 Monthly variations of surface chl-*a* concentration and SLA indices for Box A (86-90°E, 18-21°N), Box B (84-88°E, 13-17°N), Box C (81-85°E, 7-11°N), Box D (95-98°E, 7-11°N) in the Bay of Bengal

In the northern Bay, generally the VV is positive during SWM and negative during the rest of the year. Besides, positive VV dominates the region sometimes during

May and October. In general, chl-*a* concentration remains higher than  $0.4 \text{ mg m}^{-3}$  throughout the year in the northern Bay. The positive VV maximum occurs during Jul-Aug which is about  $0.3\text{-}0.68 \times 10^{-5} \text{ m s}^{-1}$  while chl-*a* high (about  $0.7\text{-}1.8 \text{ mg m}^{-3}$ ) occurs during Aug-Sep. During the post-monsoon season also high chl-*a* concentration is observed. Chl-*a* concentration is low ( $\sim 0.3\text{-}0.5 \text{ mg m}^{-3}$ ) especially during Mar-Jun, whereas VV minimum is about  $-0.22 \times 10^{-5} \text{ m s}^{-1}$  to  $-0.44 \times 10^{-5} \text{ m s}^{-1}$  during Mar-Apr in the northern Bay. There is a lag of about one month between VV and chl-*a* concentration in the northern Bay with chl-*a* variation following variations in VV. In the west-central Bay, VV is positive normally during Jun-Oct ( $\sim 0.15\text{-}0.58 \times 10^{-5} \text{ m s}^{-1}$ ) with the highest values occurring mostly in October. Chl-*a* concentration is less in west-central Bay compared to the northern Bay and is higher than  $0.2 \text{ mg m}^{-3}$  reaching  $0.6 \text{ mg m}^{-3}$  except during pre-monsoon months. VV is high mostly during post-monsoon season. Chl-*a* concentration is low ( $0.1\text{-}0.14 \text{ mg m}^{-3}$ ) during Apr-May while VV is weak and negative ( $-0.22 \times 10^{-5} \text{ m s}^{-1}$  to  $-0.35 \times 10^{-5} \text{ m s}^{-1}$ ) during Mar-Apr. In the southwestern Bay, VV is generally positive except during Dec-Apr. The mean chl-*a* concentration in this region is slightly higher than that in the west-central Bay with the maximum occurring during Jul-Dec. Average chl-*a* concentration is about  $0.21\text{-}0.5 \text{ mg m}^{-3}$  during Jul-Sep in the southwestern Bay and the VV during this time is about  $0.2\text{-}0.55 \times 10^{-5} \text{ m s}^{-1}$ . Chl-*a* concentration is the lowest during pre-monsoon season ( $0.1\text{-}0.14 \text{ mg m}^{-3}$ ) and the average VV during Jan-Mar is the lowest about  $-0.1 \times 10^{-5} \text{ m s}^{-1}$  to  $-0.2 \times 10^{-5} \text{ m s}^{-1}$ . VV is generally negative in the Andaman Sea, while positive values dominate during Mar-Apr followed by Oct-Dec. The chl-*a* concentration is high during the NEM and pre-monsoon season and is generally in the range  $0.2\text{-}0.38 \text{ mg m}^{-3}$ . The positive VV in this region is high during post-monsoon and pre-monsoon and is about  $0.1\text{-}0.3 \times 10^{-5} \text{ m s}^{-1}$ . Chl-*a* concentration is minimum ( $0.14\text{-}0.23 \text{ mg m}^{-3}$ ) during SWM and the average VV is about  $-0.5 \times 10^{-5} \text{ m s}^{-1}$  to  $-1.2 \times 10^{-5} \text{ m s}^{-1}$ . It has been observed that there is a lag of about one month between the increase in VV and corresponding increase in surface chl-*a* concentration which is most prominent in the northern Bay while the relation is weak in the west-central Bay.

### 5.7. Summary

The upwelling zones are characterised by positive Ekman pumping, high biological productivity, raised thermocline, and depression in the sea level. In this Chapter, the variability and the importance of D20 in upwelling in the BoB has been analysed. It is observed that D20 undergo considerable seasonal variations and lay deep generally from January until May, which shoals considerably upon the arrival of SWM. D20 is shallow in the western Bay compared to eastern Bay during SWM and post-monsoon season. In general there is an inverse relation between VV and D20 in the BoB, with Andaman Sea having highest correlation coefficient of -0.548 whereas in the northern Bay, the correlation is the lowest. D20 and SLA has a direct relation in the BoB with high correlation ( $\sim 0.75$ ) in the boxes in west-central Bay, southwestern Bay and Andaman Sea except in the northern Bay which has no correlation between D20 and SLA. There exists an inverse correlation between D20 and surface chl-*a* concentration with northern Bay and Andaman Sea having better correlation than western and southwestern Bay. The effect of tropical cyclones is observed with strong positive VV, an increase in chl-*a* concentration, lowering of SLA and shoaling of D20 in the analysis.

From the study of seasonal to inter-annual variations in surface chl-*a* concentration, it has been observed that on an average, SWM is the major influencing season in the increase of surface chl-*a* concentration in the BoB followed by NEM. Compared to other regions, northern Bay has the highest concentration of chl-*a*  $>0.4 \text{ mg m}^{-3}$  throughout the year. Strong positive WSC (cyclonic) and the river discharge leads to the increased chl-*a* concentration in this region during SWM and the mean concentration is about  $0.93 \text{ mg m}^{-3}$  with the maximum chl-*a* concentration occurring mostly in August. During the pre-monsoon season when the winds are weak and reduction in riverine flow occurs, chl-*a* concentration is lowest. In the west-central Bay, chl-*a* concentration is high during SWM with the maximum occurring mostly in August followed by Dec-Jan. Strong positive WSC (cyclonic) together with the flow of EICC which carries nutrient rich waters cause the high chl-*a* concentration in this

region. The average chl-*a* concentration during SWM is  $0.23 \text{ mg m}^{-3}$  and the lowest concentration occurs during pre-monsoon season in the west-central Bay. In the southwestern Bay, high chl-*a* concentration with a mean of  $0.28 \text{ mg m}^{-3}$  occurs during SWM with the chl-*a* maximum observed mostly during Aug/Sep. Open ocean upwelling by Ekman pumping and the advection of nutrient rich waters from the south of India and southern coast of Sri Lanka by the SMC to the BoB cause the high chl-*a* concentration in the southwestern Bay. Also the chl-*a* minimum occurs during pre-monsoon season in this region. In the Andaman Sea, chl-*a* concentration high of  $0.2\text{-}0.38 \text{ mg m}^{-3}$  occurs during NEM and pre-monsoon season with the maximum in Jan/Feb. The high chl-*a* concentration during Jan/Feb is attributed to the presence of coastal upwelling. Also there exists a southward flow during Oct-Jan along the eastern Bay driven by interior Ekman pumping and local alongshore winds during which high chl-*a* concentration occurs in this region. The lowest chl-*a* concentration is observed during Jun/Jul in the Andaman Sea.

From the analysis of the relationship between chl-*a* concentration and VV, it is observed that the positive correlation between these two parameters is maximum (0.571) in the northern Bay, with a lag of about one month for increase in chl-*a* concentration to appear due to an increase in VV, followed by the southwestern Bay and Andaman Sea respectively. In the northern Bay, VV is not entirely efficient due to the high surface stratification in causing upwelling and increase the surface chl-*a* concentration. There is no significant correlation between chl-*a* and VV in the west-central Bay. During NEM, equatorward EICC forces coastal downwelling along the western Bay which prevent the increase in chl-*a* concentration. In the southwestern Bay, a lag of one month is observed for the increase in chl-*a* concentration succeeding an increase in VV. Analysis of chl-*a* concentration with SLA reveals that there exists an inverse correlation between the both in BoB. In the northern Bay there is no significant correlation while in the southwestern Bay and Andaman Sea chl-*a* has good correlation ( $\sim -0.6$ ) with SLA. The strong stratification in the northern Bay reduce the effect of VV in causing upwelling and reducing the sea level. But at the same time, riverine flow brings nutrients to the surface increasing the chl-*a*

concentration. In the west-central Bay the correlation is -0.444 between chl-*a* concentration and SLA. The EICC, which carries nutrient-rich waters from the northern Bay equatorward leads to an increase in chl-*a* concentration in the west-central Bay. In the southwestern Bay where the correlation between chl-*a* concentration and VV is -0.661, advection of nutrient rich waters by SMC, open ocean upwelling driven by Ekman pumping, and the flow of EICC cause increase in chl-*a* concentration.

It has been observed from the analysis of VV and surface chl-*a* concentration that in the northern Bay, high chl-*a* concentration during SWM is accompanied by strong positive VV. The VV maximum ( $0.3-0.68 \times 10^{-5} \text{ m s}^{-1}$ ) in Jul-Aug is followed by a chl-*a* maximum ( $0.7-1.8 \text{ mg m}^{-3}$ ) in Aug-Sep. Low chl-*a* concentration ( $0.3-0.5 \text{ mg m}^{-3}$ ) especially during Mar-Jun is associated with VV minimum ( $-0.22 \times 10^{-5} \text{ m s}^{-1}$  to  $-0.44 \times 10^{-5} \text{ m s}^{-1}$ ) during Mar-Apr in the northern Bay. In the west-central Bay, positive VV during Jun-Oct ( $\sim 0.15-0.58 \times 10^{-5} \text{ m s}^{-1}$ ) reaching high mostly in October is followed by chl-*a* concentration higher than  $0.2 \text{ mg m}^{-3}$  reaching  $0.6 \text{ mg m}^{-3}$ . Surface chl-*a* concentration is low ( $0.1-0.14 \text{ mg m}^{-3}$ ) during Apr-May follows the weak VV ( $-0.22 \times 10^{-5} \text{ m s}^{-1}$  to  $-0.35 \times 10^{-5} \text{ m s}^{-1}$ ) during Mar-Apr. In the southwestern Bay, VV is generally positive except during Dec-Apr, and the low VV ( $-0.1 \times 10^{-5} \text{ m s}^{-1}$  to  $-0.2 \times 10^{-5} \text{ m s}^{-1}$ ) during Jan-Mar is associated with the chl-*a* minimum ( $0.1-0.14 \text{ mg m}^{-3}$ ) in pre-monsoon season. High VV of  $0.2-0.55 \times 10^{-5} \text{ m s}^{-1}$  during Jul-Sep is followed by chl-*a* concentration of about  $0.21-0.5 \text{ mg m}^{-3}$  in the southwestern Bay. VV is generally negative in the Andaman Sea except during Mar-Apr and Oct-Dec. During NEM and pre-monsoon season, chl-*a* concentration is high ( $0.2-0.38 \text{ mg m}^{-3}$ ) and VV is about  $0.1-0.3 \times 10^{-5} \text{ m s}^{-1}$  during post-monsoon and pre-monsoon in this region. Also chl-*a* minimum ( $0.14-0.23 \text{ mg m}^{-3}$ ) during SWM follows the low VV ( $-0.5 \times 10^{-5} \text{ m s}^{-1}$  to  $-1.2 \times 10^{-5} \text{ m s}^{-1}$ ) in this region. It has been observed that there is a lag of about one month between the increase in VV and corresponding increase in surface chl-*a* concentration which is most prominent in the northern Bay followed by southwestern Bay and Andaman Sea while the relation is weak in the west-central Bay.

It has also been observed that on an average, VV increased by 2.6-2.8 times during August in the northern Bay from the low in April. Surface chl-*a* concentration increased by 3 times during August in this region from the low values in Apr-May. In the west-central Bay, VV increased by 2.5 times in October, while the maximum increase in chl-*a* concentration is about 3 times during August. In the southwestern Bay, VV increased by about 2.5-3 times from Mar-Apr to August and surface chl-*a* concentration increased by 3 times from April to August. In the Andaman Sea an increase of about 1.4 times is observed for VV from Jul-Aug to Mar-Apr while chl-*a* concentration increased by about 1.7 times from April to August in this region. It has been observed from the analysis that the variations in VV influence the surface chl-*a* concentration in the BoB. Strong winds are able to erode the highly stratified waters of the BoB under favourable conditions and cause upwelling which increase the surface chl-*a* concentration.

## Chapter 6

# Upper ocean response to upwelling induced by tropical cyclones in the Bay of Bengal - Case studies

### 6.1. Introduction

Strong winds, heavy rainfall and storm surges associated with tropical cyclones can cause great damage to life and property in the countries bordering NIO, particularly the BoB. About 7% of the global tropical cyclones occur in the NIO (Dube *et al.*, 1997). On an average, 5 to 6 cyclones form in the BoB and Arabian Sea every year with maximum sustained wind of 34 kts or more, of which 2-3 cyclones reach severe stage with maximum sustained wind of 48 knots or more (Singh *et al.*, 2001). More cyclones occur in the BoB than in the Arabian Sea, the ratio of their frequencies being about 4:1 (Dube *et al.*, 1997). In the Bay, cyclones usually form between 8.0°N and 15.0°N along the ITCZ. There are two cyclone seasons in the NIO, viz. the pre-monsoon season (Mar - May) and post-monsoon season (Oct - Nov), with the highest frequencies in November and May. Tropical cyclones during the post-monsoon are more devastating in nature. The formation of large number of tropical cyclones in BoB are due to the presence of high SSTs (SST remains above the 28°C threshold in all seasons), a dynamically unstable atmosphere and low tropospheric wind shear during the post-monsoon and pre-monsoon seasons while they are inhibited by strong tropospheric wind shear during the monsoon season (Menkes *et al.*, 2012).

Tropical cyclone induced surface cooling is larger in the pre-monsoon season (~3°C) than in the post-monsoon season (0.5–1°C) in the BoB (Sengupta *et al.*, 2008) thereby affecting the intensity of the cyclones. Singh *et al.* (2001) showed that maximum number of severe cyclones in the NIO is during the month of November. On an average, one severe cyclone is expected to form in November every year. Cyclones during November generally move westward to west-north-westward and strike the Andhra Pradesh or Tamil Nadu coasts of India. Occasionally, these

cyclones move northward and recurve north-westward to strike the Bangladesh or Myanmar coast (Singh *et al.*, 2001). Also it is not unusual for a storm formed over the BoB to move across southern India and re-intensify over the eastern Arabian Sea.

A list of the tropical cyclones (cyclonic storms with maximum wind speed of 35-47 kts and higher categories) formed in the BoB during the period 2000-2007 is given in Table 5.1

Table 6.1 Tropical cyclones in the Bay of Bengal during 2000 to 2007. The categories of tropical cyclone with the maximum wind speed in brackets are given. CS - Cyclonic Storm (34-47 kts), SCS - Severe Cyclonic Storm (48-63) and VSCS - Very Severe Cyclonic Storm (64-119 kts)

Year	CS	SCS	VSCS
2000	27-30 Mar (45 kts) 15-19 Oct (35 kts) 25-28 Oct (35 kts)		26-30 Nov (102 kts) 23-28 Dec (90 kts)
2001	14-17 Oct (35 kts)		
2002	23-28 Nov (35 kts) 21-25 Dec (35 kts)	10-12 Nov (55 kts)	
2003		11-16 Dec (55 kts)	10-19 May (75 kts)
2004			16-19 May (90 kts)
2005	13-17 Jan (35 kts) HIBARU 17-21 Sep (35 kts) PYARR 28 Nov-2 Dec (45 kts), BAAZ 6-10 Dec (55 kts), FANOOS		
2006		27-30 Oct (55 kts)	24-29 Apr (120 kts) MALA
2007		13-15 May (65 kts) AKASH	11-16 Nov (140 kts) SIDR

The low biological productivity of the BoB compared to Arabian Sea is attributed to the strong stratification, high SST and relatively weak winds (Gomes *et al.*, 2000; Prasanna Kumar *et al.*, 2002). According to Kumar *et al.* (2004) only 20% of the nitrogen required to support the new production during pre-monsoon and post-

monsoon seasons comes from the rivers and atmosphere. They suggested that cyclones through the entrainment of subsurface water could help in brining a significant part of the remaining nitrate from deeper waters. Shortly after a cyclone event, an increase in phytoplankton biomass and productivity is frequently observed (Lin *et al.*, 2003). The nutrients injected to the well-lit euphotic zone induce the growth of plankton. Tropical cyclones with strong winds are able to erode the stratification in BoB and upwell cold nutrient rich water to the euphotic zone reducing SST and leading to high chlorophyll and PP. Deepening of mixed layer together with depressed sea level is also associated with the occurrence of tropical cyclones.

Studies on the effect of tropical cyclones on biological process have increased with the advancement in computing the regional/global PP using models. Satellite observations are able to detect the changes caused by tropical cyclones in many parts of the world ocean. In this Chapter, the response of some of the upper ocean physical and biological properties to the occurrence of tropical cyclones has been analysed. Two incidences of tropical cyclones in the BoB have been studied, of which one developed during post-monsoon season in Nov-Dec 2000 and the second during pre-monsoon in May 2003.

The tropical cyclone during 26 Nov-6 Dec 2000 was a VSCS with a maximum wind speed of 102 kts. This cyclone moved westward, made the landfall south of Cuddalore and after weakening into a low pressure system, emerged into eastern Arabian Sea which weakened later. The tropical cyclone during 10-19 May 2003 was also a VSCS with a maximum wind speed of 75 kts which moved northward and then northwestward making the landfall over Myanmar coast.

The changes in SST, chl-*a* and PP caused by the passage of the tropical cyclones are analysed using satellite observations and model outputs in both cases. The changes in MLD have been studied for the tropical cyclone in May 2003. The data sets used for the study are 8-day composite SST and chl-*a* from Terra MODIS, 8-day composite mixed layer PP (P2) estimated by the GSFC, and MLD generated by US Navy's

FNMOG averaged to the MODIS weekly period. SLA data from altimeter observations has been used for the analysis of sea surface height (SSH) variation due to the tropical cyclone in Nov 2000. Weekly averaged SST from TMI has also been used to study the changes in SST analysis of tropical cyclone during May 2003. In addition, weekly WSC data from QuickSCAT and computed VV have been used for the analysis.

### 6.2. Tropical cyclone 03B (TC 03B), 26 Nov – 6 Dec 2000

Cyclone induced productivity has been studied in the southwestern BoB for the tropical cyclone TC 03B during 26 Nov-6 Dec 2000, which is a VSCS with a wind speed of more than 65kts. A depression formed at 800 km southeast of Pondicherry at 9°N, 90°E (Fig. 6.1) in the BoB on 26 Nov 2000, and intensified into a VSCS about 300 km east of Pondicherry/Cuddalore stretch by 29 Nov 2000. It remained stationary for a day at 11.5°N, 78°E on 30 Nov 2000 and then moved to west and left the main land (west coast of India) on 1 Dec 2000. It further moved to the Arabian Sea with lower intensity of 30 kts around 5 Dec and dissipated on 6 Dec 2000. The study area is mostly along the cyclone track and its periphery, around 100 km<sup>2</sup> on either side of the track in southwestern BoB, between 10-12°N and 80-84°E.

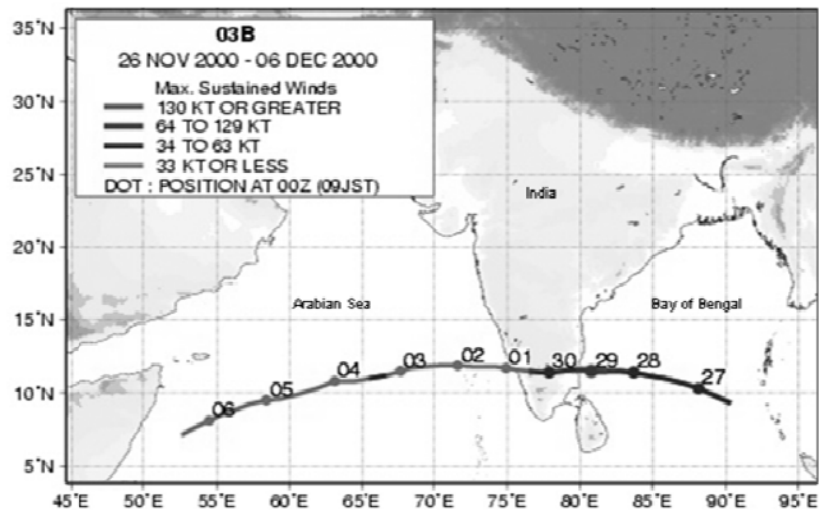


Fig. 6.1 Track of tropical cyclone 03B during 26 Nov – 6 Dec 2000 (from Rao *et al.*, 2006b)

### 6.3. Response of physical and biological properties of ocean to TC 03B

MODIS weekly (8 day) composite 4.0 km spatial resolution SST and chlorophyll images depict the distribution of SST and chl-*a* concentration prior to the development of cyclone and after its passage. In the absence of daily coverage and due to cloud cover, weekly mean SST and chl-*a* concentration are used for this study.

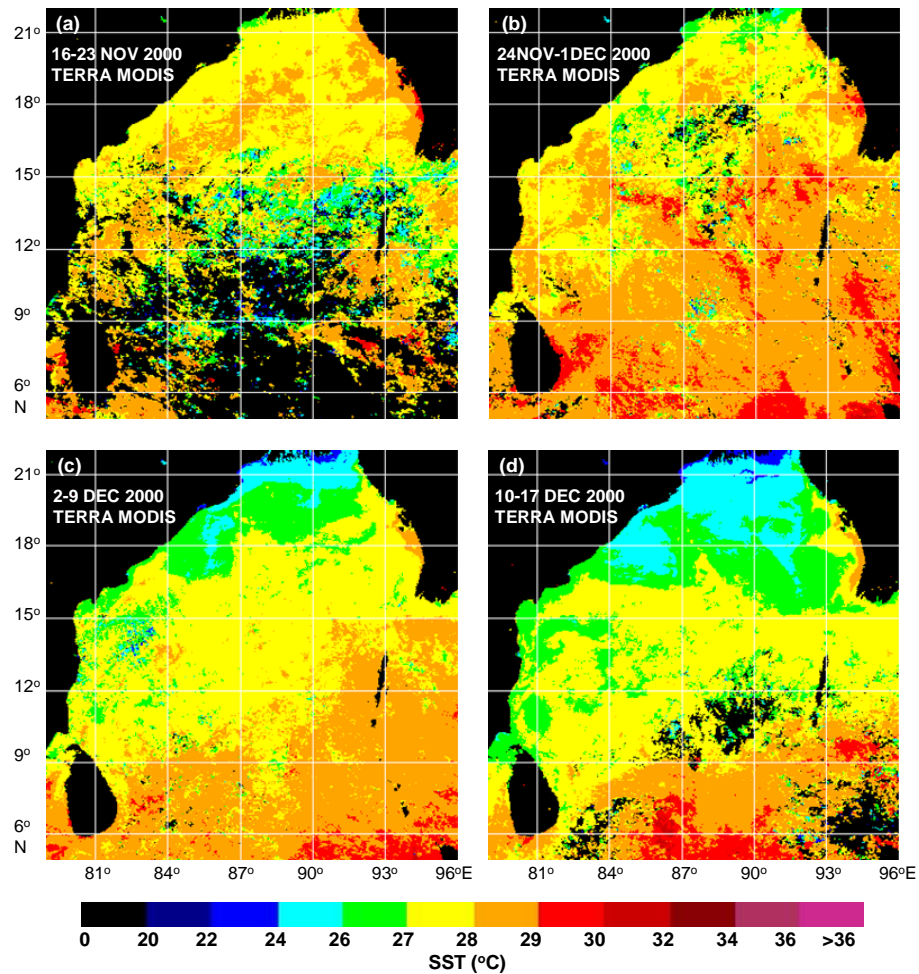


Fig. 6.2 Terra MODIS weekly sea surface temperature in °C: (a) 16-23 Nov before the cyclone; (b) 24 Nov-1 Dec during the cyclone; (c) 2-9 Dec; and (d) 10-17 Dec 2000 after the passage of cyclone

Fig. 6.2 shows the weekly mean day time SST for the periods (a) 16-23 Nov, (b) 24 Nov-1 Dec, (c) 2-9 Dec and (d) 10-17 Dec 2000. From 16 to 23 Nov 2000, SST in

the southwestern Bay was around 28.25°C. During the passage of the cyclone, SST decreased to 26.6-27°C, while in south and east of this region temperature remained high at around 29°C. One week after the passage of cyclone (2-9 Dec 2000), the surface temperature around 11°N, 81°E further reduced to about 26.5°C. During 10-17 Dec 2000, SST again decreased slightly to 26.1°C, but along the outer periphery of the track it increased to about 27°C. Maximum SST drop of 2°C was observed at 11°N, 81°E where the temperature decreased from 28.26°C before the cyclone to 26.18°C two weeks after the passage of cyclone.

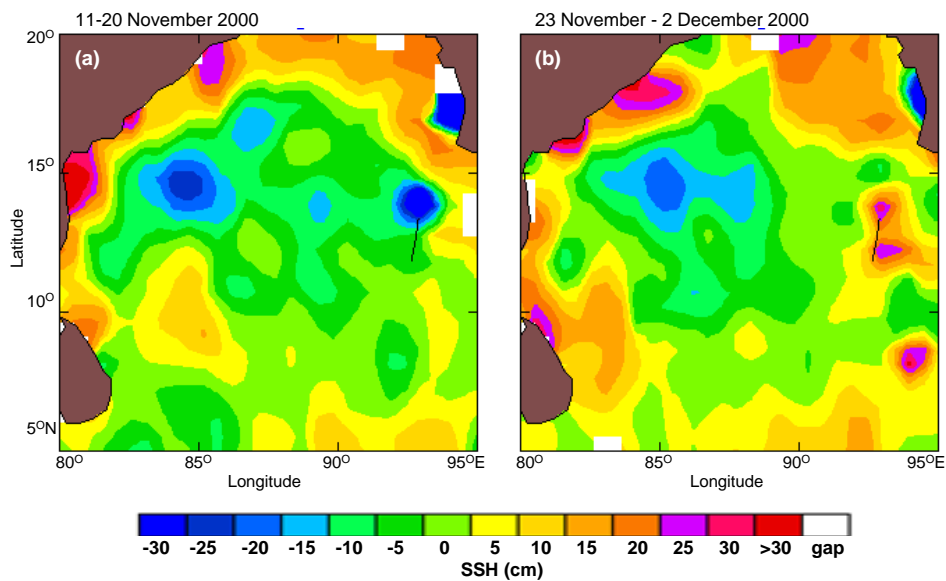


Fig. 6.3 Ten day composite of sea surface height from altimeter data during: (a) 11-20 Nov and (b) 23 Nov-2 Dec 2000

Cyclones have two effects on the SSH. Cyclonic effects raise the SSH due to the reduced atmospheric pressure and decrease it due to the divergence of water. Effect of divergence seems to dominate over that of low pressure. Due to this cyclonic storm, a small cyclonic eddy centered around 11.75°N, 81.5°E was formed (Fig. 6.3). SSH reduced by about 10 cm compared to the periphery of the eddy. The divergence caused by the cyclonic eddy resulted in upwelling of bottom waters, in turn resulting in lowering of SST and increasing the productivity. SST reduction could also have been because of increased evaporation and more cloud cover. There was an overall

increase of SSH in the entire BoB by about 10 to 20 cm in the post-cyclone period. SSH gradients were stronger after the passage of cyclone in the southwestern BoB. The locations of low SST, high chl-*a* and PP concentrations were same. However, a slight deviation was present in the cyclonic location in SSH values compared to the SST, chl-*a* and PP observations. The altimeter values are point observations along the altimeter sub satellite track over the 10 day period which were interpolated to  $0.5^\circ \times 0.5^\circ$  spatial resolution using the Cressman scheme (Cressman, 1959). The deviation in the position of the cyclonic eddy could be because of this interpolation of the 10-day composited data.

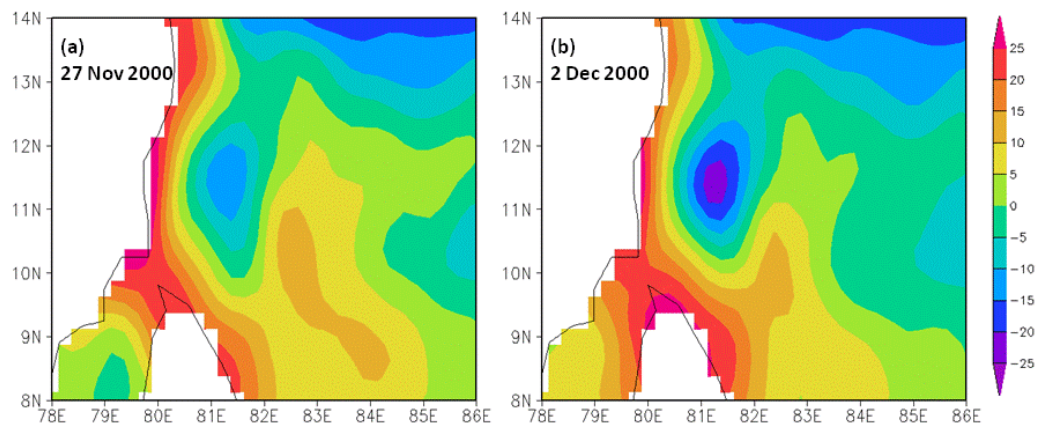


Fig. 6.4 Merged daily sea level anomaly during (a) 27 Nov 2000 before, and (b) 2 Dec 2000 after the passage of cyclone showing the decrease in sea level

The changes in SSH due to TC 03B have also been analysed using merged daily SLA data. Fig. 6.4 shows the SLA before and after the passage of cyclone in the southwestern BoB. On 27 Nov 2000, the SLA was about -15cm around  $81^\circ\text{E}$ ,  $11^\circ\text{N}$ . After the passage of cyclone during 2 Dec 2000, the SLA decreased to -25 cm and a well defined cyclonic eddy developed in this region. Due to the passage of the cyclone, a sea level decrease of 10 cm was observed in the southwestern BoB. The divergence of the upper ocean waters by the strong cyclonic winds caused the sea level to decrease due to the passage of cyclone. This was compensated by the upwelling of cooler nutrient rich subsurface waters to the surface thus enhancing productivity in this region.

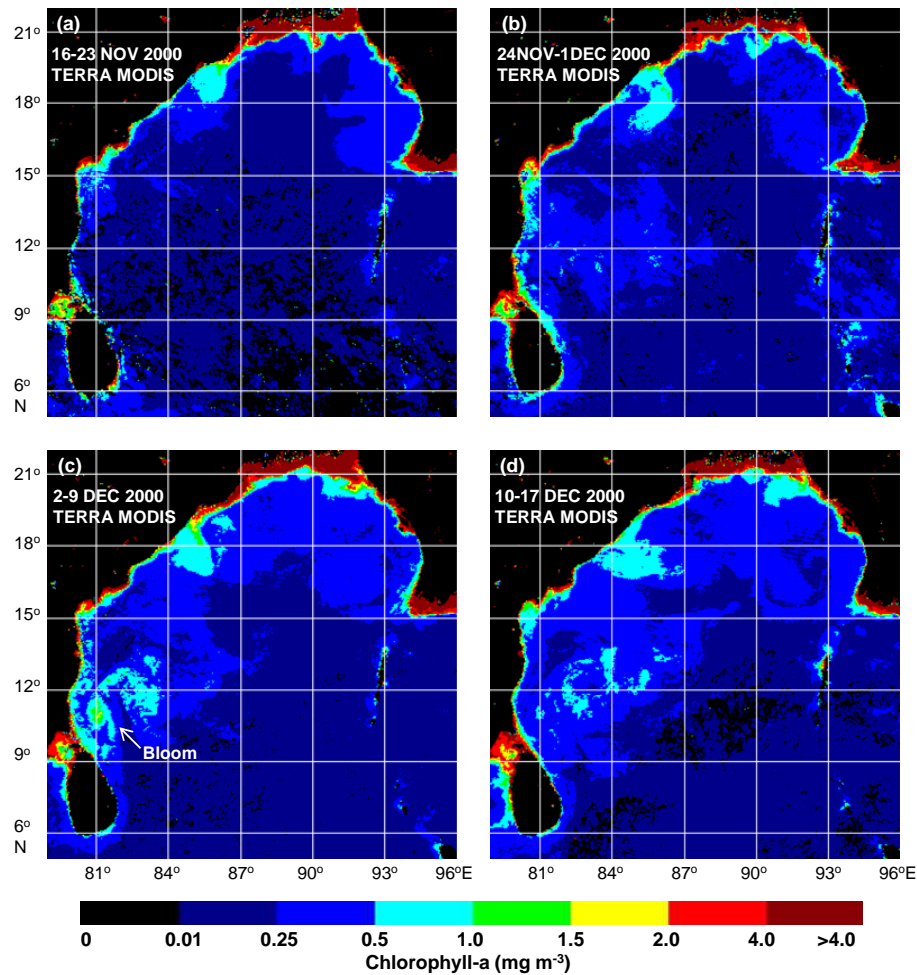


Fig. 6.5 Terra MODIS weekly chl-*a* concentration: (a) 16-23 Nov, prior to the cyclone formation; (b) 24 Nov-1 Dec during the cyclone; (c) 2-9 Dec; and (d) 10-17 Dec 2000, after the passage of cyclone showing the increase in chl-*a* concentration

During 16-23 Nov 2000, chl-*a* concentration (Fig. 6.5) in the southwestern BoB was around  $0.2 \text{ mg m}^{-3}$ . At the time of cyclone, the chl-*a* concentration in the region around  $11^{\circ}\text{N}$ ,  $81^{\circ}\text{E}$  increased to about  $0.28\text{-}0.34 \text{ mg m}^{-3}$ , while in the other parts of the BoB chl-*a* concentration remained below  $0.25 \text{ mg m}^{-3}$ . After the passage of cyclone the chl-*a* concentration increased to  $1\text{-}1.2 \text{ mg m}^{-3}$ . Maximum increase in chlorophyll concentration was located around  $11^{\circ}\text{N}$ ,  $81^{\circ}\text{E}$  where the values increased

from  $0.24 \text{ mg m}^{-3}$  to  $1.8 \text{ mg m}^{-3}$ . One week after the cyclone, during 10-17 Dec 2000, chl-*a* concentration reduced to  $0.4\text{-}0.6 \text{ mg m}^{-3}$ .

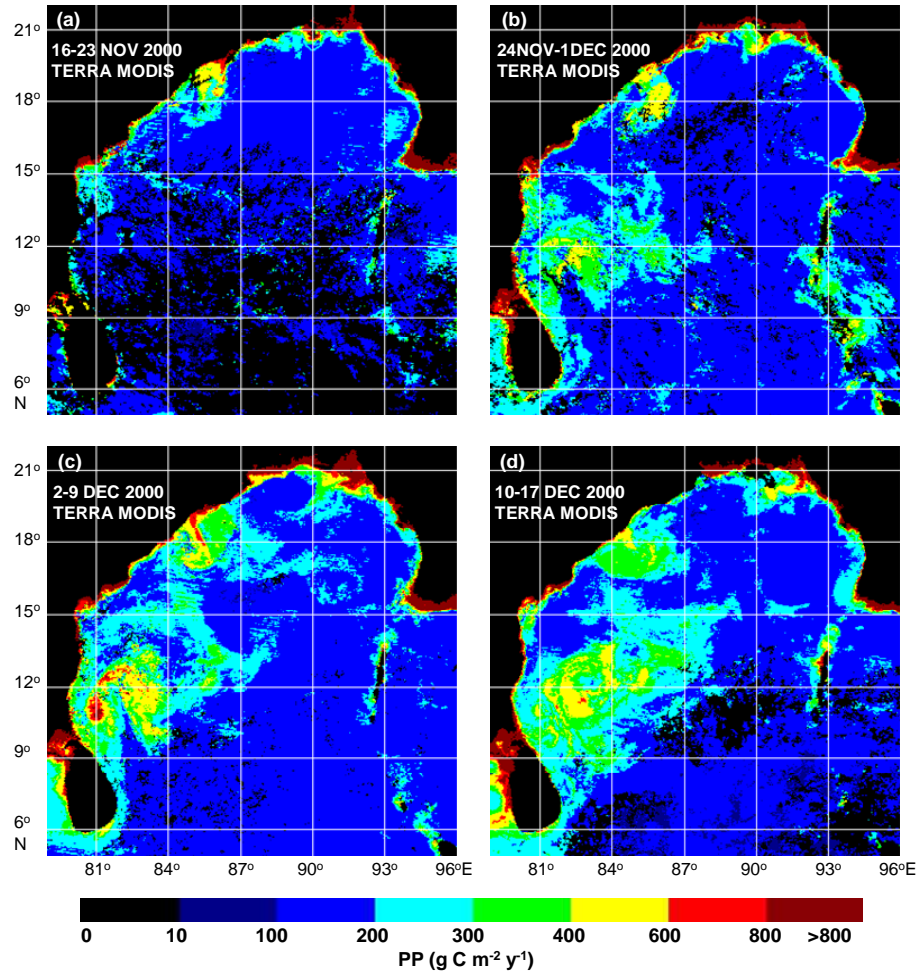


Fig 6.6 MODIS weekly primary production: (a) before the cyclone (16-23 Nov); (b) during the cyclone (24 Nov-1 Dec); (c) 2-9 Dec; and (d) 10-17 Dec 2000 after the passage of cyclone showing the increase in production

Before the cyclone, the PP in the southwestern BoB was less than  $200 \text{ g C m}^{-2} \text{ y}^{-1}$ . During the passage of cyclone, PP increased to about  $400\text{-}500 \text{ g C m}^{-2} \text{ y}^{-1}$  at around  $11.6^\circ\text{N}$ ,  $82.4^\circ\text{E}$ . Fig. 6.6 shows the spatial distribution of PP which was high along the track of the cyclone. During 2-9 Dec 2000, after the passage of cyclone the PP increased up to  $800\text{-}900 \text{ g C m}^{-2} \text{ y}^{-1}$  around  $11^\circ\text{N}$  and  $81^\circ\text{E}$ . The maximum increase in PP was located at  $11^\circ\text{N}$ ,  $81^\circ\text{E}$ , where the PP value increased from around 170 to 964

$\text{g C m}^{-2} \text{y}^{-1}$ . This coincides with the maximum increase in chl-*a* concentration in the same location. Thereafter PP concentration gradually decreased to  $350\text{-}450 \text{ g C m}^{-2} \text{y}^{-1}$ . The spatial and temporal variations in PP are similar to that of chl-*a* concentration.

MODIS weekly mean chl-*a* concentration range was between  $0.2\text{-}0.35 \text{ mg m}^{-3}$  prior to the cyclone which are in agreement with the surface chl-*a* measurements at six offshore locations in the southwestern BoB during November 1999, where the concentration ranged from  $0.22$  to  $0.49 \text{ mg m}^{-3}$  exhibiting the oligotrophic (nutrient depleted) condition. After the cyclone fully intensified and moved toward northwest, higher concentrations of chl-*a* appeared as a bloom centered about  $11^{\circ}\text{N}$ ,  $81^{\circ}\text{E}$ , with higher chl-*a* values at the centre of the cyclone influenced region (Fig. 6.5c). The bloom was located at about  $75\text{-}80 \text{ km}$  away from the coast, and looked like a round shaped cyclonic eddy of about  $100 \text{ km}$  diameter. This bloom persisted for a week and then gradually reduced and attained the normal value by the middle of Dec 2000. The forced mixed layer deepening due to intense wind stirring and cyclone-induced divergent geostrophic currents, lead to the injection of nutrients into the surface layer resulting in higher chl-*a* concentration. Vinayachandran and Mathew (2003) reported patches of phytoplankton bloom during Nov-Dec in the southwestern BoB west of  $88^{\circ}\text{E}$ . The phytoplankton population in this region during NEM is limited by nutrients. Entrainment of nutrient rich waters by wind mixing is not efficient in the BoB. The northeasterly winds during Nov-Feb do not favour coastal upwelling along east coast of India. Besides the enhanced phytoplankton blooms due to the cyclonic storm, some investigators observed the blooms which were associated with Ekman pumping (Vinayachandran and Mathew, 2003). The WSC was very high at about  $9 \times 10^{-7} \text{ N m}^{-3}$  around  $84\text{-}86^{\circ}\text{E}$ ,  $11^{\circ}\text{N}$  during the week 27Nov-3Dec 2000, while away from this location and also during the previous week WSC was about  $0.5$  to  $1 \times 10^{-7} \text{ N m}^{-3}$ . The high WSC during the tropical cyclone caused high VV of upto  $3.5 \times 10^{-5} \text{ m s}^{-1}$  in this location indicating strong divergence of surface waters and upwelling. This resulted in the reduction of SST and increase in the chlorophyll concentration at the surface.

#### 6.4. Tropical cyclone 01B (TC 01B), 11-19 May 2003

Tropical Cyclone 01B (TC 01B), a VSCS with wind speed greater than 64kts developed in the BoB on 11 May 2003 and moved slowly northward (Fig. 6.7). The description of the cyclone track is obtained from a tropical cyclone report from the NOAA, (<ftp://ftp.aoml.noaa.gov/hrd/pub/landsea/padgett/may03.sum>). On 12 May 2003, the cyclone was located near 11°N, 86°E at 06:00 UTC and reached hurricane intensity for about 24 hours. It moved northwestward at  $2.2 \text{ m s}^{-1}$  with maximum sustained winds estimated at  $28 \text{ m s}^{-1}$ , gusting to  $36 \text{ m s}^{-1}$ . On 14 May 2003, TC 01B was located near 14.4°N, 86°E at 06:00 UTC. A ridge to its east finally turned the TC 01B northward, whereupon it began to intensify, after having briefly weakened to depression strength on 18 May 2003. After weakening and remaining at minimal tropical storm intensity for several days, the cyclone rapidly intensified once again as it made landfall along the west central coast of Myanmar on 19 May 2003 with maximum sustained winds of  $23.6 \text{ m s}^{-1}$ .

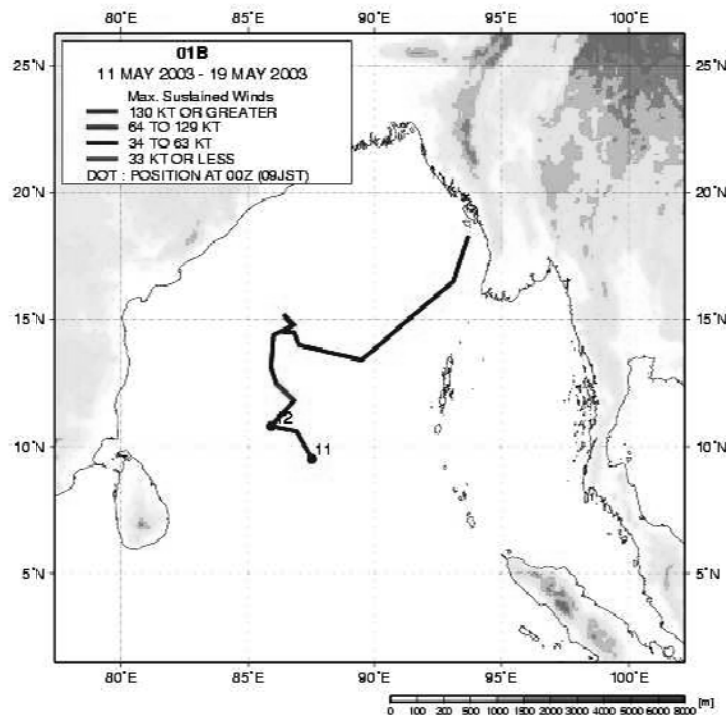


Fig. 6.7 Track of the tropical cyclone 01B during 11-19 May 2003 in the Bay of Bengal (Figure is taken from Smitha *et al.*, 2006)

**6.5. Response of physical and biological properties of ocean to TC 01B**

MODIS weekly (8 days) composite 4.0 km spatial resolution SST images (Fig. 6.8) depict the distribution of SST before, during and after the passage of the cyclone. Figures show the weekly mean day time SST for the periods (a) 1-8 May, (b) 9-16 May, (c) 17-24 May and (d) 25 May-1 Jun, 2003.

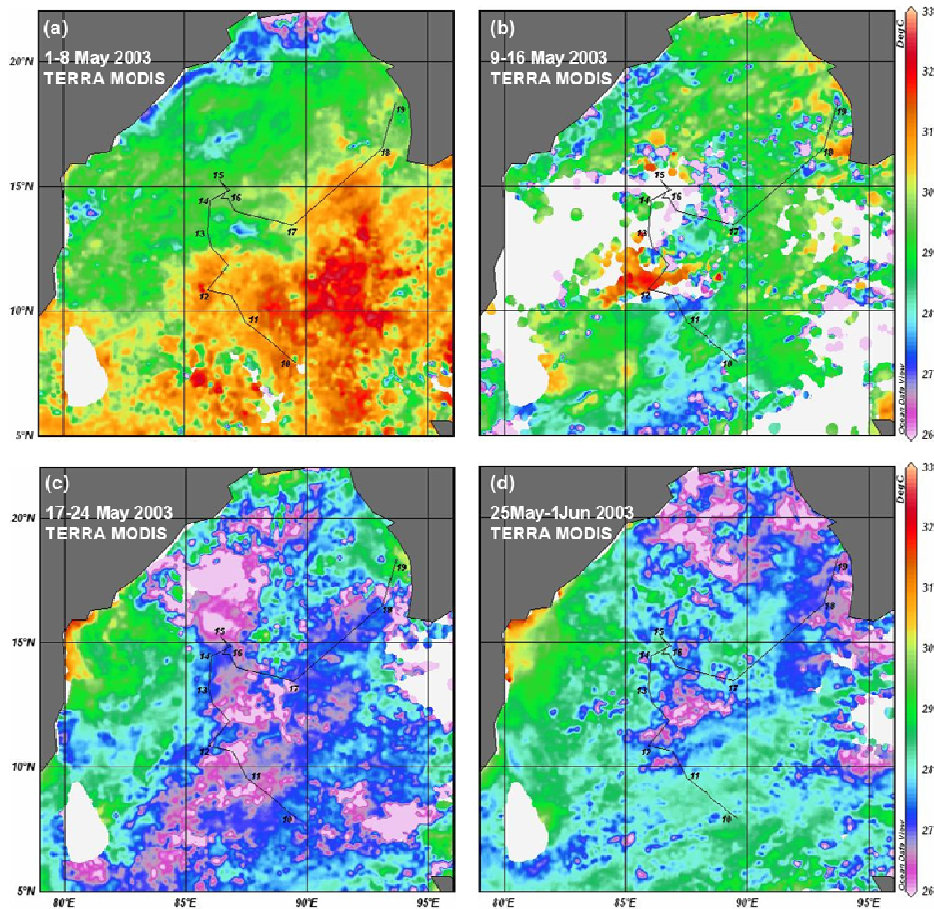


Fig. 6.8 Sea surface temperature in °C observed from Terra MODIS: (a) prior to the cyclone formation (1-8 May); (b) during the cyclone (9-16 May); (c) during 17-24 May; and (d) 25 May-1 Jun 2003 after the passage of cyclone

Before the cyclone developed, SST in the southern Bay was around 31.0°C. During the passage of cyclone, the surface temperature decreased to 27.5-28.0°C around 10°N, 87°E. After the passage of cyclone, SST further decreased to 25-26°C around

10°N, 87°E and 12°N, 87°E. During 25 May-1 Jun, 2003 the SST increased to 27-27.5°C, but was still cool (25.5°C) at some locations (around 12°N, 87°E).

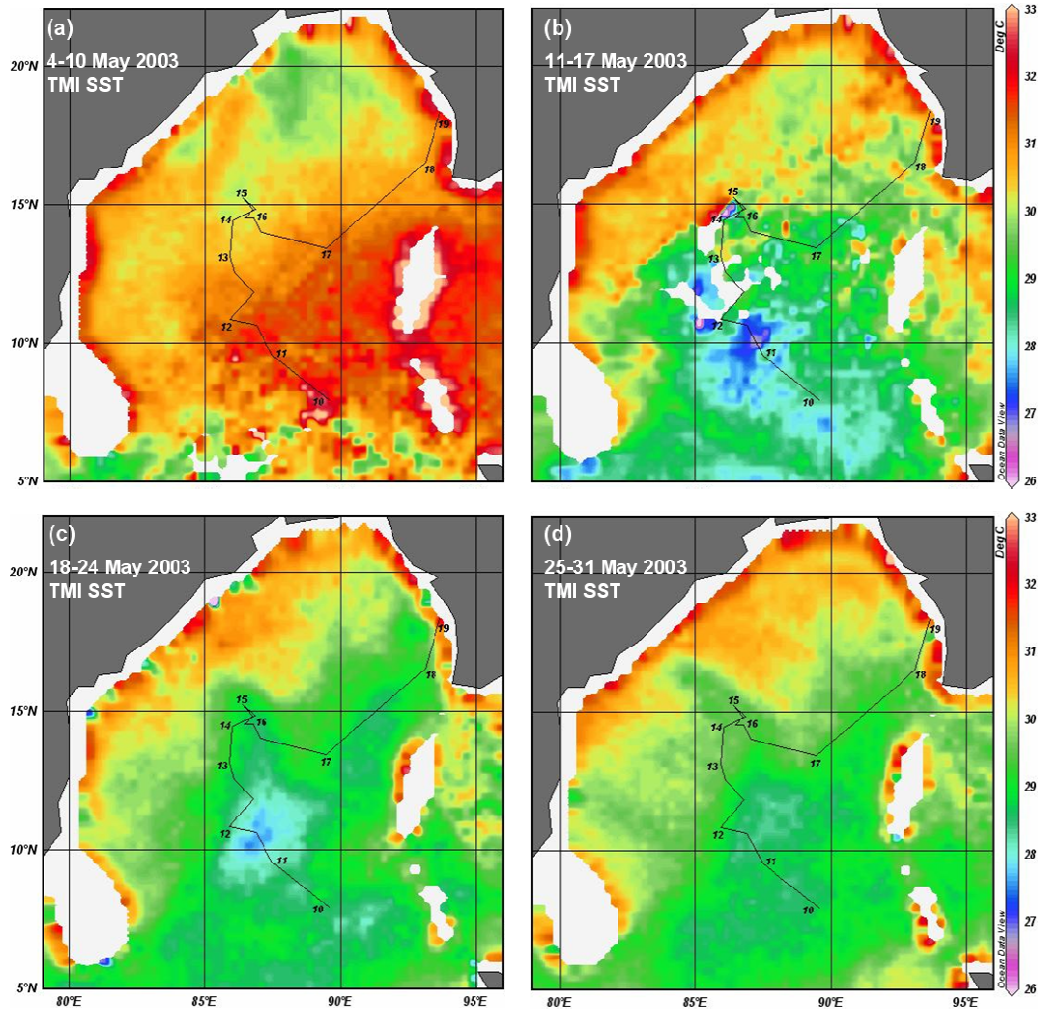


Fig. 6.9 Weekly averaged TMI data showing sea surface temperature in °C: (a) before the cyclone (4-10 May); (b) during the cyclone when cooling occurs (11-17 May); (c) during 18-24 May; and (d) 25-31 May 2003, after the passage of cyclone

SST changes due to the cyclone were also analysed using TMI SST (Fig. 6.9). SST was around 31.6°C in the southern BoB prior to the cyclone. During the passage of the cyclone, SST decreased to 26.7-27.5°C around 10-11°N and 87°E. The maximum drop in SST was observed near 10.2°N, 87°E where the SST fell from 31.5°C before

the cyclone to 26.7°C by 17 May 2003. After the passage of cyclone during 18-24 May, the temperature slowly increased to 27.7-28.2°C.

By the last week of May 2003, SST further increased to 28.4-29°C. A decrease in SST of about 5°C was observed in both MODIS and TMI, although there was a delay of one week in cooling observed from MODIS compared to TMI SST. Before the passage of cyclone, SST in the southern BoB showed a difference of 0.6°C between the TMI and MODIS data. During the passage of cyclone, SST decreased and reached a minimum of 26.7°C in TMI; whereas it was 27.5°C in the case of MODIS data. MODIS SST further decreased to 25-26°C during the subsequent week after the passage of cyclone, while the temperature slowly increased in TMI SST.

Before the cyclone, MLD at and around 10°N, 87°E was about 30 m (Fig. 6.10); in the third week, MLD increased to about 42 m. One week after the passage of cyclone, i.e. during 25 May-1 Jun 2003, MLD increased to about 45 m, possibly due to the onset of monsoon winds. The maximum SST decrease of about 5°C was observed at 10.5°N, 87°E. At this location the MLD increased from 31 m to 41 m. The maximum MLD increase due to the cyclone appeared to be 12 m. This is somewhat lower than values reported from other oceans, possibly because the southern Bay is highly stratified by both salinity and temperature in the pre-monsoon season (Sengupta *et al.*, 2002).

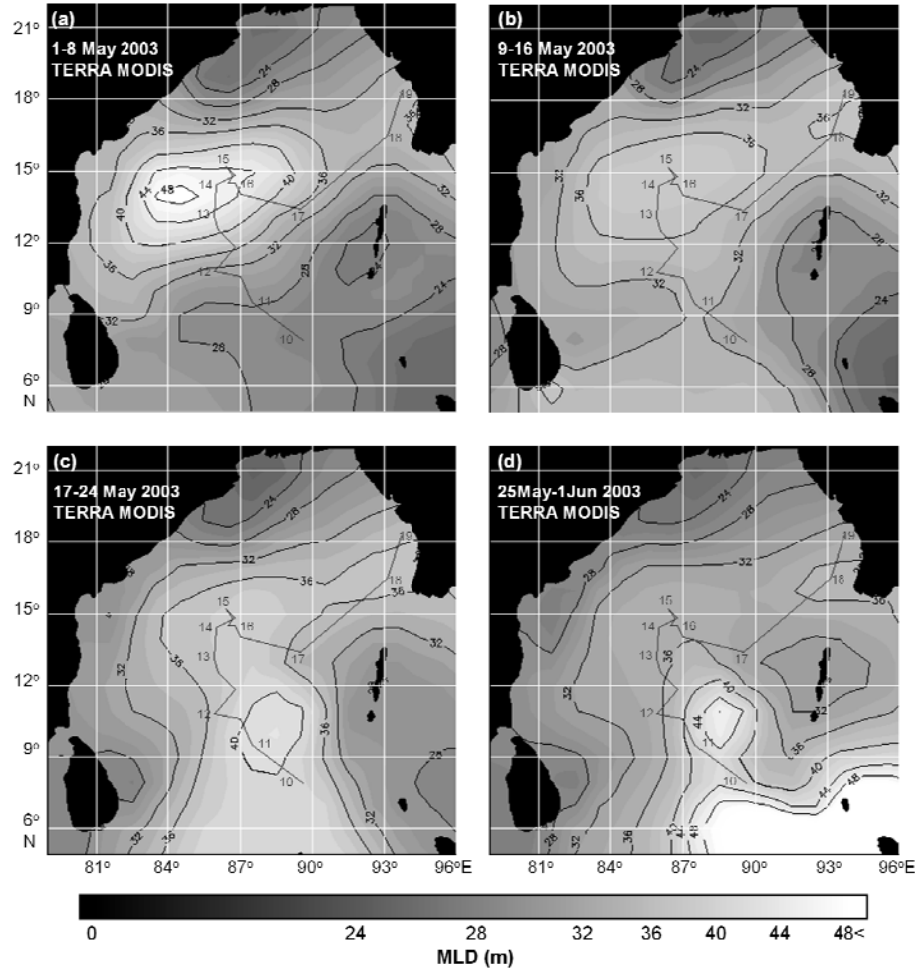


Fig. 6.10 Modeled weekly mixed layer depth (m) in the Bay of Bengal during different stages of cyclone: (a) prior to the cyclone formation (1-8 May); (b) during the cyclone (9-16 May); (c) during 17-24 May; and (d) 25 May-1 Jun 2003 after the passage of cyclone

The response of chl-*a* concentration to the passage of cyclone is shown in Fig. 6.11. During 1-8 May 2003, chl-*a* concentration in the southern BoB was 0.1-0.15 mg m<sup>-3</sup>. At the time of occurrence of the cyclone, it increased to 0.36-0.48 mg m<sup>-3</sup> in the region around 10°N, 87°E, while remaining below 0.2 mg m<sup>-3</sup> elsewhere in the Bay. During the third week, chl-*a* concentration around 10-11°N, 87°E increased to 1.5-1.9 mg m<sup>-3</sup>. The maximum increase was observed at 11.2°N, 87.3°E, where the chl-*a*

concentration increased from  $0.10 \text{ mg m}^{-3}$  to  $2.33 \text{ mg m}^{-3}$ . One week after the passage of the cyclone, chl-*a* concentration decreased to  $0.3\text{-}0.36 \text{ mg m}^{-3}$ .

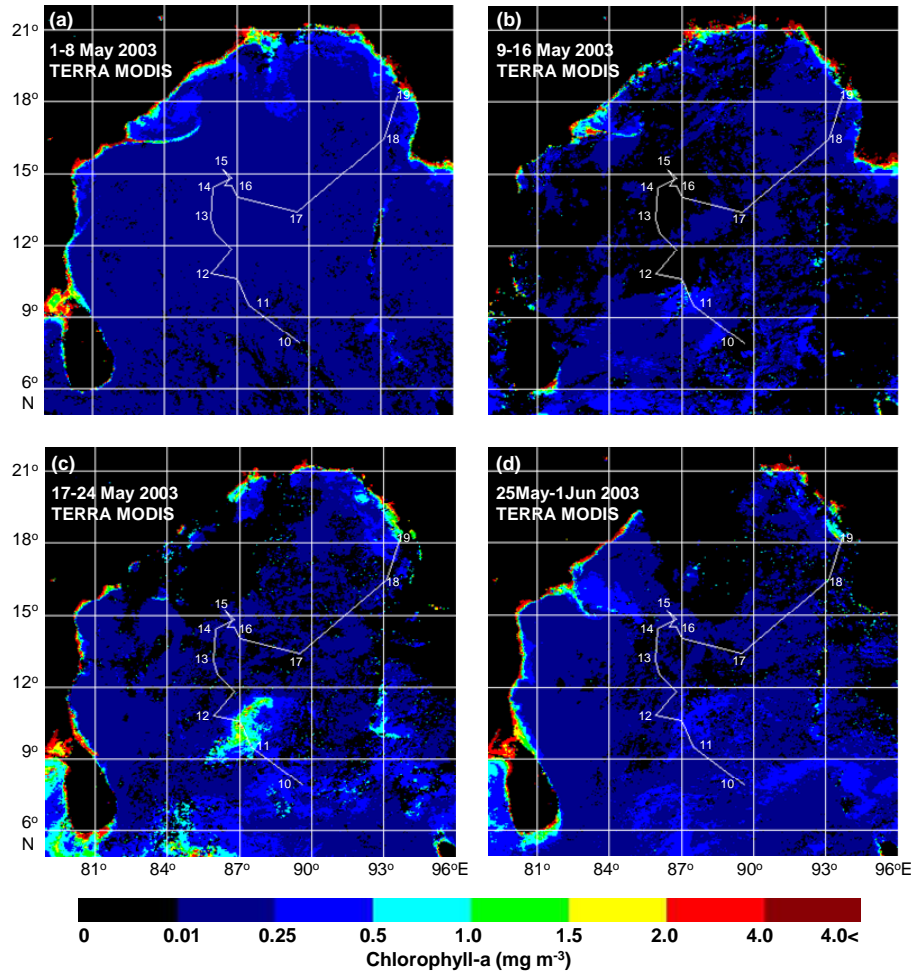


Fig. 6.11 Weekly chl-*a* concentration in  $\text{mg m}^{-3}$  observed from Terra MODIS during different stages of cyclone showing the increase in chl-*a* concentration in the cyclone affected area: (a) prior to the cyclone formation (1-8 May); (b) during the cyclone (9-16 May); (c) during 17-24 May; and (d) 25 May-1 Jun 2003 after the passage of cyclone

Difference images of SST and chl-*a* concentration from MODIS (Fig. 6.12) showed that there is a general correspondence of the region of SST cooling and enhanced chl-*a* concentration due to the cyclone. These difference plots of SST and chl-*a* concentration are based on weekly composites. Daily data is expected to provide more reliable estimates of maximum cooling and the enhancement of chl-*a*

concentration. Weekly averaged data products have been used due to the non-availability of cloud free daily data. IRS-P4 OCM having high spatial resolution (360 meters) and two day repeativity also showed thick cyclonic clouds during this period.

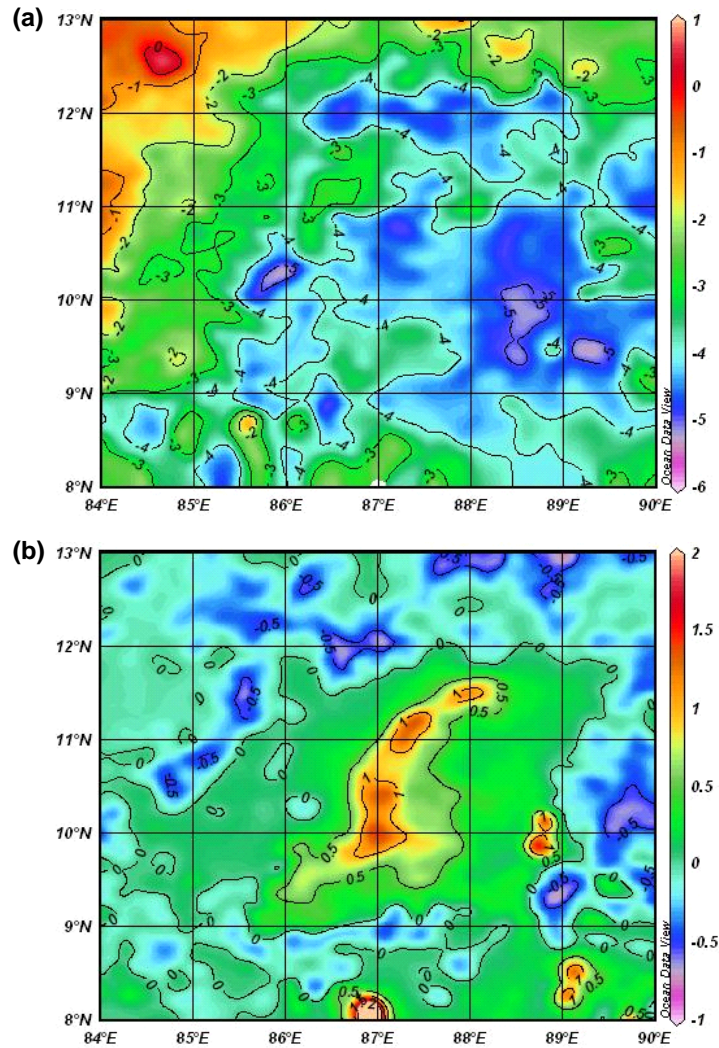


Fig. 6.12 Difference images of (a) sea surface temperature in °C and (b) chl-a concentration in mg m<sup>-3</sup> from Terra MODIS depicting the changes occurred after the passage of cyclone in May 2003

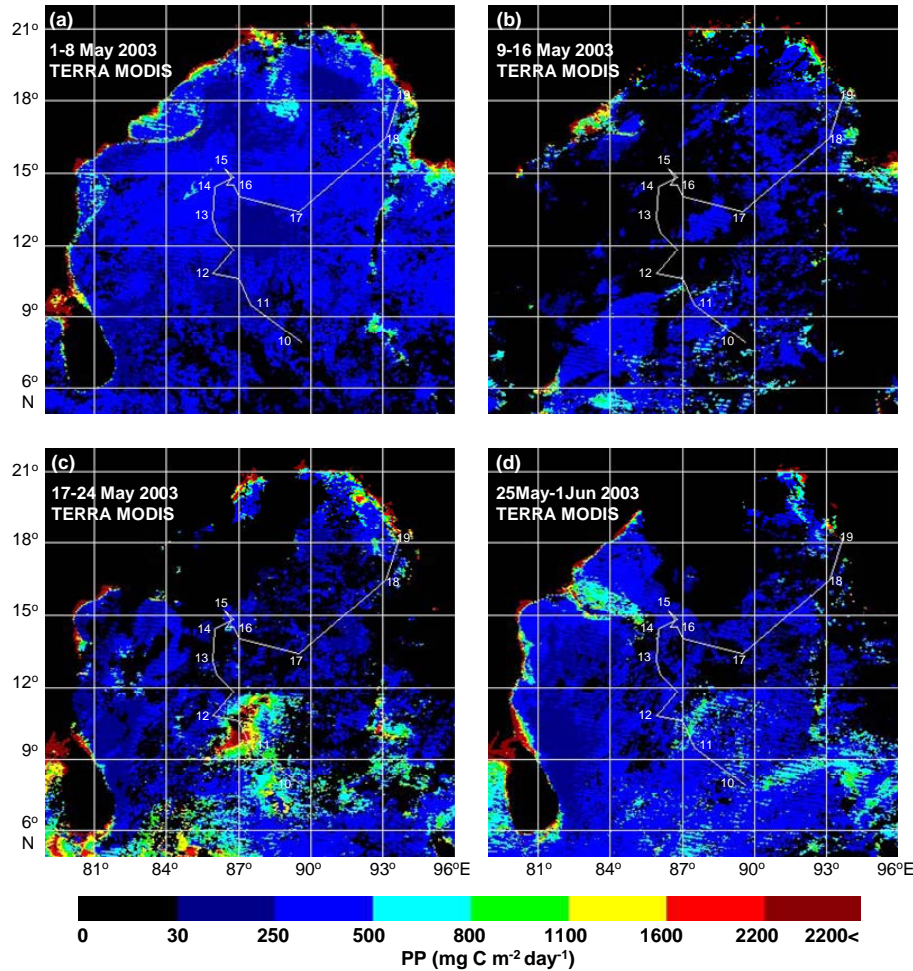


Fig. 6.13 Weekly mixed layer primary production during various stages of the cyclone: (a) prior to the formation of cyclone (1-8 May); (b) during the cyclone (9-16 May); (c) during 17-24 May; and (d) 25 May-1 Jun 2003, after the passage of cyclone showing the increase in production in the cyclone affected area

PP in the southern BoB increased significantly over a large region in response to the cyclone. Fig. 6.13 shows the spatial distribution and enhancement of PP due to the cyclone. Before the cyclone, PP in the central and southern BoB was less than  $490 \text{ mg C m}^{-2} \text{ day}^{-1}$ . During the passage of cyclone PP increased to about  $820 - 980 \text{ mg C m}^{-2} \text{ day}^{-1}$  around  $10^\circ\text{N}$ ,  $87^\circ\text{E}$ . The increase in PP was maximum during 17-24 May, in the region between  $9-11^\circ\text{N}$  and  $86-88^\circ\text{E}$ . During this week, the PP increased up to  $2460 - 4100 \text{ mg C m}^{-2} \text{ day}^{-1}$  around  $10^\circ\text{N}$ ,  $87^\circ\text{E}$ . One week after the passage of the cyclone, PP gradually decreased to  $820 - 960 \text{ mg C m}^{-2} \text{ day}^{-1}$ .

It has been shown with the help of satellite data that tropical cyclone 01B of May 2003 strongly influenced the near surface temperature and biology of the BoB. The SST dropped by 4-5°C over a fairly large region, associated with an increase in MLD by about 12 m. Lowering of SST due to the cyclone (~5°C) was significant in both MODIS and TMI data. The time lag of one week in cooling between both the data sets may be due to the slight difference in weekly periods of MODIS with that of TMI. There was moderate increase of chl-*a* concentration and large increase of biological productivity in the region directly influenced by the cyclone. During 12-18 May 2003, WSC reached up to  $12 \times 10^{-7} \text{ N m}^{-3}$  to  $16 \times 10^{-7} \text{ N m}^{-3}$  at around 86-88°E, 11-12°N while during the previous week WSC was about  $2 \times 10^{-7} \text{ N m}^{-3}$  to  $4 \times 10^{-7} \text{ N m}^{-3}$ . In this region the VV reached  $4-5 \times 10^{-5} \text{ m s}^{-1}$  during 12-18 May 2003 indicating strong upward Ekman pumping and divergence of surface water leading to upwelling. This led to an increase in surface chlorophyll concentration and decrease in SST in and around this region.

It is interesting to note that the response of SST or ocean biology was not limited to regions directly under the cyclone track. Strong eastward winds associated with the cyclone enhanced chl-*a* concentration (Fig. 6.11c) and PP (Fig. 6.13c) over a large region south and east of Sri Lanka, possibly through enhanced coastal upwelling (Fig. 6.8c) and advection of upwelled water by surface ocean currents. In response to the cyclone, production increased by about  $550 \text{ mg C m}^{-2} \text{ day}^{-1}$  over an area of at least  $1,00,000 \text{ km}^2$ . If we assume that the enhanced production sustained for a week, this single cyclone would have led to a total incremental carbon fixation of about  $0.5 \times 10^{12} \text{ g C}$ . To put this number in context, Lin *et al.* (2003) estimated that enhanced PP due to the cyclone Kai-Tak in the South China Sea was about  $0.8 \times 10^{12} \text{ g C}$ . Although the mixed layer deepening and the maximum post-storm chl-*a* concentration due to tropical cyclone 01B in the BoB were much smaller than those due to Kai-Tak, the enhancement of productivity took place over a much larger region in the case of the BoB cyclone.

**6.6. Summary**

The response of upper ocean to the passage of tropical cyclones has been analysed in this Chapter. The changes in physical and biological properties due to the effect of tropical cyclones in the BoB have been studied. BoB has low biological productivity when compared to the Arabian Sea. The chlorophyll in the upper layer of tropical oceans is limited by the availability of nutrients. Passage of intense tropical cyclones cause marked cooling of SST together with an increase in chlorophyll concentrations in the upper ocean. Intense wind stress on the ocean surface leads to the deepening of mixed layer and the entrainment of nutrient rich waters to the surface. The changes in SST, surface chl-*a* concentration and PP caused by tropical cyclones have been analysed for two cases of intense tropical cyclones in the BoB, one in Nov-Dec 2000 during post-monsoon and the other in May 2003 during pre-monsoon season. The tropical cyclone during 26 Nov-6 Dec 2000 was a VSCS with maximum wind speed of 102 kts. This cyclone moved westward, made the landfall south of Cuddalore and after weakening into a low pressure system emerged into eastern Arabian Sea which weakened later. The tropical cyclone during 10-19 May 2003 was another VSCS with a maximum wind speed of 75 kts which moved northward and then northwestward making the landfall over Myanmar coast.

For the tropical cyclone in Nov-Dec 2000, a maximum SST drop of 2°C, sea surface depression of 10 cm compared to the periphery, increase in chl-*a* concentration by about 1.5 mg m<sup>-3</sup> from 0.24 mg m<sup>-3</sup> were observed around 11°N, 81°E after the passage of the cyclonic storm. Also enhanced average mixed PP of 964 g C m<sup>-2</sup> y<sup>-1</sup> was observed in this location which was about 170 g C m<sup>-2</sup> y<sup>-1</sup> before the passage of tropical cyclone. The WSC high was about 9x10<sup>-7</sup> N m<sup>-3</sup> at around 84-86°E, 11°N during the week when the cyclone reached maximum intensity and the VV increased upto 3.5x10<sup>-5</sup> m s<sup>-1</sup>. On an average this tropical cyclone caused an increase in surface chl-*a* concentration by 6 times and PP by 5 times after the passage of cyclone. This increase was observed one week after the passage of cyclone and sustained for a week before decreasing.

During the tropical cyclone in May 2003, maximum drop of SST was about 5°C at 10.2°N, 87°E in TMI, and similar drop in SST was observed from MODIS. Around this location chl-*a* concentration increased from 0.1 to 2.33 mg m<sup>-3</sup> after the passage of cyclone. Directly under the cyclone track, PP increased from its pre-storm value by up to 3800 mg C m<sup>-2</sup> day<sup>-1</sup> (~1390 g C m<sup>-2</sup> y<sup>-1</sup>). The increase in chl-*a* concentration and productivity were not confined to the region under the cyclone track, but covered a much broader area, possibly due to forced coastal upwelling south of Sri Lanka. Decrease in SST was associated with the deepening of mixed layer by about 12 m. WSC increased to 12 x 10<sup>-7</sup> N m<sup>-3</sup> to 16 x 10<sup>-7</sup> N m<sup>-3</sup> at around 86-88°E, 11-12°N when the cyclone reached maximum intensity and the VV also increased to 4 x 10<sup>-5</sup> m s<sup>-1</sup> to 5 x 10<sup>-5</sup> m s<sup>-1</sup> during this time. After the passage of the cyclone, the SST slowly increased, and the chl-*a* concentration decreased. There was an increase in chl-*a* concentration by about 12 times and PP by 8 times due to the passage of tropical cyclone in May 2003. In this case also the increase in chl-*a* concentration and PP occurred after the passage of tropical cyclone which sustained for one week before diminishing. It has been observed that even though the maximum sustained wind speed of the tropical cyclone in May 2003 is less than that in Nov-Dec 2000, the associated increase in WSC and VV are high during May 2003 compared to Nov-Dec 2000. Hence the SST cooling is high for the May 2003. Also the increase in chl-*a* concentration and PP are high due to the tropical cyclone in May 2003 than in Nov-Dec 2000. The non-availability of cloud-free daily data makes it difficult to determine the exact dates of increase in chl-*a* concentration and PP. The enhanced PP after the passage of the cyclone supports the base of the pelagic marine food web, directly affecting the fishery productivity. The influence of tropical cyclone on enhanced chlorophyll is mainly attributed to the entrainment of subsurface nutrients. The reasons attributed for increased PP is increase of chlorophyll and availability of irradiance. This study suggests that tropical cyclones play a significant role in the annual PP of BoB.

## Chapter 7

### Summary and Conclusions

The present study is an attempt to analyze the wind induced upwelling and its effect on the surface chlorophyll distribution in the Bay of Bengal (BOB). In general, BoB is a low productive ocean basin due to high sea surface stratification caused by low salinity and high SST together with the presence of weak winds. The influence of surface winds in the generation of upwelling along with the response of physical properties of the ocean, and the ensuing changes in the distribution of surface chl-*a* concentration have been carried out using various satellite data on wind stress and wind stress curl (WSC), SST, SLA and surface chl-*a* concentration. Model outputs of water temperature, primary production (PP) and MLD have also been used along with satellite data for the analysis.

After a general introduction, the objectives and significance of the topic of study are presented in Chapter 1. Chapter 2 gives a detailed overview of all the data used in the investigation as well as the methodology, computational and analytical methods employed in the study.

The climatological variations that WSC, SST, SLA and surface chl-*a* concentration undergo in the BoB are summarized in Chapter 3. WSC and SST undergo large seasonal variations whereas the variations in concentration of surface chl-*a* are mostly confined to the coastal and near-coastal regions of the BoB. Seasonal variations in the distribution of SLA are also large in the BoB. SWM season is the major influencing event that brings about considerable changes in the distribution of these properties. The spatial distribution of WSC over the BoB depends on the prevailing surface winds which undergo seasonal reversals associated with changing seasons over the BoB. High positive (cyclonic) WSC induce divergence of the ocean surface and upwelling in the southwestern Bay, north and northwestern Bay during SWM season. Strong positive (cyclonic) WSC is observed over the southwestern

Bay during May-Sep which attains the maximum strength to the east of Sri Lanka in July and thereafter decreases. During this time high negative (anticyclonic) WSC which induces convergence of the surface waters and downwelling is observed over the southeastern Bay. The Bay experiences the lowest SST in January followed by warmest sea surface during the pre-monsoon season when the winds are weak and variable. The cold pool forms in the south-central Bay during May, develops as the SWM progresses, reaches the maximum extent during the peak of monsoon in Jul-Aug and disappears by October. The upward Ekman pumping by positive WSC leads to upwelling and lowering of SST in this region.

The variations in SLA are mainly caused by Rossby waves and Kelvin waves in the BoB which are generated by equatorial winds. Cyclonic eddies that cause upwelling are observed during the SWM and post-monsoon season in the western and southwestern Bay. The cyclonic eddy in the southwestern Bay develops as a result of the open ocean Ekman pumping by the positive WSC. During the NEM and pre-monsoon season strong anti-cyclonic eddies are observed in the Bay, which cause downwelling. Seasonal and monthly variations in surface chl-*a* concentration is less in the Bay except at certain locations such as southwestern Bay, east coast of India, northern BoB and Malacca strait. The spatial variation of surface chl-*a* is low in the BoB especially in the open ocean where it is in the range of 0.1 to 0.4 mg m<sup>-3</sup> during all the seasons. Chl-*a* concentration increases towards the coastal areas upto 8-9 mg m<sup>-3</sup> especially during SWM season. In the open ocean, surface chl-*a* concentration is lowest during pre-monsoon season. During the SWM season, a chlorophyll bloom develops in the southwestern Bay which intensifies with the progress of monsoon and disappears by October. This bloom is caused by the open ocean upwelling driven by Ekman pumping together with the advection of upwelled waters from the southern coasts of Sri Lanka by the SMC. East coast of India experiences changing coastal current patterns and receives river inputs from Krishna and Godavari, which cause increased chl-*a* concentration in that region especially during SWM season. In general, it has been observed that changing wind patterns during the SWM and NEM

seasons influence the WSC pattern, SST and SLA of the Bay. They also affect the surface chl-*a* concentration mostly along the coastal regions of the BoB.

The variability of WSC has been studied using EOF analysis in Chapter 4. Also the spatial distribution of wind stress during the SWM has been analysed. The inter-annual variations in the extent of the cold pool of the southcentral Bay have been explained in this Chapter. Ekman vertical velocity (VV) and SLA have been analysed in the regions of high wind stress in the BoB in Chapter 4. The analysis of the variability of WSC over the BoB using EOF analysis shows that first four EOF modes represent more than 64% of the total curl variance with the first mode contributing to 36% of the total variance of the WSC field. The second EOF represents 15.1% of the total variance in curl data. The spatial patterns of WSC associated with these modes describe the major elements of BoB climatology for the period of study. From the associated time series, it has been observed that most of the variance is contained in annual frequencies and the first mode EOF1 and the second mode EOF2 have annual periodicity associated with southwest and northeast monsoon respectively.

The spatial distribution of wind stress during SWM season shows that the mean wind stress is maximum ( $0.22 \text{ N m}^{-2}$ ) to the southeastern side of Sri Lanka in the southwestern BoB in July and in the west-central Bay ( $0.21 \text{ N m}^{-2}$ ) during August. During this time, wind stress is weak in the southeastern Bay followed by the east coast of India and to the east of Sri Lanka in the southwestern Bay. The cold pool of the BoB lies between  $3\text{-}10^{\circ}\text{N}$  in the south-central BoB and extends to about  $90^{\circ}\text{E}$  to the east of Sri Lanka. The SST average for JJAS shows that lowest temperature is about  $28^{\circ}\text{C}$  to the southeastern side of Sri Lanka, which is the area that experience high wind stress. The high wind stress along the southern coast of Sri Lanka leads to coastal upwelling and contribute to the SST reduction in this region. The cooler water is advected into the south-central Bay by the SMC which flow eastward south of Sri Lanka. The development of the cold pool is also due to the cyclonic curl in the local wind field which cause open ocean upwelling. The mean geostrophic currents during JJAS show a cyclonic eddy to the east of Sri Lanka in the southwestern Bay

and an anticyclonic eddy to the southeast of it. The geostrophic currents show the intrusion of SMC into the south-central BoB. Cold pool starts decaying in September, when a strong northward flow east of Sri Lanka replaces the cyclonic eddy. Analysis of the inter-annual variations of cold pool shows that the lowest SST within the cold pool occurs generally during August. The cold pool is most developed in 2000 and the SST reach the lowest of  $\sim 27.6^{\circ}\text{C}$  within the cold pool during August, while in 2007 it is least developed followed by 2003. The extent of the cold pool depends on how well developed is the pool, and it generally extent eastward upto  $88\text{-}89^{\circ}\text{E}$  with the lowest SST occurring at around  $4\text{-}7^{\circ}\text{N}$ . In 2000, the maximum cooling occurred between  $83\text{-}87^{\circ}\text{E}$  in the southwestern Bay.

Strong positive VV and high negative SLA indicate the occurrence of upwelling in a region. In the southwestern Bay, VV to the eastern side of Sri Lanka increases in strength and extends eastward into the Bay as the SWM advances and attains maximum intensity ( $2.4 \times 10^{-5} \text{ m s}^{-1}$ ) at around  $84^{\circ}\text{E}$ ,  $7^{\circ}\text{N}$  and extends upto  $86^{\circ}\text{E}$  in July. A cyclonic eddy also develops during this time to the east of Sri Lanka which is flanked by an anticyclonic eddy to the south of it. Ocean surface divergence and upward Ekman pumping by high positive WSC cause upwelling in the southwestern BoB. With the progress of SWM, anticyclonic eddy moves the cyclonic eddy northward and by September cyclonic eddy is located to the northeast of Sri Lanka. In the west-central Bay, during May before the onset of SWM, a strong anticyclonic eddy flanked in the north by a cyclonic eddy is observed and this anticyclonic eddy weakens during June. During SWM, VV becomes positive with its intensity reaching a high ( $0.55 \times 10^{-5} \text{ m s}^{-1}$ ) near  $20^{\circ}\text{N}$  in August, and north of  $18^{\circ}\text{N}$  upwelling occurs due to strong positive VV. This high VV decreases in September and in October VV increases again ( $0.55 \times 10^{-5} \text{ m s}^{-1}$ ) towards the southern side of this region. The cyclonic eddy also develops and extends eastward with two cold cores - one to the west and the other to the east in September. In October, the cold eddy develops more and is centered about  $87^{\circ}\text{E}$ ,  $18^{\circ}\text{N}$  with an SLA of  $-16 \text{ cm}$ . The EICC that flows southward along the coast during SWM forms the western side of the cold-core eddy.

The importance of D20 in upwelling in the BoB has been analysed in Chapter 5. Monthly variations of D20 have been studied and compared with VV, SLA, and chl-*a* indices in this Chapter. The seasonal and inter-annual variations in the surface chl-*a* distribution have also been analysed and explained in this Chapter. The relationship of surface chl-*a* concentration with VV and SLA has been examined for the selected regions and the results explained. It is observed that D20 undergoes considerable seasonal variation and lay deep generally from January until May, which shoals considerably upon the arrival of SWM. D20 is shallow in the western Bay compared to eastern Bay during SWM and post-monsoon season. In general there is an inverse correlation between VV and D20 in the BoB, having highest correlation coefficient of -0.548 in Andaman Sea whereas in the northern Bay, the correlation is the lowest. D20 and SLA has a direct relation in the BoB with high correlation ( $\sim 0.75$ ) in all three regions except in the northern Bay which has no correlation between D20 and SLA. There exists an inverse correlation between D20 and surface chl-*a* concentration with northern Bay and Andaman Sea having better correlation than western and southwestern Bay. The effect of tropical cyclones is observed with strong positive VV, an increase in surface chl-*a* concentration, lowering of SLA and shoaling of D20. From the study of seasonal to inter-annual variations in surface chl-*a* concentration, it has been observed that on an average, SWM is the major influencing season in the increase of surface chl-*a* concentration in the BoB followed by NEM. Surface chl-*a* has the highest concentration in the northern Bay. The relationship of surface chl-*a* concentration with VV shows that the positive correlation between both these parameters is maximum in northern Bay (0.571), followed by southwestern Bay and Andaman Sea. There is no significant correlation in the western Bay between surface chl-*a* and VV. There exists an inverse correlation between surface chl-*a* concentration and SLA in BoB. In northern Bay there is no significant correlation, while in southwestern Bay and Andaman Sea surface chl-*a* has good correlation ( $\sim -0.6$ ) with SLA. In general, it has been observed that strong winds are able to cause upwelling in the BoB and thus increase the surface chl-*a* concentration under favourable conditions.

It has been observed from the analysis of VV and surface chl-*a* concentration that in the northern Bay, high chl-*a* concentration during SWM is accompanied by strong positive VV. The VV maximum ( $0.3-0.68 \times 10^{-5} \text{ m s}^{-1}$ ) in Jul-Aug is followed by a chl-*a* maximum ( $0.7-1.8 \text{ mg m}^{-3}$ ) in Aug-Sep. Low chl-*a* concentration ( $0.3-0.5 \text{ mg m}^{-3}$ ) especially during Mar-Jun is associated with negative VV ( $-0.22 \times 10^{-5} \text{ m s}^{-1}$  to  $-0.44 \times 10^{-5} \text{ m s}^{-1}$ ) during Mar-Apr in the northern Bay. In the west-central Bay, positive VV during SWM and post-monsoon is highly variable and is followed by chl-*a* concentration of  $0.2-0.6 \text{ mg m}^{-3}$ . Surface chl-*a* concentration low of  $\sim 0.1 \text{ mg m}^{-3}$  during the pre-monsoon months follows the negative VV during Mar-Apr in this region. In the southwestern Bay, VV is generally positive except during Dec-Apr, and the negative VV of about  $-0.15 \times 10^{-5} \text{ m s}^{-1}$  during Jan-Mar is associated with the chl-*a* minimum of about  $0.12 \text{ mg m}^{-3}$  during pre-monsoon season. High VV of  $0.2-0.55 \times 10^{-5} \text{ m s}^{-1}$  during Jul-Sep is followed by surface chl-*a* concentration of about  $0.21-0.5 \text{ mg m}^{-3}$  in the southwestern Bay. VV is generally negative in the Andaman Sea except during Mar-Apr and Oct-Dec. During NEM and pre-monsoon season, chl-*a* concentration is high ( $0.2-0.38 \text{ mg m}^{-3}$ ) and VV is about  $0.2 \times 10^{-5} \text{ m s}^{-1}$  during post-monsoon and pre-monsoon in this region. Also chl-*a* minimum ( $0.14-0.23 \text{ mg m}^{-3}$ ) during SWM follows the low VV ( $-0.5 \times 10^{-5} \text{ m s}^{-1}$  to  $-1.2 \times 10^{-5} \text{ m s}^{-1}$ ) in this region. It has been observed that there is a lag of about one month between the increase in VV and corresponding increase in surface chl-*a* concentration which is most prominent in the northern Bay followed by southwestern Bay and Andaman Sea while the relation is weak in the west-central Bay.

It has been observed that the VV undergo considerable variations in the BoB together with surface chl-*a* concentration. On an average, VV increased by 2.6-2.8 times during August in the northern Bay from the low in April. Surface chl-*a* concentration increased by 3 times during August in this region from the low values in Apr-May. In the west-central Bay, VV increased by 2.5 times in October, while the maximum increase in chl-*a* concentration is about 3 times during August. In the southwestern Bay, VV increased by about 2.5-3 times from Mar-Apr to August and surface chl-*a* concentration increased by 3 times from April to August. In the Andaman Sea an

increase of about 1.4 times is observed for VV from Jul-Aug to Mar-Apr while chl-*a* concentration increased by about 1.7 times from April to August in this region.

The response of upper ocean to the passage of tropical cyclones has been analysed as part of the study in Chapter 6. The changes in SST, surface chl-*a* concentration and PP have been analysed for two VSCS in the BoB, one during 26 Nov-6 Dec 2000 (post-monsoon) with a maximum wind speed of 102 kts and the other during 11-19 May 2003 (pre-monsoon season). Satellite observations show the remarkable effects of tropical cyclones on upper ocean temperature and chl-*a* concentration. The decrease in SST is about 2°C together with a decrease in SSH of 10 cm for the tropical cyclone in post-monsoon season while it is about 5°C for the tropical cyclone in May 2003 in pre-monsoon season together with the deepening of mixed layer by about 12 m. The maximum increase in surface chl-*a* concentration is upto about 1.8 mg m<sup>-3</sup> (increase by 1.5 mg m<sup>-3</sup>) together with an increase in average mixed layer PP upto 964 g C m<sup>-2</sup> y<sup>-1</sup> around 11°N, 81°E after the passage of the tropical cyclone in Nov-Dec 2000. On an average this tropical cyclone caused an increase in surface chl-*a* concentration by 6 times and PP by 5 times after the passage of cyclone.

For the May 2003 tropical cyclone, the surface chl-*a* concentration increased upto 2.33 mg m<sup>-3</sup> (increase by 2.2 mg m<sup>-3</sup>) and the PP increased upto 4100 mg C m<sup>-2</sup> day<sup>-1</sup> (increase by 3800 mg C m<sup>-2</sup> day<sup>-1</sup> which is equivalent to ~1390 g C m<sup>-2</sup> y<sup>-1</sup>). The increase in surface chl-*a* concentration and productivity were not confined to the region under the cyclone track, but covered a much broader area, possibly due to forced coastal upwelling south of Sri Lanka. In both the cases the increase occurred one week after the passage of cyclone and sustained for a week before decreasing. An increase in surface chl-*a* concentration by about 12 times and PP by 8 times occurred after the passage of this tropical cyclone. For the tropical cyclone in Nov-Dec 2000, WSC high was about  $9 \times 10^{-7}$  N m<sup>-3</sup> at around 84-86°E, 11°N during the week when the cyclone reached maximum intensity and the VV increased upto  $3.5 \times 10^{-5}$  m s<sup>-1</sup>. For May 2003 tropical cyclone, WSC increased to  $12 \times 10^{-7}$  N m<sup>-3</sup> to  $16 \times 10^{-7}$  N m<sup>-3</sup> at around 86-88°E, 11-12°N when the cyclone reached maximum intensity and the VV also increased to  $4 \times 10^{-5}$  m s<sup>-1</sup> to  $5 \times 10^{-5}$  m s<sup>-1</sup> during this time.

It has been observed that even though the maximum sustained wind speed of the tropical cyclone in May 2003 was less than that in Nov-Dec 2000, the associated increase in WSC and VV were high during May 2003 compared to Nov-Dec 2000. Hence the SST cooling was high for May 2003. Also the increase in surface chl-*a* concentration and PP were higher due to the tropical cyclone in May 2003 than in Nov-Dec 2000. The enhanced PP after the passage of the cyclone supported the base of the pelagic marine food web, directly affecting the fishery productivity. The influence of tropical cyclone on enhanced chlorophyll is mainly attributed to the entrainment of subsurface nutrients. The reasons attributed for increased PP is increase of chlorophyll and availability of irradiance. This study suggests that tropical cyclones might play a significant role in the annual PP of BoB. Different temporal and spatial resolution satellite derived SSTs and chl-*a* concentration are able to detect the surface cooling and enhanced chlorophyll and productivity due to the passage of cyclones in BoB. Good correspondence has been observed between surface cooling area and the increase in chlorophyll concentration in these two cases studied. Passage of intense tropical cyclones cause marked cooling of SST together with an increase in chlorophyll concentrations in the upper ocean. Intense wind stress on the ocean surface leads to the deepening of mixed layer and the entrainment of nutrient rich waters to the surface.

The results of the study project the large temporal and spatial variability of the physical properties in the Bay of Bengal; such variations are important to upwelling in the ocean and hence the distribution of surface chl-*a* concentration in the region. It has been observed that the mean Ekman vertical velocity increases by about 1.4 to 3 times in different regions of the Bay of Bengal under normal conditions. The concurrent increase in mean surface chl-*a* concentration is by 1.7 to 3 times in these regions. Due to the influence of tropical cyclones, surface chl-*a* concentration in the Bay of Bengal increased by 6 to 12 times from the pre-storm values and primary production by 5 to 8 times under the area of passage of the cyclone together with a decrease in SST by 2-5°C, deepening of MLD by 12 m and a sea surface depression

by 10 cm. Hence it is seen that the inter-seasonal and intraseasonal variations in the physical parameters impact the concentrations of surface chl-*a* in the Bay of Bengal.

These variations in the concentrations of chl-*a* have large influences on the biological productivity of the region and therefore on the fish production. With growing population and the increasing need for affordable food and protein for the masses, efficient and optimal exploitation of the vast fishery resources of the region is important and urgent. Towards this goal, integrated investigations and studies involving marine biologists and physical oceanographers would be useful for planning and operational purposes.

## References

- Akhil, V.P., Durand, F., Lengaigne, M., Vialard, J., Keerthi, M.G., Gopalakrishna, V.V., Deltel, C., Papa, F. and de Boyer Montégut, C., 2014. A modeling study of the processes of surface salinity seasonal cycle in the Bay of Bengal. *Journal of Geophysical Research: Oceans*, 119(6), pp.3926-3947.
- Angel M.V, M.A. Baars., R.T. Barber., F.P. Chavez., M. Kastner, M. Leinen, J. R. E. Lutjeharms, G. Reverdin, Shimmiel, G.B., 1995. Group report: how do open ocean upwelling systems operate as integrated physical, chemical, and biological systems and influence the geological record. In: Summerhayes C.P., Emeis K-C, Angel M. V., Smith R.L., Zeitschel B. (eds) *Upwelling in the ocean: modern processes and ancient records*. Wiley, Chichester, pp.193–219.
- Antonov, J.I., Levitus, S. and Boyer, T.P., 2005. Thermosteric sea level rise, 1955–2003. *Geophysical Research Letters*, 32(12), doi:10.1029/2005GL023112.
- Banse, K. and English, D.C., 2000. Geographical differences in seasonality of CZCS-derived phytoplankton pigment in the Arabian Sea for 1978–1986. *Deep Sea Research Part II: Topical Studies in Oceanography*, 47(7), pp.1623-1677.
- Barnes, R.A., Clark, D.K., Esaias, W.E., Fargion, G.S., Feldman, G.C. and McClain, C.R., 2003. Development of a consistent multi-sensor global ocean colour time series. *International Journal of Remote Sensing*, 24(20), pp.4047-4064.
- Bauer, S., Hitchcock, G.L. and Olson, D.B., 1991. Influence of monsoonally-forced Ekman dynamics upon surface layer depth and plankton biomass distribution in the Arabian Sea. *Deep Sea Research Part A. Oceanographic Research Papers*, 38(5), pp.531-553.
- Baumgartner, A. and Reichel, E., 1975. *The world water balance; mean annual global, continental and and maritime precipitation, evaporation and run-off* (No. 628.1 B3). 179 pp., Elsevier Sci., New York
- Behrenfeld, M.J. and Falkowski, P.G., 1997. Photosynthetic rates derived from satellite-based chlorophyll concentration. *Limnology and Oceanography*, 42(1), pp.1-20.
- Behrenfeld, M.J., Randerson, J.T., McClain, C.R., Feldman, G.C., Los, S.O., Tucker, C.J., Falkowski, P.G., Field, C.B., Frouin, R., Esaias, W.E. and Kolber, D.D.,

2001. Biospheric primary production during an ENSO transition. *Science*, 291(5513), pp.2594-2597.
- Benshila, R., Durand, F., Masson, S., Bourdallé-Badie, R., de Boyer Montégut, C., Papa, F. and Madec, G., 2014. The upper Bay of Bengal salinity structure in a high-resolution model. *Ocean Modelling*, 74, pp.36-52, <http://dx.doi.org/10.1016/j.ocemod.2013.12.001>.
- Bhat, G.S., Vecchi, G.A. and Gadgil, S., 2004. Sea Surface Temperature of the Bay of Bengal Derived from the TRMM Microwave Imager\*,+. *Journal of Atmospheric and Oceanic Technology*, 21(8), pp.1283-1290.
- Black, P.G., 1983, Ocean temperature change induced by tropical cyclones. Ph. D. Dissertation, *Pennsylvania State University*, University Park, 278 pp.
- Blondeau, D., Tilstone, G.H., Vicente, V.M. And Moore, G.F., 2004, Comparison of biophysical marine products from SeaWIFS, MODIS and a bio-optical model with in situ measurements from Northern European waters. *Journal of Optics A: Pure and Applied Optics*, 6, pp. 875–889.
- Boyer, T.P., Conkright, M.E., Antonov, J.I., Baranova, O.K., Garcia, H.E., Gelfeld, R.J., Locarnini, R.A., Murphy, P., O'Brien, T.D., Smolyar, I. and Stephens, C., 2002. *World Ocean Database 2001*. Volume 2, Temporal distribution of bathythermograph profiles. NOAA Atlas NESDIS 43, 119 pp., CD-ROM, U.S. Government Printing Office, Washington, D.C.
- Boyer, T.P., Levitus, S., Antonov, J.I., Locarnini, R.A. and Garcia, H.E., 2005. Linear trends in salinity for the World Ocean, 1955–1998. *Geophysical Research Letters*, 32(1), doi:10.1029/2004GL021791.
- Brown, O. B., Evans, R.H., Minnett, P.J., Kearns, E.J., and Kilpatrick, K., 2002. Sea surface temperature measured by the MODerate resolution Imaging Spectroradiometer (MODIS). *NASA Earth Observing System Investigator Working Group Meeting*, Ellicott City, MD.
- Bukata, R.P., 2005. Satellite monitoring of inland and coastal water quality: retrospection, introspection, future directions. *CRC Press*.
- Campbell, J., Antoine, D., Armstrong, R., Arrigo, K., Balch, W., Barber, R., Behrenfeld, M., Bidigare, R., Bishop, J., Carr, M.E. and Esaias, W., 2002. Comparison of algorithms for estimating ocean primary production from surface

- chlorophyll, temperature, and irradiance. *Global Biogeochemical Cycles*, 16(3), 9–15.
- Carder, K.L., Chen, F.R., Lee, Z.P., Hawes, S.K. and Kamykowski, D., 1999. Semi-analytic Moderate-Resolution Imaging Spectrometer algorithms for chlorophyll a and absorption with bio-optical domains based on nitrate-depletion temperatures. *Journal of Geophysical Research-Oceans*, 104(C3), pp.5403-5421.
- Chang, J., Chung, C.C. and Gong, G.C., 1996. Influences of cyclones on chlorophyll a concentration and Synechococcus abundance in a subtropical western Pacific coastal ecosystem. *Marine Ecology Progress Series*, 140, pp.199-205.
- Chelton, D.B., 1982. Large-scale response of the California Current to forcing by the wind stress curl. *Calif. Coop. Oceanic Fish. Invest. Rep*, 23, pp.130-148.
- Conway, Eric D., and Maryland Space Grant Consortium (1997), An Introduction to Satellite Image Interpretation, *Baltimore MD: The Johns Hopkins University Press*.
- Cressman, G.P., 1959. An operational objective analysis system. *Monthly Weather Review*, 87(10), pp.367-374.
- Crisp, D.J., 1975. Secondary productivity in the sea. *Productivity of world ecosystems, National Academy of Sciences, Washington, D. C.*, pp.71-89.
- Dey, S. and Singh, R.P., 2003. Comparison of chlorophyll distributions in the northeastern Arabian Sea and southern Bay of Bengal using IRS-P4 Ocean Color Monitor data. *Remote Sensing of Environment*, 85(4), pp.424-428.
- Dube, S.K., Rao, A.D., Sinha, P.C., Murty, T.S. and Bahulayan, N., 1997. Storm surge in the Bay of Bengal and Arabian Sea: the problem and its prediction.
- Dwivedi, R.M., Singha, S.K., Ramana, M., Nayaka, S.R., Parabb, S. and Matondkarb, P., 2004, July. Observation of biological manifestation of physical forces with synergistic use of IRS P4 OCM & MSMR. In *XXth ISPRS congress*, 12-23 July 2004 Istanbul, Turkey, Commission 7.
- Ehret, L.L. and O'Brien, J.J., 1989. Scales of North Atlantic wind stress curl determined from the comprehensive ocean-atmosphere data set. *Journal of Geophysical Research*, 94, pp.831-841, doi:10.1029/JC094iC01p00831.

- Eigenheer, A. and Quadfasel, D., 2000. Seasonal variability of the Bay of Bengal circulation inferred from TOPEX/Poseidon altimetry. *Journal of Geophysical Research: Oceans*, 105(C2), pp.3243-3252.
- Ekman, V.W., 1905. On the influence of the earth's rotation on ocean currents. *Arkiv for Matematik, Astronomi och Fysik* 2, pp.1-53.
- Emanuel, K.A., 1999. Thermodynamic control of hurricane intensity. *Nature*, 401(6754), pp.665-669.
- Emery, K.O. and Aubrey, D.G., 1989. Tide gauges of India. *Journal of Coastal Research*, pp.489-501.
- Faghmous, J.H., Frenger, I., Yao, Y., Warmka, R., Lindell, A. and Kumar, V., 2015. A daily global mesoscale ocean eddy dataset from satellite altimetry. *Scientific data*, 2.
- Falkowski, P.G., Ziemann, D., Kolber, Z. and Bienfang, P.K., 1991. Role of eddy pumping in enhancing primary production in the ocean. *Nature*, 352, 55–58.
- Falkowski, P.G. and Raven, J.A., 1997. Photosynthesis in continuous light. *Aquatic Photosynthesis. Blackwell Science, Malden, Massachusetts*, pp.193-227.
- Gadgil, S., Joshi, N.V. and Joseph, P.V., 1984. Ocean-atmosphere coupling over monsoon regions. *Nature*, 312(5990), pp.141-143.
- Girishkumar, M.S., Ravichandran, M., McPhaden, M.J. and Rao, R.R., 2011. Intraseasonal variability in barrier layer thickness in the south central Bay of Bengal. *Journal of Geophysical Research. Oceans*, 116(3).
- Girishkumar, M.S., Ravichandran, M. and Han, W., 2013. Observed intraseasonal thermocline variability in the Bay of Bengal. *Journal of Geophysical Research: Oceans*, 118(7), pp.3336-3349.
- Gomes, H.R., Goes, J.I. and Saino, T., 2000. Influence of physical processes and freshwater discharge on the seasonality of phytoplankton regime in the Bay of Bengal. *Continental Shelf Research*, 20(3), pp.313-330.
- Gregg, W.W., 2001. Tracking the SeaWiFS record with a coupled physical/biogeochemical/radiative model of the global oceans. *Deep Sea Research Part II: Topical Studies in Oceanography*, 49(1), pp.81-105.

- Gregg, W.W., Conkright, M.E., Ginoux, P., O'Reilly, J.E. and Casey, N.W., 2003a. Ocean primary production and climate: Global decadal changes. *Geophysical Research Letters*, 30(15).
- Gregg, W.W., Ginoux, P., Schopf, P.S. and Casey, N.W., 2003b. Phytoplankton and iron: validation of a global three-dimensional ocean biogeochemical model. *Deep Sea Research Part II: Topical Studies in Oceanography*, 50(22), pp.3143-3169.
- Guo, R., 2006. Territorial disputes and resource management: a global handbook. *Nova Publishers*.
- Halpern, D., Freilich, M.H. and Weller, R.A., 1998. Arabian sea surface winds and ocean transports determined from ERS 1 scatterometer. *Journal of Geophysical Research: Oceans*, 103(C4), pp.7799-7805.
- Halpern, D., Woiceshyn, P.M., Zlotnicki, V., Brown, O.B., Feldman, G.C., Freilich, M.H., Wentz, F.J. and Gentemann, C., 2001. An Atlas of Monthly Mean Distributions of SSMI Surface Wind Speed, AVHRR Sea Surface Temperature, TMI Sea Surface Temperature, AMI Surface Wind Velocity, SeaWiFS Chlorophyll-a, and TOPEX/POSEIDON Sea Surface Topography during 1999. *NASA Jet Propulsion Laboratory, California Institute of Technology*, Publication 01-01, 102 pp.
- Han, W. and McCreary, J.P., 2001. Modeling salinity distributions in the Indian Ocean. *Journal of Geophysical Research: Oceans*, 106(C1), pp.859-877.
- Han, W. and Webster, P.J., 2002. Forcing mechanisms of sea level interannual variability in the Bay of Bengal. *Journal of Physical Oceanography*, 32(1), pp.216-239.
- Hannachi, A., Jolliffe, I.T. and Stephenson, D.B., 2007. Empirical orthogonal functions and related techniques in atmospheric science: A review. *International Journal of Climatology*, 27(9), pp.1119-1152, doi:10.1002/joc.1499.
- Hantel, M., 1970. Monthly charts of surface wind stress curl over the Indian Ocean. *Monthly Weather Review*, 98(7-12), p.765.
- Harrison, D.E. and Vecchi, G.A., 2001. El Niño and La Niña—Equatorial Pacific thermocline depth and sea surface temperature anomalies, 1986–98. *Geophysical Research Letters*, 28(6), pp.1051-1054.

- Hastenrath, S and Lamb, P.J., 1979. Climatic Atlas of the Indian Ocean. *University of Wisconsin Press, Madison, Wisconsin*, 97 p.
- Hidaka, K., 1958. Computation of the wind stresses over the oceans. *Rec. Oceanogr. Works Japan*, 4(2), pp.77-123.
- Howard, K.L. and Yoder, J.A., 1997, December. Contribution of the subtropical oceans to global primary production. In *COSPAR Colloquia Series* (Vol. 8, pp. 157-167). Pergamon.
- IOCCG, 1999. Status and Plans for Satellite Ocean-Colour Missions: Considerations for Complementary Missions. Yoder, J. A. (ed.), *Reports of the International Ocean-Colour Coordinating Group*, No. 2, IOCCG, Dartmouth, Canada.
- IOCCG, 2000. Remote Sensing of Ocean Colour in Coastal, and Other Optically-Complex, Waters. Sathyendranath, S. (ed.), *Reports of the International Ocean-Colour Coordinating Group*, No. 3, IOCCG, Dartmouth, Canada.
- Ishii, M., Kimoto, M. and Kachi, M., 2003. Historical ocean subsurface temperature analysis with error estimates. *Monthly Weather Review*, 131(1), pp.51-73.
- Ishii, M., Shouji, A., Sugimoto, S. and Matsumoto, T., 2005. Objective analyses of sea surface temperature and marine meteorological variables for the 20th century using ICOADS and the Kobe collection. *International Journal of Climatology*, 25(7), pp.865-879.
- Ishii, M., Kimoto, M., Sakamoto, K. and Iwasaki, S.I., 2006. Steric sea level changes estimated from historical ocean subsurface temperature and salinity analyses. *Journal of oceanography*, 62(2), pp.155-170.
- Jacob, D.S. and Shay, L.K., 1999. Upper ocean response to tropical cyclone wind asymmetries. *Workshop on Extratropical Transition of Tropical Cyclones*, Munich, Germany.
- Jeffrey, S.W.; Mantoura, R.F.C., 1997. Development of pigment methods for oceanography: SCOR-supported working groups and objectives, in: Jeffrey, S.W.et al.(Ed.) *Phytoplankton pigments in oceanography: guidelines to modern methods. Monographs on Oceanographic Methodology*, 10, pp. 19-36.
- Joseph, P.V., Sooraj, K.P., Babu, C.A. and Sabin, T.P., 2005. A cold pool in the Bay of Bengal and its interaction with the active-break cycle of the monsoon. *Clivar Exchanges*, 34(10), p.3.

- Kamykowski, D., 1987. A preliminary biophysical model of the relationship between temperature and plant nutrients in the upper ocean. *Deep Sea Research Part A. Oceanographic Research Papers*, 34(7), pp.1067-1079.
- Kessler, W.S., 1990: Observations of long Rossby waves in the northern tropical Pacific. *J. Geophys. Res.*, 95, 5183-5217
- Kilpatrick, K.A., Podesta, G.P. and Evans, R., 2001. Overview of the NOAA/NASA advanced very high resolution radiometer Pathfinder algorithm for sea surface temperature and associated matchup database. *J. Geophys. Res.*, 106(C5), pp.9179-9197.
- Kumar, M.D., Naqvi, S.W.A., George, M.D. and Jayakumar, D.A., 1996. A sink for atmospheric carbon dioxide in the northeast Indian Ocean. *Journal of Geophysical Research: Oceans*, 101(C8), pp.18121-18125.
- Kumar, S., Ramesh, R., Sardesai, S. and Sheshshayee, M.S., 2004. High new production in the Bay of Bengal: Possible causes and implications. *Geophysical research letters*, 31(18), doi:10.1029/2004GL021005.
- Kutzbach, J.E., 1967. Empirical eigenvectors of sea-level pressure, surface temperature and precipitation complexes over North America. *Journal of Applied Meteorology*, 6(5), pp.791-802.
- LaFond, E.C., 1957, July. Oceanographic studies in the Bay of Bengal. In *Proceedings of the Indian Academy of Sciences-Section B* (Vol. 46, No. 1, pp. 1-46). Springer India.
- Large, W.G. and Pond, S., 1981. Open ocean momentum flux measurements in moderate to strong winds. *Journal of physical oceanography*, 11(3), pp.324-336
- Lee, C.M., Jones, B.H., Brink, K.H. and Fischer, A.S., 2000. The upper-ocean response to monsoonal forcing in the Arabian Sea: seasonal and spatial variability. *Deep Sea Research Part II: Topical Studies in Oceanography*, 47(7), pp.1177-1226.
- Lin, I., Liu, W.T., Wu, C.C., Wong, G.T., Hu, C., Chen, Z., Liang, W.D., Yang, Y. and Liu, K.K., 2003. New evidence for enhanced ocean primary production triggered by tropical cyclone. *Geophysical Research Letters*, 30(13), doi:10.1029/2003GL017141.
- Linz, P. and Wang, R., 2003. *Exploring numerical methods: An introduction to scientific computing using MATLAB*. Jones & Bartlett Learning.

- Longhurst, A.R., 2010. Ecological geography of the sea. *Academic Press*. San Diego, Calif., 1998.
- Lorenz, E.N., 1956. Empirical Orthogonal Functions and Statistical Weather Prediction. Technical report, *Statistical Forecast Project Report 1*, Dept. of Meteor., MIT, 49pp.
- Ludwig, F.L., Horel, J. and Whiteman, C.D., 2004. Using EOF analysis to identify important surface wind patterns in mountain valleys. *Journal of applied meteorology*, 43(7), pp.969-983.
- Luis, A.J. and Kawamura, H., 2000. Wintertime wind forcing and sea surface cooling near the south India tip observed using NSCAT and AVHRR. *Remote sensing of environment*, 73(1), pp.55-64.
- Luis, A.J. and Kawamura, H., 2001. Characteristics of atmospheric forcing and SST cooling events in the Gulf of Mannar during winter monsoon. *Remote sensing of environment*, 77(2), pp.139-148.
- Luis, A.J. and Kawamura, H., 2002. Dynamics and mechanism for sea surface cooling near the Indian tip during winter monsoon. *Journal of Geophysical Research: Oceans*, 107(C11), doi: 10.1029/2000JC000455
- Madhu, N.V., Maheswaran, P.A., Jyothibabu, R., Sunil, V., Revichandran, C., Balasubramanian, T., Gopalakrishnan, T.C. and Nair, K.K.C., 2002. Enhanced biological production off Chennai triggered by October 1999 super cyclone (Orissa). *Current Science*, 82:12.
- Madhupratap, M., Kumar, S.P., Bhattathiri, P.M.A., Kumar, M.D., Raghukumar, S., Nair, K.K.C. and Ramaiah, N., 1996. Mechanism of the biological response to winter cooling in the northeastern Arabian Sea. *Nature*, 384(6609), pp.549-552.
- Madhupratap, M., Gauns, M., Ramaiah, N., Kumar, S.P., Muraleedharan, P.M., De Sousa, S.N., Sardesai, S. and Muraleedharan, U., 2003. Biogeochemistry of the Bay of Bengal: physical, chemical and primary productivity characteristics of the central and western Bay of Bengal during summer monsoon 2001. *Deep Sea Research Part II: Topical Studies in Oceanography*, 50(5), pp.881-896.
- Madhusoodanan, P. and James, V.V., 2003. Thermohaline features of the subsurface cyclonic Eddy the south central Bay of Bengal during August 1999. *Journal of Earth System Science*, 112(2), pp.233-237.

- Malone, T.C., Pike, S.E. and Conley, D.J., 1993. Transient variations in phytoplankton productivity at the JGOFS Bermuda time series station. *Deep Sea Research Part I: Oceanographic Research Papers*, 40(5), pp.903-924.
- Marshall, J. and Plumb, R.A., 2013. *Atmosphere, ocean and climate dynamics: an introductory text* (Vol. 21). Academic Press.
- Martin, J.M., Burton, J.D. and Eisma, D. eds., 1981. *River inputs to ocean systems. United Nations Environment Programme*, 384 pp., United Nations Press, Geneva, Switzerland, 1981.
- Martin, S., 2004. An introduction to ocean remote sensing, Chpt.6, *Cambridge University Press, Cambridge, United Kingdom*, pp 454. ISBN 0521802806.
- McCreary, J.P., Kundu, P.K. and Molinari, R.L., 1993. A numerical investigation of dynamics, thermodynamics and mixed-layer processes in the Indian Ocean. *Progress in Oceanography*, 31(3), pp.181-244.
- McCreary, J.P., Han, W., Shankar, D. and Shetye, S.R., 1996. Dynamics of the East India Coastal Current: 2. Numerical solutions. *Journal of Geophysical Research: Oceans*, 101(C6), pp.13993-14010.
- McPhaden, M.J., 1993. TOGA-TAO and the 1991–93 El Niño-Southern oscillation event. *Oceanography*, 6(2), pp.36-44.
- Meinen, C.S. and McPhaden, M.J., 2000. Observations of warm water volume changes in the equatorial Pacific and their relationship to El Niño and La Niña. *Journal of Climate*, 13(20), pp.3551-3559.
- Menkes, C.E., Lengaigne, M., Marchesiello, P., Jourdain, N.C., Vincent, E.M., Lefèvre, J., Chauvin, F. and Royer, J.F., 2012. Comparison of tropical cyclogenesis indices on seasonal to interannual timescales. *Climate dynamics*, 38(1-2), pp.301-321.
- Milliff, R.F. and Morzel, J., 2001. The global distribution of the time-average wind stress curl from NSCAT. *Journal of the Atmospheric Sciences*, 58(2), pp.109-131.
- Minnett, P.J., Knuteson, R.O., Best, F.A., Osborne, B.J., Hanafin, J.A. and Brown, O.B., 2001. The marine-atmospheric emitted radiance interferometer: A high-accuracy, seagoing infrared spectroradiometer. *Journal of atmospheric and oceanic technology*, 18(6), pp.994-1013.

- Monterey, G.I. and Levitus, S., 1997. United States. National Environmental Satellite, Data, and Information Service, *Seasonal variability of mixed layer depth for the world ocean*. US Department of Commerce, National Oceanic and Atmospheric Administration, National Environmental Satellite, Data, and Information Service.
- Morel, A. and Prieur, L., 1977. Analysis of variations in ocean color. *Limnology and oceanography*, 22(4), pp.709-722.
- Murty, C.S. and Varadachari, V.V.R., 1968. Upwelling along the east coast of India. *Bull. Nat. Inst. Sci. India*, 36, pp.80-86.
- Ning, X.R., Chai, F., Xue, H., Cai, Y., Liu, C. and Shi, J., 2004. Physical-biological oceanographic coupling influencing phytoplankton and primary production in the South China Sea. *Journal of Geophysical Research: Oceans*, 109(C10), doi:10.1029/2004JC002365.
- O'Brien, J.J. and Reid, R.O., 1967. The non-linear response of a two-layer, baroclinic ocean to a stationary, axially-symmetric hurricane: Part I. Upwelling induced by momentum transfer. *Journal of the Atmospheric Sciences*, 24(2), pp.197-207.
- O'Reilly, J.E., Maritorena, S., Mitchell, B.G., Siegel, D.A., Carder, K.L., Garver, S.A., Kahru, M. and McClain, C., 1998. Ocean color chlorophyll algorithms for SeaWiFS. *Journal of Geophysical Research: Oceans*, 103(C11), pp.24937-24953.
- O'Reilly, J.E., and 24 Coauthors, 2000: SeaWiFS Postlaunch Calibration and Validation Analyses, Part 3. *NASA Tech. Memo. 2000-206892, Vol. 11*, S.B. Hooker and E.R. Firestone, Eds., NASA Goddard Space Flight Center, 49 pp.
- Pickard, G.L. and Emery, W.J., 1990. *Descriptive physical oceanography: an introduction*. Elsevier.
- Pickett, M.H. and Paduan, J.D., 2003. Ekman transport and pumping in the California Current based on the US Navy's high-resolution atmospheric model (COAMPS). *Journal of Geophysical Research: Oceans*, 108(C10), doi:10.1029/2003JC001902.
- Platt, T. and Sathyendranath, S., 1988. Oceanic primary production: estimation by remote sensing at local and regional scales. *Science*, 241(4873), pp.1613-1620.

- Potemra, J.T., Luther, M.E. and O'Brien, J.J., 1991. The seasonal circulation of the upper ocean in the Bay of Bengal. *Journal of Geophysical Research: Oceans*, 96(C7), pp.12667-12683.
- Prasanna Kumar, S., Madhupratap, M., Kumar, M.D., Gauns, M., Muraleedharan, P.M., Sarma, V.V.S.S. and De Souza, S.N., 2000. Physical control of primary productivity on a seasonal scale in central and eastern Arabian Sea. *Journal of Earth System Science*, 109(4), pp.433-441.
- Prasannakumar, S., Madhupratap, M., Dileepkumar, M., Muraleedharan, P.M., DeSouza, S.N., Gauns, M. and Sarma, V.V.S.S., 2001. High biological productivity in the central Arabian Sea during the summer monsoon driven by Ekman pumping and lateral advection. *Current Science*, 81, pp. 1633– 1638.
- Prasanna Kumar, S., Muraleedharan, P.M., Prasad, T.G., Gauns, M., Ramaiah, N., De Souza, S.N., Sardesai, S. and Madhupratap, M., 2002. Why is the Bay of Bengal less productive during summer monsoon compared to the Arabian Sea?. *Geophysical Research Letters*, 29(24), 2235, doi:10.1029/2002GL016013.
- Prasanna Kumar, S., Nuncio, M., Narvekar, J., Kumar, A., Sardesai, S., De Souza, S.N., Gauns, M., Ramaiah, N. and Madhupratap, M., 2004. Are eddies nature's trigger to enhance biological productivity in the Bay of Bengal?. *Geophysical Research Letters*, 31(7), doi:10.1029/2003GL019274.
- Prasanna Kumar, S., Nuncio, M., Ramaiah, N., Sardesai, S., Narvekar, J., Fernandes, V. and Paul, J.T., 2007. Eddy-mediated biological productivity in the Bay of Bengal during fall and spring intermonsoons. *Deep Sea Research Part I: Oceanographic Research Papers*, 54(9), pp.1619-1640.
- Prasannakumar, S., Nuncio, M., Narvekar, J., Ramaiah, N., Sardesai, S., Gauns, M., Fernandes, V., Paul, J.T., Jyothibabu, R. and Jayaraj, K.A., 2010. Seasonal cycle of physical forcing and biological response in the Bay of Bengal. *Indian Journal of Marine Sciences*, 39, pp.388-405.
- Preisendorfer, R.W., 1988. Principal component analysis in meteorology and oceanography. Ed. Curtis D. Mobley. Vol. 425. Amsterdam: Elsevier, 1988.
- Premkumar, K., Ravichandran, M., Kalsi, S.R., Sengupta, D. and Gadgil, S., 2000. First results from a new observational system over the Indian seas. *Current Science*, 78(3), pp.323-330.

- Price, J.F., 1981. Upper ocean response to a hurricane. *Journal of Physical Oceanography*, 11(2), pp.153-175.
- Quikscat Scatterometer Mean Wind Field Products User Manual, Réf. : C2-MUT-W-03-IF, Version : 1.0, vol 2, CERSAT – IFREMER February 2002.[Available online at [ftp://ftp.ifremer.fr/ifremer/cersat/documentation/gridded/mwf-quikscat/mwf\\_vol2.pdf](ftp://ftp.ifremer.fr/ifremer/cersat/documentation/gridded/mwf-quikscat/mwf_vol2.pdf) ]
- Ramesh Kumar, M.R. and Sankar, S., 2010. Impact of global warming on cyclonic storms over north Indian Ocean. *Indian Journal of Marine Sciences*, 39, pp.516-520
- Rao, A.D., 2002. Variability of wind stress curl over the Indian Ocean during years 1970-1995. *Indian Journal of Marine Sciences*, 31(2), pp.87-92.
- Rao, A.D., Babu, S.V. and Dube, S.K., 2004. Impact of a tropical cyclone on coastal upwelling processes. *Natural Hazards*, 31(2), pp.415-435.
- Rao, A.D. and Chamarthi, S., 1997. A multi-level numerical model of coastal upwelling: A diagnostic study. *International Journal for Numerical Methods in Fluids*, 24(1), 17-59.
- Rao, A.D., Joshi, M. and Babu, S.V., 2005. A three-dimensional numerical model of coastal upwelling along the west coast of India. *Mathematical and computer modelling*, 41(2-3), 177-195.
- Rao, A.D., Joshi, M. and Ravichandran, M., 2008. Oceanic upwelling and downwelling processes in waters off the west coast of India. *Ocean Dynamics*, 58(3-4), 213-226.
- Rao, K.H., Choudhury, S.B., Das, S.K., Mishra, R.K. and SHAW, B.P., 2002a, Evaluation of VGPM model for estimation of primary productivity along Paradip coast, east coast of India. IAPRS and SIS, *Resource and Environment Monitoring*, 34, pp. 1413–1417.
- Rao, K.H., Smitha, A. and Ali, M.M., 2006b. A study on cyclone induced productivity in south-western Bay of Bengal during November-December 2000 using MODIS (SST and chlorophyll-a) and altimeter sea surface height observations. *Indian Journal of Marine Sciences*, 35(2), pp.153-160.
- Rao, L.V.G., and Shree Ram, P., 2005. Upper ocean physical processes in the Tropical Indian Ocean, *Monograph, 68pp & Figures*, NIO, Goa. (<http://hdl.handle.net/2264/93>)

- Rao, R.R., Mathew, B. and Kumar, P.H., 1993. A summary of results on thermohaline variability in the upper layers of the east central Arabian Sea and Bay of Bengal during summer monsoon experiments. *Deep Sea Research Part I: Oceanographic Research Papers*, 40(8), pp.1647-1672, doi:10.1016/0967-0637(93)90020-4.
- Rao, R.R., Kumar, G., Ravichandran, M., Samala, B.K. and Sreedevi, N., 2006a. Observed mini cold pool off the southern tip of India and its intrusion into the south central Bay of Bengal during summer monsoon season. *Geophysical research letters*, 33(6), doi:10.1029/2005GL025382.
- Rao, S.A., Behera, S.K., Masumoto, Y. and Yamagata, T., 2002b. Interannual subsurface variability in the tropical Indian Ocean with a special emphasis on the Indian Ocean dipole. *Deep Sea Research Part II: Topical Studies in Oceanography*, 49(7), pp.1549-1572.
- Rao, S.A., Saha, S.K., Pokhrel, S., Sundar, D., Dhakate, A.R., Mahapatra, S., Ali, S., Chaudhari, H.S., Shreeram, P., Vasimalla, S. and Srikanth, A.S., 2011. Modulation of SST, SSS over northern Bay of Bengal on ISO time scale. *Journal of Geophysical Research: Oceans*, 116(C9), C09026, doi:10.1029/2010JC006804.
- Rao, T.N., Rao, D.P., Rao, B.P. and Raju, V.R., 1986. Upwelling and sinking along Visakhapatnam coast. *Indian Journal of Marine Sciences*, 15(2), pp.84-87.
- Reynolds, R.W., Folland, C.K. and Parker, D.E., 1989. Biases in satellite-derived sea-surface-temperature data. *Nature* 341, 728 (1989).
- Reynolds, R.W., 1993. Impact of Mount Pinatubo aerosols on satellite-derived sea surface temperatures. *Journal of climate*, 6(4), pp.768-774.
- Ryther, J.H. and Yentsch, C.S., 1957. The estimation of phytoplankton production in the ocean from chlorophyll and light data. *Limnology and Oceanography*, 2(3), pp.281-286.
- Ryther, J.H., 1969. Photosynthesis and fish production in the sea. The production of organic matter and its conversion to higher forms of life vary throughout the world ocean. *American Association for the Advancement of Science. Science*, 166, pp.72-76.

- Sachoemar, S.I., Yanagi, T., Hendiarti, N., Sadly, M. and Meliani, F., 2010. Seasonal variability of sea surface chlorophyll-a and abundance of pelagic fish in Lampung Bay, Southern Coastal Area of Sumatra, Indonesia.
- Saji, N.H., Goswami, B.N., Vinayachandran, P.N. and Yamagata, T., 1999. A dipole mode in the tropical Indian Ocean. *Nature*, 401(6751), pp.360-363.
- Sanders, F and Charnock, Henry., "Wind Stress," *AccessScience* (McGraw-Hill Education, 2014), <http://dx.doi.org/10.1036/1097-8542.746600>
- Sarmiento, J.L., Hughes, T.M., Stouffer, R.J. and Manabe, S., 1998. Simulated response of the ocean carbon cycle to anthropogenic climate warming. *Nature*, 393(6682), pp.245-249.
- Sathyendranath, S., Gouveia, A.D., Shetye, S.R., Ravindran, P. and Platt, T., 1991. Biological control of surface temperature in the Arabian Sea. *Nature*, 349, pp. 54–56.
- Schott, F.A. and McCreary, J.P., 2001. The monsoon circulation of the Indian Ocean. *Progress in Oceanography*, 51(1), pp.1-123.
- Schott, F. A., Xie, S.-P, and McCreary Jr., J.P., 2009. Indian Ocean circulation and climate variability. *Rev. Geophys.*, 47, RG1002, doi:10.1029/2007RG000245.
- Sengupta, D., Ray, P.K. and Bhat, G.S., 2002. Spring warming of the eastern Arabian Sea and Bay of Bengal from buoy data. *Geophysical research letters*,29(15).
- Sengupta, D., Senan, R., Goswami, B.N. and Vialard, J., 2007. Intraseasonal variability of equatorial Indian Ocean zonal currents. *Journal of Climate*, 20(13), pp.3036-3055.
- Sengupta, D., Goddalahundi, B.R. and Anitha, D.S., 2008. Cyclone-induced mixing does not cool SST in the post-monsoon North Bay of Bengal. *Atmospheric Science Letters*, 9(1), pp.1-6.
- Shankar, D., McCreary, J.P., Han, W. and Shetye, S.R., 1996. Dynamics of the East India Coastal Current: 1. Analytic solutions forced by interior Ekman pumping and local alongshore winds. *Journal of Geophysical Research: Oceans*, 101(C6), pp.13975-13991.
- Shankar, D., Vinayachandran, P.N. and Unnikrishnan, A.S., 2002. The monsoon currents in the north Indian Ocean. *Progress in oceanography*, 52(1), pp.63-120.

- Shenoi, S.S.C., Shankar, D. and Shetye, S.R., 2002. Differences in heat budgets of the near surface Arabian Sea and Bay of Bengal: Implications for the summer monsoon. *Journal of Geophysical Research: Oceans*, 107(C6), doi:10.1029/2000JC000679.
- Shenoi, S.S.C., Shankar, D., Michael, G.S., Kurian, J., Varma, K.K., Kumar, M.R., Almeida, A.M., Unnikrishnan, A.S., Fernandes, W., Barreto, N. and Gnanaseelan, C., 2005. Hydrography and water masses in the southeastern Arabian Sea during March–June 2003. *Journal of earth system science*, 114(5), pp.475-491.
- Shetye, S.R., Shenoi, S.S.C., Gouveia, A.D., Michael, G.S., Sundar, D. and Nampoothiri, G., 1991. Wind-driven coastal upwelling along the western boundary of the Bay of Bengal during the southwest monsoon. *Continental Shelf Research*, 11(11), pp.1397-1408.
- Shetye, S.R., Gouveia, A.D., Shenoi, S.S.C., Sundar, D., Michael, G.S. and Nampoothiri, G., 1993. The western boundary current of the seasonal subtropical gyre in the Bay of Bengal. *J. Geophys. Res*, 98(C1), pp.945-954.
- Shetye, S.R., Gouveia, A.D., Shankar, D., Shenoi, S.S.C., Vinayachandran, P.N., Sundar, D., Michael, G.S. and Nampoothiri, G., 1996. Hydrography and circulation in the western Bay of Bengal during the northeast monsoon. *Journal of Geophysical Research: Oceans*, 101(C6), pp.14011-14025.
- Shetye, S.R. and Gouveia, A.D., 1998. Coastal circulation in the north Indian Ocean: Coastal segment (14, SW). *The Sea*, Volume 11 (Allan R. Robinson and Kenneth H. Brink, eds.), John Wiley and Sons, Inc, Ch. 18, pp. 523–556.
- Singh, O.P., Khan, T.M.A. And Rahman, M.S., 2001. Has The Frequency Of Intense Tropical Cyclones Increased In The North Indian Ocean?. *Current Science-Bangalore-*, 80(4), pp.575-580.
- Smith, L.I., 2002. A tutorial on principal components analysis. *Cornell University, USA*, 51, p.52.
- Smith, S.D., 1988. Coefficients for sea surface wind stress, heat flux, and wind profiles as a function of wind speed and temperature. *Journal of Geophysical Research: Oceans*, 93(C12), pp.15467-15472.
- Smith, R. Upwelling, volume 6, chapter 1, pages 11 – 46. University College London Press, 1968. 8

- Smitha, A., Rao, K.H. and Sengupta, D., 2006. Effect of May 2003 tropical cyclone on physical and biological processes in the Bay of Bengal. *International Journal of Remote Sensing*, 27(23), pp.5301-5314.
- Son, S., Platt, T., Bouman, H., Lee, D. and Sathyendranath, S., 2006. Satellite observation of chlorophyll and nutrients increase induced by Typhoon Megi in the Japan/East Sea. *Geophysical research letters*, 33(5), doi:10.1029/2005GL025065.
- Stewart, R. H. (1985). Methods of satellite oceanography, *Univ. of California Press*.
- Stull, R.B., 1994. *An introduction to boundary layer meteorology* (Vol. 13). Springer Science & Business Media.
- Subrahmanyam, B., Rao, K.H., Srinivasa Rao, N., Murty, V.S.N. and Sharp, R.J., 2002. Influence of a tropical cyclone on chlorophyll-a concentration in the Arabian Sea. *Geophysical Research Letters*, 29(22), doi:10.1029/2002GL015892.
- Subramanian, V., 1993. Sediment load of Indian rivers. *Current Science*, 64(11-12), pp. 928-930.
- Vinayachandran, P.N. and Shetye, S.R., 1991. The warm pool in the Indian Ocean. *Proceedings of the Indian Academy of Sciences-Earth and Planetary Sciences*, 100(2), pp.165-175.
- Vinayachandran, P. N., Seasonal Cycle of the Hydrography and Circulation of the Bay of Bengal, M Sc (Engg.) Thesis, *Indian Institute of Science, Bangalore*, 1992, pp. 61.
- Vinayachandran, P.N., Shetye, S.R., Sengupta, D. and Gadgil, S., 1996. Forcing mechanisms of the Bay of Bengal circulation. *Current Science*, 71(10), pp.753-763.
- Vinayachandran, P.N. and Yamagata, T., 1998. Monsoon response of the sea around Sri Lanka: generation of thermal domes and anticyclonic vortices. *Journal of Physical Oceanography*, 28(10), pp.1946-1960.
- Vinayachandran, P.N. and Mathew, S., 2003. Phytoplankton bloom in the Bay of Bengal during the northeast monsoon and its intensification by cyclones. *Geophysical Research Letters*, 30(11), doi:10.1029/2002GL016717.

- Vinayachandran, P.N., Chauhan, P., Mohan, M. and Nayak, S., 2004. Biological response of the sea around Sri Lanka to summer monsoon. *Geophysical Research Letters*, 31(1), doi:10.1029/2003GL018533.
- Vinayachandran, P.N., Kagimoto, T., Masumoto, Y., Chauhan, P., Nayak, S.R. and Yamagata, T., 2005. Bifurcation of the East India coastal current east of Sri Lanka. *Geophysical research letters*, 32(15), doi:10.1029/2005GL022864.
- Vinayachandran, P.N. and Kurian, J., 2007. Hydrographic observations and model simulation of the Bay of Bengal freshwater plume. *Deep Sea Research Part I: Oceanographic Research Papers*, 54(4), pp.471-486.
- Vinayachandran, P.N. and Saji, N.H., 2008. Mechanisms of South Indian Ocean intraseasonal cooling. *Geophys. Res. Lett*, 35, p.L23607.
- Vinayachandran, P.N., 2009. Impact of physical processes on chlorophyll distribution in the Bay of Bengal. *Indian Ocean Biogeochemical Processes and Ecological Variability*, pp.71-86, doi:10.1029/2008GM000705.
- Vinayachandran, P.N., Neema, C.P., Mathew, S. and Remya, R., 2012. Mechanisms of summer intraseasonal sea surface temperature oscillations in the Bay of Bengal. *Journal of Geophysical Research: Oceans*, 117(C1), <http://dx.doi.org/10.1029/2011JC007433>.
- Wentz, F.J., 1997. A well-calibrated ocean algorithm for special sensor microwave/imager. *Journal of Geophysical Research: Oceans*, 102(C4), pp.8703-8718.
- Wentz, F.J., Gentemann, C., Smith, D. and Chelton, D., 2000. Satellite measurements of sea surface temperature through clouds. *Science*, 288(5467), pp.847-850.
- Williams, R.G. and Follows, M.J., 2003. Physical transport of nutrients and the maintenance of biological production. In *Ocean Biogeochemistry* (pp. 19-51), edited by M. J. R. Fasham, chap. 2, pp. 19– 51, Springer Berlin Heidelberg.
- Yoder, J.A., McClain, C.R., Feldman, G.C. and Esaias, W.E., 1993. Annual cycles of phytoplankton chlorophyll concentrations in the global ocean: a satellite view. *Global Biogeochemical Cycles*, 7(1), pp.181-193.
- Yoder, J.A. and Kennelly, M.A., 2003. Seasonal and ENSO variability in global ocean phytoplankton chlorophyll derived from 4 years of SeaWiFS

measurements. *Global Biogeochemical Cycles*, 17(4), p.1112, doi:10.1029/2002GB001942.

Yu, L., O'Brien, J.J. and Yang, J., 1991. On the remote forcing of the circulation in the Bay of Bengal. *Journal of Geophysical Research: Oceans*, 96(C11), pp.20449-20454.

Yu, L., 2003. Variability of the depth of the 20 C isotherm along 6 N in the Bay of Bengal: Its response to remote and local forcing and its relation to satellite SSH variability. *Deep Sea Research Part II: Topical Studies in Oceanography*, 50(12), pp.2285-2304.

## List of Publications

Smitha, A., Rao, K.H. and Sengupta, D., 2006. Effect of May 2003 tropical cyclone on physical and biological processes in the Bay of Bengal. *International Journal of Remote Sensing*, 27(23), pp.5301-5314.

Rao, K.H., Smitha, A. and Ali, M.M., 2006. A study on cyclone induced productivity in south-western Bay of Bengal during November-December 2000 using MODIS (SST and chlorophyll-a) and altimeter sea surface height observations. *Indian Journal of Marine Sciences*, 35(2), pp.153-160.

## Effect of May 2003 tropical cyclone on physical and biological processes in the Bay of Bengal

A. SMITHA\*†, K. H. RAO† and D. SENGUPTA‡

†Oceanography Division, National Remote Sensing Agency, Hyderabad, India

‡Centre for Atmospheric and Oceanic Sciences, Indian Institute of Science, Bangalore, India

(Received 28 March 2005; in final form 6 August 2005)

Satellite observations are beginning to show the remarkable effects of tropical cyclones on upper ocean temperature and chlorophyll concentration. We use weekly, 4 km resolution chlorophyll-a and sea surface temperature (SST) from TERRA Moderate Resolution Imaging Spectroradiometer, weekly averaged SST at 0.25° resolution from Tropical Rainfall Measuring Mission Microwave Imager, modeled primary productivity (PP) from Goddard Space Flight Center and mixed layer depth generated by US Navy's Fleet Numerical Meteorology and Oceanography Center to study the response of upper ocean physics and biology to the passage of a tropical cyclone in the southern Bay of Bengal. Decrease in SST up to 5°C, associated with the deepening of mixed layer by about 12 m, was observed. Directly under the cyclone track, PP increased from its pre-storm value by up to 3800 mg C m<sup>-2</sup> day<sup>-1</sup>, and chlorophyll-a concentration also increased. The increase in chlorophyll-a and productivity were not confined to the region under the cyclone track, but covered a much broader area, possibly due to forced coastal upwelling south of Sri Lanka. After the passage of the cyclone the SST slowly increased, and the chlorophyll decreased.

### 1. Introduction

Wind, rain and storm surge associated with tropical cyclones cause great damage to life and property in the countries bordering the North Indian Ocean, particularly the Bay of Bengal. The Bay is a tropical basin that receives large volumes of fresh water from both continental runoff and rainfall. In the Bay, cyclones usually form between 8.0°N and 15.0°N latitude along the Inter Tropical Convergence Zone. There are two cyclone seasons in the North Indian Ocean, before and after the summer monsoon. Most cyclones occur in April to June and September to November, with the highest frequency in November and May. Tropical cyclone formation is suppressed during the monsoon season due to large vertical wind shear. The near-surface circulation of the Bay of Bengal undergoes seasonal reversal forced by monsoon winds and fresh water input as well as remote effects from the equatorial Indian Ocean. During the pre-monsoon months (March to May) there is a well-developed anticyclonic gyre in the Bay with a poleward western boundary current (Shetye *et al.* 1993). The current flows equatorward all along the coast in November-December (Shetye *et al.* 1996). During the summer monsoon (June to September) the east India coastal current flows poleward along the southern part of

---

\*Corresponding author. Email: smitha\_cusat@yahoo.com

## A study on cyclone induced productivity in south-western Bay of Bengal during November-December 2000 using MODIS (SST and chlorophyll-*a*) and altimeter sea surface height observations

K. H. Rao\*, A. Smitha & M. M. Ali

Oceanography Division, National Remote Sensing Agency, Balanagar, Hyderabad 500 037, India

\*[E-mail: [rao\\_kh@yahoo.com](mailto:rao_kh@yahoo.com) ]

Received 27 December 2004, revised 10 April 2006

MODIS (Moderate Resolution Imaging Spectroradiometer) on board TERRA weekly composite mean products of sea surface temperature (SST) and chlorophyll-*a*, and modeled ocean net primary productivity with a spatial resolution of 4.63 km and altimeter derived sea surface height (SSH) data are used to study the changes in the primary productivity (PP) induced by the November-December 2000 tropical cyclone in the Bay of Bengal. A maximum SST drop of 2°C, a sea surface depression of 10 cm compared to the periphery, increase in chlorophyll-*a* by 1.5 mg/m<sup>3</sup> and enhanced average mixed PP of 964 gC/m<sup>2</sup>/y were observed around 11.0°N and 81.0°E after the passage of the cyclonic storm. The enhanced PP after the passage of the cyclone supports the base of the pelagic marine food web, directly affecting the fishery productivity.

[**Key words:** Tropical cyclone, chlorophyll-*a*, sea surface temperature, mixed layer depth, primary productivity]

### Introduction

Bay of Bengal is a semi enclosed tropical ocean basin highly influenced by monsoonal winds and receives large volumes of fresh water from both river discharges and rainfall. Tropical cyclones are a major hazard in coastal regions, both in terms of loss of life and economic damage. The extensive coastal belt of India is very vulnerable to these tropical cyclones. Such cyclones originate in the Bay of Bengal and the Arabian Sea during the spring (April-May) and fall (October-November). The cyclones usually form between 8.0°N and 15.0°N latitude and develop as perturbations along the Inter Tropical Convergence Zone (ITCZ). It is not unusual for a storm formed over the Bay of Bengal to move across southern India and re-intensify over the eastern Arabian Sea. The surface circulation in the Bay of Bengal undergoes seasonal reversal forced by remote effects from the equatorial Indian Ocean in addition to monsoon winds and fresh water inputs<sup>1,2</sup>. These circulation features have a strong influence on the primary productivity (PP) of the Bay of Bengal, which is traditionally considered to be the region of lesser biological productivity. Recent measurements also suggest that

productivity in Bay of Bengal is less compared to Arabian Sea<sup>3,4</sup>. Prasanna Kumar *et al.*<sup>5</sup> reviewed the reasons for less productivity in the Bay of Bengal compared to Arabian Sea and attributed to the presence of strong stratified surface layer, warmer sea surface temperature (SST) and weak winds. Physical processes such as ocean currents and eddies are able to erode stratification and upwell nutrients leading to high chlorophyll in the western Bay of Bengal<sup>4</sup>.

Tropical cyclones with strong wind and heavy rainfall represent the extreme cases of the episodic disturbances that have profound influence on the abundance and production of marine phytoplankton. One of the most striking effects of a tropical cyclone on the upper ocean is the marked cooling of SST which is widely studied by many researchers over North Indian Ocean. SST cooling is mainly due to vertical mixing of cool subsurface water under the action of cyclonic winds. Premkumar *et al.*<sup>6</sup> observed a 3°C fall in SST in association with a tropical cyclone in the Arabian Sea. In the open ocean, tropical cyclones may deepen the mixed layer by 20-30 meters<sup>7</sup>. Subrahmanyam *et al.*<sup>8</sup> studied the effect of a tropical cyclone on the formation of phytoplankton blooms during the development of cyclone during 21 May to 3<sup>rd</sup> June, 2001 using IRS-P4 Ocean Colour Monitor (OCM) data in the Eastern Arabian Sea.

\* Fax : +91-40-23879869  
Phone : +91-40-23884245